



# A CONSTELLATION ARCHITECTURE FOR MONITORING CARBON DIOXIDE AND METHANE FROM SPACE

Prepared by the CEOS Atmospheric Composition Virtual Constellation Greenhouse Gas Team

Version 1.0 – 8 October 2018

© 2018. All rights reserved

Contributors:

David Crisp<sup>1</sup>, Yasjka Meijer<sup>2</sup>, Rosemary Munro<sup>3</sup>, Kevin Bowman<sup>1</sup>, Abhishek Chatterjee<sup>4,5</sup>, David Baker<sup>6</sup>, Frederic Chevallier<sup>7</sup>, Ray Nassar<sup>8</sup>, Paul I. Palmer<sup>9</sup>, Anna Agusti-Panareda<sup>10</sup>, Jay Al-Saadi<sup>11</sup>, Yotam Ariel<sup>12</sup>, Sourish Basu<sup>13,14</sup>, Peter Bergamaschi<sup>15</sup>, Hartmut Boesch<sup>16</sup>, Philippe Bousquet<sup>7</sup>, Heinrich Bovensmann<sup>17</sup>, François-Marie Bréon<sup>7</sup>, Dominik Brunner<sup>18</sup>, Michael Buchwitz<sup>17</sup>, Francois Buisson<sup>19</sup>, John P. Burrows<sup>17</sup>, Andre Butz<sup>20</sup>, Philippe Ciais<sup>7</sup>, Cathy Clerbaux<sup>21</sup>, Paul Counet<sup>3</sup>, Cyril Crevoisier<sup>22</sup>, Sean Crowell<sup>23</sup>, Philip L. DeCola<sup>24</sup>, Carol Deniel<sup>25</sup>, Mark Dowell<sup>26</sup>, Richard Eckman<sup>11</sup>, David Edwards<sup>13</sup>, Gerhard Ehret<sup>27</sup>, Annmarie Eldering<sup>1</sup>, Richard Engelen<sup>10</sup>, Brendan Fisher<sup>1</sup>, Stephane Germain<sup>28</sup>, Janne Hakkarainen<sup>29</sup>, Ernest Hilsenrath<sup>30</sup>, Kenneth Holmlund<sup>3</sup>, Sander Houweling<sup>31,32</sup>, Haili Hu<sup>31</sup>, Daniel Jacob<sup>33</sup>, Greet Janssens-Maenhout<sup>15</sup>, Dylan Jones<sup>34</sup>, Denis Jouglet<sup>19</sup>, Fumie Kataoka<sup>35</sup>, Matthäus Kiel<sup>36</sup>, Susan S. Kulawik<sup>37</sup>, Akihiko Kuze<sup>38</sup>, Richard L. Lachance<sup>12</sup>, Ruediger Lang<sup>3</sup>, Jochen Landgraf<sup>31</sup>, Junjie Liu<sup>1</sup>, Yi Liu<sup>39,40</sup>, Shamil Maksyutov<sup>41</sup>, Tsuneo Matsunaga<sup>41</sup>, Jason McKeever<sup>28</sup>, Berrien Moore<sup>23</sup>, Masakatsu Nakajima<sup>38</sup>, Vijay Natraj<sup>1</sup>, Robert R. Nelson<sup>42</sup>, Yosuke Niwa<sup>41</sup>, Tomohiro Oda<sup>4,5</sup>, Christopher W. O'Dell<sup>6</sup>, Leslie Ott<sup>5</sup>, Prabir Patra<sup>43</sup>, Steven Pawson<sup>5</sup>, Vivienne Payne<sup>1</sup>, Bernard Pinty<sup>26</sup>, Saroja M. Polavarapu<sup>8</sup>, Christian Retscher<sup>44</sup>, Robert Rosenberg<sup>1</sup>, Andrew Schuh<sup>6</sup>, Florian M. Schwandner<sup>45,1</sup>, Kei Shiomi<sup>38</sup>, Wenying Su<sup>11</sup>, Johanna Tamminen<sup>29</sup>, Thomas E. Taylor<sup>6</sup>, Pepijn Veefkind<sup>46</sup>, Ben Veihelmann<sup>2</sup>, Stephen Wofsy<sup>33</sup>, John Worden<sup>1</sup>, Debra Wunch<sup>34</sup>, Dongxu Yang<sup>39</sup>, Peng Zhang<sup>47</sup>, Claus Zehner<sup>44</sup>

<sup>1</sup> Jet Propulsion Laboratory, California Institute of Technology, Pasadena, CA, USA

<sup>2</sup> European Space Agency, European Space Research and Technology Centre (ESTEC), Noordwijk, The Netherlands

<sup>3</sup> European Organisation for the Exploitation of Meteorological Satellites (EUMETSAT), Darmstadt, Germany

<sup>4</sup> Universities Space Research Association, Columbia, MD, USA

<sup>5</sup> NASA Global Modeling and Assimilation Office, Goddard Space Flight Center, Greenbelt, MD, USA

<sup>6</sup> Cooperative Institute for Research in the Atmosphere (CIARA), Colorado State University, Fort Collins, CO, USA

<sup>7</sup> Laboratoire des Sciences du Climat et de l'Environnement, CEA-CNRS-UVSQ, Saclay, Gif-sur-Yvette, France.

<sup>8</sup> Climate Research Division, Environment and Climate Change Canada, Toronto, Canada

<sup>9</sup> School of Geosciences, University of Edinburgh, Edinburgh, UK

<sup>10</sup> European Centre for Medium-Range Weather Forecasts, Reading, United Kingdom

<sup>11</sup> NASA Langley Research Center (LARC), Hampton, VA USA

- <sup>12</sup> Bluefield Technologies, Palo Alto, CA, USA
- <sup>13</sup> Program for Atmospheric Composition Remote Sensing and Prediction, National Center for Atmospheric Research, Boulder, Colorado, USA.
- <sup>14</sup> Cooperative Institute for Research in Environmental Sciences, University of Colorado, Boulder, CO, USA
- <sup>15</sup> European Commission, Joint Research Centre, Ispra (VA), Italy
- <sup>16</sup> Earth Observation Science, University of Leicester, Leicester, UK
- <sup>17</sup> Institute of Environmental Physics (IUP), University of Bremen, Bremen, Germany
- <sup>18</sup> Empa, Swiss Federal Laboratories for Materials Science and Technology, Switzerland
- <sup>19</sup> Centre National d'Etudes Spatiales, Toulouse, France
- <sup>20</sup> Institut für Umweltphysik, University of Heidelberg, Heidelberg, Germany
- <sup>21</sup> Laboratoire Atmosphères, Milieux, Observations Spatiales (LATMOS)/Institut Pierre Simon Laplace (IPSL), Paris, France
- <sup>22</sup> Laboratoire de Météorologie Dynamique/CNRS/IPSL, Ecole Polytechnique, Palaiseau, France
- <sup>23</sup> University of Oklahoma, Norman, OK, USA
- <sup>24</sup> Sigma Space Corporation, Lanham, MD, USA
- <sup>25</sup> Centre National d'Etudes Spatiales (CNES), Paris, France
- <sup>26</sup> European Commission, Joint Research Centre, Directorate for Sustainable Resources, seconded to DG for Internal Market, Industry, Entrepreneurship and SMEs, Copernicus Services, Brussels, Belgium
- <sup>27</sup> Deutsches Zentrum für Luft- und Raumfahrt (DLR) Oberpfaffenhofen, Institut für Physik der Atmosphäre, Weßling, Germany
- <sup>28</sup> GHGSat, Montreal, Quebec, Canada
- <sup>29</sup> Finnish Meteorological Institute (FMI), Helsinki, Finland
- <sup>30</sup> NASA Goddard Space Flight Center-Retired, Greenbelt, MD, USA
- <sup>31</sup> SRON Netherlands Institute for Space Research, Utrecht, The Netherlands
- <sup>32</sup> Department of Earth Sciences, Vrije Universiteit, Amsterdam, The Netherlands
- <sup>33</sup> School of Engineering and Applied Sciences, Harvard University, Cambridge, MA, USA
- <sup>34</sup> Department of Physics, University of Toronto, Toronto, Canada
- <sup>35</sup> Remote Sensing Technology Center of Japan (RESTEC), Tsukuba Space Center, Japan Aerospace Exploration Agency (JAXA), Tsukuba-city, Ibaraki, Japan

- <sup>36</sup> Division of Geological and Planetary Sciences, California Institute of Technology, Pasadena, CA, USA
- <sup>37</sup> Bay Area Environmental Research Institute, Sonoma, CA, USA
- <sup>38</sup> Tsukuba Space Center, Japan Aerospace Exploration Agency (JAXA), Tsukuba-city, Ibaraki, Japan
- <sup>39</sup> Institute of Atmospheric Physics, Chinese Academy of Sciences, Beijing, China
- <sup>40</sup> University of Chinese Academy of Sciences, Beijing, China
- <sup>41</sup> Center for Global Environmental Research, National Institute for Environmental Studies, Tsukuba, Ibaraki, Japan
- <sup>42</sup> Department of Atmospheric Science, Colorado State University, Fort Collins, CO, USA
- <sup>43</sup> RCGC/IACE/ACMPT, Japan Agency for Marine-Earth Science and Technology (JAMSTEC), Yokohama, Japan
- <sup>44</sup> European Space Agency, European Space Research Institute (ESRIN), Frascati, Italy
- <sup>45</sup> Joint Institute for Regional Earth System Science and Engineering (JIFRESSE), University of California Los Angeles (UCLA), Los Angeles, CA, USA
- <sup>46</sup> Royal Netherlands Meteorological Institute (KNMI), De Bilt, The Netherlands
- <sup>47</sup> National Satellite Meteorological Center, China Meteorological Administration (NSMC/CMA), Beijing, China

## Contents

Executive Summary:	I
1. Introduction	1
2. Estimating Emissions from Atmospheric CO <sub>2</sub> and CH <sub>4</sub> Measurements	7
2.1 <i>In situ</i> observations and models of atmospheric CO <sub>2</sub> , CH <sub>4</sub> distributions	9
2.2 Space-based remote sensing observations of CO <sub>2</sub> and CH <sub>4</sub> concentrations	11
2.2.1 CO <sub>2</sub> and CH <sub>4</sub> concentration estimates from thermal infrared observations	11
2.2.2 Stratospheric CO <sub>2</sub> and CH <sub>4</sub> observations using solar occultation	12
2.2.3 CO <sub>2</sub> and CH <sub>4</sub> concentration estimates from observations of reflected sunlight	12
2.2.4 Space-based CO <sub>2</sub> and CH <sub>4</sub> measurements of the lower troposphere	13
2.3 Retrieving CO <sub>2</sub> and CH <sub>4</sub> concentrations from space-based observations	14
2.4 Estimating CO <sub>2</sub> and CH <sub>4</sub> fluxes from space-based atmospheric observations	15
2.5 Resolution and coverage requirements for CO <sub>2</sub> and CH <sub>4</sub> estimates	16
2.5.1 Factors limiting the resolution and coverage of space-based measurements	16
2.5.2 Expanding ground-based <i>in situ</i> GHG networks to improve coverage	17
2.6 Quantifying uncertainties in the space-based CO <sub>2</sub> and CH <sub>4</sub> estimates	18
2.6.1 Relating ground-based and space-based XCO <sub>2</sub> and XCH <sub>4</sub> estimates: TCCON	19
2.7 Linking the GHG inventory, policy and atmospheric CO <sub>2</sub> and CH <sub>4</sub> communities	20
3. Space-based CO <sub>2</sub> and CH <sub>4</sub> Measurement Capabilities and Near-term Plans	23
3.1 ENVISAT SCIAMACHY	23
3.2 GOSAT TANSO-FTS	25
3.3 OCO-2	28
3.4 TanSat Atmospheric CO <sub>2</sub> Grating Spectrometer (ACGS)	30
3.5 Sentinel 5 Precursor TROPOMI	32
3.6 Feng Yun-3D GAS and Feng Yun-3G GAS-2	33
3.7 GaoFen-5 GMI	34
3.8 GOSAT-2 TANSO-FTS-2 and GOSAT-3	35
3.9 OCO-3	37
3.10 MicroCarb	38
3.11 Sentinel 5 UVNS	40
3.12 GeoCarb	41
3.13 MERLIN	43
3.14 Future mission concepts being studied	44

4.	The Transition from Science Missions to an Operational Constellation .....	46
4.1	User Requirements Process .....	46
4.2	Timeliness .....	47
4.3	Reliability and Robustness .....	47
4.4	Traceability and Configuration Management .....	47
4.5	Reprocessing, Reproducibility and Data Preservation .....	48
4.6	Quality Assurance .....	48
4.7	Calibration and Validation Monitoring and Reporting .....	48
4.8	User Support.....	49
4.9	International Coordination and Long-Term Planning.....	49
5.	Designing an Operational LEO Constellation for Measuring Anthropogenic CO <sub>2</sub> Emissions – The Sentinel CO <sub>2</sub> Initiative.....	50
5.1	Copernicus Evolution to anthropogenic CO <sub>2</sub> emissions monitoring .....	50
5.2	The space mission .....	53
5.2.1	Auxiliary observations needed for accurate XCO <sub>2</sub> and CO <sub>2</sub> flux estimates.....	54
5.2.2	Geophysical product requirements of the space component.....	56
5.2.3	Mission requirements for the CO <sub>2</sub> observations .....	57
5.2.4	Mission requirements for aerosol and cloud observations.....	58
5.2.5	Mission requirements for NO <sub>2</sub> observations.....	59
5.3	Virtual constellation opportunities .....	59
6.	Integrating CO <sub>2</sub> and CH <sub>4</sub> Satellites into Operational Constellations.....	61
6.1	A CO <sub>2</sub> /CH <sub>4</sub> constellation architecture with LEO, GEO and HEO elements .....	63
6.1.1	LEO constellation elements .....	63
6.1.2	GEO constellation elements.....	64
6.1.3	HEO constellation elements.....	65
6.2	Cross-calibrating the sensors deployed across the constellation.....	66
6.3	Cross-validating XCO <sub>2</sub> and XCH <sub>4</sub> estimates across the constellation.....	68
6.4	Retrieval algorithm advances needed to support a CO <sub>2</sub> /CH <sub>4</sub> constellation .....	69
6.5	Atmospheric inversion systems needed to support a CO <sub>2</sub> /CH <sub>4</sub> constellation .....	70
7.	Conclusions and Way Forward.....	73
	Acknowledgements.....	77
	APPENDIX 1: Remote sensing retrieval methods for estimating XCO <sub>2</sub> and XCH <sub>4</sub> from observations of reflected sunlight .....	78

APPENDIX 2: Methods for quantifying surface fluxes of CO <sub>2</sub> and CH <sub>4</sub> from space-based XCO <sub>2</sub> and XCH <sub>4</sub> estimates .....	80
A2.1 Source pixel mass balance methods for estimating fluxes from compact sources .....	80
A2.2 Estimating CO <sub>2</sub> and CH <sub>4</sub> emissions with plume dispersion models:.....	82
A2.3 Quantifying fluxes over extended areas with atmospheric inversion systems.....	85
APPENDIX 3: Observation system simulation experiments (OSSEs).....	89
APPENDIX 4: Lessons learned from SCIAMACHY, GOSAT and OCO-2 .....	93
A4.1 Strategies for maximizing measurement precision .....	93
A4.1.1 Fitting multiple spectral lines within a band to improve precision.....	94
A4.1.2 Spatial averaging to improve measurement precision .....	96
A4.1.3 Additional insights from coincident observations of other gases .....	97
A4.2 High accuracy continues to be a challenge for space-based XCO <sub>2</sub> and XCH <sub>4</sub> estimates	98
A4.2.1 Pre-launch and on-orbit instrument calibration requirements are demanding.....	98
A4.2.2 Instrument calibration stability is critical.....	100
A4.2.3 Remote sensing retrieval algorithms require continuous improvement.....	101
A4.2.4 Validation of space-based XCO <sub>2</sub> estimates .....	105
A4.3 Resolution and coverage .....	107
A4.4 Benefits of cross-calibrating and cross-validating the GOSAT and OCO-2 products ..	109
APPENDIX 5: Greenhouse gas monitoring satellites from commercial organizations and non-governmental organizations .....	113
A5.1 GHGSat-D.....	113
A5.2 Bluefield Technologies COOL .....	113
A5.3 Environmental Defence Fund’s MethaneSAT.....	115
APPENDIX 6: Advantages of LEO, GEO and HEO vantage points .....	116
A6.1 Global observations from LEO constellations.....	116
A6.2 Time-resolved observations from GEO constellations .....	117
A6.3 High latitude observations from HEO platforms .....	119
APPENDIX 7: CEOS Agencies implementing CO <sub>2</sub> and CH <sub>4</sub> missions.....	120
Appendix 8: Acronym List .....	121
References Cited .....	127



## Executive Summary:

Since the dawn of the industrial age, human activities have substantially increased the atmospheric concentrations of carbon dioxide (CO<sub>2</sub>), methane (CH<sub>4</sub>) and other greenhouse gases (GHGs). CO<sub>2</sub> and CH<sub>4</sub> are now the primary anthropogenic drivers of climate change and their impact is expected to grow unless their emissions can be dramatically reduced. To limit the increase in the global average temperatures to less than 2 °C above pre-industrial levels, the 21st session of the Conference of the Parties (COP21) of the United Nations Framework Convention on Climate Change (UNFCCC) agreed to implement an ambitious effort to reduce GHG emissions. Parties to the COP21 Paris Agreement defined nationally-determined contributions (NDCs) to a global GHG emissions reduction effort. Each party agreed to report GHG emissions and removals to the UNFCCC, which will evaluate progress toward the NDCs at 5-year intervals through global “stocktakes”, the first of which is scheduled for 2023. These emission reports are based on “bottom-up” inventories that employ a statistical analysis of emissions and removals by known GHG sources and sinks. When fully implemented, bottom-up inventories can accurately quantify emissions sources and sinks within each country. However, some nations do not have the resources needed to compile comprehensive inventories due to rapid economic, social, or environmental change. Other sources and sinks are poorly constrained in bottom-up inventories due to uncertainties in the “activity data” or “emission factors” used in their derivation.

Atmospheric measurements of the CO<sub>2</sub> and CH<sub>4</sub> concentrations complement bottom-up inventory methods by providing an integrated “top-down” constraint on the net amount of each gas exchanged between the surface and the atmosphere. These data therefore provide additional information for compiling bottom-up inventories as well as a synergistic approach for assessing NDCs. At global scales, atmospheric CO<sub>2</sub>, CH<sub>4</sub> and other well-mixed GHGs are characterized by precise, accurate, ground-based *in situ* measurements from a series of networks coordinated by the World Meteorological Organization (WMO) Global Atmospheric Watch (GAW) program. This network now includes about 145 stations that span the globe, but still does not have the spatial resolution and coverage needed to identify or quantify sources emitting CO<sub>2</sub> and CH<sub>4</sub> into the atmosphere on the scale of individual nations, or to quantify removals by natural sinks.

Recent advances in space-based remote sensing methods provide new opportunities to augment the spatial and temporal resolution and coverage of the ground-based GHG network. High spatial resolution measurements collected by space-based sensors can be analyzed to estimate the column-averaged dry air mole fractions of CO<sub>2</sub> and CH<sub>4</sub> (hereinafter XCO<sub>2</sub> and XCH<sub>4</sub>, respectively) over the globe. The Subsidiary Body for Scientific and Technological Advice (SBSTA) of UNFCCC recently acknowledged the utility of these measurements for monitoring CO<sub>2</sub> and CH<sub>4</sub> emissions (SBSTA, 2017). The primary challenge of this approach is the need for unprecedented precision and accuracy to resolve the small (< 2%) XCO<sub>2</sub> and XCH<sub>4</sub> variations caused by surface emission sources and natural sinks.

Space agencies responded to these challenges by supporting a series of pioneering space-based instruments designed to estimate XCO<sub>2</sub> and XCH<sub>4</sub>. These experiments include the European Space Agency (ESA) ENVISAT SCIAMACHY, Japanese GOSAT TANSO-FTS, United States (US) National Aeronautics and Space Administration (NASA) OCO-2, Chinese TanSat AGCS,

Feng Yun-3D GAS and GaoFen-5 GMI, and ESA Sentinel 5 Precursor TROPOMI. These agencies are implementing six additional missions for launches between late 2018 and 2023 and several others are being planned by governments, private companies, and non-governmental organizations. Data from these space-based sensors has fostered the development of end-to-end modelling systems for estimating surface CO<sub>2</sub> and CH<sub>4</sub> fluxes from atmospheric measurements on scales ranging from individual power plants to continents.

The Committee on Earth Observation Satellites (CEOS) recognized that high-quality observations of atmospheric CO<sub>2</sub> and CH<sub>4</sub> from a constellation of space-based sensors will be an essential component of an integrated global GHG observing system designed to track progress towards NDCs and support global stocktakes. The CEOS Chair commissioned the Atmospheric Composition Virtual Constellation (AC-VC) to define a global architecture for monitoring atmospheric CO<sub>2</sub> and CH<sub>4</sub> concentrations and their natural and anthropogenic fluxes from space to (i) reduce uncertainty of national emission inventory reporting, identify additional emission reduction opportunities and provide nations with timely and quantified guidance on progress towards their emission reduction strategies and pledges (NDCs); and (ii) track changes in the natural carbon cycle caused by human activities and climate variations.

To meet these goals, this paper explains how estimates of XCO<sub>2</sub> and XCH<sub>4</sub> from space-based sensors can be integrated into a global carbon monitoring system and summarizes the state of the art in the space-based measurements and the tools needed to retrieve CO<sub>2</sub> and CH<sub>4</sub> fluxes from these data. It then provides a roadmap for existing and planned space-based CO<sub>2</sub> and CH<sub>4</sub> sensor types and performance, observing strategies, launch dates and operational timelines. It then reviews the lessons learned from SCIAMACHY, GOSAT, and OCO-2 missions and summarizes the steps needed to transition from a series of scientific experiments to an operational constellation that can support an integrated global carbon observing system. To illustrate this transition, it documents the approach being used by the European Commission Copernicus Programme to define the requirements for a future operational constellation of CO<sub>2</sub> Sentinels. Finally, it proposes an architecture of a future greenhouse gas constellation designed to address the objectives listed above, and recommends a three-step plan to implement this architecture:

- 1) Link the atmospheric GHG measurement and modeling communities and stakeholders in the national inventory and policy communities (through UNFCCC/SBSTA), to refine requirements;
- 2) Exploit the capabilities of the CEOS member agencies, Coordination Group on Meteorological Satellites (CGMS) and the WMO Integrated Global Greenhouse Gas Information System (IG<sup>3</sup>IS) to integrate surface and airborne measurements of CO<sub>2</sub> and CH<sub>4</sub> with those from available and planned space-based sensors to develop a prototype, global atmospheric CO<sub>2</sub> and CH<sub>4</sub> flux product in time to support inventory builders in their development of GHG emission inventories for the 2023 global stocktake; and
- 3) Use the lessons learned from this prototype product to facilitate the implementation of a complete, operational, space-based constellation architecture with the capabilities needed to quantify atmospheric CO<sub>2</sub> and CH<sub>4</sub> concentrations that can serve as a complementary system for estimating NDCs in time to support the 2028 global stocktake.



## 1. Introduction

Since the beginning of the industrial age, human activities have increased the atmospheric concentrations of carbon dioxide (CO<sub>2</sub>), methane (CH<sub>4</sub>) and other greenhouse gases (GHGs) to levels never before seen in human history. Fossil fuel extraction and use, biomass burning, cement production, and land use change have increased the globally averaged atmospheric CO<sub>2</sub> concentration by about 46%, from less than 277 parts per million (ppm) in 1750 to levels above 405 ppm in 2017 (Le Quéré et al., 2018). Over half of this increase has occurred since 1980 and the growth rate continues to accelerate as the share of emissions from rapidly developing economies has increased. Over this same period of time, the globally averaged atmospheric CH<sub>4</sub> concentration increased from values near 0.72 ppm in 1750 to more than 1.85 ppm today (Myhre et al., 2013). The primary anthropogenic sources of CH<sub>4</sub> include fossil fuel production and transport, livestock production, wet agriculture, and waste management practices. These sources contribute about 60% of CH<sub>4</sub> emitted into the atmosphere each year (Saunois et al., 2016).

These large changes in the atmospheric composition have raised concerns about anthropogenic climate change because both CO<sub>2</sub> and CH<sub>4</sub> are efficient GHGs, which trap thermal radiation and warm the surface (Arrhenius, 1896; Myhre et al., 2013). As of 2011, increases in the atmospheric concentration of CO<sub>2</sub>, alone, were contributing over 1.82 W/m<sup>2</sup> additional radiative forcing. These atmospheric CO<sub>2</sub> increases are also the leading cause of ocean acidification (IPCC, 2013).

While the atmospheric CH<sub>4</sub> concentration is still much smaller than that of CO<sub>2</sub>, and CH<sub>4</sub> has a much shorter atmospheric lifetime (1 decade) than CO<sub>2</sub> (> one century), the observed CH<sub>4</sub> increase could still have a substantial impact on the climate because each CH<sub>4</sub> molecule has 26 to 29 times the global warming potential a CO<sub>2</sub> molecule on 100-year time scales. As of 2011, CH<sub>4</sub> increases contributed a direct surface radiative forcing increase of 0.48 W/m<sup>2</sup> and added another 0.49 W/m<sup>2</sup> of forcing by changing the stratospheric ozone and water vapor (IPCC, 2013).

Together, CO<sub>2</sub> and CH<sub>4</sub> now account for more than 93% of the 3 W/m<sup>2</sup> increase in radiative forcing by well-mixed anthropogenic greenhouse gases. The remainder is provided primarily by changes in the concentrations of nitrous oxide (N<sub>2</sub>O), which contributes 0.17 W/m<sup>2</sup>, chlorofluorocarbons (CFCs) and hydrogenated chlorofluorocarbons (HCFCs), which together contribute 0.18 W/m<sup>2</sup>. These increases in surface radiative forcing contributed to a 0.85 °C increase in the globally-averaged surface temperature between 1880 and 2012 (IPCC, 2013).

The United Nations Framework Convention on Climate Change (UNFCCC) was established in 1994 to stabilize “greenhouse gas concentrations in the atmosphere at a level that would prevent dangerous anthropogenic interference in the climate system.” To limit the increase in the globally average temperatures to less than 2 °C above pre-industrial levels, the 21st session of the Conference of the Parties (COP21) of the UNFCCC implemented the Paris Agreement, an ambitious global effort to reduce GHG emission. Parties to the 2015 Paris Agreement defined nationally-determined contributions (NDCs) to a global GHG emissions reduction effort. Each party agreed to report their anthropogenic GHG emissions and removals to the UNFCCC, which

would evaluate their progress toward their NDCs at 5-year intervals through a “global stocktake”, the first of which is scheduled for 2023.

To track their progress toward their NDCs and the global GHG emission reduction targets, each Party agreed to provide a national inventory report of anthropogenic emissions by sources and removals by sinks of GHGs, prepared using best-practice methodologies accepted by the Intergovernmental Panel on Climate Change (IPCC). These methods are based on “bottom-up” emission inventories, compiled from a statistical analysis of emissions reported from sources in specific sectors and categories. To ensure the effectiveness of this approach, the Agreement (Article 13) defines the implementation of an enhanced “Transparency Framework” to promote the transparency, accuracy, completeness, consistency, comparability, and environmental integrity of the stocktake.

Measurements of the atmospheric concentrations CO<sub>2</sub> and CH<sub>4</sub> and their changes over space and time also provide valuable information about their emissions and removals. While bottom-up inventories provide specific information about known emission sources, “top-down” methods based on atmospheric measurements provide an integrated constraint on the net amount of each gas that is exchanged between the surface and the atmosphere by natural and anthropogenic processes. Accurate, spatially- and temporally-resolved atmospheric CO<sub>2</sub> and CH<sub>4</sub> measurements can therefore provide additional information for bottom-up inventories as well as a complementary approach for assessing NDCs.

At global scales, atmospheric concentrations of CO<sub>2</sub>, CH<sub>4</sub> and other well-mixed greenhouse gases (GHGs) are well characterized by precise, systematic, ground-based *in situ* measurements from a network of ~145 surface stations that are coordinated by World Meteorological Organization (WMO) Global Atmospheric Watch (GAW) program (WMO 2017). These data are archived and distributed by the World Data Centre for Greenhouse Gases (WDCGG; <https://ds.data.jma.go.jp/gmd/wdcgg/>). The WMO GAW GHG network now spans the globe and forms the basis of the GCOS Comprehensive Networks for CO<sub>2</sub>, CH<sub>4</sub>, and other well-mixed GHGs. While this network is generally considered to be adequate to monitor trends in N<sub>2</sub>O, CFC’s, and HCFCs (GCOS, 2016), it still does not provide the spatial resolution and coverage needed to identify or quantify the sources emitting CO<sub>2</sub> and CH<sub>4</sub> into the atmosphere on the scale of an individual nation, or to localize or quantify the natural sinks that remove these gases (i.e. Bergamaschi et al., 2018). The network is particularly sparse in the Tropics, arctic and boreal regions and over the ocean. A dramatic expansion of the GAW GHG network would be needed to identify emission “hot spots” missed by the inventories or to assess the effectiveness of national carbon emission management strategies.

The 2016 New Delhi Declaration, which was endorsed by the heads of over 60 space agencies and related agencies from around the world, recognized the key role that space-based GHG measurements could play in as a complementary system for estimating NDCs. Recent advances in space-based remote sensing methods are providing new opportunities to augment the spatial and temporal resolution and coverage of the ground-based network. Measurements collected by space-based sensors can be analyzed to estimate the column-averaged dry air mole fractions of CO<sub>2</sub> and CH<sub>4</sub> (hereinafter XCO<sub>2</sub> and XCH<sub>4</sub>, respectively). A principal advantage of this

approach is that it can yield frequent measurements at high spatial resolution over most of the globe, including areas that are too geographically or politically inaccessible to support ground-based stations. The principal challenge has been the need for unprecedented precision and accuracy in the CO<sub>2</sub> and CH<sub>4</sub> concentration measurements used to quantify surface sources and sinks.

Highly accurate estimates of XCO<sub>2</sub> and XCH<sub>4</sub> are essential because CO<sub>2</sub> and CH<sub>4</sub> fluxes are derived from spatial and temporal gradients in these quantities. High precision is needed because even the largest surface sources and sinks produce small changes in XCO<sub>2</sub> and XCH<sub>4</sub>. For example, spatially localized sources such as large cities or power plants can produce atmospheric CO<sub>2</sub> and CH<sub>4</sub> mixing ratio variations exceeding 10% within the planetary boundary layer (40 ppm for CO<sub>2</sub>; 180 ppb for CH<sub>4</sub>). However, these variations decay rapidly with altitude and horizontal distance from the source, such that only the largest sources yield XCO<sub>2</sub> and XCH<sub>4</sub> variations exceeding 0.25% (1 ppm for CO<sub>2</sub> or 4.5 ppb for CH<sub>4</sub>) on the scale of a satellite footprint (a few square kilometers; Rayner and O'Brien, 2001; Miller et al., 2007; Andrews et al., 2014; Bergamaschi et al., 2018).

Meanwhile, large scale sources and sinks, such as tropical wetland emissions of CH<sub>4</sub> or uptake of CO<sub>2</sub> by forests, which produce comparable or smaller changes in the mixing ratios of the gases within the planetary boundary layer, can interact with passing weather systems to yield larger (~2%) variations in the XCO<sub>2</sub> and XCH<sub>4</sub> distribution. These synoptic scale “carbon weather” variations can obscure compact emissions sources, such as large power plants or cities, and can introduce subtle gradients in the background XCO<sub>2</sub> and XCH<sub>4</sub> fields that must be resolved to avoid introducing biases in estimates of fluxes of these gases between the surface and atmosphere. Biases in XCO<sub>2</sub> or XCH<sub>4</sub> measurements that are spatially- or temporally-correlated on the scales of interest pose some of the largest challenges. For example, Chevallier et al. (2007) shows that regional-scale biases in XCO<sub>2</sub> no larger than a few tenths of a part per million can introduce carbon flux errors exceeding 0.7 Gigatons of carbon per year (GtC/year, where a Gigaton is 10<sup>12</sup> kg) over temperate Eurasia. This is roughly equivalent to the total, annual CO<sub>2</sub> emissions by Germany between 2009 and 2015.

Space agencies responded to these challenges by supporting a series of pioneering space-based experiments designed to retrieve spatially-resolved estimates of atmospheric CO<sub>2</sub> and CH<sub>4</sub> concentrations from high spectral resolution observations of reflected sunlight. The first of these included the European Space Agency (ESA) Environmental Satellite (ENVISAT) SCanning Imaging Absorption spectroMeter for Atmospheric Cartography (SCIAMACHY), the Japanese<sup>1</sup> Greenhouse gases Observing SATellite (GOSAT) Thermal and Near Infrared Sensor for Carbon Observation-Fourier Transform Spectrometer (TANSO-FTS), and the National Aeronautics and Space Administration (NASA) Orbiting Carbon Observaotry-2 (OCO-2) mission. The free and open distribution of the data from these missions has fostered rapid progress in the development

---

<sup>1</sup> GOSAT was a joint effort of the Japanese Aerospace Exploration Agency (JAXA), the National Institute of Environmental Sciences (NIES) and the Ministry of the Environment (MOE) of Japan.

of a new generation of remote sensing retrieval algorithms optimized to retrieve XCO<sub>2</sub> and XCH<sub>4</sub> from space-based spectroscopic measurements.

These new tools are now yielding estimates of XCO<sub>2</sub> with single sounding random errors between 0.1 and 0.3% (0.4 to 1.2 ppm) and systematic biases between 0.25 and 0.5% (1 to 2 ppm) over most of the globe (i.e. Wunch et al. 2017). This performance is approaching the levels needed to quantify natural CO<sub>2</sub> sources and sinks on regional scales (e.g. Liu et al. 2017), to detect CO<sub>2</sub> gradients across large urban areas (Schwandner et al., 2017) and in selected cases, to quantify emissions from large, coal-fired power plants (Nassar et al. 2017). For XCH<sub>4</sub>, single sounding random errors are near 13 ppb (Kuze et al., 2016) and systematic biases are between 0.2 and 0.4% (4 and 7 ppb; Buchwitz et al., 2017a). These observations are being used to estimate anthropogenic emissions (Turner et al., 2015a; Buchwitz et al., 2017b; Janardan et al., 2017; Ganesan et al., 2017). While these experiments clearly demonstrate the potential value of space-based CO<sub>2</sub> and CH<sub>4</sub> measurements, this first generation of sensors was not designed the spatial and temporal resolution and coverage needed to track anthropogenic sources and sinks on urban to national scales, with the accuracy<sup>2</sup> and precision needed to improve national CO<sub>2</sub> and CH<sub>4</sub> emission inventories.

Recognizing the need for a coordinated global system to monitor the carbon cycle's response to both human activities and the changing climate, the Group on Earth Observations (GEO) commissioned the *GEO Carbon Strategy* (Ciais et al. 2010). This report called for an Integrated Global Carbon Observing system (IGCO) within GEO and the Global Climate Observing System (GCOS) that would incorporate advanced ground- and space-based observations to meet the increasingly pressing needs for policy-relevant scientific information. The Committee on Earth Observation Satellites (CEOS) responded to the GEO Carbon Strategy report by convening a Carbon Task Force (CTF), which compiled the *CEOS Strategy for Carbon Observations from Space* (Wickland et al. 2014; hereinafter, CEOS Carbon Strategy). The CEOS Carbon Strategy report documents the state of knowledge and measurement requirements for the atmospheric, oceanic, and terrestrial domains and their interfaces, and identifies several actions to be completed by its member agencies. When CEOS published that report, remote sensing observations of the terrestrial and oceanic carbon cycle were quite mature, whereas observations of atmospheric CO<sub>2</sub> and CH<sub>4</sub> were still in their infancy and developing rapidly.

Given the recent progress with SCIAMACHY, GOSAT, and OCO-2, the CEOS Chair recognized that high-quality observations of atmospheric CO<sub>2</sub> and CH<sub>4</sub> could be an essential component of an integrated global carbon observing system, such as that advocated by the World Meteorological Organization (WMO) Integrated Global Greenhouse Gas Information System

---

<sup>2</sup> Note: As used here and throughout this document, the term “accuracy” conforms to the definition given in GCOS (2011). More specifically, it describes the closeness of the mean of an ensemble of XCO<sub>2</sub> or XCH<sub>4</sub> measurements to an accepted reference value that can be traced to CO<sub>2</sub> and CH<sub>4</sub> standards maintained by the World Meteorological Organization Global Atmospheric Watch (WMO GAW) program. Here, the accepted reference value is a coincident XCO<sub>2</sub> or XCH<sub>4</sub> estimate derived from observations collected by the Total Carbon Column Observing Network (TCCON) station, whose XCO<sub>2</sub> and XCH<sub>4</sub> estimates have been related to *in situ* atmospheric profiles of CO<sub>2</sub> and CH<sub>4</sub> collected by flask and continuous measurements on aircraft (Wunch et al., 2010, 2011a, 2017).

(IG<sup>3</sup>IS). In such systems, the space-based XCO<sub>2</sub> and XCH<sub>4</sub> estimates complement the spatial resolution and coverage of the ground-based and airborne *in situ* measurements. If the ground-based, airborne, and space-based datasets can be harmonized, they can be assimilated into atmospheric inverse systems to yield top-down global inventories of CO<sub>2</sub> and CH<sub>4</sub> fluxes with the accuracy, precision, resolution and coverage needed to serve as a complementary system for estimating NDCs, as proposed in the 2016 New Delhi Declaration. In addition, if these atmospheric data products were distributed freely and openly, in compliance with the CEOS data policy, they could support the Transparency Framework.

To advance these goals, the CEOS Chair commissioned the Atmospheric Composition Virtual Constellation (AC-VC) to define the key characteristics of a global architecture for monitoring atmospheric CO<sub>2</sub> and CH<sub>4</sub> concentrations and their natural and anthropogenic fluxes from instruments on space-based platforms to:

- reduce uncertainty of national emission inventory reporting, identify additional emission reduction opportunities and provide nations with timely and quantified guidance on progress towards their emission reduction strategies and pledges (NDCs); and
- track changes in the natural carbon cycle caused by human activities (deforestation, degradation of ecosystems, fire) and climate change (drought, temperature stress, melting permafrost and changes in ocean thermal structure and dynamics).

If these objectives can be met within the next decade, their products could inform the 2028 stocktake mandated by the Paris Agreement. To meet this ambitious goal, we propose that the CEOS member agencies adopt a three-step approach. First, we recommend that the CEOS member agencies collaborate with the ground-based atmospheric GHG measurement and modeling communities and with and stakeholders in the inventory and policy communities (through UNFCCC/SBSTA) to refine the requirements and implementation approach for global carbon monitoring system. Second, CEOS should exploit the capabilities of its member agencies and its partners in the Coordination Group on Meteorological Satellites (CGMS) and WMO IG<sup>3</sup>IS to integrate the existing and near-term space-based and ground-based atmospheric CO<sub>2</sub> and CH<sub>4</sub> measurement and analysis systems into a prototype end-to-end system that yields an unbroken record of harmonized, ground-based and space-based estimates of CO<sub>2</sub> and CH<sub>4</sub> and fluxes spanning the period from 2009 through 2021. This task should be completed in in 2021, so that this product will available in time to inform the bottom-up inventories prepared for the 2023 stocktake. The third step is to refine the requirements for a robust, operational constellation that provides interoperable CO<sub>2</sub> and CH<sub>4</sub> products with the accuracy, precision, resolution, coverage, and reliability needed to support a global atmospheric greenhouse gas monitoring system. This step will require a strong collaboration among CEOS and CGMS agencies involved in the implementation of purpose-built, space-based, operational CO<sub>2</sub> and CH<sub>4</sub> systems. It should also should fully exploit the lessons learned from the development of the prototype system to support the 2028 stocktake.

A key objective of the prototype system developed in step 2 is to identify and foster the methods needed to cross-calibrate and cross-validate products from a diverse range of space-based sensors

and observational vantage points to produce harmonized, interoperable atmospheric CO<sub>2</sub> and CH<sub>4</sub> concentration products. A coordinated effort among the CEOS AC-VC, the CEOS Working Group on Calibration and Validation (WGCV) and the WMO Global Space-based Inter-Calibration System (GSICS) would facilitate this effort.

Improved coordination among the atmospheric CO<sub>2</sub> and CH<sub>4</sub> remote sensing and flux inversion modelling communities will also be needed to produce a global atmospheric flux product by 2021, so that it can be used to support the 2023 stocktake. This ambitious goal will benefit from recent efforts such as the ESA Climate Change Initiative (CCI) and the NASA Carbon Monitoring System (CMS) and ongoing efforts such as the Copernicus Atmosphere Monitoring Service (CAMS), and the European Horizon 2020 (H2020) CO<sub>2</sub> Human Emission (CHE) and VERIFY projects to establish harmonised long-term satellite-based GHG Essential Climate Variables. In addition to supporting the 2023 stocktake, the global atmospheric flux product produced by this effort would provide a baseline in future comparisons of top-down atmospheric and bottom-up inventory products. The lessons learned by generating this product could also help to foster the development of end-to-end atmospheric data analysis systems designed to yield policy-relevant products for use by WMO IG<sup>3</sup>IS.

The third step will facilitate the implementation of a complete, operational, space-based constellation architecture with the capabilities needed to quantify atmospheric CO<sub>2</sub> and CH<sub>4</sub> concentrations that serve as a complementary system for estimating NDCs. Strong coordination in the areas of sensor and mission design, data downlink, processing and distribution systems and capacity building will help to maximize the benefits early in the life cycle of these first-generation operational systems. If these objectives are realized by 2026, the products from this space-based constellation could be available in time to support the 2028 stocktake.

This white paper is organized as follows: Chapter 2 defines the role of space-based CO<sub>2</sub> and CH<sub>4</sub> measurements within an end-to-end, global, greenhouse gas monitoring system. Chapter 3 documents the capabilities and key results of the space-based CO<sub>2</sub> and CH<sub>4</sub> missions launched over the past 16 years and describes the advances expected from missions currently being implemented and planned. Chapter 4 outlines the steps needed to transition from a series of discreet scientific experiments to an operational constellation that can routinely generate, validate and distribute products to an integrated global carbon observing system and provide the capacity building needed to yield timely, policy-relevant information about CO<sub>2</sub> and CH<sub>4</sub> emissions and trends. Chapter 5 describes the ongoing effort by the European Copernicus Programme to design an operational CO<sub>2</sub> constellation that could be deployed as part of the Sentinel program as early as 2026. Given this background, Chapter 6 describes the steps needed to integrate existing space-based sensors into a prototype constellation, and assesses the ability of this constellation to meet these requirements. It then introduces a purpose-built, space-based constellation architecture designed to more completely address the requirements for atmospheric CO<sub>2</sub> and CH<sub>4</sub> measurements. This architecture fully exploits the advantages of low Earth orbit, geostationary orbit, and highly elliptical orbits as well as ground- and aircraft-based measurements from extended networks and advanced data analysis systems. Finally, Chapter 7 summarizes the conclusions and proposes a way forward.

## 2. Estimating Emissions from Atmospheric CO<sub>2</sub> and CH<sub>4</sub> Measurements

Human activities including fossil fuel combustion, cement production, heavy industry and land use change are contributing large increases in the atmospheric CO<sub>2</sub> concentration. For 2016, inventories like those maintained by the International Energy Agency (IEA, 2012), the Carbon Dioxide Information Analysis Center (CDIAC; Boden et al., 2017) and scientific inventories such as the Emission Database for Global Atmospheric Research 4.3.2 (EDGAR v4.3.2, Janssens-Maenhout et al., 2017; Bergamaschi et al., 2018), indicate that fossil fuel use and industry alone add about 37 billion tons<sup>3</sup> of CO<sub>2</sub> to the atmosphere each year (Le Quéré et al., 2018). These estimates of the global, annual totals are thought to be accurate to within 6-10%, but estimates for individual countries are uncertain by up to several tens of percent, especially in rapidly developing countries (Ciais et al. 2014). Even with these uncertainties, fossil fuel combustion alone releases enough CO<sub>2</sub> to produce a global growth rate of over 4 ppm/year.

Anthropogenic CO<sub>2</sub> emissions are superimposed on an active natural carbon cycle, whose variability is driven primarily by photosynthesis and respiration by the land biosphere (Beer et al. 2010) and the solubility of CO<sub>2</sub> in the ocean (Ciais et al., 2013). Each year, these natural processes emit almost 20 times as much CO<sub>2</sub> into the atmosphere as human activities, but then reabsorb a comparable amount, along with more than half of the anthropogenic emissions, reducing the CO<sub>2</sub> growth rate driven by fossil fuel use by half. The identity, location, and processes controlling the natural sinks responsible for absorbing this CO<sub>2</sub> are poorly understood. In addition, the uptake of CO<sub>2</sub> by these sinks appears to vary dramatically from year to year, such that the “airborne fraction” of the anthropogenic CO<sub>2</sub> that remains in the atmosphere can vary from near zero to almost 100% from one year to the next. The airborne fraction appears to be correlated with large-scale temperature and precipitation anomalies, like those associated with major El Niño events and large-scale volcanic stratospheric aerosol injections. However, the actual mechanisms have eluded characterization, complicating efforts to predict how the sinks might perform in the future as the climate evolves in response to greenhouse gas warming.

A diverse range of human activities contribute over 60% of the CH<sub>4</sub> emitted into the atmosphere each year (Saunio et al., 2016). These include fossil fuel extraction and transport, livestock production, rice cultivation, biomass burning, landfills, and sewage treatment methods. These anthropogenic contributions add to natural CH<sub>4</sub> emissions from wetlands, lakes, rivers, wild animals, wildfire, geologic sources, oceans, permafrost regions, and termites. Together, these sources are partially offset by natural processes that destroy CH<sub>4</sub>, including atmospheric reactions with hydroxyl (OH) and chlorine (Cl) radicals in the troposphere, excited oxygen (O<sup>1</sup>D) in the stratosphere, and uptake by soils.

The “2006 IPCC Guidelines for National Greenhouse Gas Inventories” (IPCC 2006 Guidelines) mandates reports on GHG emissions and removals for each nation using a bottom-up approach

---

<sup>3</sup> Global emissions of carbon and CO<sub>2</sub> are typically expressed in either billions of tons (gigatons, Gt) or petagrams (Pg), both of which mean indicated 10<sup>12</sup> kg. A ton of carbon is combined with 2.66 tons of oxygen to yield ~3.66 tons of CO<sub>2</sub>.

that includes CO<sub>2</sub>, CH<sub>4</sub>, and other gases. These reports are source specific, listing Sectors (Energy, Industrial Processes, and Products, Agriculture, Forestry, Land Use, Waste, and Other), each of which is divided into Categories (e.g. transport) that are subdivided into sub-categories (e.g., cars). When implemented fully, bottom-up inventory methods can accurately identify and characterize emissions sources and sinks within each country (Bergamaschi et al., 2018). The source-specific information contained in these inventories is critical from a GHG policy perspective because we can only manage what we can measure. However, many developing nations do not have the resources needed to compile comprehensive bottom-up inventories in the presence of rapid economic, social, or environmental change. Other natural and anthropogenic emission sources or natural sinks of GHGs are poorly constrained due to uncertainties in the “activity data” or “emission factors” used in their derivation or because there is no global, process-based approach to represent their fluxes (e.g. lakes and rivers).

Atmospheric CO<sub>2</sub> and CH<sub>4</sub> measurements complement the bottom-up inventories by providing an integrated constraint on the exchanges of these gases between land and ocean surfaces and the atmosphere (including anthropogenic emissions) and their trends over time (Bergamaschi et al., 2018). This information is critical for estimating the impact of GHGs on the climate. While CO<sub>2</sub> and CH<sub>4</sub> fluxes inferred from atmospheric measurements are not as source-specific as the data sources typically used in inventories, they include contributions from sources that are often omitted or poorly characterized by these methods (i.e. biomass burning, wildfire, bunker fuels). To fully exploit the information included in atmospheric CO<sub>2</sub> and CH<sub>4</sub> measurements, a system level approach is needed. The key elements of that system are summarized in Figure 2-1, along with their interactions. The following sections provide a more complete description of each element of the system.

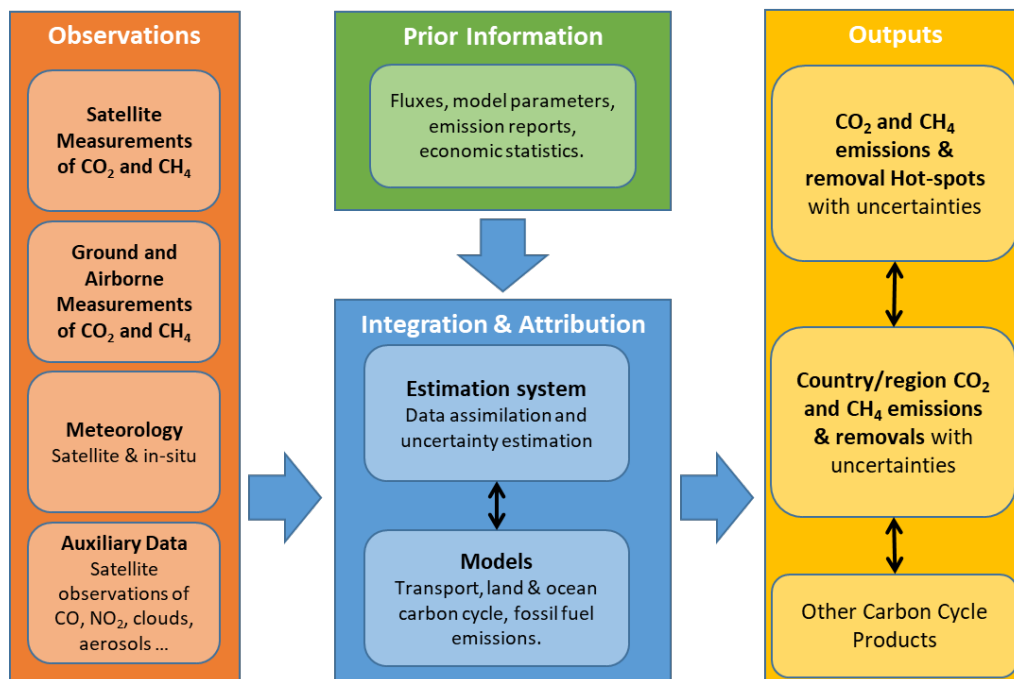


Figure 2-1: Block diagram of an atmospheric CO<sub>2</sub> and CH<sub>4</sub> monitoring system, showing the key inputs, outputs, and interactions.

## 2.1 *In situ* observations and models of atmospheric CO<sub>2</sub>, CH<sub>4</sub> distributions

Until recently, the vast majority of the atmospheric measurements of CO<sub>2</sub> and CH<sub>4</sub> and other GHGs were provided by a global network of surface-based stations managed by the WMO GAW program (Figure 2-2). This network has grown continuously since the first two stations were established by Charles David Keeling at Mauna Loa, Hawaii and the South Pole in 1958 (Brown and Keeling, 1965; Pales and Keeling, 1965) and now includes about 145 stations that report CO<sub>2</sub> and CH<sub>4</sub> to the WDCGG (WMO, 2017). Their measurements are highly precise and accurate and have provided invaluable insight into the natural and anthropogenic processes operating in the global carbon cycle (WMO 2009; 2011). In spite of these advances, this ground-based network does not have the spatial resolution and coverage needed everywhere on Earth to identify or quantify the sources emitting CO<sub>2</sub> and CH<sub>4</sub> into the atmosphere or the natural sinks that remove these gases on regional or national scales<sup>4</sup>. For example, the network is particularly sparse in potential centers of activity including the arctic, tropics, and oceans (Figure 2-2a). So, while the data from this network provides the best available record of global trends in CO<sub>2</sub> and CH<sub>4</sub>, it has not provided the information needed to identify the specific processes responsible for large year-to-year variations in the CO<sub>2</sub> airborne fraction or those responsible for the near-zero CH<sub>4</sub> growth rates observed between 1992 and 2006, which were then followed by rapid increases since then (Figure 2-2d and Saunio, et al., 2017; Rigby et al., 2017).

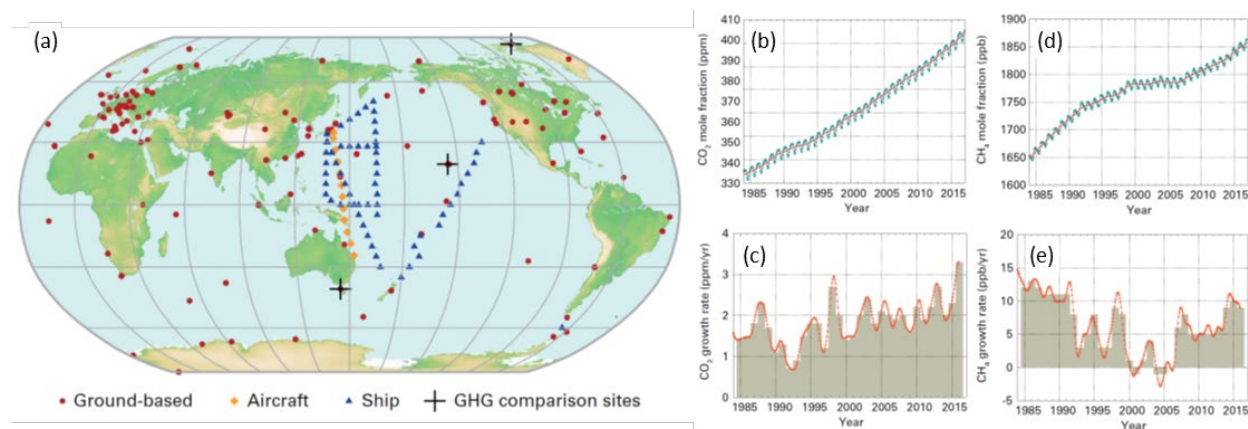


Figure 2-2: (a) Ground-based (red dots), aircraft (orange dots) and ship-borne (blue diamonds) *in situ* CO<sub>2</sub> sites managed by the WMO GAW program. (b) Globally-averaged CO<sub>2</sub> dry air mole fraction from 1984 to 2016. The blue dots show monthly measurements while the red line shows these results with the seasonal cycle removed. (c) Yearly growth rate in the globally-averaged CO<sub>2</sub> (ppm/year). (d) Same as (b) for CH<sub>4</sub>. (e) Same as (c) for CH<sub>4</sub>. (credit: WMO Greenhouse Gas Bulletin No. 13, 30 October 2017).

For historical reasons, the vast majority of these ground-based CO<sub>2</sub> and CH<sub>4</sub> monitoring stations are located in Western Europe, North America and on remote islands or coastal regions (Figure

<sup>4</sup> In the atmospheric carbon cycle literature, the term “regional scales” typically describes areas that are roughly  $4^{\circ}\times 5^{\circ}$  ( $\sim 2\times 10^4$  km<sup>2</sup>) to  $10^{\circ}\times 10^{\circ}$  ( $\sim 10^6$  km<sup>2</sup>). The largest 100 nations have areas ranging from  $1.2\times 10^4$  km<sup>2</sup> (North Korea) to  $17\times 10^7$  km<sup>2</sup> (Russia), with an average size near  $8\times 10^5$  km<sup>2</sup> (i.e. Chile or Turkey). Here, we use “regional scale” and “national” interchangeably to indicate areas ranging from  $10^4$  to  $10^7$  km<sup>2</sup>. The term “urban scale” will be used to describe cities with areas spanning a range from  $10^2$  km<sup>2</sup> (Orlando, FL) to  $600$  km<sup>2</sup> (Houston, TX).

2-2a). Most of these stations were deliberately located at sites away from large sources or sinks of CO<sub>2</sub> or CH<sub>4</sub> so that they could accurately record background concentrations of these gases and their trends. Very few sites are located in known centers of action for CO<sub>2</sub> and CH<sub>4</sub> emission or uptake such as the Eastern U.S., central and Eastern Asia, tropical Southeast Asia, South America or Africa, the Arctic/Boreal zone, or the Southern Ocean. There have been some efforts to expand into these areas in recent years, but the progress has been slow due to challenges posed by the operating environment, accessibility, or political instability.

Additional insight into the abundance, distribution and trends of atmospheric CO<sub>2</sub> and CH<sub>4</sub> has been gained from simulations using atmospheric general circulation models. In so-called “Nature Runs”, these models are initialized with an assumed distribution of these gases as well the best available information about their sources and sinks. As the spatial resolution of the transport models and the representation of the distribution and intensity of the natural and anthropogenic sources and sinks has improved, these tools have provided an improved understanding of the processes that control the spatial and temporal distribution of CO<sub>2</sub> and CH<sub>4</sub> on progressively finer scales, and how these processes change over the seasonal cycle.

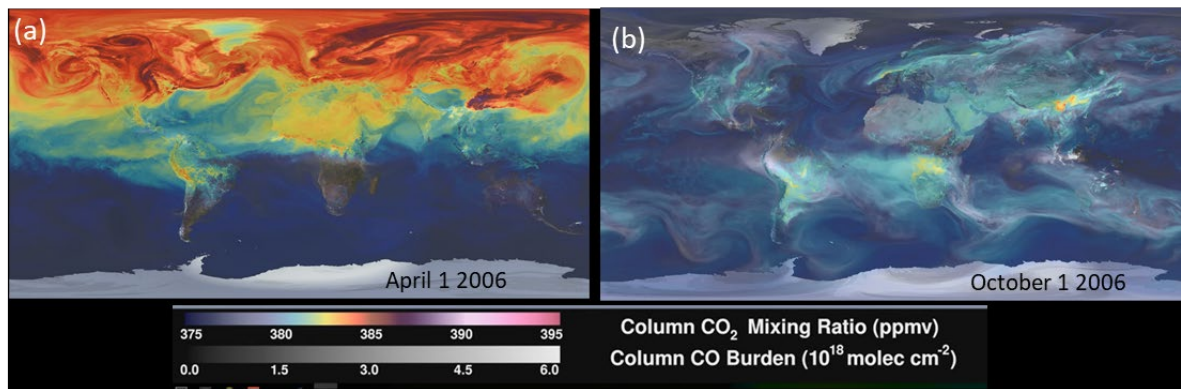


Figure 2-3: Nature runs generated using the Goddard Earth Observing System Model, Version 5 (GEOS-5) showing XCO<sub>2</sub> (rainbow colors) and column-integrated carbon monoxide, (gray) distributions for April 1, 2006 (a), when the pole-to-pole XCO<sub>2</sub> gradient is largest, and October (b), when it is near its minimum value.

For example, Figure 2-3 shows XCO<sub>2</sub> fields from a high-resolution (7 km) Nature Run (Putman et al. 2014). The impact of passing mesoscale weather systems is obvious in both the April and October snapshots shown here. In April, XCO<sub>2</sub> is highest at high northern latitudes, where the land biosphere has been dormant over the winter, and the pole-to-pole gradient in XCO<sub>2</sub> is near its maximum value of ~2%. Interestingly, variations of comparable magnitude are seen on 100-200 km scales across much of the northern mid-latitudes as passing frontal systems mix the high near-surface CO<sub>2</sub> concentrations through the troposphere. In October, when the pole-to-pole XCO<sub>2</sub> gradients are much smaller, anomalies associated with fossil fuel emissions (China) and biomass burning (central Africa) are more obvious. Given the fine structure of these XCO<sub>2</sub> fields, a sparse measurement network, such as that shown in Figure 2-2, does not provide the information needed to discriminate individual natural or anthropogenic sources and sinks.

## 2.2 Space-based remote sensing observations of CO<sub>2</sub> and CH<sub>4</sub> concentrations

One way to complement the spatial sampling and resolution of atmospheric CO<sub>2</sub> and CH<sub>4</sub> measurements is to collect measurements from sensors on orbiting satellites. Recent advances in space-based remote sensing methods are now providing new opportunities for measuring CO<sub>2</sub>, CH<sub>4</sub>, and other GHGs from this vantage point. High-resolution spectra of sunlight reflected from or thermal radiation emitted by the Earth's surface and atmosphere carry information about the thermal structure and composition of the atmosphere. These spectra can be recorded by instruments on orbiting spacecraft and analyzed with remote sensing retrieval algorithms to yield information about the atmosphere, including the distribution of CO<sub>2</sub>, CH<sub>4</sub>, and other GHGs.

The potential of atmospheric CO<sub>2</sub> and CH<sub>4</sub> observations from ground- and space-based sensors to contribute to the national inventory process was recently acknowledged by the Subsidiary Body for Scientific and Technological Advice (SBSTA) of UNFCCC (SBSTA, 2017), which stated: "The SBSTA noted the increasing capability to systematically monitor greenhouse gas concentrations and emissions, through *in situ* as well as satellite observations, and its relevance in support of the Paris Agreement".

However, as noted in the Introduction, these measurements are only useful for informing GHG inventories if they have the precision and accuracy needed to detect and quantify the small (< 0.25%) XCO<sub>2</sub> and XCH<sub>4</sub> variations associated with typical emission sources and natural sinks. The rapidly-evolving space-based observation methods and analysis techniques are summarized in the following sub-sections, along with the factors that influence their accuracy, precision, resolution, and coverage.

### 2.2.1 CO<sub>2</sub> and CH<sub>4</sub> concentration estimates from thermal infrared observations

Some of the earliest efforts to retrieve CO<sub>2</sub> and CH<sub>4</sub> information from space-based measurements used thermal infrared (TIR) observations of CO<sub>2</sub> and CH<sub>4</sub> that were routinely collected by meteorological sounders. For CO<sub>2</sub>, these include the NOAA-10 High resolution Infrared Radiation Sounder (HIRS-2; Chédin et al., 2005), the National Aeronautics and Space Administration (NASA) Atmospheric Infrared Sounder (AIRS; Crevoisier et al. 2004; Chahine et al., 2005) the Infrared Atmospheric Sounding Interferometer (IASI; Crevoisier et al. 2009a) and the Tropospheric Emission Spectrometer (TES; Kulawik et al., 2010). For CH<sub>4</sub>, these include AIRS (Xiong et al., 2008), IASI (Crevoisier et al., 2009b, 2013) and TES (Worden et al., 2012; Alvarado et al., 2015). In addition to these near-nadir-looking instruments, the Michelson Interferometer for Passive Atmospheric Sounding (MIPAS) on the ESA ENVISAT collected observations of limb emission in a wavelength range from 4.15 microns to 14.6 microns, which were used to retrieve vertical profiles of CH<sub>4</sub> and N<sub>2</sub>O in the stratosphere and mesosphere (Laeng et al., 2015; Plieninger et al., 2015; 2016).

TIR measurements like those from HIRS-2, AIRS, IASI and TES can provide information about the CO<sub>2</sub> and CH<sub>4</sub> concentrations in the middle to upper troposphere. However, early TIR measurements yielded CO<sub>2</sub> precisions no better than 1-2% and had significant systematic errors (Chevallier et al. 2005a). In addition, because TIR measurements have little sensitivity to the CO<sub>2</sub> and CH<sub>4</sub> concentrations within the lower troposphere and planetary boundary layer, their

use in retrieving surface fluxes is strongly affected by model transport errors. For these reasons, TIR measurements have not been a primary focus in studies of anthropogenic and natural sources on urban ( $\sim 10^2$  km<sup>2</sup>) to national scales.

However, there has been recent progress in the analysis of TIR products that may extend their utility. For AIRS, the accuracy of the CO<sub>2</sub> estimates improved to 1.5 ppm on daily time scales at 2° x 2° resolution at latitudes between 20S and 40N (Frankenberg et al., 2016). For TES, the CO<sub>2</sub> estimates had accuracies of 1.3 ppm at monthly intervals in 10° x 10° regions between 40S and 45N (Kulawik et al., 2013). For IASI, the CH<sub>4</sub> estimates improved to 8 ppb on daily time scales at single sounding resolution (Crevoisier et al., 2018). These measurements were used to estimate fluxes at monthly intervals at regional to hemispheric scales (Nassar et al., 2011; Cressot et al., 2014), and used in data assimilation experiments to provide CH<sub>4</sub> forecasts in the framework of the Copernicus Atmospheric Monitoring Service (Massart et al., 2014).

### 2.2.2 Stratospheric CO<sub>2</sub> and CH<sub>4</sub> observations using solar occultation

Two spacecraft sensors have collected solar occultation measurements that have been used to estimate the CO<sub>2</sub> and CH<sub>4</sub> profiles in the stratosphere. The first was the ESA ENVISAT SCIAMACHY, which operated between 2002 and 2012. SCIAMACHY measurements have recently been reanalyzed to yield profiles of both gases at altitudes between 17 and 45 km (Noël et al., 2016). Comparisons to independent standards indicate that the CO<sub>2</sub> estimates have accuracies of 2-3% (8-12 ppm) and the CH<sub>4</sub> measurements have accuracies of 5-10% (50-100 ppb). The second was the Atmospheric Chemistry Experiment (ACE) or SciSat (Bernath et al., 2005), which carries a Fourier Transform Spectrometer (FTS) that uses solar occultation in the thermal and mid-infrared to retrieve limb vertical profiles of about 40 different trace gases, including CH<sub>4</sub> (De Maziere et al., 2008) and more recently CO<sub>2</sub> (Foucher et al., 2011, Sioris et al., 2014). This dataset extends from 2004-present, and consists of profiles with a vertical resolution of  $\sim 3$  km. These SCIAMACHY and ACE-FTS datasets are valuable for studies of greenhouse gas transport, trends and processes in the upper troposphere or above (Emmert et al., 2012; Noël et al., 2016). However, since these measurements do not reach altitudes below  $\sim 5$  km, they are not of direct use for studying spatial and temporal distributions of CO<sub>2</sub> and CH<sub>4</sub> associated with surface fluxes.

### 2.2.3 CO<sub>2</sub> and CH<sub>4</sub> concentration estimates from observations of reflected sunlight

Other efforts to retrieve information about CO<sub>2</sub> and CH<sub>4</sub> sources and sinks have used high-resolution spectroscopic measurements of reflected sunlight within CO<sub>2</sub> and CH<sub>4</sub> bands at short wavelength infrared (SWIR) wavelengths. These measurements are better suited for monitoring CO<sub>2</sub> and CH<sub>4</sub> fluxes because they are more sensitive to concentration changes near the surface, where most sources and sinks are located (Buchwitz et al., 2007; 2015; Crisp et al. 2004; 2008; Yoshida et al. 2011; O'Dell et al. 2012). These data are generally analyzed to yield column-averaged dry air mole fractions of CO<sub>2</sub> and CH<sub>4</sub> (XCO<sub>2</sub> and XCH<sub>4</sub>, respectively).

The first space-based instruments designed to exploit this approach included the ESA ENVISAT SCIAMACHY, the Japanese GOSAT TANSO-FTS, and NASA's OCO-2. Recent efforts to analyze the data collected by these first-generation space-based solar SWIR sensors have

demonstrated the precision needed to resolve anthropogenic as well as natural fluxes of CO<sub>2</sub> and CH<sub>4</sub> on a range of scales. These include individual power plants (Nassar et al., 2017), cities (Schwandner et al. 2017; Ye et al. 2017), and regional-scale natural and anthropogenic sources (Schneising et al., 2013; 2014; Reuter et al. 2014; 2017b; Bloom et al. 2010; Frankenberg et al. 2011; Fraser et al. 2013; Kort et al. 2014; Hakkarainen et al. 2016; 2018; Heymann et al. 2017; Chatterjee et al. 2017; Liu et al. 2017; Patra et al. 2017). However, additional effort is needed to reduce the impact of spatially correlated biases on these scales (Chevallier et al., 2014; 2015; Locatelli et al., 2015).

These pioneering SWIR sensors were recently joined by the Chinese TanSat Atmospheric CO<sub>2</sub> Grating Spectrometer (ACGS), FengYun-3D (FY-3D) Greenhouse gases Absorption Spectrometer (GAS) and Gaofen-5 Greenhouse-gases Monitoring instrument (GMI) sensors, and by the European Commission Copernicus Sentinel 5 Precursor (S5P) TROPOMI instrument, which were being commissioned at the time of writing. Other space-based SWIR CO<sub>2</sub> and CH<sub>4</sub> sensors are being implemented and others are in the planning stages. Chapter 3 provides a more detailed description of the missions and their evolving capabilities.

#### 2.2.4 Space-based CO<sub>2</sub> and CH<sub>4</sub> measurements of the lower troposphere

Historically, top-down estimates of CO<sub>2</sub> and CH<sub>4</sub> fluxes from atmospheric inversion systems have relied on *in situ* observations from a sparse surface network (e.g. Peters et al., 2007; Chevallier et al., 2010a). Space-based SWIR measurements of the column-average dry air mole fractions of CO<sub>2</sub> and CH<sub>4</sub> provide much better coverage and spatial sampling densities than the surface network, but these measurements are sensitive to CO<sub>2</sub> and CH<sub>4</sub> variations in the free-troposphere and stratosphere as well as the planetary boundary layer, where most sources and sinks are located. These high-altitude contributions have long horizontal mixing length scales (e.g., Keppel-Aleks *et al.*, 2011, 2012; Worden *et al.*, 2013), which are sensitive to fluxes that are hundreds to thousands of kilometers away, depending on the latitude (e.g., Keppel-Aleks *et al.*, 2011, 2012; Worden *et al.*, 2013; Kulawik et al., 2017). Uncertainties in either the vertical or horizontal transport can therefore introduce significant uncertainties in the underlying fluxes or processes (e.g., Stephens *et al.*, 2007; Jiang *et al.*, 2013; Worden *et al.*, 2013; Jiang et al., 2015).

Improved space-based observations of CO<sub>2</sub> and CH<sub>4</sub> in the lower troposphere would have several advantages over both columns and surface observations for estimating fluxes:

- Flux estimates from column measurements rely on observations up to continent-scales away (Liu et al., 2015; Feng et al., 2016); whereas lower tropospheric back-trajectories show a more local influence to surface fluxes, making flux estimates more responsive to observations and less susceptible to transport error, a major driver of flux uncertainties (Houweling et al., 2015; Liu et al., 2015; Chevallier et al., 2014; Liu et al., 2011; Prather et al., 2008)
- Stephens et al. (2007) show that vertical gradient in mole fraction determined from 2 points in the atmospheric column better constrains model transport and partitioning between northern extratropical land fluxes and land fluxes further south, since vertical transport is an uncertainty in flux estimates (Deng et al., 2015; Lauvaux and Davis, 2014; Stephens et al., 2007)

- A lower tropospheric product covering the entire boundary layer, rather only at the surface, partially mitigates one source of flask assimilation error, the boundary layer height (Denning et al., 1996; Gurney et al., 2002; Rayner and O'Brien, 2001); and
- Satellites provides observations in many areas that are sparsely covered by surface-based measurements.

Several recent studies have shown that it should be possible to improve the sensitivity of space-based observations to near-surface CO<sub>2</sub> and CH<sub>4</sub> concentrations. Kulawik et al. (2017) derive a lower tropospheric CO<sub>2</sub> product from the intermediate ACOS-GOSAT CO<sub>2</sub> profile retrievals. The potential for combining TES TIR and GOSAT SWIR observations for quantifying near surface CH<sub>4</sub> was demonstrated by Worden et al. (2015). This approach could also be used to estimate near-surface CH<sub>4</sub> and CO from CrIS and TROPOMI, which are flying in tandem orbits aboard Suomi NPP and Sentinel 5p (i.e. Fu et al., 2016). Similarly, in the future, this approach could be used to combine data from IASI-NG (Crevoisier et al., 2014) and Sentinel 5 UVNS, which will fly together onboard the Metop-SG satellites, starting in 2021.

### 2.3 Retrieving CO<sub>2</sub> and CH<sub>4</sub> concentrations from space-based observations

Efforts to estimate atmospheric concentrations of CO<sub>2</sub> or CH<sub>4</sub> from space-based remote sensing measurements can be summarized as a five-step process:

1. Acquire precise high-spectral-resolution observations of reflected sunlight within CO<sub>2</sub> and CH<sub>4</sub> absorption bands at SWIR wavelengths at a spatial resolution of 5-10 km (GCOS 2011) over the globe. Co-boresighted spectra of the molecular oxygen (O<sub>2</sub>) A-band are also required for estimating the total dry air column abundance, the surface pressure, and the presence, vertical distribution, and total optical depths of clouds and aerosols;
2. Calibrate these space-based spectroscopic measurements to convert them from instrument units (i.e. time tagged data numbers) to geophysical units (i.e. photons/second/meter<sup>2</sup>/steradian/micron) and to relate them to internationally-recognized radiometric, spectroscopic, and geometric standards so that they can be cross-validated and combined with other types of measurements and model results;
3. Use a remote sensing retrieval algorithm to estimate the column-averaged dry air mole fractions of CO<sub>2</sub> and CH<sub>4</sub> (XCO<sub>2</sub>, XCH<sub>4</sub>) and other relevant atmospheric and surface state properties (i.e. surface pressure and reflectance, profiles of atmospheric temperature, water vapor, clouds and aerosols) from each sounding;
4. Validate the space-based XCO<sub>2</sub> and XCH<sub>4</sub> estimates and their estimated uncertainties against available standards, including ground-based up-looking remote sensing observations from Total Carbon Column Observing Network (TCCON) and vertical profiles of CO<sub>2</sub> and CH<sub>4</sub> obtained by aircraft or balloons; and
5. Combine the XCO<sub>2</sub> and XCH<sub>4</sub> soundings from all available space-based and ground-based CO<sub>2</sub> and CH<sub>4</sub> measurements, along with their uncertainty estimates, to produce a harmonized climate data record with the best possible spatial and temporal resolution and coverage for distribution to the user community.

To execute these steps, we need a space-based measurement system, a pre-launch and on-orbit instrument calibration program, a CO<sub>2</sub> and CH<sub>4</sub> retrieval algorithm with associated input data (i.e. laboratory measurements of gas absorption properties, top of atmosphere solar spectrum,

meteorological conditions, etc.), a data product validation capability, and a data integration, archiving, and distribution capability. A variety of methods are being explored to address these topics, and their key features are described in Appendix 1.

## 2.4 Estimating CO<sub>2</sub> and CH<sub>4</sub> fluxes from space-based atmospheric observations

Given the spatially- and temporally-dependent XCO<sub>2</sub> and XCH<sub>4</sub> fields derived from this 5-step process, these data must be combined with estimates of the atmospheric winds to estimate CO<sub>2</sub> and CH<sub>4</sub> fluxes. Three general classes of methods have been developed for this application:

- 1) Source pixel mass balance methods;
- 2) Plume dispersion models; and
- 3) Atmospheric inversion systems

Mass balance methods account for the CO<sub>2</sub> and CH<sub>4</sub> that move into and out of the domain of interest (Cambaliza et al., 2014; Karion et al., 2013; Jacob et al., 2016). These methods are best suited for estimating fluxes from compact sources where the ambient wind profile is known and nearly constant over the spatial domain and sampling interval. Plume dispersion models estimate the fluxes needed to maintain an observed plume enriched in XCO<sub>2</sub> or XCH<sub>4</sub> in the presence of entrainment and advection (White et al., 1976; Bovensmann et al., 2010; Krings et al., 2011; 2013; Conley et al. 2016; Jacob et al., 2016; Frankenberg et al., 2016; Thompson et al. 2016; Buchwitz et al., 2017a; Nassar et al., 2017; Varon et al., 2018). Over more extended regions that include multiple sources and sinks and a wind field that varies in space and time, a full 4-dimensional description of the wind field (3 spatial dimensions and time), like that used in atmospheric inversion systems, is needed to estimate CO<sub>2</sub> and CH<sub>4</sub> fluxes (Enting 2002, Bousquet et al., 2000; Rödenbeck et al., 2003; Peters et al., 2005, Baker et al., 2007; Chevallier et al., 2005b; Houweling et al., 2017; Liu et al., 2017).

The data provided by the first generation of space-based CO<sub>2</sub> and CH<sub>4</sub> sensors has fostered rapid progress in the development of all three classes of flux inversion methods. These tools are now being used to estimate CO<sub>2</sub> and CH<sub>4</sub> fluxes on scales ranging from that of large, coal-fired power plants and large urban areas to continents. While these experiments clearly demonstrate the potential of these tools, further development of all three classes of methods will be needed to fully exploit the data from future space-based CO<sub>2</sub> and CH<sub>4</sub> constellations to substantially reduce uncertainties national emission inventories or to track trends in the natural carbon cycle associated with climate change.

Appendix 2 provides a brief overview of these three classes of methods for estimating CO<sub>2</sub> and CH<sub>4</sub> fluxes from space-based XCO<sub>2</sub> and XCH<sub>4</sub> measurements. It also identifies the strengths and weaknesses of each method and illustrates the requirements that each method places on accuracy, precision, resolution, and coverage of the space-based measurements.

The end-to-end performance of a single space-based sensor or constellation of sensors, along with their remote sensing retrieval algorithms and atmospheric inversion systems can be tested within the context of Observation System Simulation Experiments (OSSEs). The key features of OSSEs for estimating CO<sub>2</sub> and CH<sub>4</sub> fluxes, as well as their random and systematic errors from space-based estimates of XCO<sub>2</sub> and XCH<sub>4</sub> are summarized in Appendix 3.

The experience gained by collecting and analysing the observations from SCIAMACHY, GOSAT, and OCO-2 has provided additional insight into the requirements for space-based measurements, retrieval algorithms, calibration and validation techniques, and methods for retrieving CO<sub>2</sub> and CH<sub>4</sub> flux estimates from these data. The principal lessons learned from these missions are discussed in Appendix 4. The methods developed to cross-calibrate the GOSAT and OCO-2 instruments and to cross-validate their XCO<sub>2</sub> estimates to yield a harmonized product are also summarized there. These methods may provide a model for integrating results from future operational XCO<sub>2</sub> and XCH<sub>4</sub> constellations.

## 2.5 Resolution and coverage requirements for CO<sub>2</sub> and CH<sub>4</sub> estimates

One of the principal advantages of space-based CO<sub>2</sub> and CH<sub>4</sub> measurements is their spatial resolution and coverage. However, while there has been good progress in improving the precision and accuracy of the space-based XCO<sub>2</sub> or XCH<sub>4</sub> estimates over the past decade, analysis efforts show that space-based CO<sub>2</sub> and CH<sub>4</sub> sensors still do not provide the spatial or temporal resolution and coverage needed to provide timely, quantified guidance on progress towards emission reduction targets (NDCs) at national scales.

### 2.5.1 Factors limiting the resolution and coverage of space-based measurements

Three factors are primarily responsible for limiting the resolution and coverage of space-based CO<sub>2</sub> and CH<sub>4</sub> measurements:

- (i) The spatial sampling strategies adopted by these first-generation sensors have low spatial resolution (SCIAMACHY), collect soundings at discrete points separated by large distances (GOSAT TANSO-FTS, FY-3D GAS) or along narrow ground tracks separated by large distances (OCO-2, TANSAT ACGS; Figure 2-4).
- (ii) Optically thick clouds and aerosols preclude full-column measurements of XCO<sub>2</sub> and XCH<sub>4</sub> for more than 90% of soundings collected by these systems.
- (iii) Passive remote sensing systems that measure reflected sunlight can only return data over the sunlit hemisphere, and typically observe near local noon, precluding observations of CO<sub>2</sub> and CH<sub>4</sub> variations over the full diurnal cycle or at high latitudes during the winter.

The first of these limitations is already being addressed to some extent by the S5P TROPOMI instrument, which records CH<sub>4</sub> and CO observations over a wide (~2600 km) swath at moderate spatial resolution (~7 km x 7 km at nadir), producing two-dimensional (2-D) “images” of XCH<sub>4</sub> and XCO from low Earth orbit (LEO). In the early 2020s, S5P will be joined by the NASA GeoCarb instrument, which will produce 2-D images of XCO<sub>2</sub> as well as XCH<sub>4</sub> and XCO at least twice each day at a comparable spatial resolution at latitudes as high as 50° over North and South America from geostationary Earth orbit (GEO).

The coverage and repeat frequency that these systems provide will still be limited by optically thick clouds and the need for sunlight. The first of these two problems can be mitigated to some extent in partially cloudy regions if the data from all available sensors can be combined, because these sensors will have different overpass times and some of the clouds will move between their observing times. Active sensors (lidars), such as the CNES/DLR MERLIN XCH<sub>4</sub> mission can also yield more useful soundings in partly cloudy regions, because they use a near vertical

illumination and observation geometry that is less contaminated by cloud shadowing and cloud reflections than solar SWIR sensors. Lidars are also expected to yield lower air mass-dependent biases than passive SWIR spectrometers as well as improved coverage of emissions during the night and at high latitudes during the winter where there is limited sunlight.

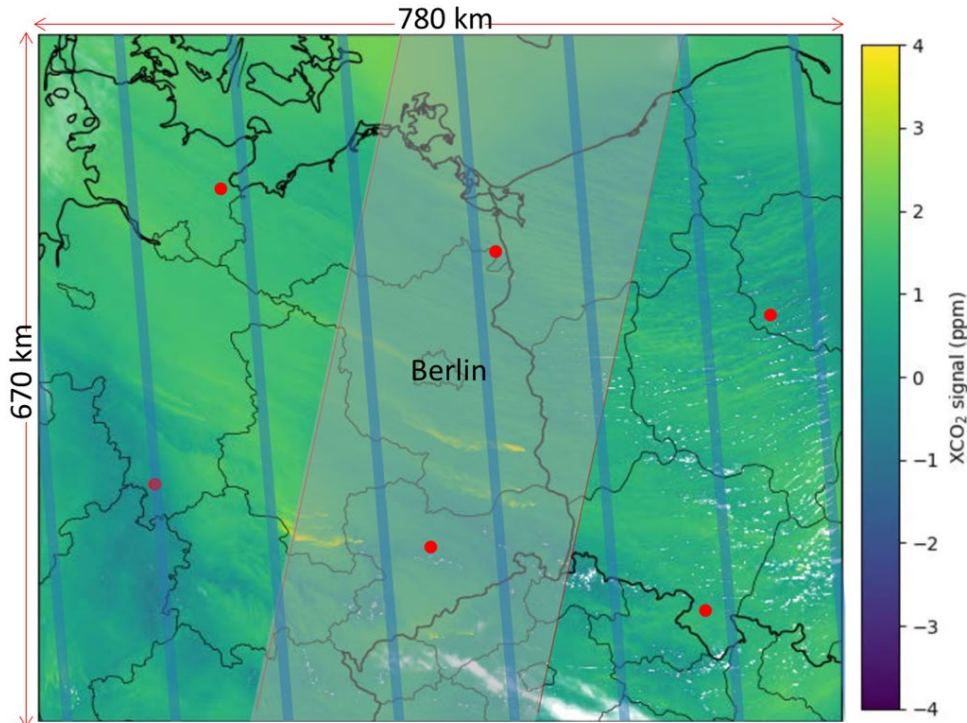


Figure 2-4: The XCO<sub>2</sub> distribution over 780 km by 670 km region centered over Berlin, Germany (adapted from Kuhlmann et al. 2018) is shown along with the spatial coverage and resolution (roughly to scale) for GOSAT (red dots), OCO-2 (blue tracks) and a proposed CO<sub>2</sub> Sentinel mission with a 250 km-wide swath (light grey region), drawn approximately to scale. GOSAT collects soundings with ~10.5 km footprints, separated by ~260 km cross-track and ~280 km down-track. OCO-2 collects soundings continuously along a 10.3 km swath. The wide swath of the CO<sub>2</sub> Sentinel is much better at capturing the CO<sub>2</sub> plumes from Berlin and the large power plants southeast and south of Berlin (Jänschwalde, Schwarze Pumpe, Turów, Boxberg, and Lippendorf; credit: ESA SMARTCARB).

### 2.5.2 Expanding ground-based *in situ* GHG networks to improve coverage

In more persistently cloudy regions, such as the Tropics and high latitudes of the winter hemisphere, the space-based remote sensing observations must be combined with ground-based *in situ* and remote sensing measurements to provide continuous year-round coverage. Continuous ground-based and tower-based measurements also complement the spatially resolved “snapshots” of the XCO<sub>2</sub> and XCH<sub>4</sub> fields acquired by orbiting spacecraft with observations acquired throughout the diurnal cycle. Flask samples, like those collected at ground stations operated by the US National Oceanic and Atmospheric Administration (NOAA) Global Atmospheric Monitoring Division (GMD) and the Integrated Carbon Observation System (ICOS) complement the spacecraft and continuous *in situ* measurements with a broad range of gases that are co-emitted with CO<sub>2</sub> and CH<sub>4</sub>, as well as isotopic species, such as carbon-14, which facilitate the discrimination of fossil fuel emissions from other emissions sources. These

ground-based data are also needed monitor the tropospheric concentrations of other well-mixed GHGs, including N<sub>2</sub>O, CFCs, HCFCs, hydrofluorocarbons (HFCs), sulfur hexafluoride (SF<sub>6</sub>) and perfluorocarbons (PFCs). The WMO GAW and Advanced Global Atmospheric Gases Experiment (AGAGE) networks are generally considered to be adequate for monitoring global trends in these gases (GCOS, 2016), but a substantially expanded ground-based network would be needed to localize or quantifying their sources on regional to continental scales.

Full-column estimates of XCO<sub>2</sub> and XCH<sub>4</sub> can only be retrieved from space-based SWIR measurements collected in cloud-free conditions while the sun is up. They must be combined with ground-based *in situ* and remote sensing measurements to track CO<sub>2</sub> and CH<sub>4</sub> variations over the entire diurnal and seasonal cycle. To harmonize the ground- and space-based data, they must be cross-validated to identify and correct any significant biases. Ground-based *in situ* measurements are more precise and accurate than the space-based estimates. The ground-based *in situ* standards maintained by the World Meteorological Organization Global Atmospheric Watch (WMO GAW) program have therefore been adopted as the internationally accepted reference values (in the context of ISO 5725) for atmospheric GHGs. The WMO GAW network also forms the basis of the GCOS Comprehensive Networks for CO<sub>2</sub> and CH<sub>4</sub> (GCOS, 2016).

## 2.6 Quantifying uncertainties in the space-based CO<sub>2</sub> and CH<sub>4</sub> estimates

A variety of processes can introduce errors and uncertainties in XCO<sub>2</sub> and XCH<sub>4</sub> estimates retrieved from space-based measurements of reflected sunlight. These include measurement errors (instrument noise or calibration errors), sampling biases (time-of-day, cloud-free skies only, etc.), and retrieval algorithm errors or oversimplifications (gas or aerosol absorption cross-section uncertainties, treatment of surface reflectance or atmospheric sphericity, assumed prior or a priori covariances, etc.), among others. For example, because the number of the CO<sub>2</sub> or CH<sub>4</sub> molecules along the optical path between the top of the atmosphere, the surface and the spacecraft sensor is estimated from the amount of sunlight absorbed by these molecules, small (~0.1 to 1%) uncertainties in absorption cross sections of these molecules can introduce systematic biases in the estimated number of molecules (Frankenberg et al., 2008a; Crisp et al. 2012; Thompson et al., 2012; Oyafuso et al. 2017). Uncertainties in the optical properties or vertical distribution of optically thin clouds and aerosols (i.e. smog, smoke, sea salt, dust) can introduce biases in the optical path length travelled by photons, and cause compensating errors in the estimated CO<sub>2</sub> or CH<sub>4</sub> concentrations along that path (Oshchepkov et al., 2012; Guerlet et al. 2013). Errors in the instrument radiometric, spectroscopic or geometric calibration can also introduce biases in the retrieved XCO<sub>2</sub> and XCH<sub>4</sub> (Gloude-mans et al., 2005; Connor et al., 2008; 2016; Crisp et al., 2017). Finally, limitations in the spatial or temporal coverage imposed by instrument performance, orbit geometry (time of day), presence of clouds, or lack of adequate signal can introduce sampling or “representativeness” errors (Corbin et al., 2009).

Fortunately, only those biases that are spatially and temporally correlated on the space and time scales of interest, and not corrected in the analysis process, can yield persistent biases in the estimated flux. Globally invariant concentration biases will complicate comparisons of the space-

based CO<sub>2</sub> and CH<sub>4</sub> estimates with *in situ* standards, but are relatively easy to identify and correct if validation standards are available. Other biases that are random or quasi-random from one sounding footprint to another will introduce flux uncertainties from sources at scales smaller than or comparable to a footprint, but will average out over larger areas and over time.

### 2.6.1 Relating ground-based and space-based XCO<sub>2</sub> and XCH<sub>4</sub> estimates: TCCON

To identify, characterize, and mitigate the impact of instrument, geophysical, or methodological biases in the space-based CO<sub>2</sub> and CH<sub>4</sub> estimates, both internationally-recognized validation standards and validation protocols are needed. The ground-based and aircraft-based *in situ* CO<sub>2</sub> and CH<sub>4</sub> measurements available through the WMO GAW program play a critical role in this activity, but cannot be used directly because they describe the concentrations of the species at a single point location or along a horizontal or vertical flight path, while the space-based results refer to an atmospheric optical path that extends from the top of the atmosphere to the surface and back to the spacecraft. The ground-based XCO<sub>2</sub> and XCH<sub>4</sub> estimates retrieved from the measurements collected by the TCCON FTS instruments provide a transfer standard between the space-based estimates and the WMO GAW standards.

Each TCCON station incorporates a high spectral resolution FTS and a solar tracker to acquire high-resolution spectra of direct sunlight from the center ~10% of the solar disk (Wunch et al., 2011a). Because they measure direct sunlight rather than sunlight scattered by the surface and atmosphere, the TCCON spectrometers have much greater sensitivity to CO<sub>2</sub> and CH<sub>4</sub> than the space-based instruments and much smaller uncertainties in the optical path length. A map of TCCON stations is shown in Figure 2-5. There are currently 23 TCCON instruments operating at latitudes between Eureka, Canada (80.05°N) and Lauder, New Zealand (45.038°S).

The data collected by these stations are analyzed to yield high precision estimates of XCO<sub>2</sub> and XCH<sub>4</sub>. To relate these estimates to the WMO GAW standard scales, *in situ* vertical profiles of CO<sub>2</sub> and CH<sub>4</sub> above the stations using fixed-wing aircraft (Washenfelder et al., 2006; Wofsy et al., 2011) and AirCore (Karion et al., 2010). Because *in situ* estimates of CO<sub>2</sub> and CH<sub>4</sub> from aircraft and AirCore form a critical link in this validation chain, expanded aircraft and AirCore networks are critically needed to support the space based elements of a future carbon monitoring system.

The TCCON team then combines aircraft and AirCore profiles with climatological upper atmosphere data, and integrates over the atmospheric column to derive XCO<sub>2</sub> and XCH<sub>4</sub>. These estimates are compared to XCO<sub>2</sub> and XCH<sub>4</sub> estimates retrieved from simultaneous TCCON measurements. A global bias correction is then applied to the TCCON estimates to reconcile any differences between the TCCON and the *in situ* standard (Wunch et al., 2010; 2015).



Figure 2-5: Spatial distribution of 23 operating TCCON stations (red dots) and 3 stations expected to come on line before 2020 (aqua; credit: TCCON and Blue Marble: Next Generation, produced by Reto Stöckli, NASA Earth Observatory, NASA Goddard Space Flight Center ).

To validate the space-based XCO<sub>2</sub> and XCH<sub>4</sub> estimates against TCCON, values retrieved from the satellite measurements collected near a TCCON station are compared to those retrieved from the simultaneous up looking measurements from that TCCON station. Biases between the TCCON and space-based XCO<sub>2</sub> and XCH<sub>4</sub> estimates are showing continuing improvements as the quality of the space-based measurements and algorithms has improved. By applying simple parametric corrections, the agreement is now less than 1 ppm for XCO<sub>2</sub> (Wunch et al. 2011b; 2017; Buchwitz et al., 2015; Hedelius et al., 2017; O’Dell et al. 2018) and 6 ppb XCH<sub>4</sub> (Yoshida et al., 2013) across the TCCON network.

## 2.7 Linking the GHG inventory, policy and atmospheric CO<sub>2</sub> and CH<sub>4</sub> communities

Stronger links between the national inventory and policy communities and the atmospheric GHG measurement and modelling communities are a critical element of any program designed to inform the national emission inventory development process because both the requirements and capabilities are evolving over time. The national inventory reports (NIRs) required by the UNFCCC are produced according to the statistical methods outlined in the 2006 Guidelines of the IPCC Task Force on National Greenhouse Gas Inventories (IPCC TFI). In 2010, the atmospheric, carbon cycle and climate change science communities produced a number of studies on the potential for atmospheric GHG concentration measurements and model analyses to independently evaluate and help to inform improved estimates of GHG emission inventories (e.g., Verifying Greenhouse Gas Emissions: Methods to Support International Climate Agreements (NAS 2010); GEO Carbon Strategy (GEO 2010); IPCC Task Force on National GHG Inventories: Expert Meeting Report on Uncertainty and Validation of Emission Inventories (IPCC 2010)). These studies concluded that a realization of this approach would require additional investment in research, increasing the density of well-calibrated atmospheric GHG measurements and improving atmospheric transport modelling and data assimilation capabilities.

In June 2015, the Seventeenth World Meteorological Congress passed a resolution initiating the development of an Integrated Global Greenhouse Gas Information System (IG<sup>3</sup>IS), based on the successes of the GAW program and the progress in atmospheric measurements and modeling since 2010. A planning team comprised of scientists and stakeholders from developed and developing countries in all six WMO regions was established to develop the IG<sup>3</sup>IS Concept Paper. IG<sup>3</sup>IS will work closely with the inventory builders and other stakeholders who need to track GHG emissions to develop methodologies for how atmospheric GHG concentration measurements (the top-down) can be combined with spatially and temporally explicit emission inventory data (the bottom-up) to better inform and manage emission reduction policies and measures. GAW GHG measurement network and standards will be essential for IG<sup>3</sup>IS success, but the focus, and location of measurement sites, must expand from remote locations to key GHG source regions where emission reduction is taking place or is needed. Over time, the IG<sup>3</sup>IS framework will be capable of continually improving the quality of and confidence in the derived information from data measured *in situ* and from the emerging satellite capabilities. IG<sup>3</sup>IS is therefore well positioned to form a bridge between the policy, inventory, and atmospheric GHG communities.

A number of less formal opportunities for interactions among these communities are also being explored. Efforts, such as the 2017 Workshop on “Atmospheric monitoring and inverse modelling for verification of GHG inventories,” hosted by the European Commission Joint Research Centre (JRC) and documented in Bergamaschi et al., (2018), are a very good example. However, a more continuous effort could yield immediate benefits for both communities. For the atmospheric GHG modelling community, this relationship could provide greater insight into the emissions from well-characterized anthropogenic sources, which are used as prior constraints in atmospheric inversion systems designed for studies of the natural carbon cycle. Similarly, observations of CO<sub>2</sub> and CH<sub>4</sub> emissions from existing and planned space-based sensors could yield timely information about the anthropogenic emissions in areas where the bottom-up inventories are known to be incomplete or highly uncertain. In the present context, a much greater level of interaction (and understanding) is needed to define the requirements for a space-based architecture designed specifically to reduce uncertainty of emission inventories and to provide extra evidence to support national inventory reports. By sampling GHG fluxes across the globe multiple times per year, the system aims to monitor localized emission sources in a transparent way, to identify additional emission reduction opportunities and to provide nations timely and quantified guidance on progress towards their emission reduction strategies and pledges (NDCs).

One approach to facilitate interactions between the inventory and atmospheric measurement communities would be to encourage the participation of the national inventory community in ongoing annual workshops, such as the International Workshop on Greenhouse Gas Measurements from Space (IWGGMS). Over the past 15 years, the IWGGMS fostered the rapid development of sensor technologies, calibration and validation techniques, retrieval algorithms, and inverse models by bringing these once diverse communities together to exchange information. The scope of this workshop could be expanded to include a session on the development of national GHG inventories, to continue the process started at the 2017 JRC

workshop. This workshop already includes interfaces with researchers supporting the scientific inventories, such as the EDGAR (Janssens-Maenhout et al., 2017; Bergamaschi et al., 2018), Carbon Dioxide Information Analysis Centre (CDIAC; Andres et al., 2012; Boden et al., 2017) and Open-source Data Inventory for Anthropogenic CO<sub>2</sub> (ODIAC; Oda and Maksyutov, 2011; Oda et al., 2018). It might be possible to exploit these interfaces to build a bridge that would attract members of the national inventory agencies. Similarly, the space-based GHG measurement and modeling community should be encouraged to participate more actively in conferences focusing on emissions, such as the biannual meeting of the Global Emissions Initiative (GEIA). ESA initiated this process by giving a keynote lecture describing the evaluation of emissions with space-based observations at the 2017 GEIA meeting. Upcoming opportunities include the next GEIA conference (University of Chile, November 2019).

A complementary approach would be to encourage more active interactions between space-based CO<sub>2</sub> and CH<sub>4</sub> measurement and modeling communities and the WMO IG<sup>3</sup>IS initiative. IG<sup>3</sup>IS plans to foster strong interactions with the inventory builders and other stakeholders to support national inventory preparation. Active participation in IG<sup>3</sup>IS would help to coordinate the space-based and ground-based measurement communities and to define best practices for incorporating atmospheric emission measurements into the bottom-up inventory development process. In addition, this association would help to support IG<sup>3</sup>IS as interface between the atmospheric measurement and the inventory communities for communications and capacity building.

In addition, the space-based CO<sub>2</sub> and CH<sub>4</sub> measurement and modeling community should also foster more direct interactions with the IPCC Task Force on Greenhouse Gas Inventories (TFI). The IPCC TFI has invited this community to participate in the review of the draft of the 2019 Refinement of the 2006 Guidelines for National GHG Inventories of, Volume 1, chapter 8 "Inverse Modeling". They particularly interested in receiving input on the increasing importance of the extra evidence inverse modeling with independent observations could give to the emission inventory community.

### 3. Space-based CO<sub>2</sub> and CH<sub>4</sub> Measurement Capabilities and Near-term Plans

When the 2014 CEOS Carbon Strategy was released, only two spacecraft carrying solar SWIR CO<sub>2</sub> and CH<sub>4</sub> sensors had been launched, the ESA ENVISAT SCIAMACHY (2002 to 2012) and the Japanese GOSAT TANSO FTS (2009-present). Since that time, these two pioneering missions have been joined by the NASA OCO-2, the Chinese TanSat, the ESA Sentinel 5 Precursor (S5P), and the Chinese Feng Yun-3D and GaoFen-5 satellites and several other solar SWIR CO<sub>2</sub> and CH<sub>4</sub> satellites are in development or in the planning stages. Each of these missions introduces new methods and observing strategies and exploits new vantage points. The following subsections summarize the key features of each of these systems.

Complementary GHG monitoring efforts by commercial organizations and non-governmental agencies have also been initiated since the 2014 CEOS Carbon Strategy was released. These include the launch of the GHGSat-D, the near term plans to launch a series of CH<sub>4</sub> imaging satellites by Bluefield Technologies, and the Environmental Defense Fund's CH<sub>4</sub> monitoring micro-satellite concept, called MethaneSAT. These concepts are described in Appendix 5.

#### 3.1 ENVISAT SCIAMACHY

SCIAMACHY was a national contribution to the ENVISAT payload provided by Germany, the Netherlands and Belgium. ENVISAT was launched on 28 February 2002 and operated through 8 April 2012 (Figure 3-1). It was deployed in a 790-km altitude, sun-synchronous polar orbit with a 100.6-minute period, a mean local time of 10 AM, and a ground track repeat period of 35 days (501 orbits/cycle). SCIAMACHY was the first space-based sensor designed to deliver NIR and SWIR spectral observations of reflected sunlight that could be used to retrieve estimates of XCO<sub>2</sub> and XCH<sub>4</sub>. SCIAMACHY collected moderate-resolution ( $\lambda/\Delta\lambda \approx 1100$ ) spectra within the short wave infrared (SWIR) CO<sub>2</sub> absorption bands near 1580 and 1610 nm and the CH<sub>4</sub> band near 1670 nm. It also collected high resolution ( $\lambda/\Delta\lambda \approx 9400$ ) spectra within the CO<sub>2</sub> bands near 1940 and 2040 nm and the CH<sub>4</sub> bands between 2265 and 2385 nm (Lichtenberg et al., 2006) although these channels were contaminated by water ice deposition on the detectors throughout much of the mission. It was also the first space-based instrument that included co-located moderate-resolution ( $\lambda/\Delta\lambda \approx 1600$ ) spectra of the near-infrared (NIR) molecular oxygen (O<sub>2</sub>) A-band at 765 nm to retrieve estimates of the dry air column (Burrows et al., 1995 Bovensmann et al. 1999, Buchwitz et al., 2005, Gottwald and Bovensmann 2011).

The analysis of SCIAMACHY measurements yielded the first maps of XCO<sub>2</sub> and XCH<sub>4</sub> over continents (Frankenberg et al., 2005; Buchwitz et al., 2005; 2015). Its broad (960-km) swath provided full coverage of the Earth at the equator on sub-weekly time scales. Its spatial resolution and sensitivity were limited by data rate on ENVISAT and instrument technologies available in the early 1990s, when the system was designed. Its relatively large single-sounding random errors (2.3 to 5.1 ppm for XCO<sub>2</sub>; 50 to 82 ppb for XCH<sub>4</sub>; Reuter et al., 2010; 2011; Buchwitz et al., 2015) and regional-scale systematic biases (0.7 ppm for XCO<sub>2</sub>, 11-15 ppb for XCH<sub>4</sub>; Buchwitz et al., 2015; 2017) limited its effectiveness for retrieving natural CO<sub>2</sub> sources

and sinks. The relatively large surface footprint size (30 km by 60 km) limited its sensitivity to compact sources of CO<sub>2</sub> and CH<sub>4</sub> emissions. It also increased the probability of contamination by clouds. Clouds-contaminated soundings were detected and screened using the simultaneous high spatial resolution, measurements from the ENVISAT Medium Resolution Imaging Spectrometer (MERIS) instrument, but this limited the coverage in regions with persistent cloud cover. Coverage of the ocean was limited by the low signal levels there. Consequently, efforts to retrieve XCO<sub>2</sub> have focused primarily on measurements over land (Figure 3-1).

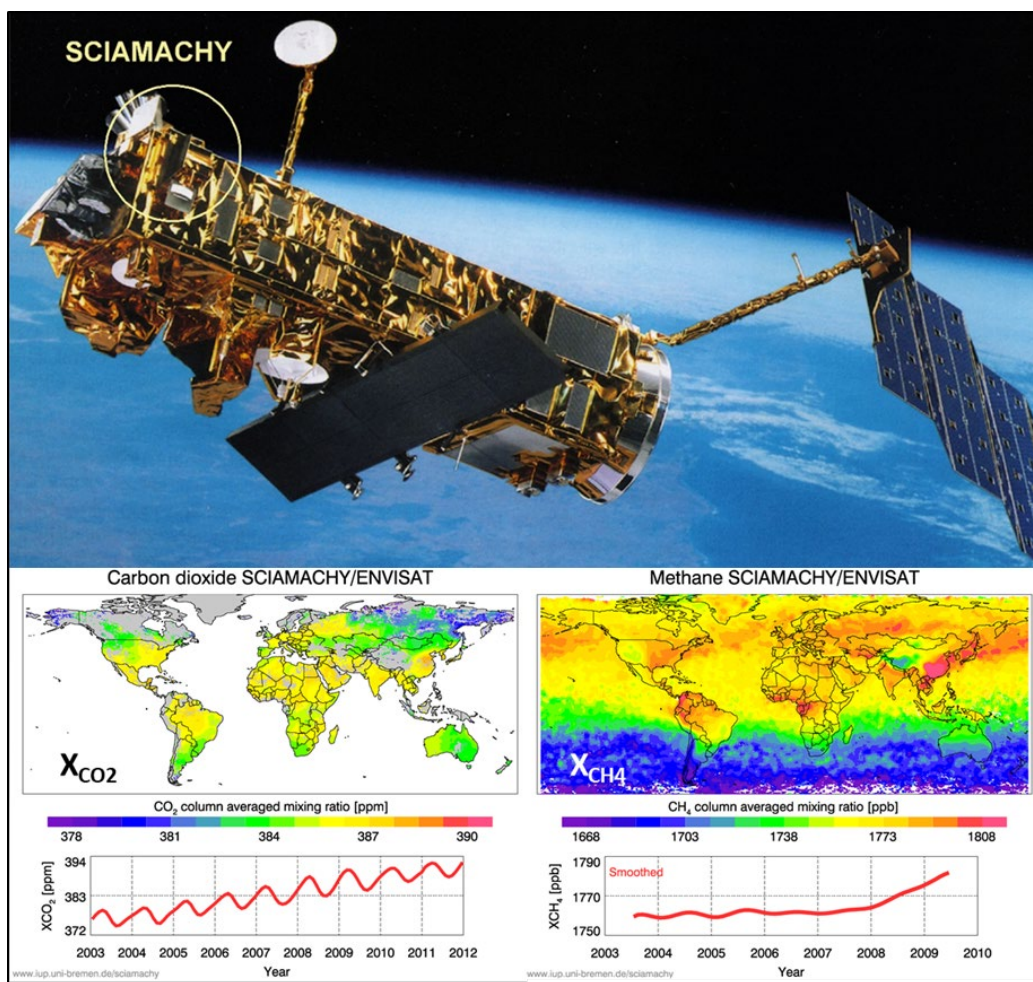


**Figure 3-1:** (top) SCIAMACHY flew on ENVISAT from 2002 to 2012 (credit: ESA), and collected observations of a broad range of trace species including CO<sub>2</sub> and CH<sub>4</sub>. Composite maps of XCO<sub>2</sub> from 2006-2011 and XCH<sub>4</sub> from 2003 to 2005 are shown in the left and right center panels respectively. The globally averaged trends of XCO<sub>2</sub> from 2003 to 2012 and XCH<sub>4</sub> from 2003 to 2009 are shown in the bottom panels (credit: Climate Change Initiative (CCI) project, <http://www.esa-ghg-cci.org/> and the University of Bremen).

An improved understanding of the instrument calibration, advances in remote sensing retrieval algorithms and the development of more comprehensive validation methods have increased the quality and value of the decade-long SCIAMACHY XCO<sub>2</sub> and XCH<sub>4</sub> data records over time. For example, while the robustness of early regional-scale CH<sub>4</sub> flux estimates inferred from SCIAMACHY measurements was limited by the need for a large bias correction (e.g. Bergamaschi et al., 2009), improved in-flight calibration, updated CH<sub>4</sub> and H<sub>2</sub>O spectroscopic

parameters and retrieval algorithms reduced the bias (Buchwitz et al., 2017a). Multi-year averages of SCIAMACHY observations have since provided insight into regional-scale CO<sub>2</sub> anomalies over Europe, North America, and East Asia (Schneising et al. 2013) and challenged the current estimate of the European carbon sink (Reuter et al. 2014; 2017b). They also facilitated the detection of fugitive CH<sub>4</sub> emissions from large emission hot spots in North America (Schneising et al., 2014; Kort et al., 2014) and around the world (Buchwitz et al 2017b). Estimates of XCO<sub>2</sub> and XCH<sub>4</sub> from SCIAMACHY data have been combined with results from TANSO-FTS (Buchwitz et al., 2017a). In this combined dataset, the globally-averaged annual CO<sub>2</sub> growth rates between 2003 and 2016 agree with estimates derived from surface observations by the National Oceanic and Atmospheric Administration (NOAA) to within 0.24 ppm/year (Buchwitz et al. 2018a). SCIAMACHY has therefore served as a pathfinder for subsequent and future sensors designed to measure XCO<sub>2</sub> and XCH<sub>4</sub> using reflected sunlight.

SCIAMACHY data products can be accessed through the ESA data portal: (<https://earth.esa.int/web/guest/data-access/browse-data-products>). Updated estimates of XCO<sub>2</sub> and XCH<sub>4</sub> from SCIAMACHY can be accessed via the European Copernicus Climate Change Service (C3S, <https://climate.copernicus.eu/>; Buchwitz et al., 2018b).

### 3.2 GOSAT TANSO-FTS

The Greenhouse gases Observing SATellite (GOSAT, also called Ibuki) is a joint effort of the Japanese Aerospace Exploration Agency (JAXA), the National Institute of Environmental Sciences (NIES) and the Ministry of the Environment (MOE) of Japan. GOSAT was launched on 23 January 2009 and has been returning science data since April 2009 (Kuze et al. 2009). GOSAT completed its nominal science mission in 2014 and is now in its extended mission. GOSAT was deployed in a 666-km altitude, 98° inclination, sun-synchronous orbit with a 3-day (44-orbit) ground track repeat period. Prior to 2016, the mean local time of the descending node was 12:49, but this time drifted later over the first 9 years of operations. In the summer of 2018, a series of maneuvers were performed to correct this local time drift.

GOSAT carries two instruments, the Thermal and Near infrared Sensor for carbon Observations (TANSO) Fourier Transform Spectrometer (FTS), and the TANSO Cloud and Aerosol Imager (CAI). TANSO-FTS is a double pendulum interferometer that records high-resolution spectra of both reflected sunlight and thermal emission (Figure 3-2). Bands 1 through 3 collect spectra of reflected sunlight within the NIR O<sub>2</sub> A-band at 765 nm (13020 cm<sup>-1</sup>), the SWIR CO<sub>2</sub> and CH<sub>4</sub> bands near 1600 nm (6250 cm<sup>-1</sup>) and 1670 nm (5990 cm<sup>-1</sup>), respectively, and CO<sub>2</sub> and H<sub>2</sub>O bands near 2060 nm (4850 cm<sup>-1</sup>). Band 5 is a broad (700 to 1800 cm<sup>-1</sup> or 5.56 to 14.3 μm) thermal infrared (TIR) channel designed to measure the absorption and emission of thermal radiation by water vapor (H<sub>2</sub>O), ozone (O<sub>3</sub>), CH<sub>4</sub>, and CO<sub>2</sub>. The spectral resolution in Band 1 is 0.37 cm<sup>-1</sup> while that in Bands 2, 3, and 4 is 0.27 cm<sup>-1</sup>.

TANSO-FTS collects interferograms at 4-second intervals within a 16 milliradian (0.9°) circular field of view (FOV) that yields a surface footprint that is about 10.5 km in diameter at nadir. A 2-axis scan mirror directs the TANSO-FTS 10.5-km field of view within ~ 35° of nadir in the

cross-track direction and within  $\sim 20^\circ$  of nadir along the spacecraft ground track, and provides image motion compensation during the 4-second exposures. Prior to August 2010, observations over land were collected using a 5-point cross-track pattern. Since that time, observations over land are collected with a 3-point cross-track pattern, with footprints that are separated by about 260 km cross-track and about 280 km along-track. Over the ocean, the pointing mechanism directs the TANSO-FTS field of view to the bright “glint” spot to ensure adequate signal for CO<sub>2</sub> and CH<sub>4</sub> retrievals. Prior to September 2014, glint measurements were collected only at solar zenith angles within  $20^\circ$  of the sub-solar latitude. Since that date, observations in the direction (azimuth) of the glint spot have been acquired to extend the ocean coverage to  $\pm 40^\circ$  of the sub-solar latitude. This spatial sampling approach yields about 10,000 soundings over the sunlit hemisphere of the Earth each day.

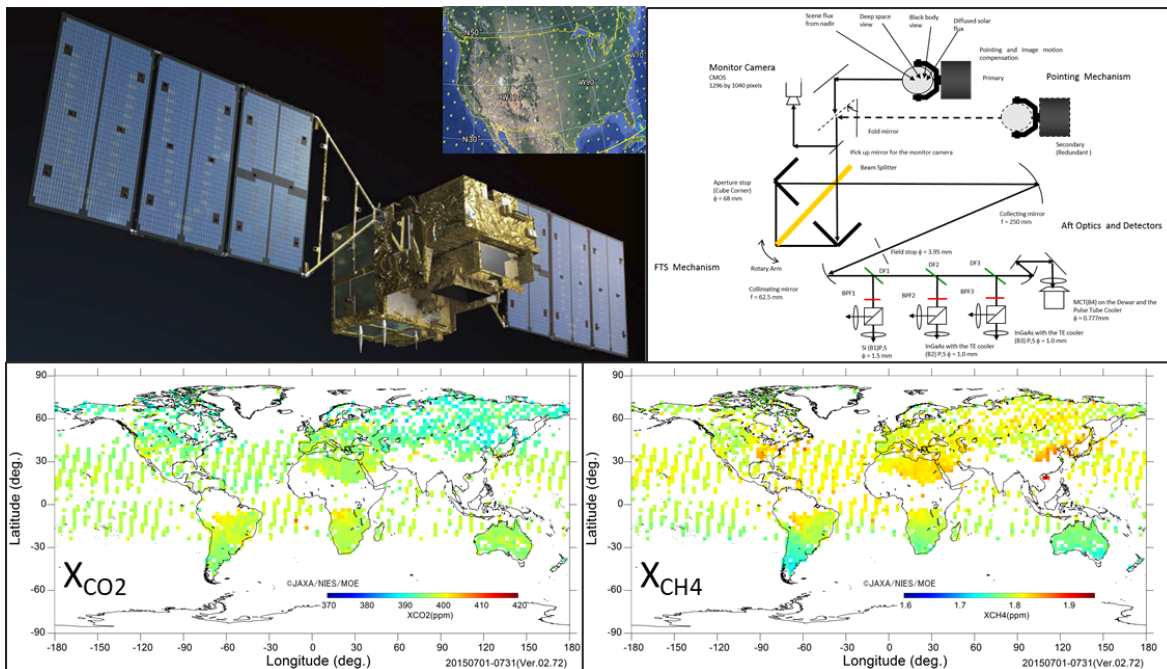


**Figure 3-2:** Top left – The GOSAT spacecraft, with inset showing 3-point cross-track scan pattern over the U.S (credit: JAXA). Top right – Schematic showing the major components and optical path of the GOSAT TANSO FTS instrument (credit: JAXA). Bottom left - monthly maps of XCO<sub>2</sub> (left) and XCH<sub>4</sub> (right) from July 1-31 2015 (credit: NIES, Version 02.72; from [https://data2.gosat.nies.go.jp/gallery/fts\\_l2\\_swir\\_co2\\_gallery\\_en.html](https://data2.gosat.nies.go.jp/gallery/fts_l2_swir_co2_gallery_en.html))

The 2-axis scan mechanism also has a flexible targeting capability, which facilitates the acquisition of data over stationary surface targets. This targeting capability is used to acquire data over well-instrumented surface calibration sites, such as Railroad Valley, Nevada, USA, and over TCCON stations, which are used for validation. Targeted observations have also been used to collect more useful measurements over island archipelagos and rain forests and to support campaigns over cities, stockyards, fossil fuel extraction fields and other points of interest.

TANSO-CAI was designed to facilitate the detection of clouds and optically thick aerosols within the TANSO-FTS field of view. The TANSO-CAI has a nadir spatial resolution of  $\sim 0.5$  km over a 900 km wide swath for spectral channels centered near 0.38, 0.674, and 0.870  $\mu\text{m}$  and

a nadir spatial resolution of  $\sim 1$  km over a 750 km swath at 1.6  $\mu\text{m}$ . Its data are used in to identify and screen clouds in the standard Level-2 retrieval algorithm implemented by NIES. On monthly time scales, between 3 and 10% of the TANSO-FTS soundings are sufficiently cloud-free and have adequate signal to yield reliable XCO<sub>2</sub> and XCH<sub>4</sub> estimates.

JAXA is responsible for generating the geolocated, radiometrically calibrated radiances (L1B products). NIES produced and distributed the official Level 2 XCO<sub>2</sub> and XCH<sub>4</sub> products (Figure 3-2; Yoshida et al., 2013), but several other teams have produced independent XCO<sub>2</sub> and/or XCH<sub>4</sub> products from the GOSAT TANSO-FTS L1B data. These included a second team at NIES (Oshchepkov et al., 2012), the NASA Atmospheric CO<sub>2</sub> Observations from Space (ACOS) team (O'Dell et al. 2012; Crisp et al., 2012), and teams at Karlsruhe Institute of Technology (Butz et al. 2011), the University of Leicester (Parker et al., 2011; Cogan et al., 2012), the ESA Greenhouse Gas Climate Change Initiative (GHG-CCI; Buchwitz et al., 2015), and Yonsei University (Jung et al., 2016; Kim et al., 2016). The close collaboration and exchange of ideas and methods among these teams fostered rapid progress in retrieval algorithm development.

GOSAT was also the first GHG mission to fully exploit opportunities for vicarious calibration over Railroad Valley, Nevada, USA (Kuze et al., 2009; 2011; 2014), and to routinely use targeted observations over TCCON sites for validation (Wunch et al., 2011b; Yoshida et al., 2013). Comparisons of GOSAT TANSO-FTS XCO<sub>2</sub> and XCH<sub>4</sub> retrievals with surface-based XCO<sub>2</sub> estimates from TCCON helped to identify and correct subtle biases associated with air mass, surface pressure, optically thick aerosols, ice-covered surfaces, and other environmental factors (O'Dell et al., 2012). Persistent spectral residuals common to TCCON and TANSO-FTS retrievals revealed limitations in the spectroscopy of CO<sub>2</sub>, CH<sub>4</sub>, and O<sub>2</sub>, which are being addressed with new laboratory measurements and analysis techniques (Long et al., 2011; 2012a,b; Thompson et al., 2012, Nikitin et al., 2015). These calibration, retrieval algorithm development, and validation activities are now yielding XCO<sub>2</sub> estimates with regional-scale errors of 1 to 2 ppm (Lindquist et al., 2015; Kulawik et al., 2017; Frankenberg et al., 2016) and XCH<sub>4</sub> estimates with regional-scale errors between 4 and 7 ppb (Buchwitz et al., 2017a) over much of the globe.

GOSAT observations have been used to constrain CO<sub>2</sub> and CH<sub>4</sub> fluxes from the biosphere and oceans on regional scales and for studies of anthropogenic sources of these gases. For example, Detmers et al. (2015) used GOSAT XCO<sub>2</sub> to document the anomalous carbon sink over Australia in 2010 associated with a strong La Niña. GOSAT observations also led to the discovery that solar induced chlorophyll fluorescence (SIF) could be detected from space in the O<sub>2</sub> A-Band, and that it had to be corrected to avoid introducing biases in the dry air column (Frankenberg et al., 2011a). Subsequent tests showed that this new product could yield additional information about gross primary productivity and thus the uptake of CO<sub>2</sub> by the land biosphere (Frankenberg et al., 2011b; Joiner et al., 2011; 2012; Guanter et al., 2012) and helped to spawn a new field of investigation. Its flexible pointing capabilities have been exploited for monitoring anthropogenic CO<sub>2</sub> emissions from megacities (Kort et al., 2012; Janardanan et al., 2016), the CH<sub>4</sub> emissions from intense livestock, coal mining, wet agriculture and oil and gas extraction (Turner et al., 2015a; Janardanan et al. 2017) and national scale CH<sub>4</sub> emissions from India (Ganesan et al.,

2017). More generally, the availability of GOSAT XCO<sub>2</sub> and XCH<sub>4</sub> data stimulated the development of remote sensing retrieval algorithms (Butz et al., 2011; O'Dell et al., 2012; Oshchepkov et al., 2012; Geddes and Bösch, 2015; Heymann et al., 2015) and atmospheric inversion systems (Alexe et al., 2015; Chevallier et al., 2005b; 2017; Maksyutov et al., 2013; Kondo et al., 2015; Houweling et al., 2015; Liu et al. 2015).

While the broad spectral coverage and high spectral resolution of TANSO-FTS provided useful products, the relatively low single-sounding precision (2 ppm for CO<sub>2</sub>, 13 ppb for CH<sub>4</sub>; Kuze et al., 2016), as well as its relatively large footprint and the sparse coverage provided by its standard 3-point and 5-point scanning modes are not ideal for monitoring compact anthropogenic emission sources. Only the largest emitters produce anomalies that are large enough to be accurately quantified within the relatively large (85 km<sup>2</sup>) footprints, even when they are well centered in the footprint. In addition, individual overpasses provide too few soundings near the source to quantify the background levels of CO<sub>2</sub> and CH<sub>4</sub>. Improved sensitivity, resolution and coverage are needed for these applications.

### 3.3 OCO-2

The NASA Orbiting Carbon Observatory-2 (OCO-2) is a “carbon copy” of the original Orbiting Carbon Observatory (OCO), which was lost in February 2009 due to a launch vehicle malfunction. OCO-2 was launched on 2 July 2014 and was inserted at the head of the 705-km altitude Afternoon Constellation (A-Train) on 3 August 2014. This 98.8-minute sun synchronous orbit has a 13:36 mean local time for its ascending node and a 16-day (233-orbit) ground-track repeat period (L'Ecuyer and Jiang, 2010). OCO-2 completed its in-orbit checkout and began returning science observations on 6 September 2014. It completed its nominal 2-year mission in October 2016, and has started a 3-year extended mission.

The OCO-2 spacecraft carries and points a single instrument, a 3-channel imaging grating spectrometer that collects co-boresighted, high-resolution spectra of reflected sunlight in the 0.765 μm O<sub>2</sub> A-Band and within the 1.61 and 2.06 μm CO<sub>2</sub> bands (Crisp et al., 2004; 2008; 2017). The instrument design was optimized for sensitivity to XCO<sub>2</sub> variations, with an unprecedented combination of spatial resolution (< 3 km<sup>2</sup>/sounding), spectral resolving power ( $\lambda/\Delta\lambda > 17,000$ , where  $\lambda$  is wavelength), and dynamic range ( $\sim 10^4$ ), so that it could yield high signal-to-noise ratio (SNR > 400) even over relatively dark surfaces (albedo < 0.05) at high solar zenith angles (SZA > 60°). Each instrument channel collects eight contiguous, spatially-resolved soundings every 1/3 second along a narrow (< 0.8°) field of view (FOV) while over the sunlit hemisphere, yielding about one million soundings each day (Figure 3-3). On monthly time scales, between 6 and 9% of these soundings are sufficiently cloud free to yield full-column estimates of XCO<sub>2</sub> with single-sounding random errors around 0.5 ppm (0.125%) at solar zenith angles as high as 70°.

For routine science operations, the spacecraft points the instrument boresight at the local nadir or near the “glint spot,” where sunlight is specularly reflected from the Earth's surface. In these observing modes, the instrument does not collect data in a conventional push-broom configuration with the long-axis of the spectrometer slits oriented perpendicular to the ground track. To mitigate errors associated with uncertainties in the degree of polarization of the

reflected solar radiation, the orientation of the slits rotates with latitude to maintain a constant angle relative to the principal plane, defined by the sun, surface footprint, and spacecraft (Crisp et al. 2017). This approach yields surface footprints with areas that decrease from  $\sim 3 \text{ km}^2$  at the southern terminator to  $\sim 0.2 \text{ km}^2$  at a point  $\sim 30^\circ$  north of the sub-solar latitude, and then increase again above that latitude to  $\sim 2 \text{ km}^2$  at the northern terminator.

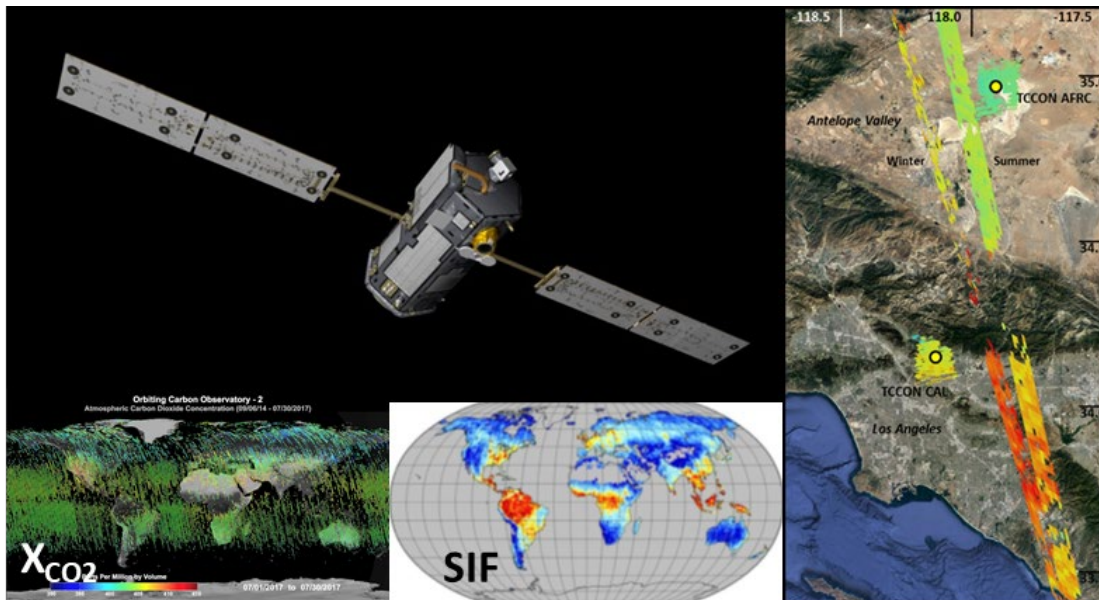


Figure 3-3: OCO-2 (top left) carries and points a high spectral resolution ( $\lambda/\Delta\lambda\sim 20,000$ ) imaging grating spectrometer that collects about 85,000 cloud free estimates each day along its narrow ( $< 10 \text{ km}$ ) ground track. Lower left - The monthly coverage for July 2017. Lower middle – Annual average SIF from 2015. Lower right – OCO-2 glint (left) and nadir (right) tracks showing enhanced XCO<sub>2</sub> over the Los Angeles basin relative to the desert north of the basin (credit: JPL/NASA).

The spacecraft can also point the instrument boresight at a stationary surface target near the ground track to collect thousands of measurements as the spacecraft flies overhead. This “target” mode is used primarily to collect data over well-instrumented surface calibration sites, such as Railroad Valley, Nevada, USA, and validation sites, including TCCON stations. In addition to these science observing modes, the spacecraft routinely points the instrument boresight at the sun or the moon for on-orbit radiometric, spectroscopic, and geometric calibration (Crisp et al., 2017; Sun et al., 2017). It also points the X-band antenna at ground stations for data downlink.

The OCO-2 glint/nadir observing strategy was refined over the first two years of operation to improve the measurement coverage and yield. The initial observing strategy recorded only glint or nadir observations over the entire sunlit hemisphere for a complete, 16-day, ground-track repeat period, and then used the other observing mode in the next 16-day cycle. This approach provided adequate coverage of oceans and continents on monthly time scales, but produced 16-day long gaps in the coverage of the ocean while in nadir mode, and limited coverage of high latitude continents while in glint mode. On 2 July 2015, this observation strategy was modified to alternate between glint and nadir observations on adjacent orbits to yield more continuous coverage of the entire sunlit hemisphere every day. On 12 November 2015, the observation strategy was optimized further to always collect glint data on orbits that are primarily over ocean, increasing the number of useful ocean observations by about 30%.

Co-boresighted observations from the 3 spectrometer channels are combined to produce soundings that are first screened for optically thick clouds (Taylor et al., 2016) and then processed with a remote sensing retrieval algorithm to estimate XCO<sub>2</sub>, SIF, and other data products (Eldering et al., 2017). OCO-2 XCO<sub>2</sub> and SIF observations returned during its first 4 years in orbit provide a high-resolution global description of the atmospheric carbon cycle. They show the intense northern hemisphere spring drawdown associated with the land biosphere. They also show persistent XCO<sub>2</sub> anomalies over regions with intense fossil fuel combustion, such as Western Europe and the east coasts of China and North America. Areas with intense biomass burning, including central Africa, the Amazon, and Southeast Asia, also show anomalously high XCO<sub>2</sub> at some times of the year (Hakkarainen et al., 2016; 2018). With its high spatial resolution, OCO-2 data have also been used to study the spatial structure of XCO<sub>2</sub> variations across megacities (Figure 3-3; Schwandner et al., 2017; Ye et al. 2017) and even to quantify fossil fuel CO<sub>2</sub> emissions from individual power plants located within or near OCO-2 ground tracks (Nassar et al., 2017).

OCO-2 data collected between March 2015 and June of 2016 provide a unique opportunity to study the carbon-climate feedbacks associated with the intense, 2015-2016 El Niño. Several teams combined OCO-2 XCO<sub>2</sub> and SIF results with data from other spacecraft instruments, including Terra MOPITT, Aura OMI, and GOSAT TANSO-FTS to provide new insights into the relative roles of changes in ocean outgassing, drought, temperature stress, and fires in controlling the atmospheric CO<sub>2</sub> buildup during this event (Heymann et al., 2017; Chatterjee et al., 2017; Liu et al., 2017; Sun et al., 2017; Patra et al., 2017).

### 3.4 TanSat Atmospheric CO<sub>2</sub> Grating Spectrometer (ACGS)

The Chinese CO<sub>2</sub> observing satellite, TanSat, launched on 22 December 2016 and began its 3-year nominal science mission nine months later. TanSat was developed by the Ministry of Science and Technology of China (MOST), the Chinese Academy of Sciences (CAS), and the China Meteorological Administration (CMA). It was initially inserted into a ~708 km altitude sun-synchronous orbit with a 98.07° inclination, 13:39 mean local time (ascending), and a 16-day (233-orbit) ground track repeat period. This orbit was ~2.5 km above the mean altitude of the A-Train constellation, but somewhat more elliptical, so that TanSat passes through the A-Train with a synodic period of ~134 days. However, there are currently no plans for TanSat to become a member of the A-Train constellation due to the complexity of the operations needed for formation flying.

TanSat carries the Atmospheric CO<sub>2</sub> Grating Spectrometer (ACGS) and the Cloud and Aerosol Polarization Imager (CAPI). ACGS soundings recorded will be used to retrieve XCO<sub>2</sub>, while data from CAPI will be used to correct cloud and aerosol interference. ACGS is a high-spectral resolution, 3-channel imaging grating spectrometer, similar to the OCO-2 spectrometer (Figure 3-4; Bi et al. 2017). It records spectra of reflected sunlight within the 0.76 μm O<sub>2</sub> A-band, and the CO<sub>2</sub> bands centered near 1.61 and 2.06 μm (Zhang et al., 2016; Yang et al., 2017). The resolving power in the A-band channel is similar to that of OCO-2 ( $\lambda/\Delta\lambda = 19,000$ ), while in the CO<sub>2</sub> channels is somewhat lower (~12,000).

ACGS acquires 20 contiguous, spatially-resolved soundings across a field of view (FOV) that is about twice as wide as that for OCO-2 (28 milliradian, or  $1.6^\circ$ ), producing a 20-km cross-track swath at nadir (Bi et al. 2017; Li et al., 2017). This FOV is sampled at  $\sim 3.7$  Hz, yielding surface footprints that are 1 km cross-track by 2.1 km down-track when the slit is oriented orthogonal to the direction of motion. Adjacent cross-track footprints are averaged together on the ground to increase the SNR, yielding 9 surface footprints with areas of about  $2 \text{ km} \times 2 \text{ km}$ .

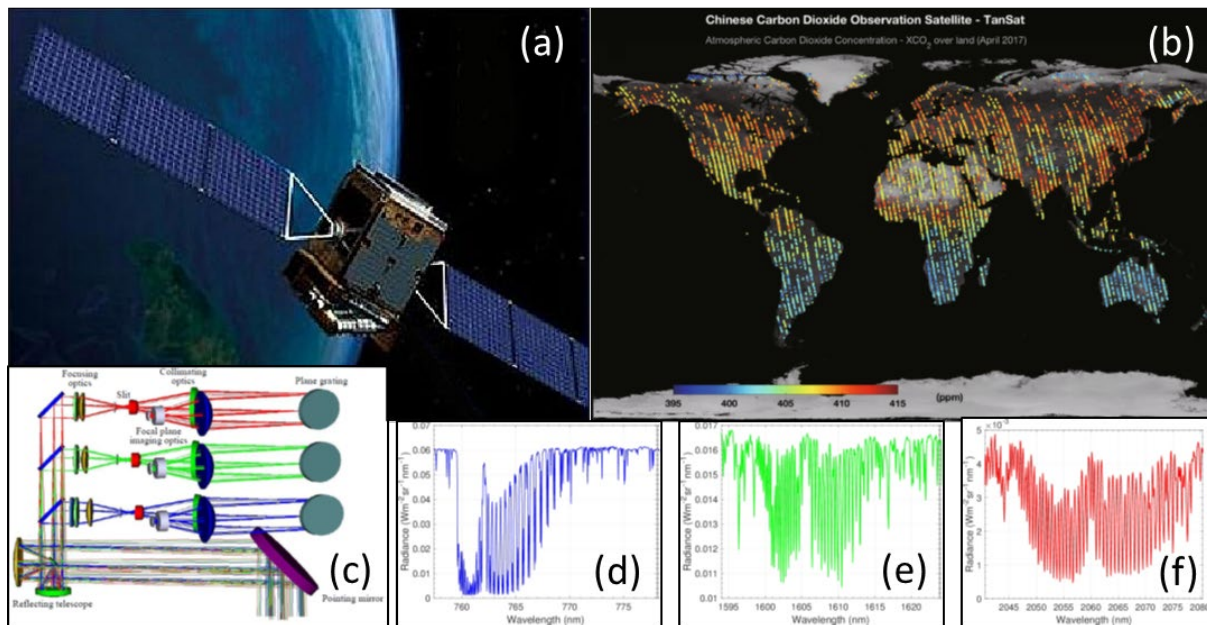


Figure 3-4: (a) Artist's rendition of the deployed TanSat spacecraft (credit: EO Portal:

<https://directory.eoportal.org/web/eoportal/satellite-missions/t/tansat>). (b) Global XCO<sub>2</sub> map from TanSat nadir mode over land for April 2017 (Yang et al., 2018). (c) ACGS optical layout, showing pointing mirror (lower right), telescope (lower left), and (bottom to top) O<sub>2</sub> A-band, 1.61 μm CO<sub>2</sub>, and 2.06 μm CO<sub>2</sub> channels (Li et al., 2017). (d-f) First light spectra from the O<sub>2</sub> A-band, 1.61 μm CO<sub>2</sub>, and 2.06 μm CO<sub>2</sub> channels (CGMS-45, CMA-WP-02, <https://www.cgms-info.org/agendas/agendas/CGMS-45>).

TanSat uses a pointing mirror in conjunction with satellite platform motions to point the ACGS boresight at the nadir, sun glint, or at stationary surface targets. This measurement approach is expected to return spectra with the sensitivity and accuracy needed to estimate of XCO<sub>2</sub> with random errors and systematic biases no larger than 1 to 4 ppm (0.25 to 1%) on regional scales (500 km x 500 km) at monthly intervals.

CAPRI records images in five spectral channels (0.38, 0.67, 0.87, 1.375, and 1.64 μm). The 0.67 and 1.64 μm channels sample three independent polarization angles. The 0.38, 0.67, and 0.87 μm channels have a spatial resolution of 0.25 km over a 400 km wide swath. The 1.375 and 1.640 μm channels have a 1-km resolution over this swath.

TanSat is operated by CMA and its data are received, processed and disseminated by the National Satellite Meteorological Center, CMA (NMSC). TanSat began collecting science observations in January 2017 and delivering radiometrically-calibrated, geolocated (Level 1B)

products on October 24, 2017 through the NMSC portal:

<http://satellite.nsmc.org.cn/PortalSite/Default.aspx>

At the time of writing, preliminary XCO<sub>2</sub> results had been shown at conferences and a brief paper describing the global XCO<sub>2</sub> fields had been published (Figure 3-4b; Yang et al. 2018). These Level 2 products were not yet distributed, but were promised in the near future. The plan is to validate these results against a comprehensive, multi-site ground-based measurement network in China as well as other internationally-recognized standards such as TCCON.

### 3.5 Sentinel 5 Precursor TROPOMI

The Copernicus Sentinel 5 Precursor (S5P) is the first of the European Sentinel satellites dedicated to monitoring of atmospheric composition. S5P was launched on 13 October 2017 and inserted into an 824-km altitude, sun-synchronous near-polar orbit with a 98.74° inclination, a 13:30 mean local time, and a ~16-day ground track repeat period. This orbit allows S5P to fly in a loose formation with the U.S. Suomi National Polar-orbiting Partnership (NPP) satellite. S5P completed its in-orbit checkout at the end of April 2018 and is beginning its 7-year mission.

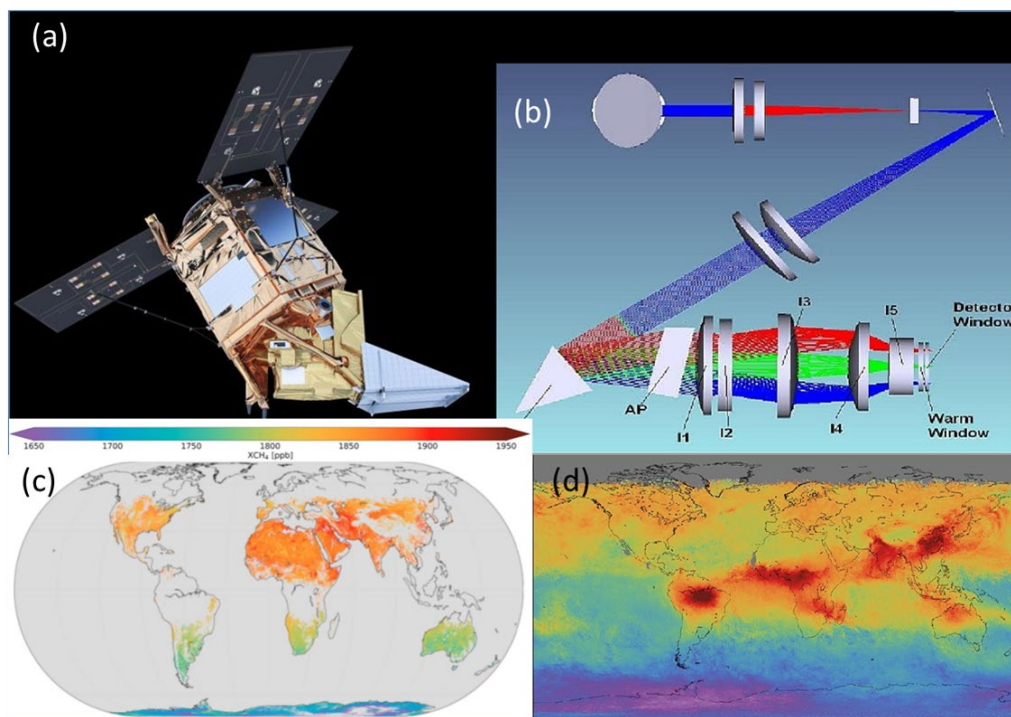


Figure 3-5: (a) Artist rendition of Sentinel-5p (Credit ESA). (b) Optical layout of the TROPOMI SWIR spectrometer including the Immersed Grating (IG), an Anamorphic Prism (AP), camera-objective lenses (I1-I5), and detector windows (image credit: SRON, TNO). (c) First map of CH<sub>4</sub> (Hu et al., 2018). (d) Preliminary map of CO (credit: SRON/ESA).

S5P carries and points a single instrument, the TROPOspheric Monitoring Instrument (TROPOMI), a wide-swath nadir-viewing push-broom imaging spectrometer developed by The Netherlands Space Office (NSO) and ESA (Figure 3-5; Veeffkind et al., 2012). TROPOMI

includes channels in the ultraviolet and visible range (270-495 nm), the NIR (675-775 nm) and the SWIR (2305-2385 nm). The NIR channel includes the O<sub>2</sub> A-band while the SWIR band covers the CH<sub>4</sub> and CO bands near 2.3 μm. The spectral resolution within the O<sub>2</sub> A-band is 0.38 nm ( $\lambda/\Delta\lambda \sim 2000$ ) while that within the CH<sub>4</sub> and CO bands is ~0.25 nm ( $\lambda/\Delta\lambda \sim 9200$ ), which is much lower than that of missions like GOSAT or OCO-2.

Besides its spectral range and relatively low spectral resolution, two features distinguish TROPOMI from other recent CO<sub>2</sub> and CH<sub>4</sub> grating spectrometers like OCO-2 and TanSat. First, TROPOMI inherits the wide-field telescope from the Ozone Monitoring Instrument (OMI), which yields observations with a near-nadir resolution of 7 km by 7 km over a 2600-km wide swath, providing high spatial resolution, 2-D images of XCO and XCH<sub>4</sub> with daily global coverage. This wide swath is resolved into 216 ground pixels, each covering a viewing angle of 0.5° (~7 km at nadir). Second, unlike OCO-2 and TanSat, which use conventional, reflective, plane holographic diffraction gratings to disperse their spectra, TROPOMI uses a silicon immersed grating as the dispersive element in the SWIR channels. This approach reduces the size and mass of the instrument. TROPOMI also differs from earlier space-based CH<sub>4</sub> sensors because it is being flown as a precursor to an operational mission (Copernicus Sentinel 5), rather than a scientific experiment.

The effort devoted to the pre-launch characterization and calibration of the TROPOMI instrument (van Hees et al. 2018; Tol et al. 2018) and the validation of its CH<sub>4</sub> and CO algorithms (Hu et al., 2016; 2018; Landgraf et al., 2016; Hasekamp et al., 2016; Borsdorff et al., 2018) provided rapid turnaround for the initial results. Only one month after the instrument was at operating temperatures, preliminary CO and CH<sub>4</sub> results were presented at the 2017 Fall Meeting of the American Geophysical Union (AGU). While these results were not yet quantitatively validated, they clearly illustrated the potential information content of 2-D imaging systems for CO and CH<sub>4</sub>. These images clearly resolved intense CO point sources over Mexico City and across northern Italy. They also showed discrete plumes from coal-fired power plants in the South African “Highveld” region (Veefkind et al. 2017). The first products, including the calibrated spectra, total columns of ozone, CO, nitrogen dioxide (NO<sub>2</sub>) and cloud & aerosol information were released to the public on July 10 2018. The first CH<sub>4</sub> products were scheduled for a later release.

### 3.6 Feng Yun-3D GAS and Feng Yun-3G GAS-2

Feng Yun 3D (FY-3D) was launched on 14 November 2017 and initiated a 6-month in-orbit checkout period. It will then enter service as the 4<sup>th</sup> satellite in the FY-3 series of Chinese polar-orbiting meteorological satellites (Figure 3-6). Once commissioned, FY-3D will begin its 5-year nominal mission from an 836 km, 98.7 degree inclination, sun-synchronous orbit with mean local time (ascending) of 14:00 (WMO OSCAR, November 2017). The FY-3 series is a cooperative program between CMA and China National Space Administration (CNSA).

FY-3D carries 10 atmospheric and space physics instruments including the Greenhouse gases Absorption Spectrometer (GAS), a high-resolution, double pendulum Fourier transform

Interferometer, similar in concept to the GOSAT TANSO-FTS. GAS has one NIR channel covering the O<sub>2</sub> A-band near 13020 cm<sup>-1</sup> (0.765 μm), and three SWIR channels covering the CO<sub>2</sub> bands near 6250 cm<sup>-1</sup> (1.60 μm) and 4850 cm<sup>-1</sup> (2.06 μm) and the CH<sub>4</sub>, carbon monoxide (CO) and nitrous oxide (N<sub>2</sub>O) bands near 4350 cm<sup>-1</sup> (2.3 μm). The NIR channel has a spectral resolution of 0.6 cm<sup>-1</sup> while the SWIR channels have a spectral resolution of 0.27 cm<sup>-1</sup>.

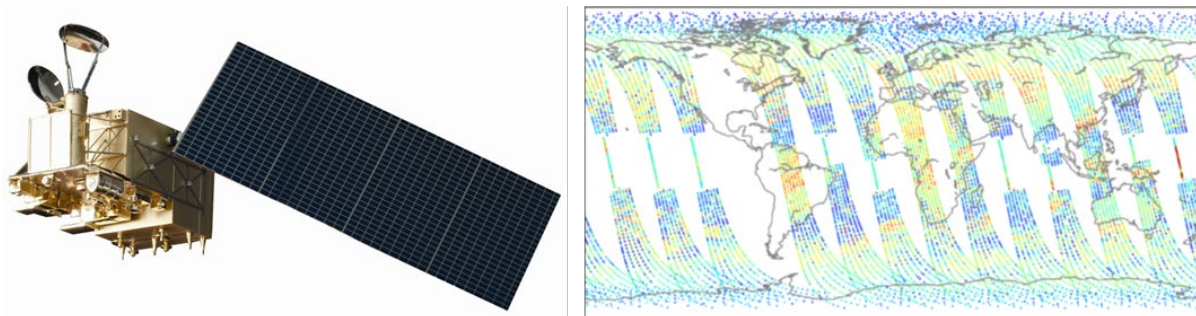


Figure 3-6: Illustration of the FY-3D satellite (left) and daily sampling pattern (right) (credit: CMA/NMSC). The scan width narrows over the ocean at low latitudes where the instrument observes the ocean glint spot.

Few details about the performance of GAS are available in the published literature. However, the June 2017 CMA report to the Coordination Group on Meteorological Satellites (CGMS) lists specifications nearly identical to of the GOSAT TANSO-FTS. The apodized spectral resolution in the 0.76-μm channel is 0.6 cm<sup>-1</sup>, while the SWIR channels have a resolution of 0.27 cm<sup>-1</sup>. The SNR values listed there are 320, 260-300, 160-300, and 140-300 in the 0.76, 1.61, 2.0, and 2.3 μm channels, respectively. The values in the first three channels are identical to those quoted for TanSat, but other aspects of the instrument performance were not available at the time of writing.

GAS collects measurements within a circular FOV with a diameter of 16 milliradian (0.9°), yielding a 13.7-km diameter surface footprint. This is slightly larger than that of the GOSAT TANSO-FTS footprint. Also like GOSAT, GAS uses a pointing mirror to direct its FOV in a grid pattern with 7 footprints across a ~1200-km wide cross-track swath, with the individual footprints separated by ~202 km cross-track and 117 km down-track (Figure 3-6; Yang et al., 2017). Estimates of the precision accuracy of its XCO<sub>2</sub>, XCH<sub>4</sub> and XCO retrievals were not available at the time this report was written.

CMA plans to deploy a second-generation CO<sub>2</sub> / CH<sub>4</sub> / CO instrument, called GAS-2, on the Feng Yun-3G, a satellite, which is scheduled to launch in the early 2020's. GAS-2 will be a broad-swath imaging grating spectrometer instead of an FTS. It will collect measurements over a 100-km swath, with a resolution of < 3 km and SNR values near 300 (Lu et al., 2017). Little additional information about this instrument is currently available.

### 3.7 GaoFen-5 GMI

GaoFen-5 is the fifth member of the China High-Resolution Earth Observation System (CHEOS) fleet of civilian remote sensing satellites flown by CNSA (Chen, 2016; Figure 3-7a). Gaofen-5 was launched on 8 May 2018 and deployed in a 708-km, sun-synchronous polar orbit with a  $98.1^\circ$  inclination, and a 13:30 mean local time (descending). Its nominal operational lifetime is 8 years.

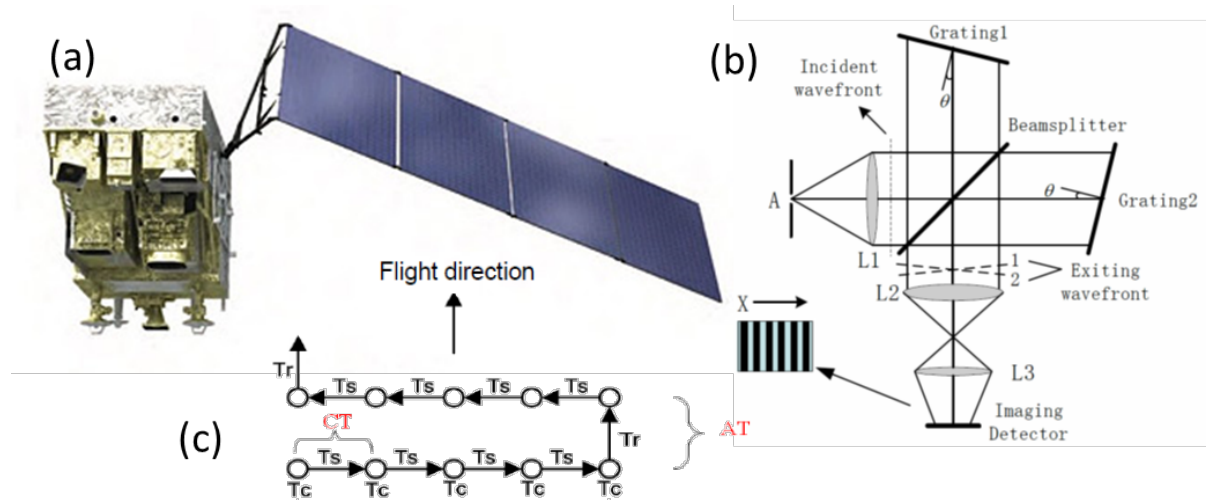


Figure 3-7: (a) Image of the GaoFen-5 spacecraft. (b) Optical layout of GMI. (c) Scan pattern of GMI (credit: Chen, 2016).

GaoFen-5 carries a suite of six instruments, including the Greenhouse-gases Monitoring instrument (GMI; Chen, 2016, Liu 2017). GMI is a 4-channel spatial heterodyne spectrometer (Harlander, et al. 1992; 2002) designed to measure the  $0.765\text{-}\mu\text{m}$   $\text{O}_2$  A-band,  $1.57\text{-}\mu\text{m}$   $\text{CO}_2$  band,  $1.65\text{-}\mu\text{m}$   $\text{CH}_4$  band, and the  $2.05\text{-}\mu\text{m}$   $\text{CO}_2$  band. A spatial heterodyne spectrometer is essentially a static Michelson interferometer with the fixed and moving mirrors replaced by fixed diffraction gratings to produce a Fizeau fringe pattern at the focus that is recorded by a 2-D focal plane array (Figure 3-7b). These instruments have been used for ground-based astronomical observations, but this is the first application to space-based  $\text{CO}_2$  or  $\text{CH}_4$  measurements. The spectral resolution is  $0.6\text{ cm}^{-1}$  in the  $\text{O}_2$  A-band and  $0.27\text{ cm}^{-1}$  in the  $\text{CO}_2$  and  $\text{CH}_4$  bands, similar to that of GOSAT TANSO FTS and FY-3D GAS (Chen, 2016). Also, like those two instruments, GMI has a 14.6 milliradian diameter circular FOV that yields a 10.3 km diameter footprint at nadir from its 708 km orbit. A 2-axis scan mirror directs the FOV to produce a grid pattern over land with 5, 7, or 9 cross-track points with along-track and cross-track distances of 100, 130, 130 km and 212, 142, 106 km, respectively (Chen, 2016; Liu, 2017; Figure 3-7c). Little additional information about this instrument or the intended accuracy and precision of its data products was available in the open literature when this report was compiled.

### 3.8 GOSAT-2 TANSO-FTS-2 and GOSAT-3

JAXA, NIES, and the MOE, are developing GOSAT-2 as a follow-on mission for GOSAT (Figure 3-8a). At the time this report was written, GOSAT-2 was preparing for a launch scheduled in October 2018. GOSAT-2 will be deployed in a 613-km, sun synchronous orbit with

a 6-day ground track repeat period and a mean local time of  $1300 \pm 15$  minutes. Like GOSAT, it has a nominal operational lifetime of 5 years.

GOSAT-2 carries two instruments, the TANSO Fourier Transform Spectrometer-2 (TANSO-FTS-2) and the TANSO Cloud Aerosol Image-2 (TANSO-CAI-2). Both instruments are substantially-upgraded versions of their predecessors. For example, while the GOSAT TANSO-FTS data yielded  $XCO_2$  and  $XCH_4$  estimates with precisions of  $\sim 0.5\%$ , TANSO-FTS-2 is being designed to return random errors near  $0.125\%$  ( $0.5$  ppm) for  $XCO_2$  and  $0.25\%$  ( $5$  ppb) for  $XCH_4$  on  $500 \text{ km} \times 500 \text{ km}$  scales at monthly intervals. In addition, a third SWIR spectral channel was added to record spectra of the CO and  $CH_4$  bands centered near  $2.3 \mu\text{m}$ . To meet its demanding new precision requirements, TANSO-FTS-2 includes larger optics ( $74 \text{ mm}$  diameter input aperture vs  $63 \text{ mm}$  for TANSO-FTS) and more sensitive detectors and readout electronics to produce larger signal to noise ratios for similar (4-second) integration times, spectral resolutions, and surface footprint sizes ( $9.7 \text{ km}$  diameter vs  $10.5 \text{ km}$  for TANSO-FTS). The spectral ranges and spectral resolution within each spectral channel have been optimized to yield improved sensitivity to  $O_2$ ,  $CO_2$  and  $CH_4$  variations.

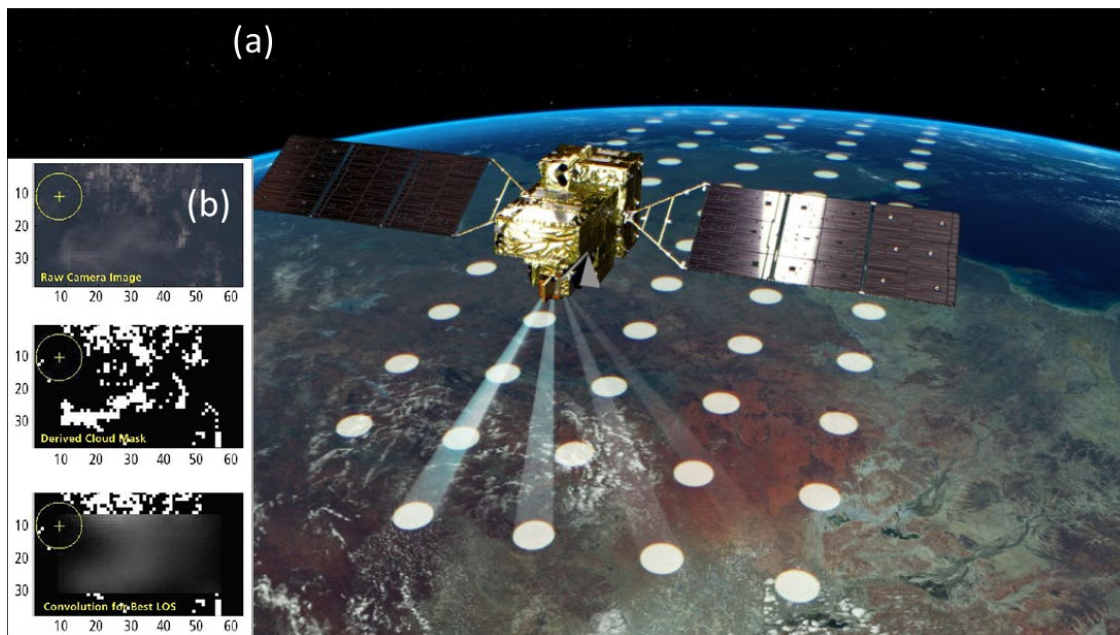


Figure 3-8: (a) Artists rendition of GOSAT-2, showing the 5-point cross-track sampling pattern (credit: JAXA). (b) Cloud-free region identification for intelligent pointing (credit: Harris Corp).

These TANSO-FTS-2 updates will be combined with an intelligent pointing algorithm that allows the instrument to select the most cloud-free of 9 possible footprint positions within a  $\sim 30 \text{ km}$  by  $50 \text{ km}$  area, which is expected to increase the number of cloud-free soundings by more than a factor of 2 (Figure 3-8b). The sub-nadir scan range has been expanded to facilitate observations of the bright ocean glint spot over twice the range of latitudes to improve the instrument's sensitivity to  $CO_2$  changes over the ocean. The expanded glint coverage is also expected to yield factor of 2 increase in the number of glint soundings collected each day.

TANSO-CAI-2 also includes improvements in performance to meet the much more demanding GOSAT-2 goals. For example, while TANSO-CAI was a nadir-viewing push-broom radiometer, TANSO-CAI-2 includes both forward-looking and backward looking channels, inclined at  $\pm 20^\circ$  of nadir. It also includes new or modified channels in the near ultraviolet (333-353 nm), blue (443-453 nm), and visible (540-560 nm). These changes are expected to improve the accuracy of aerosol optical depth retrievals.

The Japanese GOSAT/GOSAT-2 partners have initiated discussions of GOSAT-3, as a follow-on to GOSAT-2. As currently conceived, GOSAT-3 will be deployed in 2023 and will measure  $\text{CO}_2$ ,  $\text{CH}_4$ , and  $\text{CO}$  with substantially better spatial resolution and coverage than GOSAT and GOSAT-2. Both broad-swath imaging grating spectrometers and imaging FTS instruments were being studied at the time this report was compiled. Other details, including the orbit and lifetime were not yet available.

### 3.9 OCO-3

As part of the OCO-2 mission, NASA authorized the development of a flight spare instrument to minimize schedule impacts of any delays introduced by problems with the flight instrument development. In 2012, NASA approved plans to adapt this instrument for deployment on the Japanese Equipment Module Exposed Facility (JEM-EF) on the International Space Station (ISS) as the Orbiting Carbon Observatory-3 (OCO-3) mission (Figure 3-9a, b).

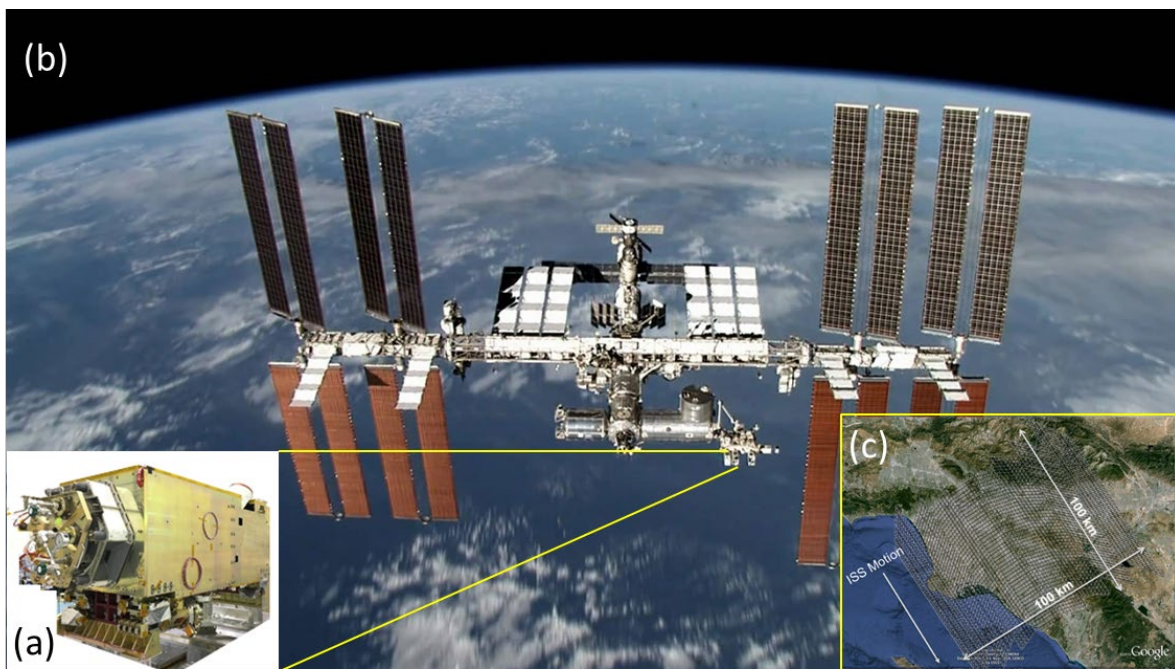


Figure 3-9: (a) The OCO-3 instrument will be deployed on the JEM-3F module on the ISS (b) in 2019. (c) The snapshot mode of its fast, 2-axis pointing mechanism will allow OCO-3 to map out areas as large as 100 km  $\times$  100 km as it flies over the Los Angeles basin or other compact  $\text{CO}_2$  sources (credit: JPL/NASA).

Because OCO-3 incorporates the OCO-2 flight spare instrument assembly, its physical characteristics, capabilities, and performance are expected to be very similar to those of the OCO-2 instrument. For OCO-2, the instrument's field of view is pointed by the spacecraft bus. To enable glint and target pointing capabilities from the nadir-pointing ISS, an agile, 2-axis pointing mechanism was added to the OCO-2 flight spare instrument. The pointing system introduces varying polarization angles for glint and target measurements. This change, combined with modifications of the telescope to maintain a footprint size similar to that of OCO-2 from the much lower (~350 km) ISS orbit, introduces a range of signal to noise values for OCO-3 that includes both lower and higher values than those seen by OCO-2. The pointing system also provides new opportunities for mapping compact targets, such as cities, power plants, or coastlines. For example, this mechanism can map out 100-km by 100-km areas to characterize the XCO<sub>2</sub> distribution within a large urban area (Figure 3-8c).

Unlike all earlier space-based CO<sub>2</sub> sensors that have flown in near-polar, sun-synchronous orbits, ISS flies in a low inclination orbit, which overflies latitudes equatorward of 51°. This orbit precludes coverage of higher latitudes, but provides somewhat better coverage of mid-latitudes where human activities emit the most CO<sub>2</sub>. Mid-latitude measurements from OCO-3 would be most easily interpreted if they were acquired along with others from a polar orbiting system, like OCO-2 or GOSAT. The orbit precession will allow OCO-3 to sample different parts of the Earth at different times of day. This will provide the first opportunity to search for variations in XCO<sub>2</sub> and other carbon cycle variables, such as SIF, across the entire range of local times, from dawn to dusk, from a single space-based platform.

The deployment of OCO-3 on the ISS will also enable synergistic measurements of terrestrial ecosystem properties with other co-manifested instruments, including the NASA Global Ecosystem Dynamics Investigation (GEDI), and Ecosystem Spaceborne Thermal Radiometer Experiment on Space Station (ECOSTRESS) and the JAXA Hyperspectral Imager Suite (HISUI). GEDI will measure of the three-dimensional structure of the canopy, ECOSTRESS will measure the water use efficiency, and HISUI will measure the canopy composition. These data can be combined with OCO-3 XCO<sub>2</sub> and SIF observations to provide a unique, diurnally-varying description of the ecosystem productivity (Stavros et al., 2017).

The OCO-3 instrument completed final testing as this document was being written. It will be launched to the ISS in the “trunk” of the Falcon 9 Dragon as part of a resupply mission in early 2019. It will then be installed in Exposed Facility Unit 3 (EFU3) on the JEM-EF for a 3-year nominal mission.

### 3.10 MicroCarb

MicroCarb is the first European satellite specifically designed to measure atmospheric CO<sub>2</sub> from space with the precision and resolution needed to characterize CO<sub>2</sub> sources and sinks at regional scales (Figure 3-10). MicroCarb being developed by the French Space agency, Centre National d'Études Spatiales (CNES), in partnership with several research organizations and with the United Kingdom Space Agency (UKSA).

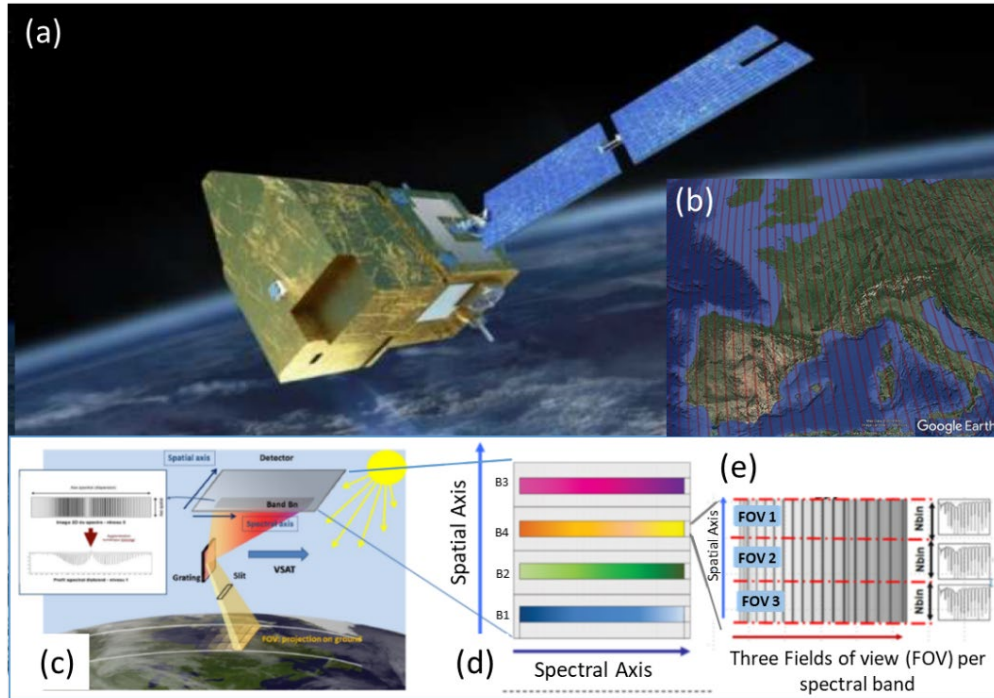


Figure 3-10: (a) Artist's concept of MicroCarb satellite in orbit. (b) Spatial distribution of ground tracks over Europe for a descending orbit. (c) The compact, 4-channel spectrometer collects spatially-resolved spectra in push-broom fashion. (d) All 4 spectral ranges are recorded on different parts of a single  $1024 \times 1024$  pixel FPA. (e) Spatially-resolved spectra are collected in three cross-track footprints in each range.

The MicroCarb satellite carries two instruments. The  $\text{CO}_2$  instrument is a compact, high-resolution, 4-channel, imaging Echelle grating spectrometer. It is accompanied by an imager that uses a single broad filter, centered at  $0.625 \mu\text{m}$  to facilitate the detection and screening of soundings contaminated by clouds.

To minimize the size of the  $\text{CO}_2$  spectrometer, a split-pupil telescope is used to image the same instantaneous FOV onto the 4 spatially separated spectrometer slits. In addition, the spectra produced by all four channels will be recorded on a single 2-D focal plane array (Figure 3-10c, d). The spectrometer channels measure the absorption of reflected sunlight in  $\text{O}_2$  A-Band at  $0.76 \mu\text{m}$  and  $1.27 \mu\text{m}$  bands and the  $\text{CO}_2$  bands near  $1.61$  and  $2.06 \mu\text{m}$ . Each channel has a spectral resolving power,  $\lambda/\Delta\lambda \sim 26,000$  and SNR values similar to those of OCO-2 and OCO-3. A polarization scrambler deployed in front of the entrance telescope makes the instrument insensitive to the polarization due to the observed scenes or scattering aerosols, thus eliminating a potential cause for regional bias. The scrambler also avoids the loss of flux for highly-polarized scenes (e.g. observation over oceans).

The  $1.27 \mu\text{m}$  channel has not been included in other space missions designed for  $\text{CO}_2$  monitoring due to airglow contamination in the  $\text{O}_2$   $^1\Delta_g$  band. Radiative transfer studies performed during the MicroCarb preparation phase concluded that this airglow contribution can be distinguished from the  $\text{O}_2$  absorption if the spectral resolution and SNR are adequate. The  $1.27 \mu\text{m}$  channel can then be used in combination with the  $0.76 \mu\text{m}$  channel to estimate the surface pressure, dry air mass,

and atmospheric optical path length, which are affected by the presence of scattering by aerosols and clouds. If the airglow contamination can be removed, the 1.27  $\mu\text{m}$  channel has two potential advantages over the 0.76  $\mu\text{m}$  band, which has been used for XCO<sub>2</sub> normalization by other similar missions. First, the absorption lines are not saturated, providing more sensitivity to the dry air mass. Second, the band is spectrally closer to the 1.61 and 2.06  $\mu\text{m}$  CO<sub>2</sub> bands, potentially reducing optical path length biases introduced by uncertainties in the wavelength-dependent optical properties of aerosols.

All four channels record three simultaneous, co-boresighted samples across a  $\sim 21$  milliradian ( $1.2^\circ$ ) wide cross-track FOV at  $\sim 1.3$  second intervals, yielding sounding footprints that are  $\sim 4.5$  km x 9 km at nadir. A single-axis scan mirror mechanism can direct the FOV over a  $\pm 35^\circ$  range which, in combination with the satellite agility, permits the instrument to collect science observations at nadir, glint, or over stationary targets, such as TCCON stations. It can also acquire separated samples over a  $\pm 200$  km-wide grid pattern, or over a contiguous 40-km by 40-km area to map out the XCO<sub>2</sub> distribution within an urban area. In addition, the scan mechanism can direct the FOV to a lamp or solar port for calibration or to the limb to characterize the airglow within the O<sub>2</sub>  $^1\Delta_g$  band at 1.27  $\mu\text{m}$ . With these science observation and calibration capabilities, the MicroCarb mission is expected to yield XCO<sub>2</sub> estimates with single sounding random errors between 0.5 and 1 ppm and regional-scale biases  $< 0.2$  ppm.

The MicroCarb project is currently in its realization phase (Phase C), with the integration of both the instrument and the spacecraft starting in 2019. It is expected to launch as early as 2021 as a secondary payload. It is being designed to operate for at least 5 years in a 649 km sun-synchronous orbit with a 25-day ground track repeat period. The mean local time will either be 10:30 (descending) or 13:30 (ascending), depending on launch opportunities, which were still under review when this document was written.

### 3.11 Sentinel 5 UVNS

The Copernicus Sentinel 5 mission will deploy the Ultra-Violet/Visible/Near Infrared/SWIR (UVNS) Spectrometer on the MetOp-SG-A spacecraft, an operational meteorological satellite operated by the European Organisation for the Exploitation of Meteorological Satellites (EUMETSAT). The primary objective of the mission is to monitor reactive gases (ozone, nitrogen dioxide, sulfur dioxide, formaldehyde, CO), CH<sub>4</sub> and aerosol optical depth operationally. The first MetOp-SG-A spacecraft is scheduled for launch in 2021 and is expected to have a 7.5-year nominal lifetime. The current plan is to launch pairs of identical satellites at 7-year intervals to yield a system lifetime of 21 years. MetOp-SG-A will launch into an 817-km, sun synchronous orbit with a  $98.7^\circ$  inclination, a mean local time (descending) of 09:30, and a 29-day (412 orbit) ground track repeat period.

The MetOp-SG-A carries 8 instruments including UVNS, a push-broom imaging spectrometer. UVNS inherits the wide-field telescope from TROPOMI and adds a slit homogenizer to reduce errors introduced by non-uniform illumination of the spectrometer slit. It includes 6 spectral channels covering the spectral regions from 270-310 nm (UV1), 300-500 nm (UV2VIS), 685-

710 nm (NIR1), 745-755 nm (NIR2a), 755-773 nm (NIR2), 1590-1675 nm (SWIR-1) and 2305-2385 nm (SWIR-3). The NIR2 channel includes the O<sub>2</sub> A-Band, the SWIR-1 channel includes the CO<sub>2</sub> band near 1.61 μm and the CH<sub>4</sub> band near 1.67 μm, and the SWIR-3 channel covers the CH<sub>4</sub> and CO bands near 2.3 μm (Figure 3-11). The NIR2 channel has a spectral resolution of 0.4 nm ( $\lambda/\Delta\lambda \sim 1900$ ), while the spectral resolution of the SWIR1 and SWIR3 bands is 0.25 nm ( $(\lambda/\Delta\lambda \sim 6440$  and 9200, respectively). This is comparable to the resolution of TROPOMI, but substantially lower than that of other CH<sub>4</sub> monitoring missions.

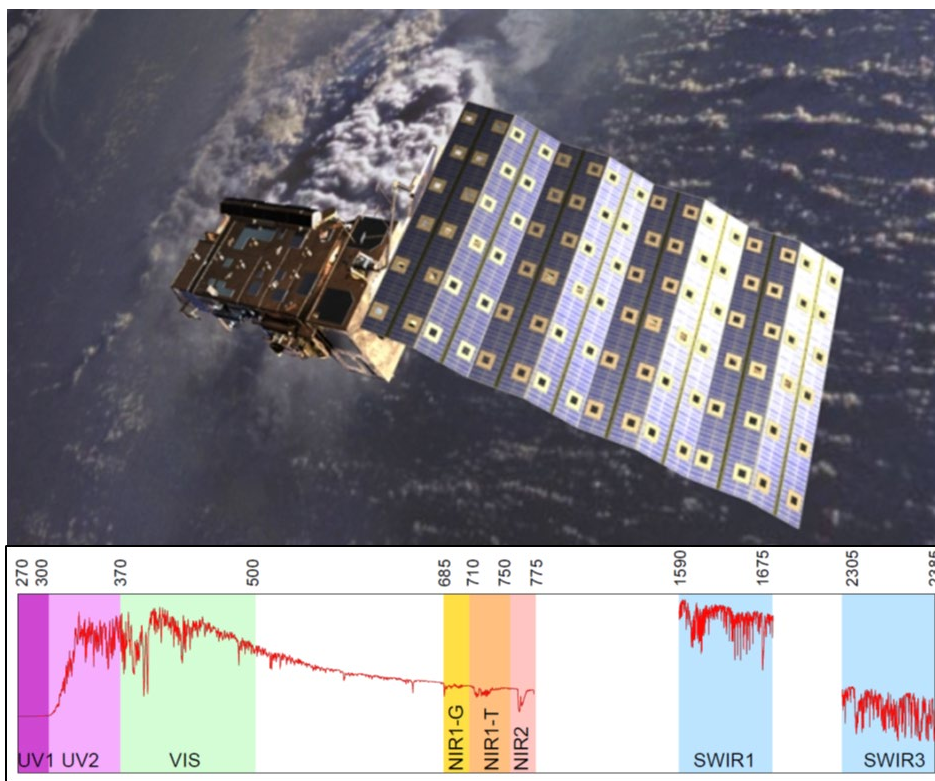


Figure 3-11: Top – Artist’s rendition of the MetOp-SG spacecraft in orbit. Bottom: spectral ranges covered by the UVNS instrument. XCH<sub>4</sub> will be retrieved from SWIR3 (credit: ESA).

Like TROPOMI, UVNS employs a wide swath (108.4°, ~2715 km) and a 1-Hz readout time to yield 7 km x 7 km footprints near nadir and near-global coverage at latitudes > 12° every day. The SWIR 3 channel is expected to yield CO and CH<sub>4</sub> results with sensitivities comparable to those produced by TROPOMI.

### 3.12 GeoCarb

The NASA Geostationary Carbon Cycle Observatory (GeoCarb) is the first satellite designed to collect spatially resolved observations of the column-averaged dry air mole fractions of CO<sub>2</sub>, CH<sub>4</sub>, CO and SIF from geostationary orbit (GEO). The GeoCarb mission is currently under development for a mid-2022 launch as a hosted payload on an SES Government Solutions satellite that will be deployed in a GEO orbit between 75° and 100° West longitude. From this

vantage point, its high-resolution imaging spectrometer will produce maps of XCO<sub>2</sub>, XCH<sub>4</sub>, XCO and SIF at a spatial resolution of 10-20 km at latitudes as high as 50° over North and South America several times each day in order to better understand the natural and anthropogenic carbon cycles on regional scales.

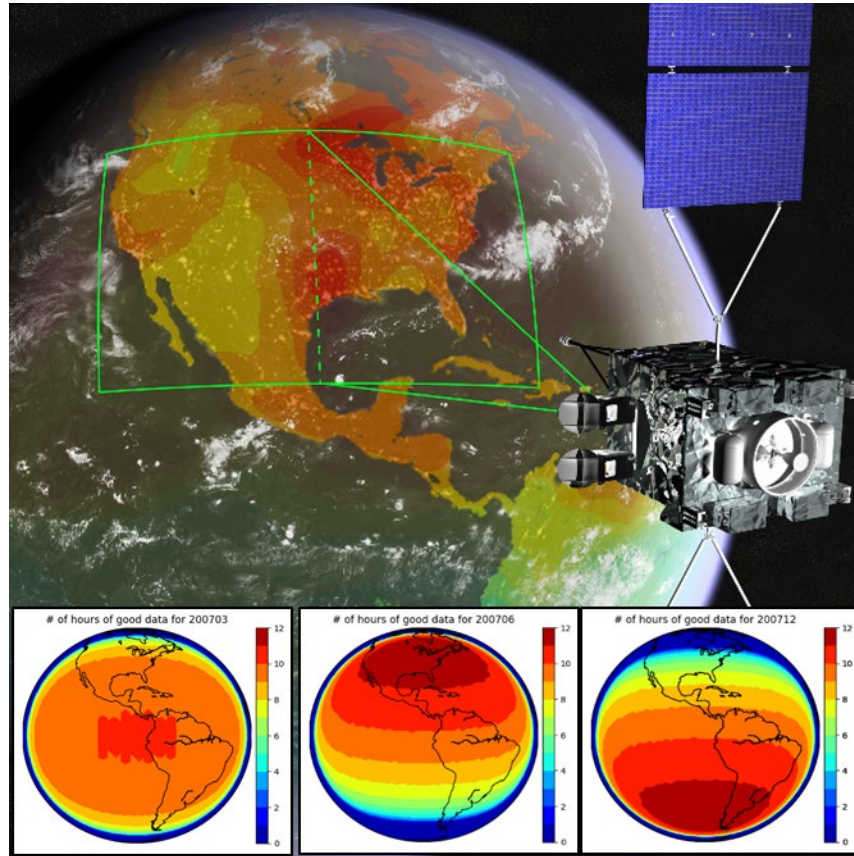


Figure 3-12: (Top) Artist's rendition of the GeoCarb host spacecraft over the western hemisphere. (Bottom) From this GEO vantage point, the number of hours of illumination over visible hemisphere changes with season from March (left) to June (center) to December (right).

GeoCarb carries a 4-channel imaging grating spectrometer that records high-resolution spectra ( $15,000 < \lambda/\Delta\lambda < 16100$ ) of O<sub>2</sub> and SIF near 0.765  $\mu\text{m}$ , CO<sub>2</sub> near 1.61  $\mu\text{m}$  and 2.06  $\mu\text{m}$ , and CH<sub>4</sub> and CO near 2.320  $\mu\text{m}$ . The spectrometer's field of view is defined by a 0.15 milliradian (0.0086°) wide by 77-milliradian (4.4°) long slit. The long axis of the slit is resolved into 1016 ~12 km by ~3 km footprints along a 2750-km field of view that is oriented north-south, and scanned east-west to yield spatially-contiguous 2-D images. The instrument field of regard can be scanned  $\pm 10^\circ$  east-west and  $\pm 9.25^\circ$  north-south of the sub-spacecraft nadir. From the ~36000 km altitude, this scan range covers most of South America, Central America, and North America at latitudes between 50° S and 50° N at least twice each day, although the available illumination changes somewhat with season (Figure 3-12). Selected regions will be observed at more frequent intervals. GeoCarb is not designed to collect data over the oceans, as the reflectivity over the oceans is too low to provide useful data without glint illumination (Polonsky et al., 2014; O'Brien et al. 2016).

The GeoCarb data will cover the major urban and industrial regions in the Americas, large agricultural areas, and the expansive South American tropical forests and wetlands. GeoCarb maps will be analyzed to resolve the variability in CO<sub>2</sub>, CH<sub>4</sub>, and CO fluxes and to provide critical insight into the relationship between the carbon cycle and climate change. By demonstrating that GeoCarb can be flown as a hosted payload on a commercial satellite, the mission will strengthen NASA’s partnerships with the commercial satellite industry and provide a model that can be adopted by NASA’s international partners to expand these observations to other parts of the world.

### 3.13 MERLIN

The Methane Remote Sensing Lidar Mission (MERLIN) is currently scheduled for launch in mid-2024 timeframe. It will be deployed in a 500 km altitude, sun-synchronous orbit with a 06:00/18:00 mean local time, a 97.4° inclination, and a 28-day revisit time (Ehret et al., 2017). MERLIN is a joint mission by the German Space Agency (DLR), which is in charge of payload and part of ground segments, and the French Space Agency (CNES), which is responsible of the platform, system and launch as well as the general ground segment. This project is being executed as a strong partnership with French and German science organizations (leadership at LSCE and DLR Institute).

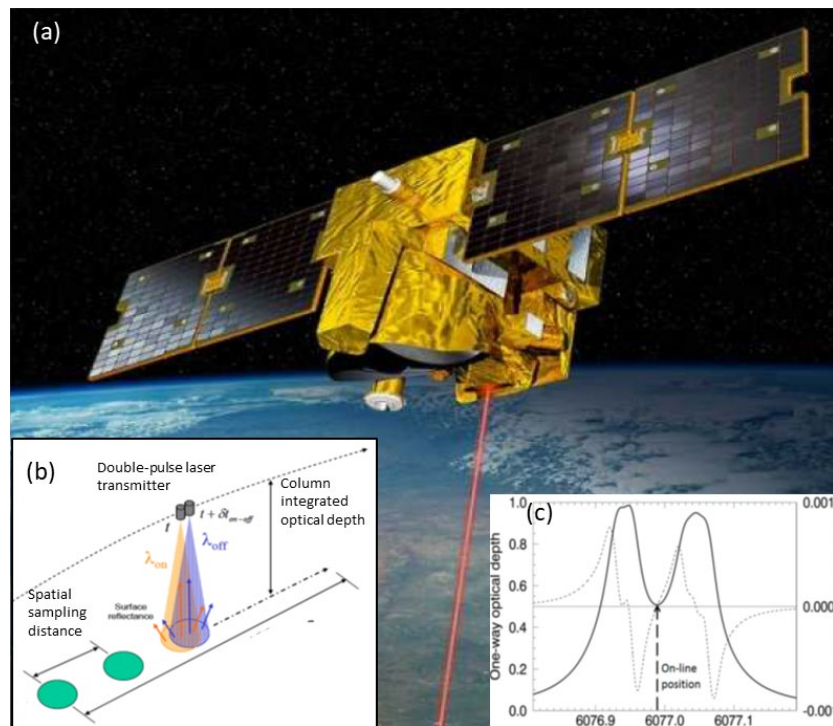


Figure 3-13: (a) Artist’s rendition of the MERLIN spacecraft in orbit. (b) Illustration of the IPDA measurement approach, where on-line and off-line measurements are acquired in succession. (c) A substantial relaxation in the frequency knowledge requirement for the on-line measurement was achieved by selecting a frequency between two overlapping CH<sub>4</sub> lines (credit: MERLIN/CNES).

MERLIN is the first mission to use Integrated Path Differential Absorption (IPDA) Light Detecting and Ranging (Lidar) for measuring XCH<sub>4</sub> (Figure 3-13). It will therefore be the first space-based sensor that can provide the observations needed to estimate CH<sub>4</sub> sources at high latitudes in the winter hemisphere, when the sun is too low to provide adequate signal for passive SWIR sensors. Because the lidar transmits and receives photons along a near-vertical path, MERLIN is expected to yield a higher fraction of useable soundings in partially cloudy regions, where passive measurements are compromised by cloud reflections and cloud shadows. These observations should contribute to our understanding of the regional distribution of CH<sub>4</sub> fluxes in partly cloudy regions, including emissions hot spots in the Tropics.

The primary strength of this active sensing approach is that it can collect measurements during both day and night, in all seasons and at all latitudes. The MERLIN lidar transmitter uses an Optical Parametric Oscillator (OPO) that is pumped by a Nd:YAG laser. For each single measurement, the lidar emits two 20-nanosecond pulses at two frequencies around a methane line multiplet at 1.64  $\mu\text{m}$ . The temporal separation of these pulses is 250 microseconds while the measurement frequency is 20 Hz. One wavelength is locked to a spectral feature of the CH<sub>4</sub> absorption manifold while the other frequency is selected to have negligible CH<sub>4</sub> absorption and is used as the reference. The receiver uses an avalanche photodiode to detect the reflected pulses (Ehret et al., 2017; Bousquet et al., 2018).

The very narrow ( $\sim 120$  m), near-nadir beam and selective sampling techniques will allow MERLIN to collect some useful data in partially cloudy regions. However, unlike passive instruments, the lidar will not make an oxygen measurement to infer the dry air mass. Instead, the retrieval algorithm will use assimilated meteorological data products for surface pressure, temperature, and water vapor information. The expected XCH<sub>4</sub> measurement precision is  $\sim 27$  ppb over a 50-km track. The ambitious target for systematic errors is  $< 3.7$  ppb on regional scales. With these capabilities, it is expected to significantly improve our knowledge of methane sources from global to regional scales, with emphasis on poorly-accessible regions at high latitudes in the winter hemisphere and in cloudy regions in the Tropics.

### 3.14 Future mission concepts being studied

In addition to the CO<sub>2</sub> and CH<sub>4</sub> missions described above, several others are in the early planning stages. These include the Chinese Feng Yun-3G and Japanese GOSAT-3 satellites mentioned above. A GHG mission was also recommended in the US National Academy's Earth Science Decadal Survey as one possible concept that could compete as part of the newly-defined Earth Science Explorer program.

An ambitious CO<sub>2</sub> Sentinel constellation is under development by the European Commission Copernicus Programme (Ciais et al. 2015; Pinty et al., 2017). This constellation will deploy 3 or 4 broad-swath (200-350 km) imaging grating spectrometers CO<sub>2</sub>, CH<sub>4</sub>, and NO<sub>2</sub> from spacecraft in LEO. The objective is to yield global, high spatial resolution (2 km x 2 km) operational images of XCO<sub>2</sub> and XCH<sub>4</sub> distributions at daily to weekly intervals. The approach adopted for defining the requirements for this constellation is described in Chapter 5.

In China, the Shanghai Advanced Research Institute (SARI) and Shanghai Engineering Center for Microsatellites (MicroSat) in the Chinese Academy of Sciences and ShanghaiTech University have begun working on a constellation of CO<sub>2</sub>/CH<sub>4</sub>/CO satellites, called TanSat-2. As currently conceived, this constellation will include 6 satellites, with 3 flying in morning sun-synchronous orbits and 3 flying in afternoon sun-synchronous orbits. The primary instrument on each satellite will measure CO<sub>2</sub> (1.61 and 2.06 μm), CH<sub>4</sub> and CO (2.3 μm) as well as the O<sub>2</sub> A-band (0.76 μm) across a 100-km cross-track swath.

Other GHG missions are being developed by commercial organizations and non-governmental organizations (NGOs) including GHGSat, Bluefield Technologies, and the Environmental Defense Fund. These satellites complement the global space-based monitoring capabilities being deployed by CEOS agencies by collecting high spatial resolution images of intense CH<sub>4</sub> emission plumes, rather than global monitoring. These missions are described in Appendix-5 for completeness.

## 4. The Transition from Science Missions to an Operational Constellation

Today, all existing and planned SWIR CO<sub>2</sub> and CH<sub>4</sub> missions, with the exception of the Sentinels, are “science” missions, developed to address specific, well-defined scientific questions and to identify optimal methodologies for measuring CO<sub>2</sub> and CH<sub>4</sub>. The initial phases of a scientific mission generally involve extensive scientific assessment and development within the scientific project team before results and data are made available to the wider community.

The focus of an operational mission is fundamentally different in that the final aim is to produce an overall end-to-end system to provide end users with products and services for a set of well-defined user needs. In this case, the objective is to deliver policy-relevant CO<sub>2</sub> and CH<sub>4</sub> products focused on anthropogenic emissions within a specified time frame. While a strong scientific underpinning is required for an operational mission, pure research and scientific investigation is not the primary focus. Operational systems are specifically designed to provide robust, long-term delivery of products and services with a guaranteed quality, reliability and timeliness. Additional services such as user support, training, data preservation, and reprocessing capabilities are also typically provided by an operational system.

Following the model developed by the operational meteorological satellite operators, any future CO<sub>2</sub>/CH<sub>4</sub> constellation will also need to focus on orbit and mission coordination, data distribution, data exchange, and data format requirements, including relevant ancillary and meta-data. Robustness of the overall system, including the satellite component, and the ability to ensure high quality observations in a changing environment are of particular importance. For this application, free and open data policies will be critical to ensure the traceability and support the Transparency Framework of the Paris Agreement. Finally, to fully exploit these data from future CO<sub>2</sub>/CH<sub>4</sub> constellations, the missions will also have to invest in training and capacity building, as well as public outreach. CEOS should exploit the experience of WMO, CGMS and other organizations to foster the development of these capabilities. Other specific changes needed to transition from a series of scientific missions to an end-to-end operational system are summarized in the following subsections.

### 4.1 User Requirements Process

The overall performance of an operational system is driven by the requirements of the end user of the products and services to be provided by the system. In order to establish these requirements, a consultation process with the end users is required. This process will allow the basic characteristics of the system, such as observation requirements, timeliness, accuracy, frequency of product generation and so forth, to be determined. This is typically an iterative process to allow for user involvement in any critical trade-off decisions to be taken during system design. The final, end-user requirements will underpin the design of the overall system and provide requirements against which the performance of the overall system can be verified.

## 4.2 Timeliness

Timeliness requirements in operational systems are typically driven by end user needs. An end-to-end requirement for data product latency and services must be allocated to requirements for timeliness of all elements of the system including data acquisition, data reception, processing and dissemination, and the requirement for production of higher-level products. There can also be tradeoffs between the requirements for timeliness and reliability, as a more relaxed data latency requirement can provide opportunities for backlog processing in case of data loss via transmission outages, for example. The overall system design may also drive timeliness requirements in terms of pipe-line processing versus off line processing of data.

For operational meteorological systems, data must be delivered in near real time to meet timeliness requirements. Near-real time dissemination may or may not be required for anthropogenic greenhouse gas emission monitoring. Yet, the end-to-end operational system must still be designed to deliver data to the end user community reliably, within the required time for data dissemination, throughout the mission lifetime.

## 4.3 Reliability and Robustness

An operational system is expected to be reliable with pre-defined service levels that must be met for delivery of products and services. All elements of the system that can potentially impact the delivery of products or services must be considered in the assessment of reliability. This includes any observation infrastructure (ground-based, satellite, or others), data transmission, processing and dissemination systems etc. In order to guarantee reliability, redundancy is usually required in the system and a robust, forward planning process is essential to ensure continuity of service. The degree of redundancy that is implemented will typically be part of a risk to cost analysis and should account for the availability of infrastructure from other contributing systems.

Reliability and robustness also require that all elements of the system are robust to changes in observing conditions over the mission lifetime, including changes of the space, atmosphere, surface and ground reception and processing environment. This is especially relevant and demanding for a mission addressing the long-term monitoring of a changing environment.

## 4.4 Traceability and Configuration Management

An operational product or service must be fully traceable in terms of the observations, auxiliary data, and versions of data processing systems used in the product generation. This implies that all products and services must be produced in a configuration-controlled environment, including the use of well-defined and documented product release processes. Use of configuration management systems is essential. This is of particular importance if the products or services are expected to be used in a regulatory environment. For full traceability and transparency, it is also

required that documentation of the end-to-end systems, including the scientific basis for, and validation of, the data products and services are also available and configuration-controlled.

#### 4.5 Reprocessing, Reproducibility and Data Preservation

An operational system must also be fully capable of reproducing data, products, and services on the basis of a fully-traceable configuration-controlled environment. A necessary requirement for reproducibility is also data preservation and archiving, including all ancillary, instrument characterization or other data required for the data processing. This may necessitate duplication of data archives for redundancy and security purposes. The capability for reprocessing of long-term data sets to take advantage of improvements in data processing, advances in scientific knowledge and policy needs or constraints, or to account for changing instrument performance is also an important capability that needs to be built into the overall system design.

#### 4.6 Quality Assurance

Quality Assurance is an essential pillar of any successful operational system. This implies that not only should the quality of the final products be demonstrated by comparison to external validation sources, a comparison that should be documented in a validation report, but also that all elements of the overall system should be verified, documented and that products are produced using well defined processes which also contributes to the guarantee of the final quality of the product. Traceability and configuration management are important elements of quality assurance.

#### 4.7 Calibration and Validation Monitoring and Reporting

An operational system requires continuous calibration of the end-to-end system at the instrument and ground-processing level, in order to ensure that product quality is maintained over the full mission lifetime. This monitoring must often be performed in the context of changing instrument performance, as well as changing observation environments and requires the continuous evaluation of instrument performance and validation of product quality. Routine and continuous monitoring and reporting to facilitate early recognition of product processing and delivery issues is essential. In order to support this activity, it is necessary to put automated monitoring and reporting functions in place and to ensure the availability of routinely available ground-based or other validation data sets. These data sets are also required to be made available in a timely, traceable, configuration-controlled manner. This implies the need to ensure long-term continuity of resources to support the provision of such validation data to ensure long-term traceable maintenance of product quality.

## 4.8 User Support

A fully operational system should also provide a User Helpdesk with defined levels of service and the ability to respond appropriately and in a timely manner to user requests, track responses to user queries, issue announcements of upcoming processor or product changes, and alert users to outages in service provision. Training and public outreach is also an element of user support and can facilitate improved uptake of products and services as well as provide the opportunity for users to familiarize themselves with the upcoming or new products or services by provision of advance test data and hosting of User preparation workshops.

## 4.9 International Coordination and Long-Term Planning

An additional element to consider when establishing an operational system, particularly one involving high cost assets such as satellite systems, is international coordination, cooperation and partnership. These elements are particularly important in the design of an overall constellation to optimize the use of available resources, facilitate the smooth and controlled sharing of data, including in the definition of product formats and to introduce redundancy in the system. International coordination in the meteorological context is facilitated by such bodies as the Coordination Group on Meteorological Satellites (CGMS) and by the WMO Space Program. These organizations promote availability and utilization of satellite data and products for weather, climate, water and related applications to WMO Members and coordinate environmental satellite matters and activities throughout all WMO Programs. They also provide guidance on the potential of remote-sensing techniques in meteorology, hydrology and related disciplines. These activities are further supported by bilateral agreements between partner Agencies.

There is extensive experience in the operational meteorological community, and in particular the operational meteorological satellite operators, in all aspects described above. This experience can be usefully applied to the development of a robust operational anthropogenic CO<sub>2</sub> and CH<sub>4</sub> monitoring capability.

## 5. Designing an Operational LEO Constellation for Measuring Anthropogenic CO<sub>2</sub> Emissions – The Sentinel CO<sub>2</sub> Initiative

The European Commission (EC) and the European Space Agency (ESA) are considering the further development of the first generation Copernicus Space Component. Among the highest priorities is a self-standing, robust and operational global observation system for monitoring anthropogenic emissions of CO<sub>2</sub>. Together with the support of the European Organisation for the Exploitation of Meteorological Satellites (EUMETSAT) and the European Centre for Medium-range Weather Forecasts (ECMWF), the EC and ESA have initiated several studies to support this decision. Based on the recommendations documented by a team of experts (Ciais et al. 2015), a pair of task forces were established. Task Force A defined the preliminary requirements for the space-based elements of a CO<sub>2</sub> monitoring constellation. Task Force B defined the remainder of an end-to-end system for monitoring CO<sub>2</sub>. In early 2018, Task Force A completed the first version of the Mission Requirements Document (MRD) for the satellite system, and was replaced by an international Mission Advisory Group (MAG) to oversee studies of the satellite system, which then transitioned to the preliminary design phase (Phase A/B1) and evolve the MRD. An outline of the intended overall capability is described in this chapter, together with details related to the space component.

### 5.1 Copernicus Evolution to anthropogenic CO<sub>2</sub> emissions monitoring

Because Copernicus is a user-driven program, the first step in its evolution was the collection of User Requirements, which were then expressed in terms of Observation Requirements. The importance and pertinence of a Copernicus data or information product group is also determined by its capability to provide useful information to the policy sectors of the European Union. In this context, the Union has reinforced its strategy from 2020 to 2050 to tackle climate change at European and international levels (COM, 2011). This includes climate adaptation and mitigation, emission trading, reduction of CO<sub>2</sub> and CH<sub>4</sub> emissions, monitoring of emissions from forestry and agriculture, support of international climate action, efficient use of energy sources, and transition to renewable energy.

Based on these factors, a preliminary list of additional measurements that would complement the existing data for climate change services was identified. This list included measurements that could be analyzed to estimate anthropogenic CO<sub>2</sub> emissions. This high-level requirement was supported unanimously by the participants of the Workshop on Copernicus User Requirements, organized by the Commission on September 14, 2017. An anthropogenic CO<sub>2</sub> emissions monitoring system was also requested in a resolution of the European Parliament "Towards a new international climate agreement in Paris" (2015/2112(INI) see: <http://www.europarl.europa.eu/sides/getDoc.do?pubRef=-//EP//TEXT+REPORT+A8-2015-0275+0+DOC+XML+V0//EN>). Furthermore, the potential of atmospheric measurements to support the Paris Agreement has recently been recognized by the Subsidiary Body for Scientific and Technological Advice (SBSTA) of UNFCCC (3), which stated: "The SBSTA noted the

increasing capability to systematically monitor greenhouse gas concentrations and emissions, through *in situ* as well as satellite observations, and its relevance in support of the Paris Agreement" (see <https://unfccc.int/resource/docs/2017/sbsta/eng/l21.pdf>).

In the context of the Copernicus Programme and its evolution, in 2015 the Commission tasked an international group of experts to propose a roadmap for monitoring anthropogenic CO<sub>2</sub> emissions. The overarching objective was to provide the European and international community with the capability to assess the effectiveness of the Paris Agreement and COP21 decisions with regard to their impacts on anthropogenic CO<sub>2</sub> emissions and the overall CO<sub>2</sub> budget at country and regional/megacity scales. This expert group recommended the implementation of a Copernicus CO<sub>2</sub> Monitoring system based on spatial images of atmospheric CO<sub>2</sub> from space-based observations (Ciais et al., 2015). The required spatial and temporal coverage could be provided by a constellation of CO<sub>2</sub> satellites. In addition, the expert group has highlighted the need for a strong ground-based infrastructure consisting of a measurement component with *in situ* networks and an integration component involving global and regional scale modelling together with statistical inventories.

To quantify anthropogenic CO<sub>2</sub> emissions and their trends at the scale of large urban areas, important industrial sites, nations, and the Earth as a whole, an operational system is needed that integrates four complementary components:

1. Atmospheric CO<sub>2</sub> measurements obtained from dedicated space-borne sensors, complemented by *in-situ* networks and ancillary observations;
2. The operational provision of bottom-up fossil fuel CO<sub>2</sub> emission maps and other anthropogenic emission maps (i.e. biomass burning, land use change), with high spatial and temporal resolution, and short time updates;
3. An operational data-assimilation system, which will integrate atmospheric measurements with bottom-up information into consistent and accurate estimates of anthropogenic CO<sub>2</sub> emissions and their trends.
4. A decision support tool that can use this information to inform the inventory process.

In this context, “fossil CO<sub>2</sub> emissions” were defined as the sum of CO<sub>2</sub> emissions from fossil fuel combustion, CO<sub>2</sub> emissions from cement production and metal (ferrous and non-ferrous) production, and the CO<sub>2</sub> emissions from urea production, urea application and agricultural lime. In addition, other anthropogenic emissions include emissions from the combustion of biofuel (assumed to be carbon neutral over one year) and from land-use, land-use change and forestry (including large-scale biomass burning of forest or peat fires).

Current efforts to limit and reduce fossil CO<sub>2</sub> emissions, whether they are voluntary or part of international agreements, use self-reported data to the UNFCCC to define baselines and assess the effectiveness of climate and energy policies over time. Self-reported inventories of CO<sub>2</sub> emissions are primarily based on energy-use statistics collected for different sectors. They offer limited transparency and their accuracy and completeness cannot be assessed independently. Because emission inventories in developing nations, where emissions are growing the fastest, are thought to be less accurate than those from developed countries, the uncertainty associated with fossil CO<sub>2</sub> emissions and their trends has increased enough to undermine the credibility and the

stability of future climate agreements. Within the 2015 Paris Agreement, each country proposed Intended NDCs, described in the national climate action plans) as a measure to reduce greenhouse gas emissions. The Paris Agreement also called for a transparency framework to monitor energy- and fossil fuel-intensive national and global activities using a Measuring-Reporting-Verifying (MRV) framework.

In 2017, Task Force B issued a complementary report (Pinty et al., 2017) as a first step in advancing the definition and development of the envisaged system. That report proposed that the system operate on a global scale but with the capability of providing detailed information over a specific region such as Europe. Section 2 of that report provides the methodological background for establishing operational monitoring and verification capabilities based on advanced inverse modeling and data assimilation techniques. Furthermore, the potential to use *in situ* and remote sensing measurements combined with inverse modelling to verify reported bottom-up GHG emission inventories has been reviewed in a recent EU report (Bergamaschi et al., 2018).

Neither ground- nor space-based techniques, alone, are capable of providing the information needed across the full range of spatial and temporal scales required. Consequently, a Monitoring and Verification Support (MVS) system is proposed that is capable of integrating a wide range of observations that are heterogeneously distributed in space and time. The main building blocks of the system are illustrated in Figure 2-1. The core of the system is the integration component. This component makes extensive use of models of the Earth system and of the processes governing fossil fuel emissions. These sources of information are combined to generate anthropogenic emission fields at the required temporal and spatial scales, together with uncertainty information.

A number of advances in the observing system and modeling capability are required to implement this MVS system. In addition, an end-to-end simulation platform is needed to optimize the overall system performance and to refine the required contributions from the individual system elements and prioritize development steps according to their impact on the system performance. The functional elements, i.e. data assimilation, models, observations, prior information, and data output dissemination, are described in greater detail in section 2.2 of Pinty et al. (2017).

The first global stocktake is planned for 2023 at the COP29, where the total sum of reported GHG emissions inventories of 2021/2022 will be assessed and attributed to the estimated global budget of GHGs. After this first exercise, the Parties will be asked to revise and strengthen their NDCs. A crucial global stocktake will occur in 2028 with inventories of 2026/2027. This global stocktake of 2028 is expected to show a reduced global total, but independent assessment with top-down observations will be needed to gain confidence on the GHG emission trends.

The CO<sub>2</sub> constellation envisaged in the framework of the Copernicus Programme could significantly contribute to this second global stocktake if it starts operation before 2026 (Figure 5-1). The CO<sub>2</sub> MVS system could become an essential service to the UNFCCC to support the emission expert team with the independent information on, e.g. CO<sub>2</sub> emissions trends for certain activities to verify and consolidate the national inventories and reports.

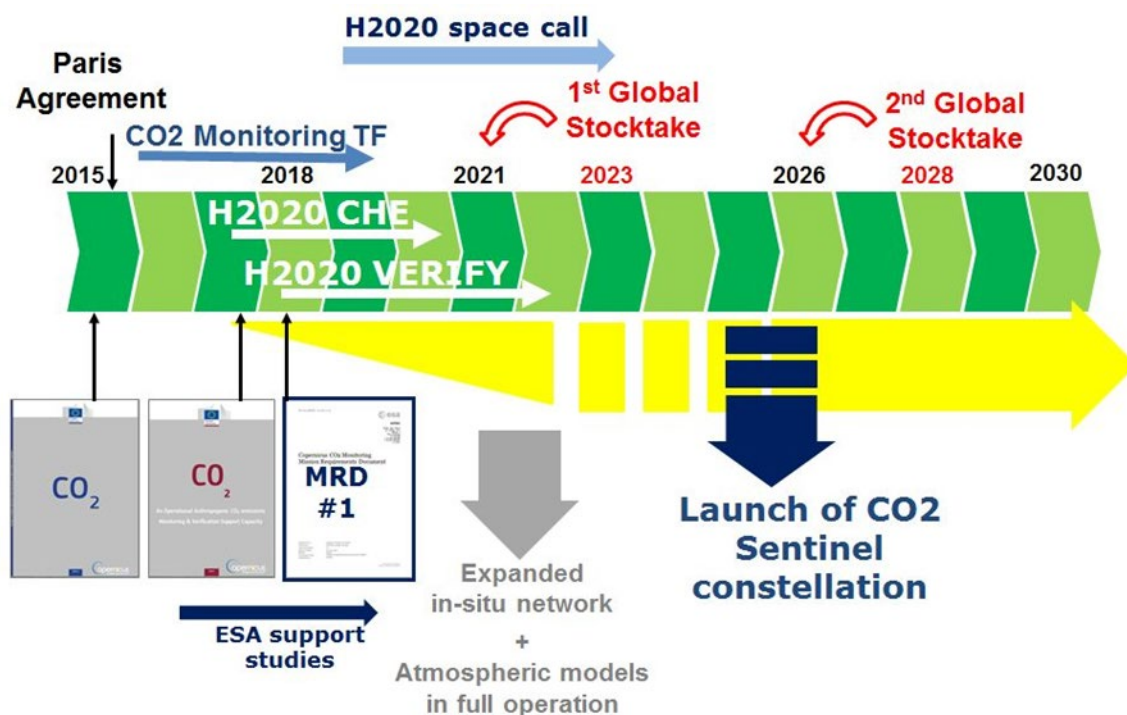


Figure 5-1: CO<sub>2</sub> task force outputs and planning of various interleaving activities.

## 5.2 The space mission

The primary objective of the CO<sub>2</sub> Monitoring mission is to collect spatially-resolved images of column averaged CO<sub>2</sub> dry air mole fraction with the resolution, accuracy, temporal sampling and spatial coverage required to provide the key space component input of the Operational Anthropogenic CO<sub>2</sub> Emissions MVS system. The mission objectives of the space-based components of this system are to provide the observations needed to:

1. detect emitting hot spots, such as large urban areas and power plants;
2. monitor trends in hot spot emissions to assess emission reductions and increases;
3. assess emission changes against local reduction targets to monitor impacts of NDCs; and
4. assess national emissions and changes in 5-year time steps to inform the global stocktake.

Anthropogenic CO<sub>2</sub> emissions vary on sub-weekly to monthly scales during a year (Andres et al., 2012; Nassar et al., 2013) due to economic and climate-related drivers. Capturing this variability requires frequent sampling with an operational constellation of satellites (Velzco et al. 2011). Emitting areas must be sampled as frequently as possible to quantify annual budgets. In practice, cloud presence will significantly limit the number of days during which emissions can be locally quantified, and passive instruments will not sample the highest latitudes from the autumn to the spring equinox in the northern hemisphere. The number of days per year per 1° × 1° with satellite overpasses that can be exploited to obtain CO<sub>2</sub> emissions from selected cities and point sources has been estimated for different numbers of LEO satellites (Table 5.1). The assumed swath width

is 200 km and only cloud-free observations were considered using cloud information from MODIS. The number of days with cloud-free conditions has been scaled by 0.4, based on results from Pillai et al. (2016) for point sources.

Monitoring emission trends over several years (section 1.3, Pinty et al., 2017) is one of the most policy-relevant capabilities expected from the Copernicus CO<sub>2</sub> monitoring initiative. As such, the design of the CO<sub>2</sub> Monitoring mission must ensure excellent operational measurement stability over the long term. Yet ensuring the consistency of the trends found in XCO<sub>2</sub> observations requires traceability of the accuracy of the products over time through the whole operational chain, including instrument drifts, cross-satellite calibration and seamless processing and re-processing of data products.

Table 5.1: Estimated number of days per year with LEO satellite overpasses per 1°x1° around selected major cities, which can be exploited to obtain their CO<sub>2</sub> emissions

City	1 satellite	2 satellites	3 satellites	4 satellites
Berlin	14	22	38	52
Paris	15	28	34	51
New York	14	26	39	54
Moscow	12	24	36	46
Cairo	18	34	52	69
Beijing	14	27	45	56
Los Angeles	16	31	47	64

Other products from the CO<sub>2</sub> Monitoring mission will improve the detection and quantification of anthropogenic CO<sub>2</sub> emissions, and provide a better understanding of natural sources and sinks:

- Measurements of XCO<sub>2</sub> concentration gradients over regions dominated by natural fluxes will improve the quantification of ocean and terrestrial ecosystem fluxes, which will help to better separate anthropogenic emissions from natural CO<sub>2</sub> fluxes in XCO<sub>2</sub> images.
- Measurements of SIF will yield improved estimates of gross primary productivity and terrestrial net ecosystem exchange of CO<sub>2</sub> during the growing season. These measurements are valuable for discriminating the contribution of green areas within and around cities to XCO<sub>2</sub> plumes.

### 5.2.1 Auxiliary observations needed for accurate XCO<sub>2</sub> and CO<sub>2</sub> flux estimates

Scattering of solar radiation by clouds and aerosols introduces uncertainties in the optical path length that affect the accuracy of the XCO<sub>2</sub> retrieval. Spectra of the O<sub>2</sub>-A band and the strong CO<sub>2</sub> band at 2.0 μm contain some information about aerosol scattering, but this may not be adequate to eliminate cloud and aerosol related biases. The presence of small, optically thick clouds in the planetary boundary layer can significantly alter this light path, leading to systematic

errors. The CO<sub>2</sub> monitoring mission would significantly benefit from a cloud imaging capability that could detect low clouds that cover > 5% of the footprint (Threshold) with 1% as the goal.

Optically thin clouds and aerosols can also introduce XCO<sub>2</sub> biases. In a simulation study led by SRON, the performance of XCO<sub>2</sub> retrievals was assessed accounting for different types and loading of aerosol in the atmosphere at different levels. For (fine) aerosol in the boundary layer, they found that the XCO<sub>2</sub> bias was limited but that it could be significant for larger aerosol optical depth (AOD) greater than 0.2 and at larger solar zenith angles (SZAs). For coarse aerosols around 8 km altitude, such as dust and thin cirrus, the XCO<sub>2</sub> bias also depends on AOD and can grow to several ppm and even further for larger SZAs.

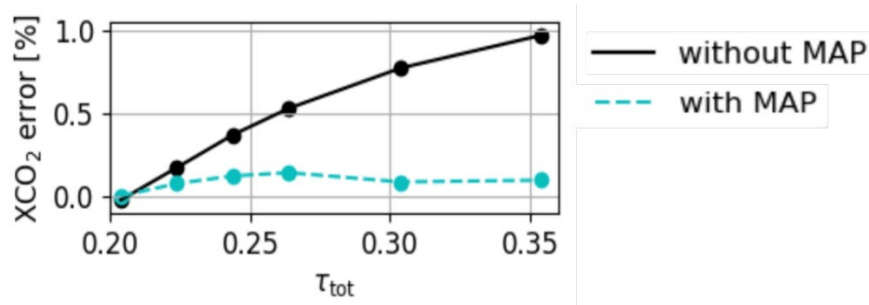


Figure 5-2. Simulated XCO<sub>2</sub> error as function of total aerosol optical depth ( $\tau$ ) with and without prior aerosol knowledge from multi-angle polarimeter observations (credit: ESA).

To mitigate these aerosol-related biases, simulated XCO<sub>2</sub> retrievals were performed with additional information from a dedicated multi-angle polarimeter (MAP). The results (Figure 5-2) indicate that aerosol-related biases in XCO<sub>2</sub> could be reduced substantially using these additional observations, even at larger SZAs and total AOD up to 0.5. This would allow the acquisition of useful observations in more aerosol-laden conditions than existing systems, such as OCO-2, which screen out observations with AOD above 0.3 (Eldering et al., 2017a; O’Dell et al., 2018).

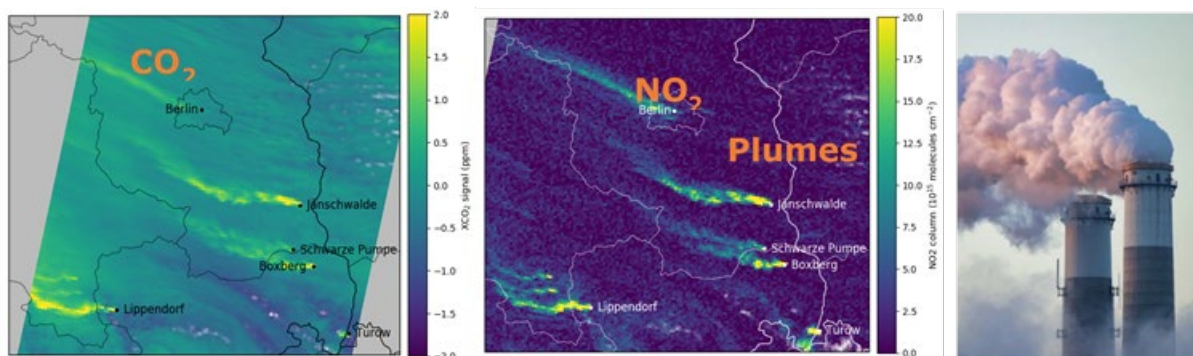


Figure 5-3 Simulated XCO<sub>2</sub> and NO<sub>2</sub> plumes originating from power plants and other emission sources in a larger area around Berlin. Simulated data come from the COSMO-GHG model as used in the SMARTCARB study simulating a swath width of 250 km. (credit: ESA SMARTCARB).

Auxiliary observations of NO<sub>2</sub> and CO, two key species co-emitted with anthropogenic CO<sub>2</sub> in the fossil fuel combustion process, were considered to better localize the plumes of anthropogenic CO<sub>2</sub> (Pinty et al. 2017). Of these two species, NO<sub>2</sub> is easier to detect at the same spatial scale as XCO<sub>2</sub>. NO<sub>2</sub> is also more characteristic of high temperature combustion of fossil fuels than CO. The SMARTCARB study simulated plumes of NO<sub>2</sub> and XCO<sub>2</sub> from power plants

and cities in eastern Germany (Figure 5-3; see Kuhlmann et al., 2018). Because of its relatively short chemical lifetime (several hours), the NO<sub>2</sub> plumes can be easily detected above their background concentrations with a measurement precision of  $2 \times 10^{15}$  molecules/cm<sup>2</sup> in a sampling area equal to the XCO<sub>2</sub> measurement footprint. The SMARTCARB study also investigated the effect of plume rise from power plants stacks. The heat content in the exhausted gas (a mix of CO<sub>2</sub> and nitrogen oxides, NO<sub>x</sub>) results in the plume rising to a different altitude level than the height of the stack. If the wind speed or direction changes with altitude, and these changes are not accounted for in the flux calculation, this can introduce error in the CO<sub>2</sub> emission estimate. Coincident observations of NO<sub>2</sub> with XCO<sub>2</sub> facilitated the detection of the plume in these conditions.

### 5.2.2 Geophysical product requirements of the space component

To meet the objectives outlined in the previous section, a CO<sub>2</sub> task force was assembled to define the mission requirements. The main driving requirements identified by this group are summarized in Table 5.2.

Table 5.2: Characteristics of the geophysical product as required from the space component of the anthropogenic CO<sub>2</sub> monitoring system. The designation, (T), indicates the minimum performance threshold, while (G) indicates the goal.

Parameter	Level-2 requirement
XCO <sub>2</sub> precision	0.5 ppm (G) and 0.7 ppm (T) for vegetation scenario (albedo = 0.1 in NIR, 0.05 in SWIR) at SZA of 50 degrees
XCO <sub>2</sub> systematic error	Less than 0.5 ppm
XCO <sub>2</sub> spatial resolution	Less than or equal to 4 km <sup>2</sup> / footprint with an aspect ratio less than or equal to 2.
XCO <sub>2</sub> plume image	Contiguous sampling over a >200 km swath
XCO <sub>2</sub> plume temporal coverage	At least once every week, on average, assuming data are on average 1/3 cloud free resulting in a coverage requirement of 2–3 days for latitudes above 40 degrees, where the strongest emitting areas are located
Auxiliary information for accurate XCO <sub>2</sub> retrieval	High accuracy XCO <sub>2</sub> retrieval requires the following spatially and temporally-collocated measurements: 1) aerosol & cloud information (e.g., vertical profile, optical depth, size distribution and composition) needed to calculate their effect on optical path length in CO <sub>2</sub> spectral bands, 2) detection of low cloud coverage (>1% (G), >5% (T)) of optically thick (AOD > 1) clouds within each FOV, 3) measuring CH <sub>4</sub> spectral bands (allowing proxy retrieval of XCO <sub>2</sub> ), 4) measuring solar induced fluorescence (SIF) for correction in O <sub>2</sub> -A band radiances and estimating gross primary production contributions.
Auxiliary information for CO <sub>2</sub> plume characterisation	Spatially and temporally-collocated observations of NO <sub>2</sub> should be collected to identify the source, plume direction and local wind speed. These measurements should be collected at the same (or better) spatial resolution as the XCO <sub>2</sub> observations and with a single-sounding precision of $1-2 \cdot 10^{15}$ molecule/cm <sup>2</sup>

Note 1: Aerosol and (thin) cloud information are expected to also come from both O<sub>2</sub> A-band measurements and auxiliary measurements using a multi-angle polarimeter (MAP).

Note 2: A single LEO satellite cannot deliver the required geometrical coverage. Therefore, the overall system requirements will be satisfied after the full deployment of 3–4 satellites (depending on the selected swath) flying in a constellation.

Note 3: High XCO<sub>2</sub> precision of 0.5–0.7 ppm shall have priority over the swath.

Note 4: XCO<sub>2</sub> systematic error is assumed to be after bias correction.

Note 5: Aerosol measurements serve for correction purposes, but will also generate, as a by-product, aerosol height with ~500 m uncertainty and AOD with uncertainty of ~0.05.

Note 6: CH<sub>4</sub> band measurements for the proxy CO<sub>2</sub> retrieval will also generate, as a by-product, XCH<sub>4</sub> products with uncertainty of about ~10 ppb.

### 5.2.3 Mission requirements for the CO<sub>2</sub> observations

Observations should be collected at a local time close to noon to exploit the better illumination conditions at that time of day. This also allows easier access to sun-glint observations over water bodies and minimizes the solar zenith angles at high latitudes (current CO<sub>2</sub> missions have good performance at solar zenith angles up to about 70 degrees). The target for the equator crossing-time is in the morning close to noon (e.g., 11:30). All land surface areas shall be covered in 2 to 3 days for latitudes above 40°.

In order to distinguish spatial gradients in XCO<sub>2</sub> introduced by mesoscale meteorology and regional- to local-scale emission sources from the natural background CO<sub>2</sub> levels, city-scale and local emission areas need to be observed within the context of their background. Therefore, a minimum swath is required that is larger than the typical size of these sources and includes their cleaner surroundings. The minimum across-track swath width shall be 200 km contiguously sampled. The product of the spatial resolution along-track and across-track shall cover an area smaller than 4 km<sup>2</sup>.

The requirements for the CO<sub>2</sub> spectrometer were determined through a series of OSSEs (Bovensmann et al., 2010, Buchwitz et al., 2013; ESA 2015; Pillay et al., 2016; Broquet et al., 2018) and experience from the analysis of SCIAMACHY, GOSAT, and OCO-2 observations. The required spectral bands of the imaging spectrometer are provided in Table 5.3.

Table 5.3: Requirements on spectral range, resolution and sampling ratio (number of samples across the full width at half maximum of the instrument spectral response function) for the CO<sub>2</sub> instrument. Note that the SWIR-2A will be used as an imager for detecting cirrus clouds.

<b>Band ID</b>	<b>Spectral range [nm]</b>	<b>Spectral resolution [nm]</b>	<b>Spectral sampling ratio</b>
NIR	747–773	0.12	3
SWIR-1	1590–1675	0.3	3
SWIR-2A	1936–1941 (G)	5.0	1
SWIR-2B	1990–2043 (G&T)	0.55	3
SWIR-2C	2043–2095 (G&T)	0.55	3

The requirements for the signal-to-noise ratio (SNR) per band are provided in Table 5.4 for top of atmosphere (TOA) radiance measurements. The absolute radiometric accuracy of the (top-of-atmosphere) radiance measurement shall be better than 3%.

Table 5.4: SNR requirements for terrestrial signals. The SNR requirements are valid per spectral channel (i.e. not per full width at half maximum of the instrument spectral response function) assuming the spectral sampling specified above. The designation, (T), indicates the minimum performance threshold, while (G) indicates the goal.

Band ID	$L_{ref}$ [photons/s/nm/cm <sup>2</sup> /sr]	SNR <sub>ref</sub> *
NIR	$4.2 \times 10^{12}$	260 (T) / 330 (G)
SWIR-1	$2.1 \times 10^{12}$	335 (T) / 480 (G)
SWIR-2	$1.15 \times 10^{12}$	335 (T) / 480 (G)
* The total XCO <sub>2</sub> random error budget has a contribution from the spatial co-registration error (as a pseudo-noise). Therefore, as a minimum, the T value of the SNR shall be selected in combination with the G value for the spatial co-registration requirement, and vice versa.		

#### 5.2.4 Mission requirements for aerosol and cloud observations

Scattering of sunlight by clouds and aerosols introduces uncertainties and biases in the XCO<sub>2</sub> estimates. The added benefit of dedicated aerosol and cloud observations is currently being assessed in scientific support studies. The primary objectives of these studies are to identify and screen out scenes with sub-footprint clouds and to characterize the optical path uncertainties introduced by scattering by optically thin clouds and aerosols in the presence of realistic scattering by surfaces. The required aerosol and cloud parameters are:

- Fraction of each footprint covered by optically thick (AOD > 1) clouds
- Layer height(s) of optically thin (0.01 < AOD < 1.0) clouds, ideally a profile, with accuracy ~500 m (of Gaussian profile height),
- optical depth is in the range 0.01–1.0, with an uncertainty better than 0.01,
- Wavelength-dependent AOD, single scattering albedo, particle phase function, size distribution (and refraction index).

A high-spatial-resolution imager is needed to identify and screen soundings whose footprints are partially filled by optically thick clouds and those that are contaminated by scattering or shadowing from nearby clouds. The wavelength chosen, radiance precision, and spatial resolution of the imager will be optimized to identify optically thick clouds that occupy more than 1% (goal) or 5% (threshold) of any footprint. A high spatial resolution cloud imager that uses two or three bands centered around 565 nm, 760 nm, and 1380 nm is being studied to detect both optically thick low clouds and high, thin cirrus.

The polarimetric observations will be taken in a number of different viewing angles along the spacecraft track to sample various observation zenith angles for each cross-track spatial sample used to retrieve XCO<sub>2</sub>. The observation zenith angles shall cover 0 degree (nadir) +/-40 degrees

in the cross-track direction and +/-60 degrees in the along-track direction. The along-track angles will be centered around the nadir view. For each cross-track sample and each along-track angle, the multi-angle polarimeter (MAP) will provide measurements of top-of-atmosphere (TOA) Earth radiance (Stokes parameter, I, in W/m<sup>2</sup>/sr) in a number of spectral channels and the Degree of Linear Polarisation (DoLP) in all or a subset of the spectral channels. The polarimetry data from the MAP will be retrieved by combining different viewing directions and shall be (spatially) resampled to the XCO<sub>2</sub> spatial samples. The aerosol product shall be retrieved across the full, cross-track swath used to retrieve XCO<sub>2</sub> estimates.

The number of observation zenith angles can be traded against the number of spectral bands. The minimum number of observation zenith angles is 5 and the minimum number of spectral bands is 6, but the product of zenith angles and spectral bands should be around 80 (e.g., 5 observation zenith angles and 20 DoLP bands or 10 observation zenith angles and 10 spectral bands).

### 5.2.5 Mission requirements for NO<sub>2</sub> observations

Based on the outcome of the SMARTCARB study and discussions with experts, NO<sub>2</sub> has been selected as an auxiliary measurement for improving anthropogenic CO<sub>2</sub> emission estimates. The benefit of such dedicated NO<sub>2</sub> observations is currently assessed in a scientific support study. The requirements for these observations include the following:

- The Level-2 product precision for NO<sub>2</sub> shall be between  $1-2 \cdot 10^{15}$  molecules/cm<sup>2</sup>
- In order to exploit parts of plumes originating outside the swath of the CO<sub>2</sub> instrument, the NO<sub>2</sub> observations shall include context outside the nominal CO<sub>2</sub> swath. This could enhance the number of CO<sub>2</sub> sources for which the emissions can be quantified.
- The NO<sub>2</sub> data must be interpolated to the same spatial grid as the CO<sub>2</sub> data. If the same instrument is used, then the sampling should be the same. If a separate instrument is used, then sampling should be high enough to allow the NO<sub>2</sub> data to be resampled at the CO<sub>2</sub> measurement resolution. In the latter case, the spatial sampling distance is expected to be twice as high in both the along-track and cross-track directions.
- The absorption spectrum of NO<sub>2</sub> consists of a continuum with a weak absorption features superimposed. This absorption can be exploited to retrieve total column NO<sub>2</sub> in the visible spectral range from 405 to 490 nm at moderate spectral resolution (0.6 nm).

## 5.3 Virtual constellation opportunities

The satellite constellation currently under consideration by the EC will constitute the backbone of the required space-based component of a robust, standalone, operational global observation system for monitoring anthropogenic CO<sub>2</sub> emissions. The EC also encourages and fosters international collaboration to complement the system with the creation of a virtual constellation. In particular, the USA, Japan and China will launch several satellites dedicated to CO<sub>2</sub> monitoring from space during the coming decade. If these satellites could be integrated into a virtual constellation, this effort would facilitate the development and testing of the space-based component of the end-to-end MVS system. In the long term, this experience would enhance the measurement capability and the overall contribution of atmospheric measurements to the emission inventory process.

Other observations and capabilities that would enhance the CO<sub>2</sub> constellation include:

- Observations of CO<sub>2</sub> and CH<sub>4</sub> from geostationary platforms.
- Space-based lidars that can acquire CO<sub>2</sub> and CH<sub>4</sub> measurements with the precision and accuracy needed to cross-validate measurements from the constellation of CO<sub>2</sub> imagers.
- Additional satellites in LEO with comparable capabilities and performance to enhance the observation frequency.
- Ground-based calibration and validation data to facilitate the on-orbit calibration of the satellite instrument and validation of its products in representative areas.
- Faster, more accurate satellite CO<sub>2</sub> and CH<sub>4</sub> retrieval algorithms to speed up the processing and enhance the product reliability and range of validity.

Ensuring the robust quantification of anthropogenic CO<sub>2</sub> emissions and emission trends also requires the continuous traceability of XCO<sub>2</sub> measurements from the CO<sub>2</sub> constellation through to the international atmospheric CO<sub>2</sub> mole fraction scale maintained by the WMO. This traceability will enable combining the CO<sub>2</sub> Monitoring mission data with measurements from other XCO<sub>2</sub> satellites and *in situ* data throughout the period of operations. Transfer standards, including TCCON (Wunch et al., 2011a, 2011b, 2017) and AirCore (Karion et al., 2010), will be essential for maintaining this traceability. Additional information, including CO<sub>2</sub> profiles from fixed-wing aircraft (Gatti et al., 2010; Wofsy et al., 2011; Masarie et al., 2014; Matsueda et al., 2015; Filges et al., 2015), *in situ* measurements of <sup>14</sup>CO<sub>2</sub> (Miller et al., 2012), and CO<sub>2</sub> fluxes from flux tower networks (Falge et al., 2017) will be critical for validating CO<sub>2</sub> fluxes in regions with strong anthropogenic emissions.

## 6. Integrating CO<sub>2</sub> and CH<sub>4</sub> Satellites into Operational Constellations

To provide useful information about CO<sub>2</sub> and CH<sub>4</sub> sources and sinks, atmospheric measurements must detect concentration changes associated with local sources and sinks and discriminate these changes from those originating from atmospheric transport. This places stringent requirements on the accuracy, precision, and resolution, and coverage of these measurements. For example, the 2011 update for the Global Climate Observing System (GCOS) Systematic Observation Requirements for Satellite-Based Data Products for Climate (GCOS, 2011) and GCOS 2016 Implementation Plan (GCOS, 2016) recommend a target sampling resolution of 5-10 km, a temporal resolution of 4 hours, and accuracies of 1 ppm and 10 ppb for CO<sub>2</sub> and CH<sub>4</sub>, respectively (Table 6.1). Recent efforts indicate these values may be adequate for specifying single sounding random errors, but spatially- and temporally-coherent systematic biases must be much smaller to enable atmospheric flux inversions on regional scales. It may not be necessary to meet these spatial and temporal resolution requirements everywhere on the planet (i.e., Antarctica during the southern winter). However, the ability to meet or exceed these requirements will be critical for discriminating anthropogenic emissions from natural sources and sinks in regions where either may be changing on spatial scales that are as small as an urban area or temporal scales that are shorter than a day. For example, recent work suggests that a horizontal resolution of < 4 km<sup>2</sup> is preferred for monitoring CO<sub>2</sub> emissions from large cities (Broquet et al., 2018). CH<sub>4</sub> leak detection can benefit from even higher (sub-km) resolution.

Table 6.1: GCOS CO<sub>2</sub> and CH<sub>4</sub> Requirements (GCOS, 2011).

Variable / Parameter	Horizontal Resolution	Vertical Resolution	Temporal Resolution	Accuracy *	Stability/Decade
Tropospheric CO <sub>2</sub> column	5-10km	N/A	4 h	1 ppm	0.2 ppm
Tropospheric CO <sub>2</sub>	5-10 km	5 km	4 h	1 ppm	0.2 ppm
Tropospheric CH <sub>4</sub> column	5-10 km	N/A	4 h	10 ppb	2 ppb
Tropospheric CH <sub>4</sub>	5-10 km	5 km	4 h	10 ppb	2 ppb
Stratospheric CH <sub>4</sub>	100-200 km	2 km	Daily	5%	0.3%

\* See definition on pg. 7 of GCOS, 2011.

A space-based CO<sub>2</sub> and CH<sub>4</sub> monitoring system that fully meets these demanding precision, accuracy, resolution and coverage requirements may be beyond the resources (or interests) of a single nation. However, the implementation cost and schedule could be reduced by exploiting international partnerships by adopting a model similar to the one pioneered for delivering operational meteorological measurements.

As discussed in Chapter 3, more than a dozen CO<sub>2</sub> and CH<sub>4</sub> satellites will be launched before 2025 (Figure 6-1). A logical first step in the implementation of an operational space-based CO<sub>2</sub> and CH<sub>4</sub> monitoring capability would be to integrate these systems into a virtual constellation.

Efforts to cross-calibrate the observations and cross validate their products will provide the experience needed to foster the development of future, purpose-built CO<sub>2</sub> and CH<sub>4</sub> constellations and provide the inputs needed to develop and validate a prototype end-to-end atmospheric inventory system.

Integrating existing and planned satellite systems into a multi-satellite virtual constellation would provide resiliency to the loss or degradation of individual systems, a feature that is critical to any operational observation system. CEOS could play a critical role in this effort by facilitating the coordination of the space-based assets that are operating or planned. CEOS could also contribute to efforts to cross validate their products, so that they can be integrated into a self-consistent, continuous, global climate data record that supports the atmospheric inversion efforts.

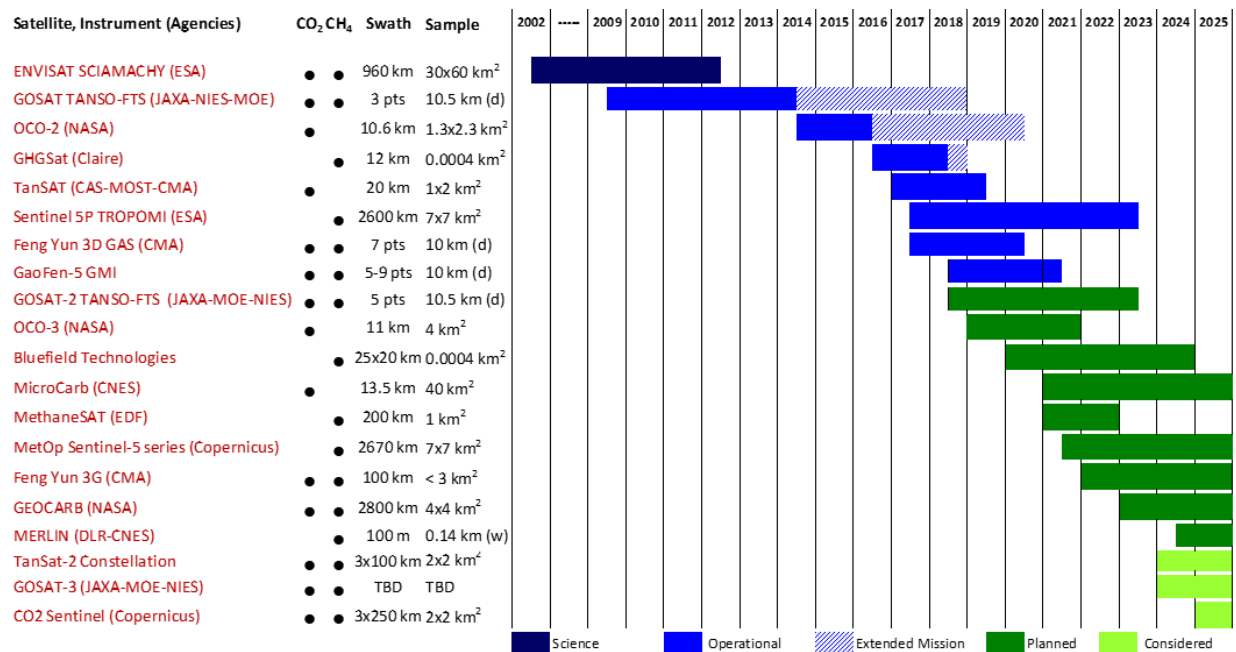


Figure 7-1: The CO<sub>2</sub> and CH<sub>4</sub> satellite time line.

Once validated, these space-based data must be integrated with data from ground-based and aircraft sensors and analyzed with atmospheric inversion systems to produce emission estimates on spatial scales ranging from large point sources (power plants) to metropolitan areas, to nations, to the globe (Pinty et al., 2017). This would provide the space-based measurements needed for an end-to-end test of a global CO<sub>2</sub> and CH<sub>4</sub> monitoring system like that described in Chapters 2 and 5 and envisioned by the WMO IG<sup>3</sup>IS (DeCola et al., 2017).

If these atmospheric measurement and modelling systems can be integrated by 2020, preliminary products could be ready in time to support the 2023 stocktake. Although this prototype, space-based product may not have the accuracy, resolution, and coverage needed to greatly improve GHG inventories in the industrialized world, it is likely to provide useful insights into CO<sub>2</sub> and CH<sub>4</sub> inventories in poorly characterized regions of the developing world. In addition, the experience gained from the development of this virtual constellation will provide information critical for defining the requirements for a future operational atmospheric CO<sub>2</sub> and CH<sub>4</sub>

monitoring system, and will help to identify gaps in the measurement and analysis systems that will have to be addressed by that future system.

The next step would be to incorporate the lessons learned from the virtual constellation into a purpose-built CO<sub>2</sub> / CH<sub>4</sub> constellation that addresses the resolution and coverage requirements specified by GCOS. Appendix 6 summarizes the principal advantages and limitations of the LEO, GEO, and HEO vantage points. A candidate constellation architecture that exploits these advantages to more completely address the precision, accuracy, resolution, and coverage requirements of the space-based component of a global carbon monitoring system is described below. Other critical elements needed to fully exploit the space-based measurements in a global Monitoring and Verification Support system are then summarized. These include methods for cross calibrating the measurements from different parts of the space- and ground-based measurement system, retrieving estimates of XCO<sub>2</sub> and XCH<sub>4</sub> from these measurements, cross validating these estimates against internationally accepted standards, and retrieving CO<sub>2</sub> and CH<sub>4</sub> fluxes on scales ranging from individual power plants to nations.

## 6.1 A CO<sub>2</sub>/CH<sub>4</sub> constellation architecture with LEO, GEO and HEO elements

A constellation of CO<sub>2</sub>/CH<sub>4</sub> satellites that fully exploits the assets of the LEO, GEO, and HEO vantage points will be needed to meet the demanding GCOS requirements for precision, accuracy, spatial and temporal resolution and coverage summarized in Table 6.1. The following sub-sections describe a point design for a NIR/SWIR constellation architecture that addresses these requirements over continents, while providing somewhat lower resolution and coverage over the ocean. One or more of the LEO platforms would have to carry active CO<sub>2</sub> and CH<sub>4</sub> Lidars to provide useful constraints on XCO<sub>2</sub> and XCH<sub>4</sub> over the nighttime hemisphere. Lidar measurements could also provide global constraints on systematic biases in passive SWIR observations associated with variations in the solar illumination and viewing geometry.

### 6.1.1 LEO constellation elements

A LEO constellation consisting of three or more satellites carrying wide-swath CO<sub>2</sub> and CH<sub>4</sub> imaging spectrometers, deployed along a common, sun-synchronous orbit could provide high spatial resolution observations of the sunlit hemisphere at weekly intervals. Each satellite should carry passive imaging spectrometers that record high-resolution spectra of reflected sunlight within the 0.765 μm O<sub>2</sub> A-band, the CO<sub>2</sub> bands at 1.61 and 2.06 μm and the CH<sub>4</sub> bands near 1.67 or 2.33 μm. The O<sub>2</sub> A-band channel must be wide enough to include the solar Fraunhofer lines near 0.757 and 0.772 μm to quantify and remove contamination from SIF. Each satellite should also include a spectrometer channel that records reflected sunlight within the 0.43 μm NO<sub>2</sub> band and/or the 2.33 μm CO band for use in identifying the spatial extent of discrete emission plumes.

To provide full coverage of the sunlit hemisphere at roughly weekly intervals, all spectrometer channels should acquire co-boresighted spectra within all bands at a spatial resolution of < 5 km<sup>2</sup> over a wide (> 200 km) swath. Instruments with wider swaths could increase the repeat frequency, but observations acquired at the largest cross-track angles are likely to be more contaminated by optically thick clouds and aerosols. The CO<sub>2</sub> and CH<sub>4</sub> spectrometers must

return measurements with the resolution, accuracy, and stability needed to yield single sounding random errors in  $XCO_2 < 0.125\%$  (0.5 ppm) and  $XCH_4 < 0.25\%$  (4.5 ppb) and vanishingly small systematic biases ( $< 0.06\%$ ) on scales ranging from cities ( $\sim 100 \text{ km}^2$ ) to continents ( $10^7 \text{ km}^2$ ).

Even though this constellation will collect data over the entire surface of the Earth at weekly intervals, optically thick clouds and aerosols will preclude full-column estimates of  $XCO_2$  and  $XCH_4$  over 80 to 90% of that area. The coverage and accuracy of these products could therefore be improved by adding instruments designed to screen and/or characterize the optical properties and vertical distribution of clouds and aerosols within the  $CO_2$  and  $CH_4$  spectrometer footprints. For maximum benefit, these cloud/aerosol instruments should be co-boresighted with the  $CO_2/CH_4$  spectrometers, and should have adequate spatial resolution and sensitivity to detect optically thick clouds and aerosols that occupy more than 5% of the  $5 \text{ km}^2$  area of any footprint. The field of view should span the full extent of the swath and extend at least 20 km beyond its edge to identify clouds and aerosols outside of the swath that cast shadows or reflect solar radiation into the outermost footprints of the swath.

Over the ocean, only the LEO platforms can routinely obtain measurements with adequate sensitivity for retrieving  $XCO_2$  and  $XCH_4$ . Passive NIR/SWIR spectrometers must observe the glint spot to obtain these measurements. These observations will only illuminate a fraction of the swath for a wide swath instrument, reducing their ocean coverage. Fortunately, there are few known compact sources or sinks over the ocean. If each satellite in the baseline, three-satellite LEO constellation orbits the Earth about 15 times each day, the  $\sim 45$  pole-to-pole tracks provided by the constellation should provide adequate resolution and coverage to track synoptic-scale  $XCO_2$  and  $XCH_4$  anomalies. Active  $CO_2$  and  $CH_4$  Lidars deployed on LEO platforms can also obtain high SNR observations over a narrow (100 – 200 m) swath at the local nadir. Lidar measurements can be collected over both the sunlit and nighttime hemispheres, yielding dozens of additional tracks each day. The Lidar measurements could also be used to remove biases in  $XCO_2$  and  $XCH_4$  retrieved from the passive sensors.

### 6.1.2 GEO constellation elements

Dawn to dusk observations from a constellation of GEO satellites stationed along the equator at longitudes centered over North and South America, Europe and Africa, and South and East Asia would complement the global measurements from LEO. This could be achieved by a constellation of 3 (or more) GEO satellites stationed near  $85^\circ \text{ W}$ ,  $20^\circ \text{ E}$  and  $105^\circ \text{ E}$ , respectively. A similar approach has been adopted by the air quality GEO constellation, consisting of TEMPO, Sentinel 4, and GEMS (Al-Saadi et al., 2017), although this group of missions is primarily focused on the Northern Hemisphere. Each platform should carry imaging spectrometers that record high-resolution spectra of reflected sunlight within the same spectral ranges used by the LEO constellation described. To meet the GCOS sampling frequency, the spectrometers on each platform should collect co-boresighted spectra at a spatial resolution of  $4 \text{ km}^2$  to  $10 \text{ km}^2$ , at 4-hour intervals between sunup and sundown across the land masses within their fields of regard. As for the LEO  $CO_2$  and  $CH_4$  spectrometers, complementary instruments to characterize SIF and screen and/or correct for contamination by clouds, aerosols, and SIF within the spectrometer fields of view are highly desirable. Methods to optimize the observing strategy

in near real time to avoid persistently cloudy areas and maximize the yield of cloud-free soundings in partially-cloudy regions should be pursued. Time resolved measurements of NO<sub>2</sub> and/or CO would also be of great value in identifying and tracking CO<sub>2</sub> emission plumes associated with fossil fuel and biomass burning.

Time-resolved measurements from this GEO constellation would provide critical constraints on diurnal variations in CO<sub>2</sub> and CH<sub>4</sub> emissions associated with fossil fuel extraction, transportation, and use. Long-term observations of CO<sub>2</sub>, and SIF from GEO could also yield valuable insights into diurnal, seasonal, and longer-term variations in CO<sub>2</sub> uptake by the land biosphere, as it responds to heat and drought stress associated with climate change. Multiple observations throughout the day may also improve the chances of observing cloud-free scenes in the persistently-cloudy tropical land regions. Coincident observations of both NO<sub>2</sub> and CO may be critical for discriminating CO<sub>2</sub> emission plumes from the “cleaner” background in tropical regions, where fossil fuel combustion produces compact plumes that include both NO<sub>2</sub> and CO, while biomass burning contributes larger-scale plumes that include CO<sub>2</sub> and CO. Proxy measurements will be even more important for tracking plumes if the GEO CO<sub>2</sub> and CH<sub>4</sub> spectrometers have larger footprints or lower CO<sub>2</sub> sensitivities, because both factors will reduce the detectability of given mass of CO<sub>2</sub> that is emitted into the atmosphere.

### 6.1.3 HEO constellation elements

The GEO instruments can meet the GCOS revisit requirements over tropical and mid-latitude land masses, but cannot provide useful data at higher latitudes where viewing angles become too large. The LEO instruments will provide more frequent overpasses of high latitudes, due to the convergence of the meridians, but are still not likely to provide data at as often as 4-hour intervals throughout sunlit portion of the day. High latitude observations from instruments on HEO platforms are needed to meet these requirements for the boreal and Arctic regions. Observations from HEO would also overlap with those from the northern reach of GEO missions to provide inter-comparison opportunities spanning the diurnal cycle.

At least two HEO platforms would be needed for continuous daytime observing (equivalent to GEO), but even a single HEO platform working in conjunction with the LEO constellation could act as a proof-of-concept and help to detect major emission events. The instrument complement on these platforms should be similar to the NIR/SWIR sensors on the GEO and LEO satellites. In particular, the spectrometers on each platform should collect co-boresighted high-resolution spectra of the O<sub>2</sub> A-band at 0.76 μm, the CO<sub>2</sub> bands at 1.61, and 2.06 μm, the CH<sub>4</sub> bands at 1.67 or 2.3 μm at a spatial resolution of 4 km<sup>2</sup> to 10 km<sup>2</sup>, at 4-hour intervals while the sun is up. For the highest latitudes, this would yield between 12 and 24 hours of potential observing time in the summer and 0-12 hours during the winter. During winter, when the highest northern latitudes are dark and cannot be observed with passive measurements, a HEO mission could focus on mid-latitudes for increased overlap with GEO observations.

As for the LEO and GEO platforms, coincident observations of NO<sub>2</sub> or CO would facilitate the interpretation of the HEO XCO<sub>2</sub> and XCH<sub>4</sub> observations. A dedicated cloud/aerosol imager may be even more beneficial for detecting and correcting the effects of scattering particles at these high latitudes. SIF observations would be useful for constraining the spatial extent of CO<sub>2</sub> uptake

during the brief, intense growing season. All of these sensors will have to be optimized for use at high latitudes, where the solar illumination is reduced and snow and ice-covered surfaces have reduced reflectances at wavelengths in the SWIR. They should also be designed to collect multiple observations each day or employ cloud avoidance strategies like those suggested above for GEO platforms to increase the likelihood of obtaining some cloud-free observations in the predominately cloudy arctic and boreal regions.

## 6.2 Cross-calibrating the sensors deployed across the constellation

To integrate the measurements collected by instruments deployed on a constellation of satellites into a common climate data record, these instruments must be cross-calibrated against common standards to characterize the precision, accuracy and information content of their measurements. The XCO<sub>2</sub> and XCH<sub>4</sub> estimates retrieved from these measurements must then be validated against common standards before they can be combined in atmospheric inversion systems to estimate CO<sub>2</sub> and CH<sub>4</sub> fluxes. Both of these efforts pose challenges for a constellation that employs multiple instrument types that observe from different vantage points and must meet unprecedented accuracy and precision requirements. Fortunately, the GOSAT and OCO-2 teams pioneered methods for addressing these challenges.

As part of their pre-launch testing programs, the GOSAT and OCO teams visited each other's test facilities and cross-calibrated their radiometric standards (Sakuma et al., 2010). These measurements benefited both teams by identifying subtle errors and uncertainties in their pre-launch calibration hardware and testing procedures. Many of the lessons learned from the OCO-GOSAT pre-launch calibration were adopted as parts of the OCO-2, OCO-3, and GOSAT-2 pre-launch calibration programs and have been incorporated into the GeoCarb calibration plan.

The OCO-2 and OCO-3 teams took a further step by enlisting the direct participation of the National Institute of Standards and Technology in the pre-launch radiometric calibration process (Rosenberg et al. 2017). Similar methods and instruments can be adopted across the constellation to radiometrically calibrate high-spectral-resolution NIR and SWIR spectrometers. It was not possible to directly cross-calibrate the geometric, spectroscopic or polarimetric performance of the OCO/OCO-2/OCO-3 and GOSAT/GOSAT-2 instrument families prior to launch, but the teams exchanged information on experience and best practices in each of these areas. The information provided a basis for diagnosing and correcting trends in performance of these instruments discovered after launch. Currently, there are no programs supporting the cross-calibration of radiometric standards used in pre-launch testing of CO<sub>2</sub> and CH<sub>4</sub> sensors. CEOS should strongly encourage its member agencies to support these efforts.

Once GOSAT was successfully launched, the GOSAT team worked closely with the ACOS/OCO-2 teams to develop the Railroad Valley Vicarious Calibration site, and then incorporate observations of this site into both GOSAT and OCO-2 in-flight calibration programs (Kuze et al., 2011; 2014). Earlier missions had used this site to monitor the radiometric calibration of broadband radiometers (MISR, MODIS) that were designed to measure surface reflectance in spectral regions with little or no atmospheric absorption. To monitor the

radiometric performance of the GOSAT and OCO-2 instruments, which were designed to measure high-resolution spectral radiances at wavelengths occupied by O<sub>2</sub>, CO<sub>2</sub>, and CH<sub>4</sub> bands, the vicarious calibration strategy used for those earlier missions had to be updated with additional atmospheric measurements.

The routine surface reflectance and atmospheric aerosol measurements were augmented with radiosonde profiles of pressure, temperature, and water vapor. The NASA/Ames Alpha Jet collected vertical profiles of CO<sub>2</sub> and CH<sub>4</sub> above the playa. These data were augmented with surface CO<sub>2</sub> and CH<sub>4</sub> measurements (Yates, et al. 2011) and with up-looking XCO<sub>2</sub> and XCH<sub>4</sub> measurements from ground-based Bruker EM27/Sun instruments. These data provided a much more comprehensive description of the atmospheric extinction above the site, and allowed a comprehensive assessment of the spectrally-dependent radiances throughout each of the spectral bands of interest. Railroad Valley observations then provided a spectroscopic as well as a radiometric standard. If the ground-based measurement campaigns initiated by the GOSAT and OCO-2 teams can be maintained, this site can be used by future CO<sub>2</sub> and CH<sub>4</sub> missions operating over North America. Similar sites in the Asian/Oceania and Europe/African domains would be needed to cross calibrate GEO orbiters operating over these areas. CEOS could play an important role in coordinating the development of these sites and distributing ground-based calibration data collected during calibration campaigns.

The GOSAT and OCO-2 teams also collaborated with the Robotic Lunar Observatory (ROLO) team (Andersen et al., 1999) to refine and then use the moon as a common radiometric and geometric calibration target at the wavelengths shared by the two instruments. Lunar observations are especially advantageous for calibrating SWIR CO<sub>2</sub> and CH<sub>4</sub> sensors, since the moon has no atmosphere and thus no strong absorption by O<sub>2</sub>, CO<sub>2</sub>, or CH<sub>4</sub> in the spectral ranges used for routine science observations. Also, unlike the sun, the moon can be observed directly with the optical train used to acquire science observations, without the need for additional optical elements that could degrade. Lunar observations are challenging, however, because lunar topography casts sharp shadows on the lunar surface that produce significant changes in the lunar surface reflectance as the illumination and observing geometry changes.

At wavelengths where the Earth's atmosphere is relatively transparent, these radiometric changes can be carefully calibrated using ground-based observations. Unfortunately, ground-based lunar observations are somewhat less reliable within the strong O<sub>2</sub>, CO<sub>2</sub>, and CH<sub>4</sub> bands used by these sensors. To create a lunar calibration standard with accuracies as high as 1%, the polarization of the lunar surface must also be considered. Using the ROLO data, the GOSAT and OCO-2 teams pioneered methods for tracking radiometric drifts. However, after May 2014, when one of GOSAT's two solar panels failed, it could no longer acquire lunar calibration observations. The OCO-2 team was eventually able to use lunar observations to track relative radiometric drifts as small as 1%/year within its three spectral channels. Additional ground- and space-based measurement campaigns and comparisons with other spacecraft will be needed to improve this standard beyond that level or to extend it to other wavelength ranges.

CEOS and CGMS could play a significant role in coordinating these efforts. In the short term, these lessons represent best practices that should be extracted and generalised by the

CEOS/CGMS Working Group on Calibration and Validation (WGCV) and the Global Space-based Intercalibration System (GSICS) so that they are available as calibration "protocols" for space agencies that are now considering missions that could contribute to a future constellation. In addition, the strategy for cross-calibrating the GOSAT and OCO-2 instruments has employed common standards, including observations of the sun, Moon, and surface vicarious calibration sites, such as Railroad Valley, Nevada, U.S.A. Additional effort by WGCV and GSICS is needed to maintain and improve the quality of these standards to better address the calibration needs of space-based CO<sub>2</sub> and CH<sub>4</sub> sensors.

### 6.3 Cross-validating XCO<sub>2</sub> and XCH<sub>4</sub> estimates across the constellation

To cross-validate the XCO<sub>2</sub> estimates from GOSAT and OCO-2, the science teams from both missions worked closely with the TCCON consortium and aircraft programs to develop internationally-recognized standards for validating space-based XCO<sub>2</sub> and XCH<sub>4</sub> estimates. The ~21 TCCON stations now provide the primary method for tracing the space-based CO<sub>2</sub> and CH<sub>4</sub> measurements to the ground-based *in situ* standards maintained by the WMO GAW network. This validation approach involves two steps (Wunch et al., 2011a; 2011b). First, XCO<sub>2</sub> and XCH<sub>4</sub> estimates derived from measurements obtained at individual TCCON stations are validated against vertical profiles of *in situ* measurements obtained by high altitude aircraft flying above the stations. Data collected by both high-altitude fixed-wing aircraft (Washenfelder et al., 2006; Wunch et al. 2011a) and balloon-borne AirCore systems (Karion et al. 2010) are being used for this application. XCO<sub>2</sub> and XCH<sub>4</sub> estimates from coincident space-based and TCCON measurements are then compared to relate these remote sensing results.

The TCCON network is currently providing a cross-validation standard with accuracies near 0.1% (~0.4 ppm) (Wunch et al., 2017). The ~21 stations are adequate for identifying and correcting biases on regional to hemispheric scales, but a much denser network may be needed to support a constellation designed to quantify anthropogenic as well as natural CO<sub>2</sub> and CH<sub>4</sub> fluxes on national scales. In particular, the current network, whose stations are primarily located in North America, Western Europe, Japan, and Oceania (Australia, New Zealand, Philippines) will have to be expanded to Africa, South America, and China to support the GEO elements of the constellation. Additional stations in the Arctic and boreal regions will be needed to support the HEO elements of the constellation.

The TCCON network is now managed as a loose confederation individual Principal Investigators, most of whom are funded from year to year from a variety of sources to operate the stations, archive and distribute their data. This funding model has limited the number and geographic distribution of TCCON stations and does not provide the resiliency needed to support an operational space-based CO<sub>2</sub> and CH<sub>4</sub> constellation. Given the importance of this network to any future CO<sub>2</sub> or CH<sub>4</sub> constellation, CEOS should strongly encourage its member agencies to identify a more coordinated and sustainable method for supporting and expanding the TCCON network and the distribution of its products.

As the CO<sub>2</sub>/CH<sub>4</sub> constellation grows, spacecraft-to-spacecraft validation opportunities should become more common. For example, as mentioned above, cross validation of XCO<sub>2</sub> and XCH<sub>4</sub> estimates from coincident observations from LEO, GEO and HEO platforms should be strongly encouraged. Also, if the broad-swath imaging CO<sub>2</sub>/CH<sub>4</sub> spectrometers on one or more of the LEO platforms could be combined with an active CO<sub>2</sub> and/or CH<sub>4</sub> Lidar, the Lidar would serve two purposes. First, as noted above, it would provide some coverage of the night side hemisphere and Polar Regions during polar night. XCO<sub>2</sub> or XCH<sub>4</sub> measurements retrieved from a selected footprint of the passive spectrometer could be compared to Lidar observations co-boresighted with that footprint to identify persistent systematic biases in both instruments, since passive solar and active Lidar instruments are affected differently by uncertainties in clouds, aerosols, and other sources of bias. CEOS and CGMS should encourage their member agencies and partners to support these and other cross-platform validation activities.

#### 6.4 Retrieval algorithm advances needed to support a CO<sub>2</sub>/CH<sub>4</sub> constellation

Since the launch of SCIAMACHY, substantial progress has been made in the development of remote sensing retrieval algorithms for estimating XCO<sub>2</sub>, XCH<sub>4</sub>, and SIF from space-based observations of reflected sunlight. These methods are now yielding estimates with accuracies approaching 1 ppm for XCO<sub>2</sub> (Wunch et al. 2011b; 2017; Buchwitz et al., 2015; 2017b; Hedelius et al., 2017; O'Dell et al. 2018) and 6 ppb for XCH<sub>4</sub> (Yoshida et al., 2013; Parker et al., 2015) on regional scales after applying quality filters. Advanced methods for identifying and correcting regional scale biases have also been developed to further reduce the impact of known biases (O'Dell et al., 2018; Osterman et al., 2018). In spite of this progress, substantial improvements in both the forward models and inverse methods used in these algorithms are needed to yield the accuracy, precision, coverage, reliability, and computational speed required to fully exploit the quality and quantity of data expected from a future operational CO<sub>2</sub> and CH<sub>4</sub> constellation. For example, uncertainties in gas absorption cross sections still introduce biases on a range of spatial scales. More reliable methods for identifying cloud-free footprints and detecting or correcting contamination of clear-sky footprints by scattering or shadowing by nearby clouds are needed. A more reliable treatment of the scattering by optically thin clouds and aerosols is critical for retrieving XCO<sub>2</sub> and XCH<sub>4</sub> in the presence of fossil fuel or biomass plumes, since aerosols are often co-emitted with CO<sub>2</sub> and CH<sub>4</sub>. Improvements in computational speed are also required since the most accurate methods are computationally-demanding even for current data volumes, and a future CO<sub>2</sub>/CH<sub>4</sub> constellation will return hundreds to thousands of times as much data.

Progress is being made in each of these areas, but must be fostered to support a CO<sub>2</sub>/CH<sub>4</sub> constellation within the next decade. CEOS should encourage its member agencies to support these retrieval algorithm developments and intercomparison efforts, and should encourage the free exchange of gas and aerosol optical properties and other types of input and validation data. CEOS should also support the development of remote sensing retrieval algorithms that can analyze the data from the full array of instruments that will be deployed in the CO<sub>2</sub>/CH<sub>4</sub> constellation, so that these data can be used to create a harmonized multi-sensor global product that can be used by the atmospheric inversion community. Finally, since bias correction of the

XCO<sub>2</sub> and XCH<sub>4</sub> retrievals is an important step of the process at the moment, further work into harmonizing the retrieval schemes used to process the satellite and TCCON should be encouraged, to reduce possible representation errors caused by the different schemes.

## 6.5 Atmospheric inversion systems needed to support a CO<sub>2</sub>/CH<sub>4</sub> constellation

To date, atmospheric inversion systems have been used primarily for assessing CO<sub>2</sub> fluxes from the natural biosphere and CH<sub>4</sub> fluxes from wetlands. These systems will require substantial advances to support applications as demanding as supporting urban- to national-scale GHG emission inventories and monitoring natural carbon cycle responses to climate change.

Transport models currently represent one of the weakest components of atmospheric inversion systems. Several ongoing efforts are needed to improve horizontal resolution and vertical transport representation in the specific context of atmospheric inversion. The assimilation and inversion systems will also have to accommodate a broader range of data types with their associated uncertainties. Current atmospheric inversion systems can simultaneously assimilate XCO<sub>2</sub>, XCH<sub>4</sub>, and SIF data from one or two LEO spacecraft along with data from TCCON and the *in situ* surface and tower networks. In the future, to meet the demanding spatial and temporal resolution and coverage requirements, these systems may have to assimilate data from a much broader array of passive and active instruments deployed on LEO, GEO, and HEO spacecraft, and commercial aircraft (CONTRAIL, Machida et al., 2008; IAGOS, Filges et al., 2015) as well as an expanded ground-based *in situ* network. Efforts to improve the efficiency of global inversions should also be encouraged so that they can estimate fluxes at the highest spatial resolutions that the increased data density of upcoming constellation will allow.

The availability of high-spatial-resolution maps of XCO<sub>2</sub> and XCH<sub>4</sub> from a constellation of satellites like the one described above will also provide opportunities to expand the utility of atmospheric inversion systems to produce a more independent assessment of inventories. Currently, most mesoscale to global atmospheric inversion experiments use data from gridded inventories, such as EDGAR (Janssens-Maenhout et al., 2017) or ODIAC (Oda and Maksyutov, 2011; Oda et al., 2018) to specify the well-documented fossil fuel emission sources as part of the flux prior, and then derive the residual fluxes. This approach is not ideal because the final answer is strongly dependent on the assumed prior in places where the observations do not adequately constrain the flux estimate. Once high spatial resolution space-based data are available (along with proxies such as NO<sub>2</sub> or CO for identifying discrete plumes), it might be possible to use mass balance and plume dispersion techniques to provide an independent assessment of the spatial distribution fluxes from compact sources, replacing the gridded inventories.

Uncertainties in the input meteorological fields limit the accuracy of atmospheric inversion systems since the inferred fluxes depend on the product of the atmospheric transport and the CO<sub>2</sub> or CH<sub>4</sub> anomaly (Polavarapu et al., 2018; Patra et al., 2011). Systems that use both surface *in situ* and space-based column averaged data would benefit from improvements in both the vertical and horizontal resolution of the atmospheric transport model. Improved estimates of the vertical transport through the planetary boundary layer are especially critical for inferring urban scale

fluxes from both ground-based *in situ* and space-based column observations. Improvements in the stratospheric transport and chemistry are also critically needed for interpreting XCH<sub>4</sub> observations, since the CH<sub>4</sub> mixing ratio decreases rapidly throughout the stratosphere.

One promising way to improve our understanding of the accuracy of the atmospheric transport is to perform atmospheric inversions that simultaneously assimilate measurements of multiple species including long-lived greenhouse gases and their isotopes and short-lived reactive gases that affect air quality, like NO<sub>2</sub> and CO, since all of these species are transported by same winds. Models that produce adequate fits to all species should therefore produce more reliable flux estimates. Alternately, the Carbon Cycle Data Assimilation System (CCDAS) approach employs prognostic land surface models constrained by other well observed state variables (temperature, land cover, etc.) to provide *a priori* estimates of fluxes and their uncertainties as well as dynamical guidance (Rayner et al., 2005; 2011; Scholze, et al., 2007).

Another limiting factor of atmospheric inversion systems is the lack of robust uncertainty estimates of the assumed prior fluxes, including fossil fuel, biospheric and oceanic fluxes. This is critical because the inversion system depends on the assumed prior flux uncertainties and the sensitivities of observations to underlying fluxes (simulated by transport) to allocate the mismatch between observations and model simulated values to a quantitative adjustment in prior fluxes. In most existing studies, *ad hoc* prior flux uncertainties (variances and covariances) are assumed. More research is needed to develop robust estimates of prior flux uncertainties, and a close collaboration between atmospheric inversion community and biogeochemical modeling and bottom-up inventory community should be encouraged.

More generally, advanced methods for validating the fluxes estimated using these atmospheric inverse systems are critically needed, both to facilitate model improvements and to certify the accuracy and reliability of the estimated emissions products (Liu and Bowman, 2016). Currently, atmospheric inverse modelers validate fluxes by comparing *a posteriori* CO<sub>2</sub> and CH<sub>4</sub> fields against *in situ* measurements of CO<sub>2</sub> and CH<sub>4</sub> profiles collected by aircraft (Liu et al., 2017; Bergamaschi et al., 2018). If the atmospheric inversion system reduces the difference between the *a priori* and observed profiles, they assume that the flux uncertainty has been reduced as well. This approach may work on regional scales, but may not be adequate for quantifying fluxes and their uncertainties on scales ranging from urban to national scales.

On these smaller scales, comparisons of biospheric fluxes from atmospheric inversions to estimates from individual flux towers or mesoscale flux tower networks are challenging because it is difficult to up-scale flux tower estimates to spatial scales reliably constrained by atmospheric inversions or to co-locate flux towers within (sparsely sampled) satellite footprints (Kondo et al., 2015). These issues should be mitigated to some extent as the resolution and coverage of the satellite observations improve, and as denser ground-based flux monitoring networks are deployed. For individual large power plants or large, isolated urban areas, where anthropogenic fluxes dominate and are reasonably well known, these data can be used to validate atmospheric inversion results (Conley et al., 2016; Hedelius et al., 2017; Ye et al., 2017).

To inform anthropogenic emission inventories with space-based measurements, CEOS should continue to encourage its member agencies to support the development of advanced atmospheric inversion systems. These efforts should span all scales of interest, from global models, to mesoscale models, to urban scale and point source models, and should encourage the use of data from the broadest range of space-based and ground-based sources. They should also encourage the development and testing of innovative ways to validate atmospheric inversion products.

## 7. Conclusions and Way Forward

Measurements of atmospheric CO<sub>2</sub>, CH<sub>4</sub>, and other GHGs provide an integrated constraint on the net exchange of these gases between the surface and the atmosphere. If these atmospheric measurements can be integrated into a comprehensive atmospheric GHG monitoring system, like that outlined in Chapters 2 and 6, they could form the basis of top-down approach that complements the bottom-up inventories used for NDCs. They could also provide timely insight into changes in the natural carbon cycle as it evolves in response to climate change. Estimates of XCO<sub>2</sub> and XCH<sub>4</sub> from space-based observatories could play a crucial role in this atmospheric carbon monitoring system by providing the spatial resolution and coverage needed to discriminate emission hot spots and improve the quantification of both natural and anthropogenic fluxes on national scales. While great progress has been made in space-based atmospheric CO<sub>2</sub> and CH<sub>4</sub> measurement techniques and analysis methods over the past 15 years, additional advances are needed to meet the increasingly demanding requirements for precision, accuracy, resolution, and coverage. The continued involvement of research agencies will therefore be critical as operational agencies begin to design and deploy the first generation of dedicated operational systems that can deliver CO<sub>2</sub> and CH<sub>4</sub> products and services with a guaranteed quality, reliability and timeliness.

This report represents the first comprehensive analysis of the state-of-the art of space-based atmospheric greenhouse gas monitoring capabilities in support of international, regional and national climate policy. It also provides a reference document for individual agencies planning missions in this domain as well as for the broader coordination of virtual and dedicated constellations of space-based CO<sub>2</sub> and CH<sub>4</sub> sensors among space agencies through CEOS and CGMS. To advance the state of the art and build a strong foundation for the space-based elements of an operational atmospheric CO<sub>2</sub> and CH<sub>4</sub> monitoring system that can be implemented within the next few years, this report recommends a series of specific steps:

1. A prototype system, based on available space-based and ground-based atmospheric measurement assets and modelling capabilities, should be designed and implemented in time to inform the first global stocktake in 2023. To support this stocktake, the initial global atmospheric CO<sub>2</sub> and CH<sub>4</sub> flux products must be available by 2021.
2. The initial operational system should exploit the lessons learned from the development and use of the prototype product as well as new space-based measurement and modelling capabilities to produce space-based CO<sub>2</sub> and CH<sub>4</sub> flux products in time to support the second global stocktake in 2028.
3. To meet these goals within a decade, it is imperative that individual research and operational space agencies work within CEOS, CGMS and other international coordination bodies (i.e. WMO IG<sup>3</sup>IS, GCOS, GEO-C) to define a roadmap with specific programmatic milestones for developing virtual and then dedicated constellations that can deliver harmonized, space-based climate data records for CO<sub>2</sub> and CH<sub>4</sub>.

4. The preparation of this report has demonstrated the benefits of the complementary viewpoints provided by CEOS and CGMS for advancing the implementation of system that incorporates both research and operational elements within the timeframe available. In particular, the CGMS partners could provide insight into the process of gathering user requirements for timeliness, reliability, traceability, reprocessing, quality assurance, and providing user support for an operational product. A continued engagement by both entities is required and some formalisation of the relationship would be advantageous. The joint CEOS/CGMS Working Group on Climate could lead this effort.
5. As recognised in Chapter 2, a broad system approach is required to develop a top-down atmospheric inventory approach that complements the bottom-up inventories. This system integrates the satellite observations, *in situ* (surface, aircraft, and balloon) measurements, modelling components (retrieval, inversion, biogeochemical processes and transport), prior information and ancillary data.
6. To ensure that the space agencies are working together and building the necessary partnerships with the relevant stakeholders (i.e. UNFCCC/SBSTA) to address the overall system implementation goals, they should work through CEOS and CGMS to strengthen the ties to these stakeholders.
7. In Chapter 6, the GCOS requirements were adopted as the basis in the formulation of a baseline operational CO<sub>2</sub>/CH<sub>4</sub> constellation because GCOS provides an independent basis for the requirements. However, these requirements predated the Paris Agreement, which changed the focus of CO<sub>2</sub> and CH<sub>4</sub> monitoring efforts to anthropogenic emissions at national scales. Further analysis and revision of the space-based measurement and analysis requirements are needed to address this new focus. The CEOS and CGMS agencies should work with GCOS and other partner organizations and stakeholders in an iterative approach to further refine those requirements over the next few years.
8. CEOS, CGMS and their partners should continue to support the necessary OSSE experiments, which remain of critical importance in further refining the detailed requirements of the space-based elements of the constellation (sensor precision, accuracy, and resolution, orbit and mission coordination). The near-term objective is to develop a prioritized list of the required OSSE experiments and end-to-end system simulations to optimize the overall system design, resolve system-level uncertainties, and facilitate the coordination of activities among the CEOS and CGMS agencies. The output from these experiments should be made available to the CEOS and CGMS Principals periodically, in a format conducive to discussions with their mission and orbit planning organizations.
9. Over the last 15 years, research missions have provided considerable insight into instrument calibration, validation and the broader aspects of uncertainty quantification and quality control. Appendix 4 of this report summarizes the lessons learned from SCIAMACHY, GOSAT, and OCO-2. In the short-term, these lessons represent best practices that should be extracted and generalised by the CEOS/CGMS Working Group on Calibration and Validation (WGCV) and the Global Space-based Intercalibration

System (GSICS) so that they are available as Cal-Val strategy "protocols" for space agencies that are now considering missions.

10. The strategy for cross-calibrating the GOSAT and OCO-2 instruments has employed common standards, including observations of the sun, Moon, and surface vicarious calibration sites, such as Railroad Valley, Nevada, U.S.A. Additional effort by WGCV and GSICS is needed to maintain and improve the quality of these standards to better address the calibration needs of space-based CO<sub>2</sub> and CH<sub>4</sub> sensors.
11. TCCON has provided the primary transfer standard to relate space-based XCO<sub>2</sub> and XCH<sub>4</sub> estimates to the ground-based *in situ* standards maintained by the WMO GAW network. This network must be maintained and augmented using portable, ground-based remote sensing instruments (e.g. EM27/SUN), *in situ* sensors on fixed-wing aircraft (commercial aircraft, such as CONTRAIL, IAGOS) and balloons (AirCore), and airborne remote sensing instruments (MAMAP, CHARM-F etc.) to provide a more robust and accurate operational validation approach.
12. CGMS and CEOS should work with their member agencies to identify and promote standards in product specification, formats, pre-processing etc. and product inter-comparisons should be routinely undertaken and supported on a sustained basis to produce seamless, interoperable datasets that can be used in the broader system implementation.
13. Agencies should consider a centralized (but possibly geographically distributed) repository for hosting quality-controlled CO<sub>2</sub> and CH<sub>4</sub> products, with internal capability for product inter-comparison.
14. The capabilities required to meet the needs of the UNFCCC and the Parties to the Convention are already at the limit of the state-of-the-art for existing, space-based measurement technology. The CEOS and CGMS agencies should therefore continue to pursue complimentary technologies for both sensors (e.g. wide swath passive CO<sub>2</sub> and CH<sub>4</sub> imagers, active lidar) and mission design (e.g. HEO). These development efforts should be coordinated to keep the Principals updated on additional needs and capabilities that would be useful to consider for future mission opportunities.
15. There is a significant need for systematically produced ancillary measurements. These measurements are needed both to improve the accuracy of the XCO<sub>2</sub> and XCH<sub>4</sub> retrievals (i.e. coincident observations of clouds and aerosols) and to facilitate their interpretation within the context of the anthropogenic and natural carbon cycle (i.e. SIF, NO<sub>2</sub> and CO). Here, the proposed atmospheric CO<sub>2</sub> and CH<sub>4</sub> monitoring system could substantially benefit from the full scope of carbon cycle observations included in the CEOS Carbon Strategy. The CEOS partner agencies should therefore continue to support that strategy. The coordination mechanism identified to address follow-up to the current work should provide an assessment of prioritized products to be addressed in a coherent way, across agencies, to ensure seamless input to the system.

16. To ensure that the initial operational constellation and associated atmospheric CO<sub>2</sub> and CH<sub>4</sub> monitoring system can meet the sustained operational needs, a system engineering effort should be undertaken early in the implementation. This effort is needed to ensure that the requirement-reliability-traceability-fitness-for-purpose cycle is adequately planned and that the user uptake, user support and training and capability building elements are defined and prototyped. The CEOS and CGMS agencies and their partners at WMO have the necessary competences to start addressing these requirements and can help to assess the scope of these activities at the different levels of the implementation.

This summary describes some areas where initial efforts are required to ensure that the space agencies are ready to make the critical contributions needed on the timescale identified in point "1" above. These ambitious time constraints, require substantial programmatic commitments at the level of individual agencies. They also demand strengthened cooperation amongst space agencies (through CEOS and CGMS) as evidenced in point "2" as well as between CEOS/CGMS and the relevant external partners/stakeholders i.e. UNFCCC/SBSTA, WMO, GCOS and GEO. Finally, the CEOS agencies should establish and nurture strong, continuous engagement with the national inventory agencies as well as the stakeholders listed above. Frequent interactions with the inventory community will be critical to ensure that the products CO<sub>2</sub> and CH<sub>4</sub> produced by the CEOS agencies are well understood, and can support the Transparency Framework and can serve as a complementary Measurement, Reporting, and Verification System for nationally determined contributions.

The CEOS agencies can exploit a number of existing elements and competences. which include: the all-encompassing CEOS Carbon Strategy which provides the broader template for CEOS' work on the Carbon Cycle, the CEOS CGMS Joint Working Group on Climate which provides the direct link to the policy needs through UNFCCC/SBSTA and GCOS and for which the activities presented here would represent a concrete example of the realisation of the Climate Monitoring Architecture from Space (for atmospheric GHG monitoring), the Atmospheric Composition Virtual Constellation where there technical competences on the missions and instruments are located and other relevant competences for calibration (WGCV), information systems (WGISS) and capacity building and training (WGCapD). CGMS also have several relevant working groups and experts group which bring complimentary competences.

In summary, the needs are clear, the architecture implementation, though challenging, is within the means of agencies and the coordination mechanisms. We have a clear understanding of how we fit into the broader system and with which external stakeholders we need to engage. As summarized here, we also understand short-to-mid-term priorities that should be addressed to advance implementation, most importantly we have the necessary competences within CEOS and CGMS, and their technical working groups and other entities as well as their respective agencies, to address these priorities. So, with the appropriate decisions and direction from space agency Principals, we can and should strive to build the necessary constellation and associated system interfaces over the next decade.

## **Acknowledgements**

Part of this research was carried out at the Jet Propulsion Laboratory, California Institute of Technology, under a contract with the National Aeronautics and Space Administration.

## APPENDIX 1: Remote sensing retrieval methods for estimating XCO<sub>2</sub> and XCH<sub>4</sub> from observations of reflected sunlight

State-of-the-art atmospheric remote sensing retrieval algorithms are needed to estimate XCO<sub>2</sub>, XCH<sub>4</sub> and other properties of the atmospheric and surface state from each spectrum collected by a space-based instrument. A typical solar SWIR retrieval algorithm includes five major components. The first is a preprocessor that specifies the initial guess for the “state vector,” consisting of atmospheric structure, vertical profile of absorbing and scattering gases and airborne particles (clouds, aerosols), and the surface optical properties. It then screens out soundings contaminated by optically thick clouds. The second is a surface-atmosphere radiative transfer model that produces a synthetic spectrum of the solar radiation reflected by the surface and atmosphere for the specified viewing geometry. Typical radiative transfer models also generate “spectral Jacobians,” which specify the rate of change of the radiance at each wavelength due to changes in the state properties at any level of the atmosphere or at the surface.

The third is an instrument model that simulates the spectrally-dependent performance of the flight instrument (i.e. spectrally-dependent throughput, spectral coverage and resolution, instrument line shape, polarization sensitivity, etc.). The fourth is an inverse model that uses a constrained, non-linear least-squares approach to optimize the atmospheric and surface state properties to minimize the differences between the observed and the synthetic spectrum. The final component is a post-processor that assesses the quality of the retrieved state properties. These components are illustrated in Figure A1-1.

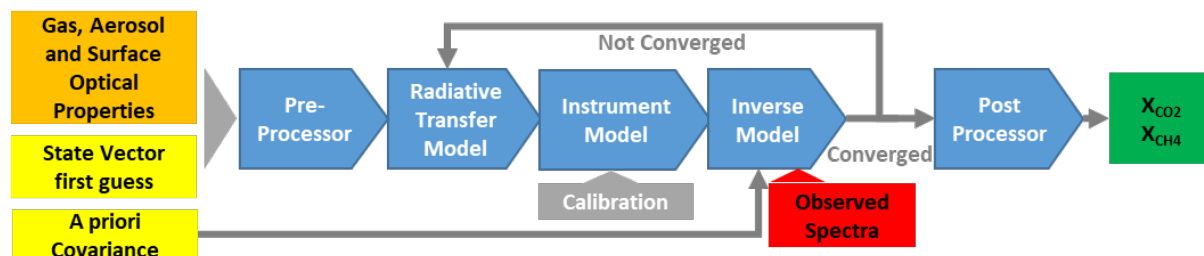


Figure A1-1: A typical remote sensing retrieval algorithm incorporates multiple inputs into the forward radiative transfer model and instrument model, which generate synthetic spectra that are compared to the observed spectra. The inverse model updates the atmospheric and surface state to improve the fit between the observed and synthetic spectra. This process is repeated until the convergence criteria are met. The products (XCO<sub>2</sub>, XCH<sub>4</sub>, etc.) are then generated from the retrieved state vector (credit: JPL/NASA).

Given an initial guess for the atmospheric and surface state and the observing geometry for a specific sounding, the radiative transfer model generates a high-resolution synthetic radiance spectrum and radiance Jacobians for spectral ranges sampled by the space-based instrument. These typically include the O<sub>2</sub> A-band, the CO<sub>2</sub> bands centered near 1.61 and 2.06 μm (Figure A1-2) and the CH<sub>4</sub> bands at 1.67 or 2.3 μm. This synthetic spectrum fully resolves the wavelength-dependent structure of the solar spectrum at the top of the atmosphere, the absorption and scattering cross sections and scattering phase functions for each absorbing gas, all

cloud and aerosol particle types included in the state vector, and the optical properties of the reflecting surface.

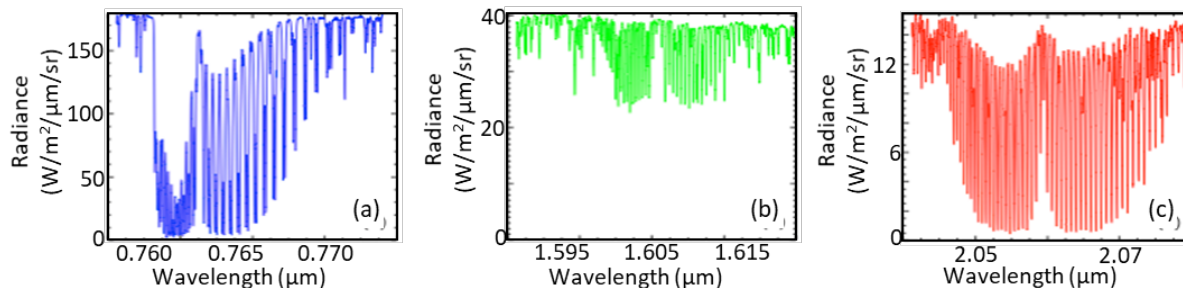


Figure A1-2: Typical spectra from the (a) O<sub>2</sub> A-band, (b) 1.61 μm CO<sub>2</sub> band and (c) 2.06 μm CO<sub>2</sub> band collected by OCO-2. Each spectrum has a resolving power,  $\lambda/\Delta\lambda \cong 19,000$ , to resolve the individual O<sub>2</sub> and CO<sub>2</sub> absorption lines from the adjacent continuum (credit: JPL/NASA).

The instrument model then convolves this full-resolution synthetic radiance spectrum with the instrument line shape (ILS) function and corrects for instrument throughput and polarization to simulate the spectrum recorded by the instrument. An inverse method based on optimal estimation (Rodgers, 2000; Connor et al.; 2008; 2016; Bösch et al., 2006; 2011) or Philipps-Tikhonov regularization (Butz et al., 2009) then determines the differences between the observed and simulated spectrum and updates the state vector to minimize differences between the observed and simulated spectra. The radiative transfer model then generates an updated synthetic spectrum and spectral Jacobians, and this process is repeated until the differences between the observed and synthetic spectra meet their convergence criteria or the fit fails to converge. The post-processor then generates the final state properties and assesses their quality (i.e. convergence, quality of fit, compliance with screening criteria, etc.).

Accurate but computationally-fast forward radiative transfer models are essential to meet the demanding requirements for retrieving XCO<sub>2</sub> and XCH<sub>4</sub>. For example, to resolve XCO<sub>2</sub> differences as small as 0.25% (1 ppm out of the 400 ppm background), the radiative transfer model must produce high-resolution synthetic radiance spectra with accuracies near 0.1% to simulate spectra with spectral resolving powers near  $\lambda/\Delta\lambda \sim 20,000$  (where  $\lambda$  is the wavelength of interest and  $\Delta\lambda$  is the spectral sampling interval), because a 0.25% change in XCO<sub>2</sub> rarely produces larger changes in the reflected radiance spectrum (Crisp et al., 2017). To meet this requirement, the radiative transfer model must accurately account for the spectrally-dependent absorption, multiple scattering, and polarization of the incident sunlight by gases and airborne particles (clouds, aerosols, dust) and the surface. It must also be fast enough to process the large volume (tens of thousands to millions) of cloud-free soundings collected each day. A substantial amount of progress has been made to address the speed and accuracy of these methods since the launch of SCIAMACHY, GOSAT, and OCO-2. However, substantial improvements in retrieval algorithm precision and accuracy are needed to provide products that can be used to inform inventories or track subtle changes in the natural carbon cycle associated with climate change. Dramatic improvements in algorithm speed are needed to support the demanding resolution and coverage requirements of these new applications.

## APPENDIX 2: Methods for quantifying surface fluxes of CO<sub>2</sub> and CH<sub>4</sub> from space-based XCO<sub>2</sub> and XCH<sub>4</sub> estimates

The methods used to derive CO<sub>2</sub> and CH<sub>4</sub> fluxes from spatially resolved estimates of their column-averaged concentrations can be broadly classified as analytic mass balance, plume dispersion, or atmospheric inversion methods. All three approaches predict or optimize surface fluxes needed to reproduce the observed XCO<sub>2</sub> and XCH<sub>4</sub> distributions in the presence of the time-varying wind field. However, each approach places distinct requirements on the precision, accuracy, resolution, and coverage of the atmospheric CO<sub>2</sub> and CH<sub>4</sub> estimates. These differences are illustrated in the following three subsections.

### A2.1 Source pixel mass balance methods for estimating fluxes from compact sources

A series of methods have been developed for estimating emissions from point sources. Perhaps the simplest example is the Source Pixel Mass Balance method (see Varon et al., 2018), which has been adopted here for illustration.

For emission sources that are smaller than the instrument footprint size, the minimum detectable mass or change depends on the footprint area,  $A$ , and the minimum detectable change in  $\Delta XCO_2$  or  $\Delta XCH_4$ , which may be associated with the single sounding random error (precision), or the footprint-to-footprint biases. To illustrate this, we note that the total mass of a hydrostatic atmosphere per unit area is given by  $M_{ATM} = P_{surf}/g$ , where  $P_{surf}$  is the surface pressure and  $g$  is the acceleration due to gravity. At sea level, the total mass of dry air is  $M_{ATM} \approx 101000 \text{ Pa} / 9.8 \text{ m/s}^2 = 10300 \text{ kg/m}^2$ . If the CO<sub>2</sub> volume mixing ratio,  $[CO_2] = 400 \text{ ppm}$  or  $4 \times 10^{-4} \text{ mol/mol}$ , the mass of CO<sub>2</sub> per unit area,

$$M_{CO_2} = [CO_2] \times M_{ATM} \times \mu_{CO_2} / \mu_{air},$$

where  $\mu_{CO_2}$  is the molecular mass of CO<sub>2</sub> (44 kg/kmole) and  $\mu_{air}$  is the molecular mass of dry air (29 kg/kmole). The total mass of CO<sub>2</sub> per unit area is therefore,  $M_{CO_2} = 44 / 29 \times 4 \times 10^{-4} \times 10300 = 6.24 \text{ kg/m}^2$  and a 1 ppm change in CO<sub>2</sub> throughout the column is equivalent 1/400 of that or  $0.0156 \text{ kg/m}^2$  or  $0.0156 \text{ kilotons/km}^2$ , where 1 kiloton (kt) is  $10^6 \text{ kg}$ . If a sensor can detect a 1-ppm difference in XCO<sub>2</sub> within a  $1 \text{ km}^2$  footprint, it can therefore detect a CO<sub>2</sub> mass anomaly,  $\Delta M_{CO_2} = 0.016 \text{ kt}$  change in the CO<sub>2</sub> within that footprint. Because the detection limit scales with the area of the footprint, if it can detect a 1-ppm change within a  $10 \text{ km} \times 10 \text{ km}$  ( $100 \text{ km}^2$ ) footprint, it can detect a mass change of  $\Delta M_{CO_2} = 1.6 \text{ kt CO}_2$  (Figure A2-1).

The minimum detectable flux or flux change depends on the minimum detectable mass change, the footprint size and the effective wind speed and direction across the footprint (here defined as the mass-weighted averaged wind profile). To visualize this, assume that the CO<sub>2</sub> flux from a point source,  $F$ , is constant over a time interval,  $t$ , and that an effective, horizontal wind speed,  $u(\theta)$ , is blowing across the footprint in direction,  $\theta$ , over this time interval.

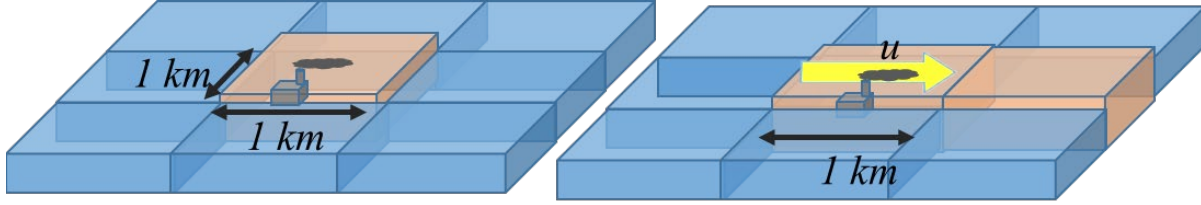


Figure A2-1: Left – In the absence of transport, an emission source that adds  $\Delta M \sim 16$  tons of  $\text{CO}_2$  to the air within a  $1 \text{ km} \times 1 \text{ km}$  footprint will raise the  $\text{XCO}_2$  within that footprint by  $\sim 1$  ppm. Right - The flux needed to maintain this  $\text{XCO}_2$  anomaly in the presence of a steady wind, increases linearly with the wind speed,  $u$ .

The corresponding change in the mass of  $\text{CO}_2$ ,  $M_{\text{CO}_2}$ , is given by  $\Delta M_{\text{CO}_2} = F \cdot t$ . If the effective footprint has a horizontal projection,  $L(\theta)$ , in direction,  $\theta$ , then the mean residence time,  $t$ , in the footprint (assuming the point source is roughly centered within the footprint) is  $t = 0.5 L / u$ . The change in  $\text{CO}_2$  mass within a footprint is therefore related to the corresponding flux by a relation of the form:

$$\Delta M_{\text{CO}_2} = 0.5 \cdot F \cdot L / u .$$

Rearranging (and ignoring horizontal convergence and divergence), we can express the minimum detectable flux,  $F_{\text{min}}$  in terms of the mass change, associated with the instrument precision,  $\Delta M_{\text{CO}_2} (\Delta \text{XCO}_{2\text{min}})$ :

$$F_{\text{min}} = 2 \cdot u \cdot \Delta M_{\text{CO}_2} (\Delta \text{XCO}_{2\text{min}}) / L .$$

As noted above, at a concentration of 400 parts per million, an instrument that has a single sounding precision of  $\Delta \text{XCO}_2 = 1$  ppm can detect a  $\text{CO}_2$  mass anomaly with an amplitude,  $\Delta M_{\text{CO}_2} (\Delta \text{XCO}_{2\text{min}}) \approx 0.016 \text{ kg/m}^2$  or  $0.016 \text{ kt/km}^2$ . If we assume a conservative, effective stack-height averaged wind velocity of  $u = 10 \text{ km/hr}$ , this indicates a minimum detectable flux of  $0.312 \text{ kt/hr}$  in a single overpass. If this flux was maintained continuously, it would correspond to a flux of  $2.7$  megatons of  $\text{CO}_2$  ( $\text{Mt CO}_2$ ) per year. For comparison, the average  $\text{CO}_2$  emissions from the 10 largest coal fired power plants in the U.S. is around  $15 \text{ Mt CO}_2/\text{year}$  (see <https://ghgdata.epa.gov/ghgp/main.do#/listFacility/>), while the Paris metropolitan area (the densest urban area in Europe) emits  $40$  to  $52 \text{ MtCO}_2/\text{year}$  (Staufner et al., 2016; Broquet et al. 2018) from an area of  $\sim 17000 \text{ km}^2$ .

Tables A2.1 a-c illustrate the impact of  $\Delta \text{XCO}_{2\text{min}}$  and footprint size for effective, emission-level-averaged wind speeds of  $5$ ,  $10$ , and  $20 \text{ km/hr}$  ( $1.4$ ,  $2.8$ , and  $5.6 \text{ m/sec}$ ). These results clearly demonstrate the value of high precision and a small footprint size for constraining the emissions from compact sources. They also show that the precision needed to detect a given change in flux increases linearly with the ambient wind speed at the emission level. Only sensors with the highest precisions ( $0.25$  to  $0.5 \text{ ppm}$ ) and the smallest footprint sizes considered here ( $1$ - $2 \text{ km}^2$ ) may yield flux estimates for large coal-fired power plants with uncertainties that approach the reported state of the art for inventories in the developed world (Ciais et al., 2014).

Table A2.1 Point source flux sensitivity in megaton per year (Mt/yr) with footprint area (km<sup>2</sup>) and single sounding precision (ppm) for winds at (a) 5 km/hr, 10 km/hr, and 20 km/hr. The numbers shown here are the minimum fluxes detectable with the footprint size and XCO<sub>2</sub> enhancement.

(a) 5 km/hr

Footprint Area (km <sup>2</sup> )	$\Delta XCO_{2min}$ (ppm)					
	0.25	0.50	1.00	2.00	4.00	
1.0	0.34	0.68	1.40	2.70	5.50	
2.0	0.48	0.97	1.90	3.90	7.70	
4.0	0.69	1.40	2.70	5.50	11.0	
10.0	1.10	2.20	4.30	8.70	17.0	
50.0	2.40	4.80	9.70	19.0	39.0	
85.0	3.10	6.30	12.6	25.0	50.0	
1800.0	14.0	29.0	57.8	120.	230.	

(b) 10 km/hr

Footprint Area (km <sup>2</sup> )	$\Delta XCO_{2min}$ (ppm)					
	0.25	0.50	1.0	2.0	4.0	
1.00	0.68	1.40	2.70	5.50	11.0	
2.00	0.97	1.90	3.90	7.70	15.0	
4.00	1.40	2.70	5.50	11.0	22.0	
10.00	2.20	4.30	8.70	17.0	35.0	
50.00	4.80	9.70	19.0	39.0	77.0	
85.00	6.30	13.0	25.0	50.0	100.	
1800.00	29.0	58.0	115.	230.	460.	

(c) 20 km/hr

Footprint Area (km <sup>2</sup> )	$\Delta XCO_{2min}$ (ppm)					
	0.25	0.50	1.00	2.00	4.00	
1.00	1.40	2.70	5.47	11.0	22.0	
2.00	1.90	3.90	7.73	15.0	31.0	
4.00	2.70	5.50	11.0	22.0	44.0	
10.00	4.30	8.70	17.0	35.0	69.0	
50.00	9.70	19.0	39.0	77.0	160.	
85.00	13.0	25.0	50.0	100.	200.	
1800.00	58.0	115.	230.	460.	930.	

## A2.2 Estimating CO<sub>2</sub> and CH<sub>4</sub> emissions with plume dispersion models:

As the effective stack-height winds increase above 10 km/hour, even the most sensitive sensors considered here will face significant challenges detecting and characterizing fluxes with measurements obtained from individual soundings, like those described above. One way to reduce flux uncertainties in these cases is to acquire high spatial resolution images of the emission plumes formed as the winds transport emissions away from the source. All XCO<sub>2</sub> or

XCH<sub>4</sub> estimates from soundings within the plume can then be used in the emission estimate, which has a similar effect to averaging data to improve precision. The XCO<sub>2</sub> or XCH<sub>4</sub> values can be compared to spatial averages of soundings outside the plume to determine anomalies associated with the plume.

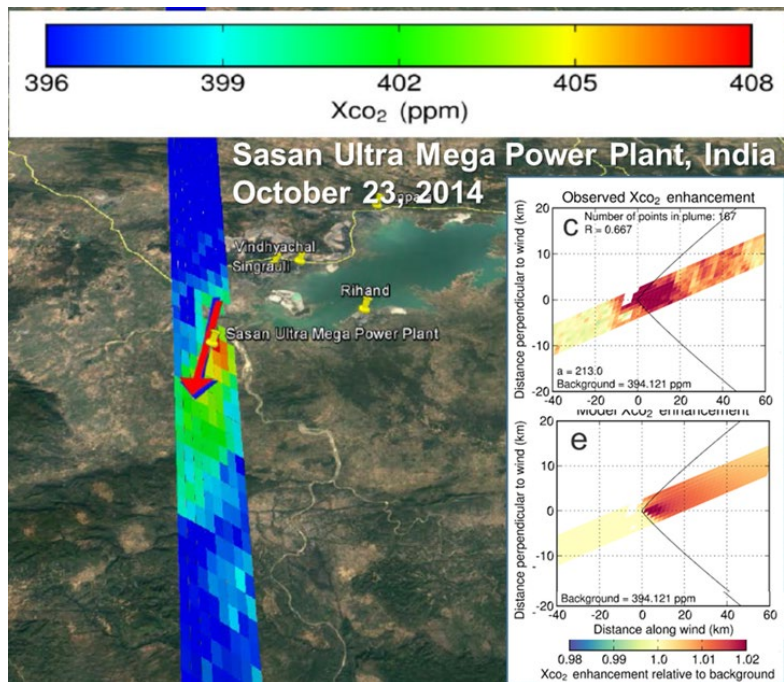


Figure A2-2: Nassar et al. (2017) used a Gaussian Plume model to estimate the CO<sub>2</sub> emissions from coal-fired power plants that were located along or close to OCO-2 ground tracks. Here, the OCO-2 ground track captured the plume of the Sasan Ultra Mega Power Plant in Northern India. The Gaussian plume model yielded a flux estimate of  $68 \pm 10$  kt/day, which was 13% higher than that of that projected in Sasan’s Clean Development Mechanism application to the UNFCCC (credit: Ray Nassar, ECCC and JPL/NASA).

By fitting the observed XCO<sub>2</sub> or XCH<sub>4</sub> enhancements to a plume from a dispersion model with some prior emissions, a scaling factor can be determined that gives the best fit. One such approach, which was pioneered for analyzing aircraft observations of emission plumes, assumes that the plume profile can be modeled as Gaussian distribution in height and width that expands as it is transported downwind by the local wind field. However, when using XCO<sub>2</sub> or XCH<sub>4</sub>, the problem is simplified to two dimensions by vertically integrating the plume (Bovensmann et al., 2010). This approach was successfully applied to data collected by OCO-2 to estimate the emissions from individual coal fired power plants, yielding estimates within 1%, 4% and 17% of reported daily emission values for power plants in the United States (Nassar et al., 2017; Figure A2-2). Once validated, these methods were applied to power plants in other countries where accurate emission data are not as reliable or not as readily available.

To reduce flux uncertainties using Gaussian plume models or other spatial averaging techniques, the soundings contaminated by the plume must be accurately discriminated from the background. This should be relatively straightforward once high spatial resolution imaging observations of XCO<sub>2</sub> and XCH<sub>4</sub> are available, as long as the plume is well within the detection limits of individual soundings. However, it will be much more challenging for soundings where the mass

anomaly is near or below the detection limit. These and other challenges are described by Ye et al., (2017) and Varon et al. (2018).

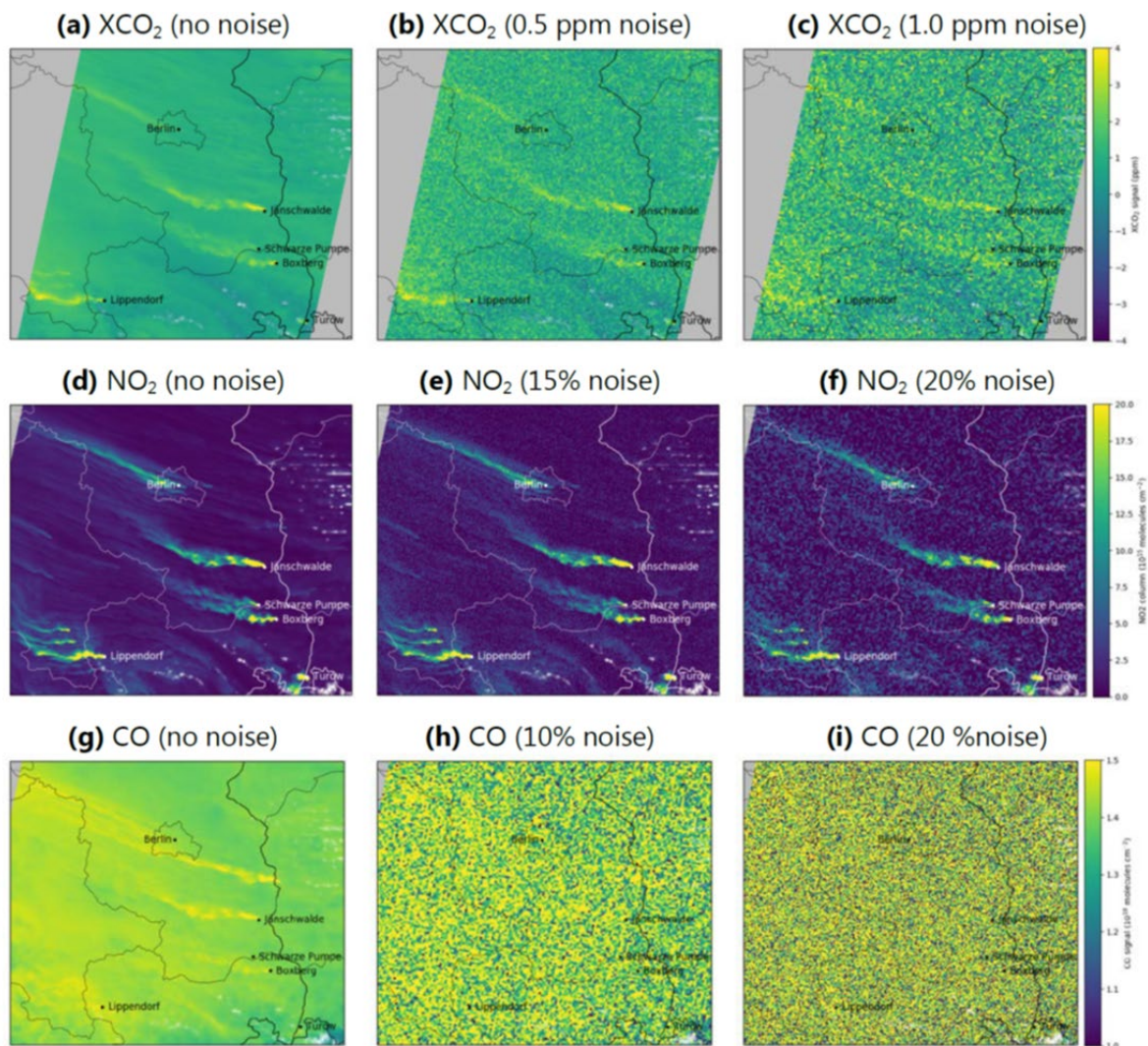


Figure A2-3: Simulated  $XCO_2$ ,  $NO_2$ , and CO distributions over Germany derived as part of the European Space Agency (ESA) Project SMARTCARB. The left-hand panels (a, d, e) show the simulated  $XCO_2$ ,  $NO_2$  and CO fields without noise. The middle panels (b, e, h) and right-hand panels (c, f, i) illustrate the impact of adding random noise to the fields. The  $XCO_2$  and XCO plumes become much less distinct as the noise increases, while the structure of the  $NO_2$  plumes is preserved, even when the noise increases to 20% (credit: ESA/SMARTCARB).

One way to discriminate an isolated plume from its background is to acquire spatially- and temporally-coincident observations of species co-emitted with the species of interest. For example, CO,  $NO_2$ , and  $SO_2$  are often co-emitted with  $CO_2$  by fossil fuel combustion, and all three of these gases are routinely measured from space for monitoring air quality (Figure A2-3). In general, measurements of these gases, alone, cannot be used to estimate  $CO_2$  emissions because their emission ratios can vary widely, depending on the combustion source, and some decay rapidly as they react with the environment. However, they can provide excellent tools for

identifying the location of the plume because they are usually emitted with concentrations that much larger than those in the background, and can be detected in space-based observations over much larger distances from the source, even in the presence of significant entrainment and diffusion. This approach may be of less value for tracking CH<sub>4</sub> plumes because the known co-emitted species (i.e. ethane from fracking) are even more difficult to detect from space.

### A2.3 Quantifying fluxes over extended areas with atmospheric inversion systems

The observed atmospheric CO<sub>2</sub> and CH<sub>4</sub> mole fractions are influenced by surface fluxes, atmospheric transport, and, where relevant, atmospheric chemistry. Because surface fluxes impose spatial and temporal gradients in the concentrations of these gases, atmospheric CO<sub>2</sub> and CH<sub>4</sub> measurements contain information about the geographical location, intensity, and timing of surface fluxes. Computational models of atmospheric transport are typically used to improve upon prior estimates of surface fluxes (derived from biogeochemical models for natural fluxes and inventories for anthropogenic fluxes) by relating them to spatially- and temporally-resolved atmospheric CO<sub>2</sub> and CH<sub>4</sub> measurements collected at sites around the world.

The approach most commonly adopted in atmospheric inverse modeling of sources and sinks is based on Bayesian inverse modeling (Enting 2002, Ciais et al., 2010). These atmospheric inverse methods assimilate CO<sub>2</sub> and CH<sub>4</sub> concentration data and adjust their surface fluxes to minimize a cost function, a mathematical expression that describes the agreement or mismatch of a model simulation and observations, accounting for their respective uncertainties. Indeed, the value of this approach relies on a reasonable description of observation and prior uncertainties. The prior knowledge and the derived (posteriori) inference is described by probability distribution functions (PDFs), which are typically assumed to be Gaussian, but in practice this is likely only to be an approximation. Most methods can be adapted to address non-Gaussian statistics (e.g. Bergamaschi et al., 2010) although many studies assume the Gaussian approximation.

A wide range of approaches are used by the atmospheric inverse modelling community to solve the inverse problem. The dominant methods are Bayesian synthesis, variational data assimilation, ensemble Kalman filter, and the Markov Chain Monte Carlo (e.g. Bousquet et al., 2000; Rödenbeck et al., 2003; Chevallier et al., 2005b; Peters et al., 2005, Baker et al., 2006a; Meirink et al., 2008; Lunt et al., 2016; Houweling et al., 2017). This community has also employed different ways of defining the inverse problem. For example, they use different approaches to define the state vector (grid based, eco-region based, process specific flux patterns or amplitudes, domain partitioning driven by observational constraint, orthogonal decomposition, etc., as discussed by Enting 2002; Kaminski et al., 2001; Michalak et al., 2004; Stohl et al., 2009; Turner et al., 2015b; Zhuravlev et al., 2011; Tian et al 2014). There are advantages and disadvantages of each method, associated with development time, computational efficiency and flexibility. As a consequence, there is a strong justification for supporting the development of these independent methods as they can provide different insights into the inverse problem.

From a mathematical perspective, the estimation of net surface fluxes (emissions minus uptake) from atmospheric measurements represents an underdetermined (i.e., the total number of fluxes

to be estimated is much greater than the number of observations available) and ill-posed (i.e., several different solutions exist that are equally consistent with the available measurements) inverse problem. In other words, there are insufficient data (in time and space) to determine a unique solution. Because of this, prior knowledge about fluxes is required to regularize the inverse problem, allowing posterior fluxes to be determined that are consistent with this prior knowledge and with the atmospheric CO<sub>2</sub> and CH<sub>4</sub> measurements and their respective uncertainties.

Historically, CO<sub>2</sub> and CH<sub>4</sub> measurements were available from a small number (30-200) of surface stations, most of which were located in North America, Western Europe or associated territories. Pioneering synthesis Bayesian inversions were constructed to estimate fluxes for a small number of pre-defined continental regions (e.g. Bousquet et al., 2000; Gurney et al., 2003; Baker et al., 2006b). Specifying the spatial patterns of fluxes within such large regions led to aggregation errors (e.g. Kaminski et al., 2001), whereby the atmospheric measurements are sensitive to variability in the fluxes at finer scales than the scale at which the inversion is allowed to adjust the fluxes. As more atmospheric CO<sub>2</sub> and CH<sub>4</sub> data have become available from expanded surface networks and space-based observations, recent studies have attempted to address this problem by estimating fluxes at finer scales spanning the native resolution of transport models to regional spatial domains.

Prior knowledge about the fluxes includes the magnitude and gridded distribution of emissions and uptake from anthropogenic and natural processes. Anthropogenic CO<sub>2</sub> emissions are generally better quantified than natural fluxes (i.e. Le Quéré et al., 2018). Indeed, a common assumption for the inverse problem, especially for atmospheric CO<sub>2</sub> inversions at global scale, is perfect knowledge of the magnitude and distribution of emissions from fossil fuel combustion and cement production. Without this assumption it is difficult to independently quantify the anthropogenic and natural fluxes, because, depending on the GHG being studied, natural fluxes can originate from different parts of the land (soil, grasses, trees, etc.) and ocean (physical and biological processes), and in some regions anthropogenic and natural fluxes may overlap. This assumption will clearly have to be revisited to enable future atmospheric inversion studies designed to inform anthropogenic inventories. For CH<sub>4</sub>, no such assumption is made, but many inversions only solve for total methane emissions.

For CO<sub>2</sub>, ocean flux priors are either determined by climatologies (e.g. using pCO<sub>2</sub> ocean measurements) or from ocean circulation models. The climatologies implicitly assume that correlations are valid on spatial scales long enough (1000s of km) so that point measurements can be extrapolated, while circulation models explicitly describe ocean transport and biology. Both climatologies and models provide estimates of the atmosphere-ocean exchange processes. Land flux priors for CO<sub>2</sub> can be derived from biospheric carbon cycle models that may incorporate satellite data to improve changes in the spatial and temporal distributions (e.g. leaf area index, water inundation from microwave data, precipitation). Natural CH<sub>4</sub> emissions are poorly known and to date only wetland emissions are modelled using process-based approaches. Describing the uncertainty of these models is difficult and has not received much attention so far. It is possible to estimate uncertainties from statistical analyses with dependent (Michalak et al.

2005) or independent data (Chevallier et al. 2006), but most studies have empirically tuned a couple of uncertainty parameters (e.g., error correlation lengths or a scaling factor to the global annual error budget) or neglect correlated errors.

Atmospheric transport is an integral component of the inverse method that establishes the relationship between fluxes (or the model parameters that describe those fluxes) and atmospheric CO<sub>2</sub> and CH<sub>4</sub> measurements. Most atmospheric inversion systems use “off-line” or pre-computed meteorological fields to estimate the transport of CO<sub>2</sub> and CH<sub>4</sub>. These models have a horizontal resolution between two and four degrees and up to 50 vertical levels (ranging from the surface to the model top, typically far above the stratosphere) that are resolved every 3-6 hours. Other “on-line” methods numerically solve the full mass continuity equation, at high spatial (sub-degree) and temporal resolution. The main advantage of off-line models is that they impose a substantially smaller computational burden, but this benefit decreases with increasing spatial and temporal resolution, where input/output becomes a more significant bottleneck. The main advantage of the on-line approach is the ability to account for transport error due to imperfectly known meteorological analyses (e.g. Liu et al., 2011; Polavarapu et al., 2016; 2018).

The use of on-line models in inversion systems limits errors that may arise from the spatial and temporal interpolation of the meteorological fields from the high-resolution global circulation model grid to the coarser off-line inverse transport model grid. Yu et al. (2018) have shown that degrading the meteorological fields in an off-line model to a temporal resolution of three hours, while maintaining the horizontal resolution of the parent model, results in the loss of some of the resolved vertical transport processes, therefore weakening vertical transport in the off-line model. They also found that the reduced vertical transport relative to the on-line model was further exacerbated by degrading the horizontal resolution of the off-line model. It remains to be determined how this error depends on the numerical formulation of the off-line model, such as whether the model employs interpolated winds or mass fluxes for atmospheric transport. Employing the native resolution (spatial and temporal) of the parent models in the off-line models to alleviate this problem would be computationally expensive, in part because of the cost of storing and reading the high-resolution fields. This cost can be much larger for some iterative inverse methods, such as the variational schemes, that may require numerous sequential simulations of the atmospheric model.

With progressive improvements in data density and quality and a better understanding of other sources of uncertainty, atmospheric transport model uncertainty will soon become the single largest source of uncertainty in flux inversion (Basu et al., 2018). Several approaches have been studied to quantify model transport uncertainty (e.g. Lauvaux et al., 2009; Polavarapu et al., 2018). Inverse methods could use these results to better weigh the measurements with respect to the propagated state information in the cost function, but the technical implementation is challenging and transport uncertainties therefore remain largely uncompensated in these models.

Much of what we know about the global carbon cycle is based on *in situ* flask and continuous measurements of GHGs collected within inter-calibrated, but geographically disaggregated networks. Measurements from individual flux towers provide direct information about surface fluxes of GHGs on relatively small scales. Across much of the globe, the sparse spatial

distribution of *in situ* atmospheric GHG measurements has precluded robust GHG flux estimates on subcontinental scales. Exceptions include regions such as the Upper Midwest of the U.S., where a network of towers was deployed as part of the North American Carbon Program (i.e. Miles et al., 2013). Gaps in measurement coverage over the Tropics and the high boreal latitudes compromise the flux estimates over these regions. Resulting posterior GHG fluxes deviate little from prior knowledge, with any changes contributed by downwind constraints diluted by atmospheric transport.

In the context of atmospheric inversion systems, satellite observations of the column-averaged CO<sub>2</sub> and CH<sub>4</sub> dry air mole fractions have major advantages, including global coverage and dense spatial sampling. Measurements collected at SWIR wavelengths are more sensitive than TIR measurements to CO<sub>2</sub> and CH<sub>4</sub> changes in the lower troposphere, where surface emissions and uptake operate. However, as noted earlier, these SWIR measurements are limited to the sunlit hemisphere and only return data at high latitudes during summer months, subject to viewing geometry constraints. SWIR CO<sub>2</sub> and CH<sub>4</sub> measurements are also more easily compromised by cloud and aerosol scattering. These limitations may introduce a clear-sky bias (Corbin et al., 2009; Parazoo et al., 2012) and a latitudinal bias (Liu et al., 2014; Byrne et al., 2017). Yet the increased availability of SWIR CO<sub>2</sub> and CH<sub>4</sub> observations from recent space-based remote-sensing instruments, especially for CO<sub>2</sub> (i.e., JAXA's GOSAT, NASA's OCO-2), has led to a proliferation of inverse modelling studies using satellite data over the last decade (e.g. Rayner et al., 2010; Basu et al., 2013; 2014; 2018; Bergamaschi et al., 2013; Maksyutov et al., 2013; Chevallier et al., 2014; Liu et al., 2014; Takagi et al., 2014; Alexe et al., 2015; Houweling et al., 2015; Deng et al., 2016; Feng et al., 2016; and Wang et al., 2017).

### APPENDIX 3: Observation system simulation experiments (OSSEs)

Advances in remote sensing methods are ushering in a “golden era” of satellite-based carbon observations. These observations have the potential to dramatically improve our understanding of the carbon cycle. They also provide independent data that can be used to support societal needs driven international agreements such as the Paris Accord (Pacala et al., 2010; Ciais et al., 2015; Battersby, 2018; Bergamaschi et al., 2018). The information that this “constellation-of-opportunity” can contribute to advancing these scientific and societal needs must be quantified. Moreover, the design of future measurements should quantify their added benefit in the context of the existing ground-based, aircraft, balloon, and space-based measurement systems. These include multiple trace gases that are sensitive to different processes controlling the carbon cycle over a range of scales (e.g. Brioude et al., 2013; Rayner et al., 2014; Bowman et al., 2017; Liu et al., 2017; Silva et al., 2013, 2017). Furthermore, as older satellites leave the constellation and are replaced by newer ones, the impact of changes in the constellation architecture on inferred trends in carbon fluxes must be assessed.

For these reasons, observing system simulation experiments (OSSEs) are critical tools in the design and evaluation of observing systems. The purpose of an OSSE is to quantitatively assess the impact of a set of observations on the predicted state of a geophysical field, e.g., XCO<sub>2</sub>, or the reduction in uncertainty of a physical process, e.g., sources and sinks of CO<sub>2</sub>. OSSEs can be used to assess the relative merits of the resolution or coverage provided by a given measurement strategy (i.e. spatial resolution, swath width, time of day, repeat frequency) or to evaluate techniques used to estimate fluxes from observed XCO<sub>2</sub> or XCH<sub>4</sub> fields. These tools were originally developed in the Numerical Weather Prediction (NWP) community in the 1950’s or earlier (Arnold and Dey, 1986) and are now routinely used to evaluate the impact of existing or new satellite observations (e.g., Tan *et al.*, 2007; Masutani et al., 2010).

More recently, these tools have been applied to the assessment of observing systems and instruments designed to constrain estimates of CO<sub>2</sub> and CH<sub>4</sub> sources and sinks from atmospheric observations of these gases (e.g., Rayner et al., 1996; 2014; Jones et al., 2003; Houweling et al., 2004; Edwards et al., 2009; Hungershofer et al., 2010; Liu et al. 2014). OSSEs are particularly valuable in these applications because they can provide an end-to-end method for assessing how well a given measurement system, observing strategy, atmospheric transport model or inverse system can reduce CO<sub>2</sub> or CH<sub>4</sub> flux uncertainties to meet specific scientific or operational requirements. For example, OSSEs performed by Bousseres et al. (2016) indicate that TIR and SWIR observations from a geostationary platform could be combined to constrain CH<sub>4</sub> emissions at a resolution of 100km × 100km over source hotspots with emissions > 4 × 10<sup>5</sup> kg day<sup>-1</sup>.

The elements of a typical OSSE adapted for the design of a CO<sub>2</sub> or CH<sub>4</sub> satellite are shown in Figure A3-1. The reference model field, called the Nature Run, is a model representation of the “true” atmospheric system generated at global (as in the Figures A3-1 and 2-11), regional (Figure A2-3), or local scales producing distributions of CO<sub>2</sub>, CH<sub>4</sub> and their sources and sinks. These fields are subsequently sampled in space and time by an Observation Simulator that samples the Nature Run in a way that corresponds to the sampling strategy adopted by a specific

observing system to produce realistic Simulated Observations. In parallel, a Control Run, preferably from a second model that is independent of the Nature Run model in terms of process description, meteorology etc., produces an alternate description of the atmospheric system. The extent to which the Nature Run differs from the Control Run should mimic the difference between the true atmospheric system and our ability to represent this in a model, as is required for a priori purposes in a retrieval of CO<sub>2</sub> or CH<sub>4</sub>, for example. A third model run, the Assimilation Run, produces an assimilation of the Simulated Observations into the Control Run. The differences between the Nature Run and Control Run, compared to the differences between the Nature Run and Assimilation Run, then allows for an examination of the impact of the Simulated Observations in constraining CO<sub>2</sub>, CH<sub>4</sub> and their sources and sinks. If the Simulated Observations are useful, then the Assimilation Run should tend to the Nature Run. Otherwise, more work on the Observation Simulator and sampling strategy will be required.

In the carbon modelling community, most Observation Simulators approximate the actual performance of the sensor by a simplified model (i.e. a measurement precision or accuracy that depends on sun angle, surface albedo, aerosol loading, or other environmental parameter) or set of high level requirements (i.e. an assumed single sounding random error). The major limitation of most simplified Observation Simulators is their ability to accurately represent the impact of small, regionally correlated systematic errors in synthetic datasets. Other common limitations include incorrect estimates of uncertainties in the *a priori* fluxes and the often-used assumption of perfect transport, but these limitations may be less important for comparing the performance of different observing systems or sampling strategies.

To assess the information provided by a particular instrument design or retrieval algorithm approach, a more comprehensive Observation Simulator is needed. Such systems typically use a radiative transfer model to simulate the spectrally-dependent radiances at the top of the atmosphere that are consistent with the geophysical conditions observed in each sounding (surface reflectance and pressure, air temperature, trace gas and aerosol profiles, illumination and observing geometry). Each spectrum is then processed with an instrument simulator that mimics the spectral resolution, signal-to-noise ratio, dynamic range, and other aspects of an existing or planned instrument. Each simulated spectrum is then analyzed with a remote sensing retrieval algorithm and instrument model, like those introduced in Appendix 1, to yield estimates of XCO<sub>2</sub>, XCH<sub>4</sub>, and other retrieved geophysical properties, along with their estimated uncertainties. To assess the impact of uncertainties in the radiative transfer model or instrument calibration, the radiative transfer and instrument models included in the retrieval algorithm can include features that differ from those used to generate the synthetic top-of-atmosphere radiance spectra. These approaches are consistent with the more advanced techniques developed by the NWP community (e.g., Errico et al., 2017).

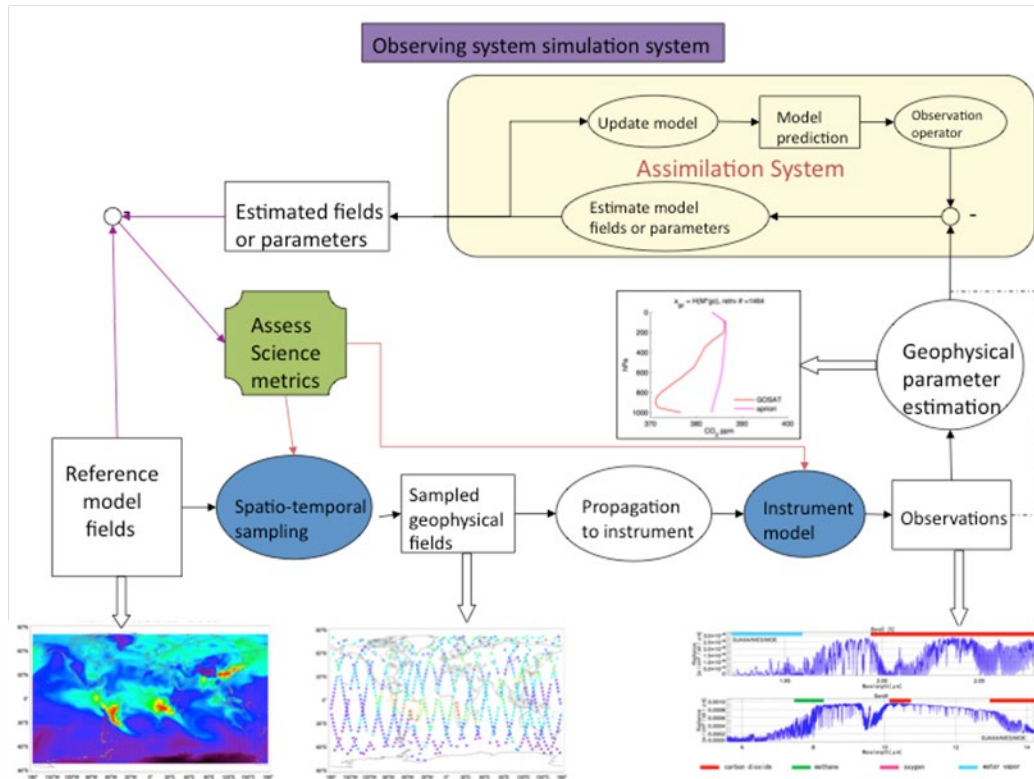


Figure 2-11: Satellite-based observing system simulation experiment. Boxes represent outputs and ovals represent processes. The pictures are illustrative of the different outputs in the system. The blue ovals indicate those processes that can be assessed by the outcome of the OSSE.

Simulated XCO<sub>2</sub> and XCH<sub>4</sub> datasets can be ingested into a data assimilation system (described in more detail in A 2.3) to evaluate the impact of the proposed observations. The simplest assimilation systems treat all errors as random errors in the measurements (Hungershofer et al., 2010). More realistic OSSEs include some components that are substantially different from those used to generate the nature run (e.g., a different transport model, different flux boundary conditions) or can add systematic as well as random errors to simulate realistic observations (i.e. ESA, 2015; Bousquet et al., 2018). The data assimilation system will then adjust the surface fluxes based on the ingested data (Ciais et al., 2010). For CO<sub>2</sub> or CH<sub>4</sub> source and sink estimation, the estimated fluxes are compared with the fluxes used to generate the nature run model fields. The specified science metrics are applied to the differences between the estimated and reference fluxes. If the estimated fluxes do not meet the thresholds defined by those metrics, then the spatial and temporal sampling and instrument model characteristics are modified and the process is repeated. Note that the extension to multiple instruments and platforms (including surface networks) is relatively straightforward.

An alternative OSSE approach can be used to study how error statistics (biases, variances and covariances) propagate from the radiation measured by the observing system down to the estimated fluxes. This can be done analytically, using algebraic formulae under a linear model assumption (Houweling et al., 2004), or through a robust Monte Carlo ensemble of inversions (Chevallier et al., 2007). A key advantage of such systems is that they require only a description

of observation uncertainties and of prior flux uncertainties, but do not require simulated observations themselves. Both approaches, through perturbations of the Nature run or through the end-to-end propagation of error statistics, should yield consistent results as long as input hypotheses on the perturbations and on the error statistics are consistent (Michalak et al., 2017).

OSSEs with varying degrees of sophistication have been used to study augmentations of surface networks (Gloor et al., 2000; Suntharalingam et al., 2003) or the addition of remote sensing measurements (Rayner et al., 2001) at both global and regional scales (Law et al., 2003, Carouge et al., 2010). More recently, OSSEs have been constructed to assess the impact of individual satellites on fluxes (Chevallier et al., 2007; Miller et al., 2007; Baker et al., 2010; Liu et al., 2014) and comparisons between different platforms (Hungershofer et al., 2010). Despite this progress, carbon OSSE capabilities remain much less mature than those in the NWP community. Transport error has been a well-known challenge for accurate flux estimates of CO<sub>2</sub> (Peylin et al., 2002; Patra et al., 2003; Baker et al., 2006b). Some OSSEs have attempted to represent the influence of transport error on flux estimates (Chevallier et al., 2010b), though more research in this area is critically needed. Spatio-temporally varying bias in the retrieval of trace gas concentrations can have a significant impact on inferred fluxes (Takagi et al., 2014) that is not included in many carbon OSSE studies. Radiance retrieval simulations can help quantify those biases, resulting in more robust OSSEs, but these efforts are currently limited by the computational cost of the retrieval algorithm.

It is also challenging to weigh the benefit of new information in the context of other existing and planned satellites. For example, it is difficult to evaluate the benefit of ancillary trace gas observations (e.g. CO, NO<sub>2</sub>) because few existing data assimilation systems are able to use multi-species correlation information for attribution. Assessing the value added to a growing constellation of space-based CO<sub>2</sub> and CH<sub>4</sub> sensors is an emerging challenge. The carbon OSSE community is only beginning to deal with the complexity of simulating multiple passive datasets with realistic random and systematic error, and then ingesting these into data assimilation models. As the size of the carbon observing constellation increases, so will the computational demands of OSSEs. Coordination among the world's modeling centers could help relieve the burden on scientists by providing nature runs and synthetic datasets, and to increase the transparency of OSSEs. However, such activities currently lack sustained support.

## APPENDIX 4: Lessons learned from SCIAMACHY, GOSAT and OCO-2

When the CEOS Carbon Strategy (Wickland et al. 2014) was being written, space-based CO<sub>2</sub> and CH<sub>4</sub> measurements were still in their infancy. SCIAMACHY had completed its decade-long mission and GOSAT was near the end of its nominal 5-year mission. Their measurements substantially increased the density of atmospheric carbon cycle observations, but the XCO<sub>2</sub> and XCH<sub>4</sub> estimates from these two sensors still had errors exceeding 0.5% on regional scales. These data had to be integrated over months to years to identify carbon flux trends, or to discriminate anthropogenic changes from natural variability (Kort et al., 2012; Schneising et al. 2013; 2014; Reuter et al. 2014; Turner et al., 2015; Janardanan et al., 2016; 2017; Ganesan et al., 2017).

The 2014 launch of OCO-2 provided substantial improvements to the precision, spatial resolution and sampling density of space-based CO<sub>2</sub> estimates. Its measurements were analyzed to yield between 50,000 and 100,000 XCO<sub>2</sub> soundings over the sunlit hemisphere each day, with single sounding random errors near 0.125% (0.5 ppm; Eldering et al. 2017) and a mean bias near 0.4 ppm relative to TCCON (Wunch et al., 2017). The OCO-2 XCO<sub>2</sub> estimates have been cross-calibrated with those from GOSAT (Kataoka et al., 2017) and the XCO<sub>2</sub> estimates from both missions were cross-validated against TCCON measurements and other standards to yield a combined, harmonized dataset that spanned the lifetimes of both missions. This combined dataset is now being used to study the carbon cycle (Chatterjee, et al., 2017; Liu et al., 2017; Sun et al. 2017; Patra et al. 2017).

Early studies indicated that space-based remote sensing observations of XCO<sub>2</sub> with accuracies of 0.25% (1 ppm) on regional scales could substantially improve our understanding of surface sources and sinks (Rayner and O'Brien, 2001). XCO<sub>2</sub> estimates from OCO-2 are now exceeding this target (Eldering et al., 2017b; Wunch et al., 2017). However, more recent studies indicate that systematic, regional-scale biases must be reduced to values much smaller than this (0.025% to 0.125%) to preclude large errors in CO<sub>2</sub> fluxes (e.g. Chevallier et al., 2014). So, in spite of this progress and that anticipated from the growing fleet of CO<sub>2</sub> and CH<sub>4</sub> missions, substantial improvements in precision, accuracy, resolution and coverage of space-based measurements and analysis systems are needed to provide timely information about anthropogenic emission inventories and trends on the scale of individual nations. The specific factors that drive the requirements for precision, accuracy, resolution, and coverage are summarized below, along with the lessons learned as we attempted to address these requirements with the first generation of SWIR CO<sub>2</sub> and CH<sub>4</sub> missions.

### A4.1 Strategies for maximizing measurement precision

As noted above, high precision is critical for resolving the small variations in XCO<sub>2</sub> and XCH<sub>4</sub> associated with both natural and anthropogenic sources and natural sinks. Two practical approaches have been developed to optimize the precision of XCO<sub>2</sub> and XCH<sub>4</sub> retrievals collected by passive solar NIR/SWIR instruments like those carried by SCIAMACHY, GOSAT, and OCO-2. The first exploits the information contained in high-resolution spectra collected over

broad spectral regions. The second exploits spatial averages of nearby samples. The principle features of these two methods are summarized below.

#### A4.1.1 Fitting multiple spectral lines within a band to improve precision

As sunlight passes through the atmosphere and is reflected back to space by the surface, molecules such as O<sub>2</sub>, CO<sub>2</sub>, and CH<sub>4</sub> absorb only certain colors or wavelengths of this light, producing narrow dark absorption lines, superimposed on a bright continuum (e.g. Figure A1-2). At NIR and SWIR wavelengths, these molecular absorption lines are organized into “bands” whose structure is determined by the vibrational and rotational motions of the molecules, which, in turn, are dictated by quantum mechanics. The wavelength dependence of the absorption within the NIR and SWIR O<sub>2</sub>, CO<sub>2</sub> and CH<sub>4</sub> bands is described in terms of an absorption cross-section per molecule, which is characterized by detailed laboratory measurements.

Along atmospheric paths, the amount of light absorbed by each spectral line depends on the spectrally-dependent optical depth,

$$\tau = \int \sigma(\lambda, s) N(s) ds ,$$

which depends on the integral of wavelength-dependent absorption cross section of each molecule,  $\sigma(\lambda, s)$ , the number density of the molecules along the optical path,  $N(s)$ , and the length of the path,  $s$ . In general, the amount of light present within a given absorption line decreases exponentially with increasing optical depth. When the optical depth is very small, the absorption near the line center increases almost linearly with the number of molecules along the path. As the optical depth increases, almost all of the light is absorbed at the center of the line, such that it is “saturated”. For a weakly-absorbing line, a 0.25% (1 ppm CO<sub>2</sub> or 4.5 ppb CH<sub>4</sub>) change in the concentration of the absorbing gas therefore produces a comparable change in the absorption. As the line becomes saturated, the rate of change associated with a given change in concentration is much smaller. A very sensitive instrument is needed to detect these small changes.

Passive NIR/SWIR spectrometers like those used by OCO-2 or TanSat spectrometers produce an image of a spectrum of an O<sub>2</sub>, or CO<sub>2</sub> band on a 2-D focal plane array (FPA) detector, and record that spectrum at rapid intervals as the spacecraft moves along its orbit track. For OCO-2, the spectrum is dispersed along one dimension of the array, while the other dimension captures spatial information along the spectrometer slit. A Fourier transform Interferometer Spectrometer (FTS), like the one used on GOSAT, records an “interferogram” of the incoming light, which is then processed to yield a wavelength-dependent spectrum. In both cases, the intensity of the light incident on each detector is maximized through careful design of the spectrometer optics. The noise is minimized by careful choice of the detector and design of its control and readout electronics and by limiting unwanted sources of stray light within the instrument. The integration time is then optimized to yield the highest possible signal-to-noise ratio (SNR) to maximize the sensitivity to changes in the incident radiation.

Both OCO-2 and GOSAT produce spectra that have adequate spectral resolution to reveal the bright continuum between the lines throughout much of the O<sub>2</sub>, CO<sub>2</sub> and CH<sub>4</sub> (for GOSAT)

absorption bands that they record (Figure A4-1). However, these spectrometers do not completely resolve the absorption lines from the nearby continuum. The detectors recording the light within the absorption lines also record some light from the continuum. This mixing of the line core and continuum further reduces the sensitivity to intensity changes associated with changes in the concentration of the absorbing gases.

At the spectral resolving power of OCO-2 ( $\lambda/\Delta\lambda\sim 19,000$ ), a 0.25% change in  $X_{CO_2}$  rarely produces intensity changes larger than 0.1% at any spectral sample. An instrument SNR of  $> 1000$  would therefore be needed to detect this change with a single spectral line. For instruments like SCIAMACHY, which have lower spectral resolution, the intensity changes associated with a 0.25% change  $X_{CO_2}$  are even smaller, requiring an even larger SNR. Fortunately, the throughput of an instrument is intrinsically higher at lower spectral resolution. A careful tradeoff between spectral resolution and SNR is therefore needed to achieve the optimum sensitivity.

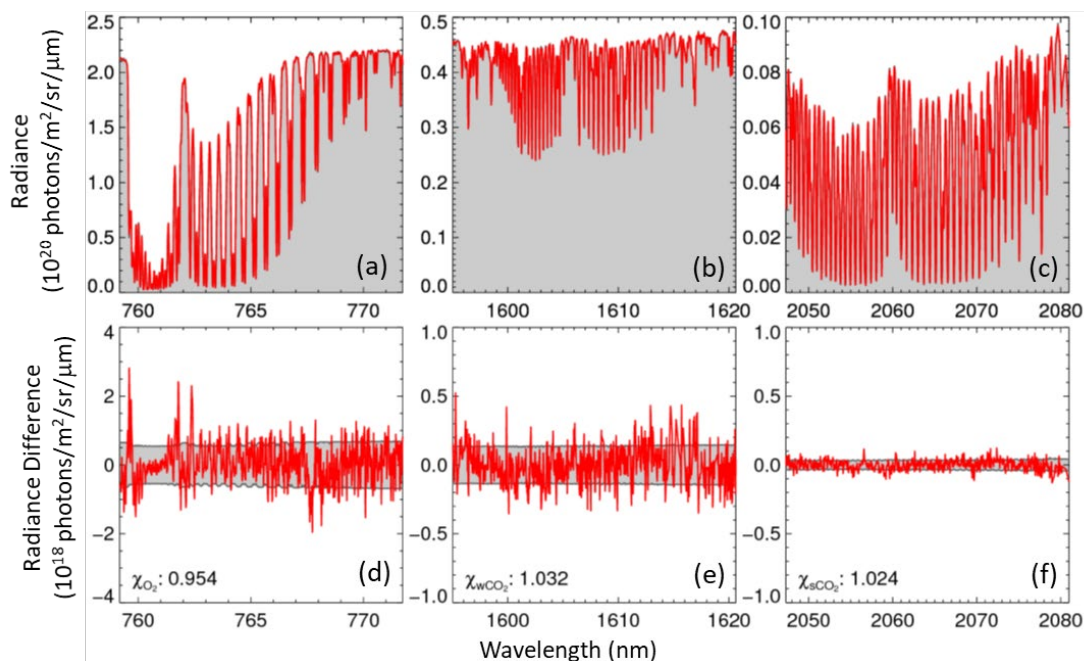


Figure A4-1: OCO-2 spectra collected near Hamburg, Germany June 6, 2015, 12:01 UTC in the (a) 765 nm  $O_2$  A-band (b) 1610 nm  $CO_2$  band and (c) 2060 nm  $CO_2$  band, along with the spectrally-dependent differences between the synthetic spectrum and the observations (d-f). In the spectral difference plots (d-f), the gray band indicates the approximate amplitude of the measurement noise (credit: Reuter et al., 2017).

Each OCO-2 spectrum records the intensity at more than a thousand discrete wavelengths within each band, sampling the continuum and the absorption within dozens of discrete absorption lines. To retrieve estimates of  $X_{CO_2}$  from these spectra, a constrained least squares fitting process is used to fit a synthetic spectrum to the observed spectrum (Figure A4-1). If the optical properties of the continuum and the gas absorbers are well represented by the synthetic spectrum, this process can exploit information across the entire band (or even multiple bands) to improve the precision of the  $X_{CO_2}$  estimate. For example, for OCO-2, a spectrum with a mean SNR of  $\sim 200$  in the continuum can clearly distinguish  $X_{CO_2}$  variations as small as 0.25%. This approach also works for spectrometers that have somewhat lower spectral resolution, but cover wider spectral

ranges, like SCIAMACHY, but requires an even more detailed understanding of the processes controlling the intensity of the continuum and gas absorption throughout the spectral range sampled. Active instruments, like MERLIN, which sample only a few spectral points, cannot exploit this advantage, and must have very high SNR at each spectral point sampled.

#### A4.1 2 Spatial averaging to improve measurement precision

Another way to improve the effective precision of the measurement is to acquire observations at high spatial resolution, and then average nearby results. In ideal conditions, where  $X_{CO_2}$  and  $X_{CH_4}$  fields and other atmospheric and surface properties vary slowly, this approach can theoretically yield estimates whose precision increases with the square root of the number of spatial samples included in the average. In practice, spatial averaging rarely works that well. Even in regions where the  $X_{CO_2}$  and  $X_{CH_4}$  gradients are small, spatial variations in other atmospheric or surface properties introduce correlated biases that limit the benefits of co-adding additional samples. Kulawik et al. (2016) find that a point of diminishing returns is reached after averaging as few as 10 SCIAMACHY samples or 4 GOSAT samples, but that the precision rarely increases by more than a factor of 2 (Figure A4-2). Zhang et al. (2016; 2018) find similar results for OCO-2 observations acquired near TCCON stations. This conclusion has important implications for the role of single sounding precision in the identification and correction of biases in space-based  $X_{CO_2}$  and  $X_{CH_4}$  estimates. More specifically, it suggests that it may be difficult or impossible to characterize biases much smaller than the single sounding random error through comparisons with TCCON stations or other standards.

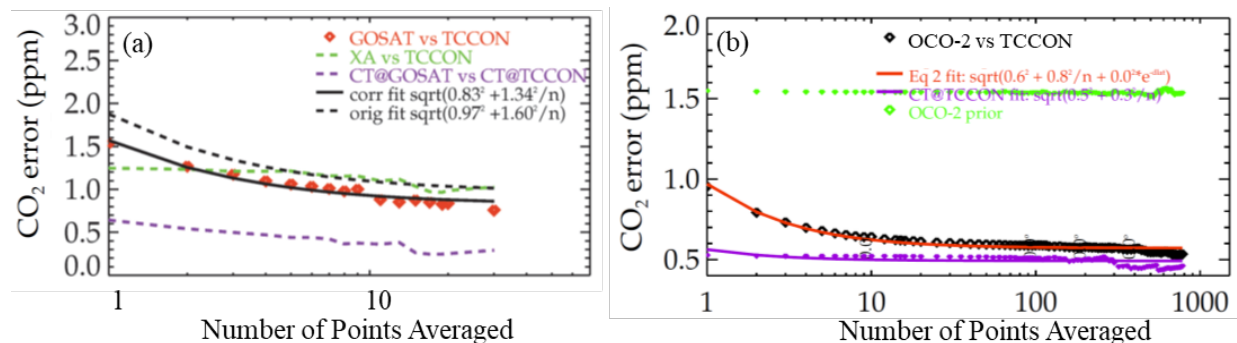


Figure A4-2: Effect of averaging of soundings from GOSAT and OCO-2 near the Lamont TCCON Station. (a) For GOSAT, averages for both the bias corrected (red diamonds and fitted solid black line) and uncorrected (dashed black line) are shown. The dashed green line (XA vs TCCON) shows the difference between the initial guess and the TCCON standard deviation over a 90-minute period. (b) For OCO-2, averages of bias-corrected values (black diamonds) are shown along with a fit (red line). The purple lines in both panels show the standard deviation in the CarbonTracker  $X_{CO_2}$  relative to TCCON over the geometric area used. As the number of soundings included in the average increases, the standard deviation of the space-based  $X_{CO_2}$  estimates decrease relative to TCCON, but the rate of decrease is much slower than  $n^{-1/2}$  for both GOSAT and OCO-2 (credit: Kulawik et al., 2016 and S. Kulawik, personal communication, 2018).

If a plume from the point source extends over several footprints and can be clearly resolved from the background, information from multiple footprints can be combined to improve the measurement precision. Bovensmann et al. (2010) describes an approach that fits the observed  $X_{CO_2}$  anomalies with a simple Gaussian plume model. The  $CO_2$  mass in the fitted model is then compared to that obtained from a hand-picked “background” population to define the  $CO_2$  mass

emitted by the point source. This information is then combined with information about the wind speed to estimate the flux. This approach was used by Schwandner et al. (2017) to derive volcanic CO<sub>2</sub> fluxes and by Nassar et al. (2017) to retrieve power plant CO<sub>2</sub> fluxes from OCO-2 observations.

This simple Gaussian Plume approach is limited by several factors. First, few realistic plumes can be fit by this simple model (e.g. Figure A2-3) since complex terrain and changes in wind speed or direction introduce changes in the plume that make it difficult to track and fit. In other cases, the plume is rapidly entrained into the background and difficult to identify over many spatial samples. In others, the background is difficult to define, or can be contaminated by other plumes with amplitudes that are just at or below the detection limit. In these cases, other methods are needed to identify the spatial samples within the plume and those in the background.

#### A4.1.3 Additional insights from coincident observations of other gases

As noted in Appendix 2 (Figure A2-3), one way to discriminate the plume from the background is to acquire spatially- and temporally-coincident observations of species co-emitted with the species of interest. For example, CO and NO<sub>2</sub> are often co-emitted with CO<sub>2</sub> by fossil fuel combustion. Hakkarainen et al. (2016) showed that tropospheric NO<sub>2</sub> columns retrieved from OMI measurements were spatially correlated with the XCO<sub>2</sub> anomalies retrieved from OCO-2 measurements collected a few minutes later along the same orbit track (Figure A4-3).

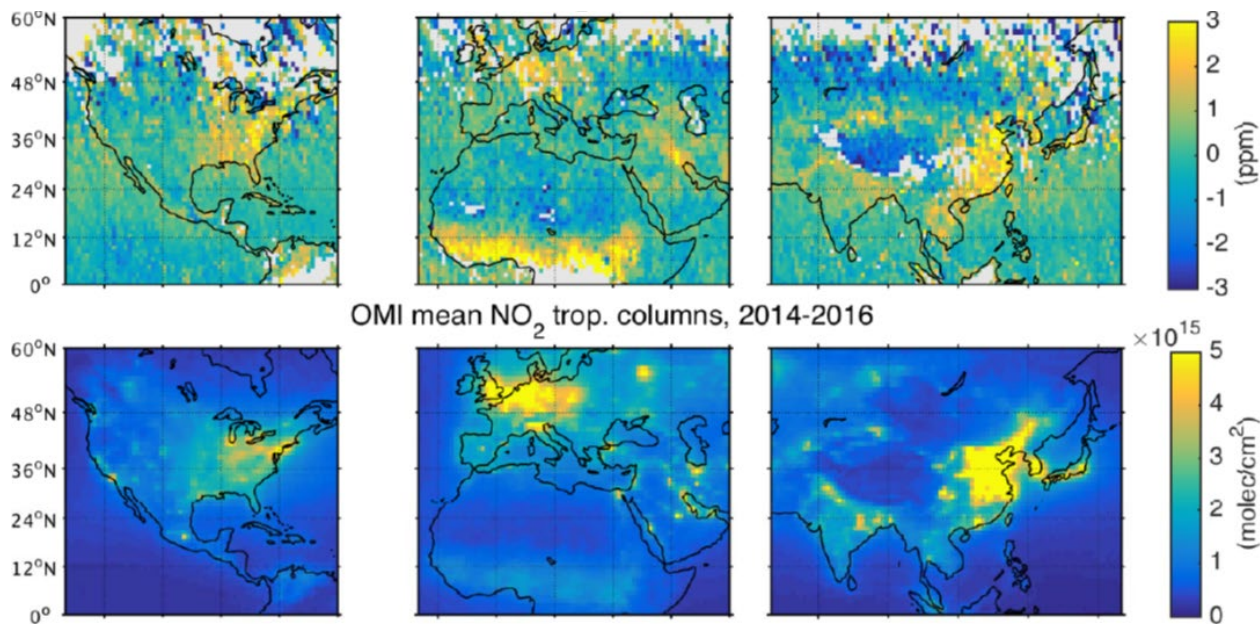


Figure A4-3: XCO<sub>2</sub> anomalies (top) derived from OCO-2 observations over Northeast U.S., central Europe, the Persian Gulf and East Asia are well correlated with tropospheric NO<sub>2</sub> columns observed by OMI (bottom), suggesting that they are associated with high temperature combustion. The correlation is much lower for the XCO<sub>2</sub> anomalies over central Africa and Southeast Asia, where biomass burning is a critical source of CO<sub>2</sub> (credit: Hakkarainen et al., 2016).

This approach worked well on scales of 1° × 1° for soundings with XCO<sub>2</sub> and tropospheric NO<sub>2</sub> columns that were well above the single sounding detection limits of the OCO-2 and OMI,

respectively. To fully exploit this approach for discriminating plumes from smaller sources at much finer spatial scales in the presence of a time-varying wind field, co-boresighted measurements from instruments on the same platform will be needed.

## A4.2 High accuracy continues to be a challenge for space-based XCO<sub>2</sub> and XCH<sub>4</sub> estimates

As noted in the Introduction, here, the term “accuracy” specifies the closeness of the mean of an ensemble of XCO<sub>2</sub> or XCH<sub>4</sub> measurements to results derived from *in situ* atmospheric profiles of CO<sub>2</sub> and CH<sub>4</sub> that can be traced to CO<sub>2</sub> and CH<sub>4</sub> standards maintained by the World Meteorological Organization Global Atmospheric Watch (WMO GAW) program. The need for high accuracy in space-based estimates of CO<sub>2</sub>, CH<sub>4</sub>, and other GHGs was recognized early in the design phases of the SCIAMACHY, GOSAT and OCO-2 missions. Methods to achieve and maintain high accuracy were therefore key drivers in their implementation and operation strategies for pre-launch and on-orbit calibration, retrieval algorithm development, and data product validation approaches. In spite of these efforts, all three missions encountered challenges throughout their nominal missions to meet their originally-targeted accuracy requirements. The methods adopted to overcome these challenges are documented in the refereed literature, and are only summarized here. With the new focus on quantifying anthropogenic emissions of CO<sub>2</sub> and CH<sub>4</sub> in the context of the natural background fluxes, even greater efforts are needed to ensure high accuracy.

### A4.2.1 Pre-launch and on-orbit instrument calibration requirements are demanding

All three missions included comprehensive, pre-launch instrument calibration programs that characterized the instrument performance, and demonstrated unprecedented measurement accuracy (Noël et al., 2003; Lichtenberg et al., 2006; Shiomi et al. 2007; Suto et al., 2009; Kuze et al. 2009; Frankenberg et al., 2014; Lee et al., 2017; Rosenberg et al. 2017). These measurements provided an essential baseline for the radiometric, spectroscopic, and geometric performance of these instruments. For other aspects of instrument performance, they provided the only opportunity to perform an end-to-end calibration (detector linearity, instrument line shape, polarization). The GOSAT, OCO, and OCO-2 teams took a step beyond this, by conducting an intercomparison of the radiometric standards used in their pre-launch calibration activities (Sakuma et al., 2010).

SCIAMACHY, GOSAT TANSO-FTS and OCO-2 instruments deployed comprehensive on-orbit calibration systems that combined on-board sources (lamps, laser diodes) and targets as well as astronomical (sun, moon) calibration targets (Gottwald et al., 2002; Noël et al., 2003; Kuze et al., 2012; Shiomi et al., 2013; Crisp et al., 2017). GOSAT and OCO-2 augmented these activities with joint, annual vicarious calibration campaigns in Railroad Valley, Nevada (Kuze et al., 2011; 2014; 2015). These on-board capabilities were fully exploited throughout these missions to address calibration changes associated with anomalies and more routine performance degradation (Gloude-mans et al., 2005; Kuze et al., 2017, Crisp et al. 2017).

For example, both SCIAMACHY and OCO-2 experienced time-dependent radiometric and spectroscopic calibration changes due to dead and hot pixels and the rapid buildup of ice on their detectors. Ice contamination of channels 7 and 8 of SCIAMACHY reduced the performance of these channels (Lichtenberg et al., 2006). The impact of ice buildup on the OCO-2 performance was a surprise because the instrument design employed mitigation strategies designed to limit ice accumulation on the FPAs. While these methods effectively prevented accumulations as thick as 1  $\mu\text{m}$ , ice buildups as small as 50 nm produced substantial (20%) reductions in throughput by temporarily degrading the performance of the anti-reflection coatings on the FPAs (Crisp et al., 2017). Both on-board lamps and astronomical calibration sources were critical for tracking and correcting these errors, mitigating their impact on instrument performance and accuracy. Similarly, both GOSAT and OCO-2 experienced long-term reductions in instrument throughput due to optical coating degradation. These changes were tracked and corrected using observations of the moon and surface vicarious calibration targets (Kuze et al., 2017, Crisp et al. 2017).

Pointing and geolocation knowledge also played a more critical role than anticipated in the accuracy of the XCO<sub>2</sub> and XCH<sub>4</sub> products in regions with significant topographic variability. For OCO-2, the original pointing accuracy requirement was one milliradian (0.057°). This corresponds to about ½ the angular width or 1/3 the down-track length of a typical footprint. Compliance with this requirement was validated early in the mission using observations of the lunar disk and observations of coastline crossings. However, as the dataset expanded, significant variations in XCO<sub>2</sub> became apparent in regions with significant topography (Wunch et al., 2017). For example, XCO<sub>2</sub> estimates retrieved from target observations over the Lauder TCCON site showed up to 3 ppm biases that were spatially correlated with the ~150-200 m hills just south of the TCCON station (Figure A4-4a,b). Similar variations were seen in routine nadir and glint observations over regions with significant topography, such as Death Valley, California, U.S.A and the Atacama Desert, Chile.

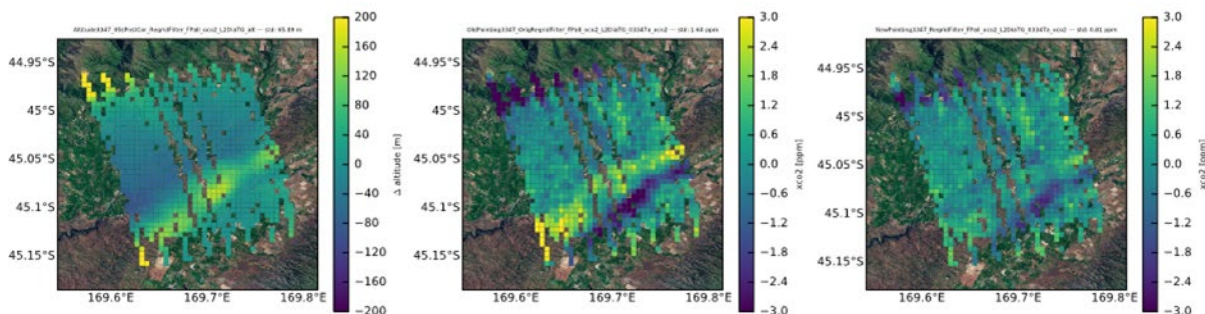


Figure A4-4: (a) topographic elevation variations near the Lauder TCCON station. (b) Estimates of XCO<sub>2</sub> retrieved from OCO-2 observations collected near the Lauder station and in other regions with significant topography showed anomalous variations that were strongly correlated with topographic slopes. An investigation traced these errors to a small (0.03°) pointing error (< 1/6 the angular size of the sounding footprint). (c) Correcting the pointing error reduces by XCO<sub>2</sub> bias by more than half.

A more detailed investigation showed that these spurious XCO<sub>2</sub> variations were more strongly correlated with topographic slopes than topographic elevation. These biases were attributed to a small (0.03°) pitch error in the pointing of the OCO-2 instrument boresight. The ACOS Level 2

Full Physics (L2FP) algorithm and its associated pre-screeners were utilized to analyze the effects of miss-pointing. An *a posteriori* correction reduces the correlation between XCO<sub>2</sub> variance and topographic slope (Figure A4-4c).

While the on-board calibration systems carried by SCIAMACHY, TANSO-FTS and OCO-2 provided the information needed to track most of the critical instrument calibration properties, there were a few aspects of the instrument performance that could not be validated directly after launch. For example, none of these three missions included an on-board system to monitor changes in the linearity of their radiometric response. This was recognized as a significant issue for the TANSO-FTS (Suto et al., 2011) and OCO-2 (Crisp et al., 2017) instruments. While the TANSO-FTS included an on-board laser diode to monitor changes in its instrument line shape (ILS) and OCO-2 used Doppler shifted observations of solar Fraunhofer lines for this purpose, none of the three missions provided a means to recover from changes in instrument ILS. While ILS uncertainties have been identified as a leading driver of XCO<sub>2</sub> bias in linear error analysis experiments (Connor et al., 2016), the actual amplitude of these errors has been impossible to quantify inflight. Finally, none of these three instruments provided a way to calibrate their polarimetric response once in orbit. These aspects of the instrument performance introduced additional uncertainties in the calibration for all three instruments, but, fortunately, they did not preclude the missions from eventually meeting their overall accuracy requirements.

#### A4.2.2 Instrument calibration stability is critical

Instrument calibration stability is another critical need for CO<sub>2</sub> and CH<sub>4</sub> instruments, because high calibration accuracy must be preserved on time scales that exceed the recalibration intervals. Some instrument performance characteristics can only be calibrated or related to internationally recognized standards during pre-launch testing on the ground. These capabilities must therefore maintain their calibration requirements through on-ground flight qualification tests, instrument transport, storage, spacecraft integration, and on-orbit operations. For grating spectrometers (i.e. SCIAMACHY, OCO-2), these properties included the linearity of the response of the FPAs and readout electronics to the incident radiation as well as the spectrally dependent shapes of instrument line shape functions (width, contrast, far-wing response). For interferometers (i.e. TANSO FTS), examples include the radiometric linearity of the detectors and their readout electronics and the modulation efficiency of the interferometer optics.

Other aspects of the instrument performance can be recalibrated in orbit, but these methods will work only if the instrument performance remains stable over periods that exceed the time between calibration opportunities. For example, if observations of the sun are used to detect trends in the radiometric or spectroscopic calibration, and these observations can only be obtained once in every orbit, these instrument properties must remain stable over the orbital period. If the observations of the full moon are needed for radiometric or geometric calibration, these instrument properties must remain stable on monthly time scales (Crisp et al., 2017). If observations of surface vicarious calibration targets are required to trend the long-term radiometric, spectroscopic or geometric performance of the flight instrument, and the surface site is only calibrated during annual vicarious calibration campaigns (Kuze et al. 2015), those aspects of the instrument performance must remain stable, or at least vary smoothly, on yearly intervals.

### A4.2.3 Remote sensing retrieval algorithms require continuous improvement

Advanced remote sensing retrieval algorithms have been developed and then continuously refined during the SCIAMACHY, GOSAT and OCO-2 missions. These efforts substantially improved the reliability and accuracy of the XCO<sub>2</sub> and XCH<sub>4</sub> estimates, but additional refinements will be needed to meet the increasing demands on accuracy and coverage.

During the development phases of these missions, accurate, physics-based forward transfer models and inverse methods were created and validated against available standards. Intercomparisons of these tools further facilitated their rate of development. These tests showed that the accuracy of the retrieved XCO<sub>2</sub> products was critically dependent on the forward radiative transfer model's treatment of gas absorption, cloud and aerosol scattering, surface reflectance and polarization state, and knowledge of the instrument performance (SNR, ILS, polarization). They also showed that the reliability of the inverse models depended on the accuracy and completeness of the *a priori* atmospheric state and its assumed uncertainties (Buchwitz et al., 2006; Connor et al., 2006; 2016; Aben et al., 2007; Boesch et al., 2006; 2011; Yoshida et al., 2011; O'Dell et al. 2012; Guerlet et al. 2013). Several methods were implemented to improve the computational speed of the radiative transfer forward models while maintaining their accuracy (Buchwitz et al., 2000; Hasekamp et al., 2002; Spurr et al., 2001; Natraj et al., 2007; O'Dell et al., 2009; Reuter et al., 2017a; Somkuti et al., 2017; Bril et al, 2017).

In addition to these "full physics" retrieval algorithms, simplified "proxy methods" have been developed for retrieving CH<sub>4</sub> abundances from SCIAMACHY and GOSAT measurements. These methods account for the effects of instrument artifacts and optical path length uncertainties introduced by aerosols and clouds empirically, by comparing the absorption by CH<sub>4</sub> with that of CO<sub>2</sub> in a nearby absorption band. They rely on the assumption that instrument calibration and/or optical path length uncertainties will affect the two gases the same way, such that these artifacts will divide out in ratios of the CH<sub>4</sub> and CO<sub>2</sub> absorption. XCH<sub>4</sub> estimates derived using the proxy method are described by Schepers et al. (2012) and Parker et al. (2015).

The accuracy of the radiative transfer forward models depends critically on the accuracy and completeness of the input data. Shortcomings in two critical input data sets dominated the error budgets early in the evolution of these three pioneering CO<sub>2</sub> and CH<sub>4</sub> missions. The first was the gas absorption spectroscopy for O<sub>2</sub>, CO<sub>2</sub>, CH<sub>4</sub>, and other gases that absorb within the spectral bands used to retrieve XCO<sub>2</sub> and XCH<sub>4</sub>. When SCIAMACHY started collecting data in 2002, the near infrared and short wave infrared absorption cross sections for the strongest CO<sub>2</sub> and O<sub>2</sub> lines within the bands used to retrieve XCO<sub>2</sub> and XCH<sub>4</sub> were known to an accuracy of 3-5%. Meanwhile, an accuracy of ~0.1% was needed to return XCO<sub>2</sub> estimates with an overall accuracy of 1 ppm (Miller et al., 2007).

Over the past decade, a considerable amount of effort has been devoted to improvements in the accuracy of the spectroscopic input for relevant molecules and spectral ranges. These efforts have led to advances in theoretical calculations of absorption line shape, line mixing and other line parameters as well as advances in laboratory measurements and their analysis (e.g. Tran and

Hartmann, 2008; Lamouroux et al., 2015; Long et al., 2011; 2012). For example, in the OCO-2 spectral regions, advanced multi-spectrum fitting techniques (Benner et al., 1995) were used to derive line parameters simultaneously from laboratory measurements collected from a broad range of temperatures, pressures and optical path lengths, in order to derive self-consistent sets of line parameters (Benner et al., 2016; Devi et al., 2016; Drouin et al., 2017). These parameters were then used to calculate gas absorption cross-sections, which have been carefully validated using ground-based atmospheric spectra from the TCCON network (Thompson et al., 2012; Oyafuso et al., 2017; Drouin et al., 2017) and have been shown to reduce biases and root-mean-square errors in spectral residuals and retrievals.

In spite of these advances, uncertainties in gas absorption cross-sections continue to be a leading limitation on the accuracy of the OCO-2  $X_{CO_2}$  product (Connor et al., 2016). An example of the impact of outstanding uncertainties in the spectroscopic input on the retrievals is shown in Figure (A4-5). The  $O_2$  A-band gas absorption cross sections were updated between the OCO-2 Version 7 (V7) and Version 8 (V8) products, following analysis of laboratory measurements by Drouin et al. (2017). This update substantially reduced the spectrally-dependent differences between the observed and calculated  $O_2$  A-band spectra, and reduced biases in the surface pressure, dry air mass, and aerosol estimates over many regions. Unfortunately, this change also introduced a systematic, latitude-dependent bias in surface pressure estimates with an amplitude of 6-10 hPa (Figure A4-5). This error was accompanied by a reciprocal error in the standard V8  $X_{CO_2}$  product. Fortunately, because of the large-scale, spatially smooth nature of this bias, it was relatively straightforward to identify and correct in the bias-corrected products used by most of the community (O'Dell et al., 2018). Nonetheless, this issue points to a need for further improvements in the accuracy of spectroscopic input for the retrieval algorithm.

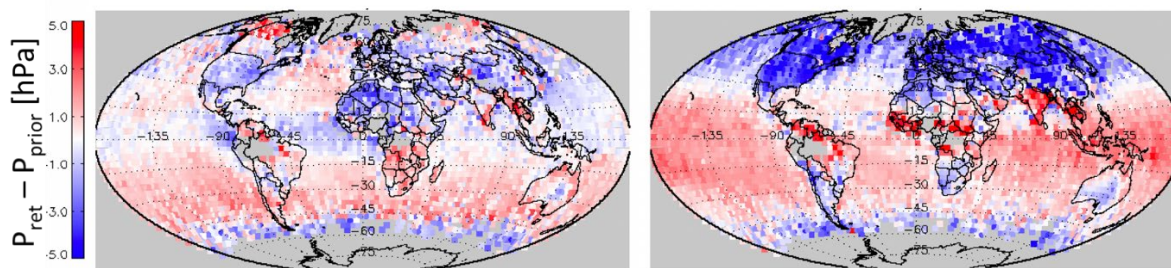


Figure A4-5: (a) Seasonal (March-April-May) difference between surface pressures from the European Center for Medium Range Weather Forecasting (ECMWF) prior and the retrieved surface pressure from the OCO-2 Build 7 retrieval algorithm. (b) Same as (a) for the Build 8 (right) algorithm. While this update improved the overall fit between the observed and simulated spectra, and substantially reduced the surface pressure and air mass biases in some places, it introduced an enhanced, latitude-dependent (credit: Chris O'Dell, personal communication, 2018).

To address these issues, the OCO-2 team is incorporating new analysis of data from three state-of-the-art laboratory measurement techniques (Figure A4-6). Long-path Fourier Transform Spectroscopy is being used to characterize the entire absorption bands over broad ranges of temperature, pressure, and optical path length. Frequency-Stabilized Cavity Ring-Down Spectroscopy (FSCRDS) measurements are being used to provide details of spectral line shapes.

Photo-Acoustic Spectroscopy (PAS) measurements can provide the ultra-high sensitivity and range of pressures needed to characterize line mixing and continuum absorption.

Similar efforts are ongoing for CH<sub>4</sub> and CO. Examples of recent efforts for other missions include precise CH<sub>4</sub> FS-CRDS absorption measurements in the 1.64 μm band and corresponding analysis of these measurements using advanced line shapes for the MERLIN mission (Delahaye et al., 2016) and new FTS and CRDS measurements and analysis in the 2.3 μm region used for TROPOMI CH<sub>4</sub> and CO retrievals (Birk et al., 2018). Teams and committees behind widely used spectroscopic databases such as the HITRAN compilation (Gordon et al., 2017) are actively working with the international spectroscopy community to incorporate advances in line shape and continuum parameterizations as new theory, measurements and analysis become available. This continues to be an active area of research and continued advances are needed in order to achieve stated goals for retrieval accuracy.

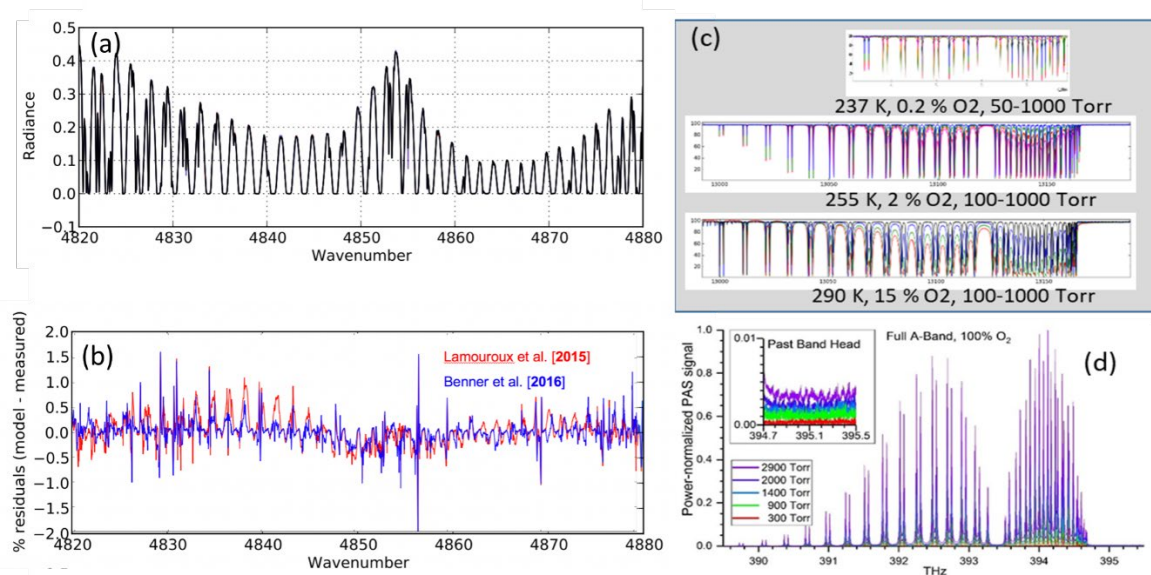


Figure A4-6: Improvements in the acquisition and analysis of laboratory measurements of CO<sub>2</sub> and O<sub>2</sub> have facilitated improvements in the accuracy of fits to observed spectra. (a) CO<sub>2</sub> absorption cross sections derived from high-resolution laboratory spectra of the 2.06 μm CO<sub>2</sub> band, using a self-consistent treatment of line-shape and line mixing, were used to fit atmospheric spectra collected by the Lamont TCCON station (Oyafuso et al., 2017). (b) These CO<sub>2</sub> cross sections substantially reduced the amplitude of the spectral differences between the observed and best-fit spectrum compared to the pre-existing state of the art, but residual features above the level of the instrument noise remain. State-of-the-art FS-CRDS and PAS are being used to improve our understanding of the relative roles of line shape, line mixing and continuum absorption over the full range of temperatures and pressures encountered along atmospheric paths. (c) Temperature-dependent spectra of the O<sub>2</sub> A-band collected by FS-CRDS are providing new insights into the temperature dependence of line mixing and continuum absorption (Drouin et al., 2018). (d) PAS spectra of the O<sub>2</sub> A-band are providing addition information about the absorption associated with far wings, line mixing, and continuum over a range of pressures (Cich et al., 2017).

As noted above, the presence of optically thick clouds and aerosols precludes observations of CO<sub>2</sub> and CH<sub>4</sub> near the surface, where most of their sources and sinks are located. Even those soundings with scattering optical depths substantially less than unity can introduce large uncertainties in XCO<sub>2</sub> and XCH<sub>4</sub> estimates if the cloud and aerosol particle distribution and

optical properties are not accurately characterized by the retrieval process. Efficient methods are therefore needed to identify, characterize, or screen out soundings with substantial cloud or aerosol scattering. For soundings with optically-thin clouds and aerosols ( $\tau < 0.3$ ), accurate gas absorption cross-section (especially in the O<sub>2</sub> A-band) are also critical for retrieving the total optical depth and vertical distribution to minimize optical path length errors.

Advanced methods for identifying and screening out optically thick clouds, based entirely on the high-resolution spectra, were developed and used for both GOSAT (Taylor et al. 2012) and OCO-2 (Taylor et al., 2016). These methods reduced, but did not eliminate, the need for co-boresighted imaging observations of clouds. Cloud imagers are still of value for identifying the contamination of cloud-free pixels by scattering and shadowing by nearby clouds (Massie et al., 2017). The OCO-2 cloud screening process detects and eliminates some, but not all, of the soundings contaminated by these 3-d cloud effects. Contaminated soundings that are missed by the cloud screening methods can introduce substantial bias. More effective methods for identifying and then screening or correcting these biased soundings are under development.

Optically thin clouds and aerosols (optical depth,  $\tau < 0.3$ ) continue to introduce uncertainties in the retrieved products. In the earliest OCO-2 XCO<sub>2</sub> products, the largest errors were seen at middle to high latitudes of the southern hemisphere over the ocean, where biases as large as 3 ppm were common during the southern winter (Figure A4-7). These errors were traced to the omission of an optically thin ( $\tau < 0.01$ ) stratospheric aerosol layer in the retrieval algorithm. (Wunch et al. 2017; O'Dell et al., 2018).

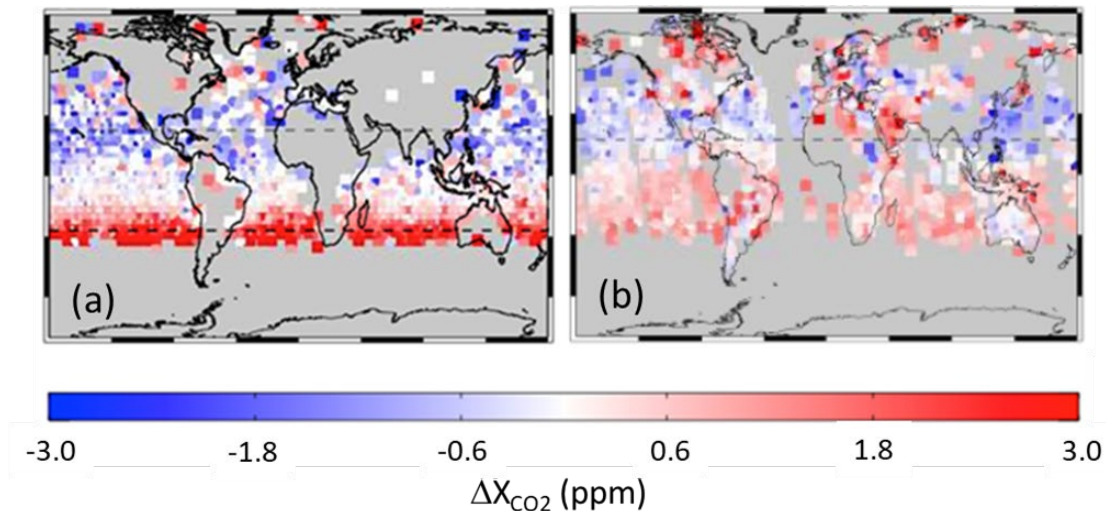


Figure A4-7: (a) Differences between the OCO-2 V7 XCO<sub>2</sub> data product from August 2015 and the median XCO<sub>2</sub> from a suite of six carbon cycle models (O'Dell et al., 2018). The OCO-2 V7 product had large (2-3 ppm) positive biases relative to the models over the ocean in southern mid-latitudes during the southern winter. This bias was traced to the omission of an optically thin ( $\tau \approx 0.01$ ) stratospheric aerosol layer in the retrieval algorithm. (b) The same comparison is shown for the OCO-2 V8 XCO<sub>2</sub> data product, in which this bias is largely eliminated by retrieving stratospheric aerosols.

The largest biases were seen at these latitudes during the winter because of the large solar illumination and observation zenith angles, which maximized the optical path lengths through

the aerosol layer. In 2015, the impact of these aerosols was enhanced further by the eruptions of the Calbuco (Chile), Wolf and Cotopaxi (Ecuador) volcanos, which injected substantial amounts of SO<sub>2</sub> into the stratosphere, which led to the formation of sulfate aerosols there. This problem had not been seen in SCIAMACHY or GOSAT retrievals because these instruments could not collect ocean glint data at latitudes this far south during the southern winter. For OCO-2, this problem was addressed in the OCO-2 version 8 product by including a stratospheric aerosol layer as part of the prior atmospheric state, and then retrieving the optical depth of the aerosols in this layer for each sounding.

These retrieval algorithms have been complemented by comprehensive data product screening and bias correction methods (O'Dell et al., 2012; Mandrake et al., 2013; O'Dell et al., 2018) and uncertainty quantification methods (Connor et al., 2016; Worden et al., 2017; Wunch et al. 2017). These methods are now being used to support studies of the natural carbon cycle on regional scales (Chatterjee et al., 2017; Liu et al., 2017; Heymann et al., 2017; Patra et al. 2017). They are also being used to investigate emissions from megacities (Schwandner et al. 2017) and quantify emissions from individual power plants (Nassar et al., 2017). However, the retrieval algorithms still may not have the accuracy, and the datasets may not have the resolution and coverage needed to improve the CO<sub>2</sub> and CH<sub>4</sub> emission inventories in well characterized regions like North America, Western Europe, or Japan.

#### A4.2.4 Validation of space-based XCO<sub>2</sub> estimates

The products derived from the SCIAMACHY, GOSAT, and OCO-2 retrieval algorithms have been validated against the WMO CO<sub>2</sub> *in situ* standard using an array of transfer standards. These include TCCON XCO<sub>2</sub> and XCH<sub>4</sub> estimates and profiles collected by *in situ* sensors on fixed-wing aircraft and AirCore (Wunch et al., 2011a, b; 2017; Frankenberg et al., 2015; Kulawik et al., 2016; Wu et al., 2017). This validation architecture was developed in parallel with these space-based systems.

For example, the precision and accuracy of the GOSAT and OCO-2 XCO<sub>2</sub> data products were validated through comparisons with XCO<sub>2</sub> estimates from TCCON (Wunch et al., 2011b; 2017), AirCore (Karion et al. 2010), and other aircraft experiments. After identifying and correcting known biases in the OCO-2 V7 product, the median difference between co-located OCO-2 and TCCON XCO<sub>2</sub> estimates is less than 0.4 ppm and the root-mean-square differences are typically less than 1.5 ppm. However, as noted above, biases with amplitudes as large as 3 ppm were seen at high southern latitudes over the ocean during the southern winter (Figure A4-7). Other, smaller biases were traced to subtle shortcomings in the instrument calibration (Crisp et al. 2017), gas absorption coefficients (Oyafuso et al., 2017) and the retrieval algorithm (O'Dell et al., 2018).

Many of these issues were subsequently corrected in the OCO-2 Build 8 processing system. In late 2017, the entire OCO-2 data record was reprocessed using the Build 8 algorithms and delivered to the NASA Goddard Earth Science Data and Information Services Center (GES DISC) as the Version 8 (V8) product for distribution to the science community. Comparisons of OCO-2 V8 XCO<sub>2</sub> with TCCON indicate substantial reductions in bias (Figure A4-8). The OCO-2 V8 product was then compared to coincident observations from GOSAT and aircraft

measurements from the NASA Atmospheric Carbon and Transport – America (ACT-America) and Atmospheric Tomography (ATom) aircraft campaigns to further validate the data quality.

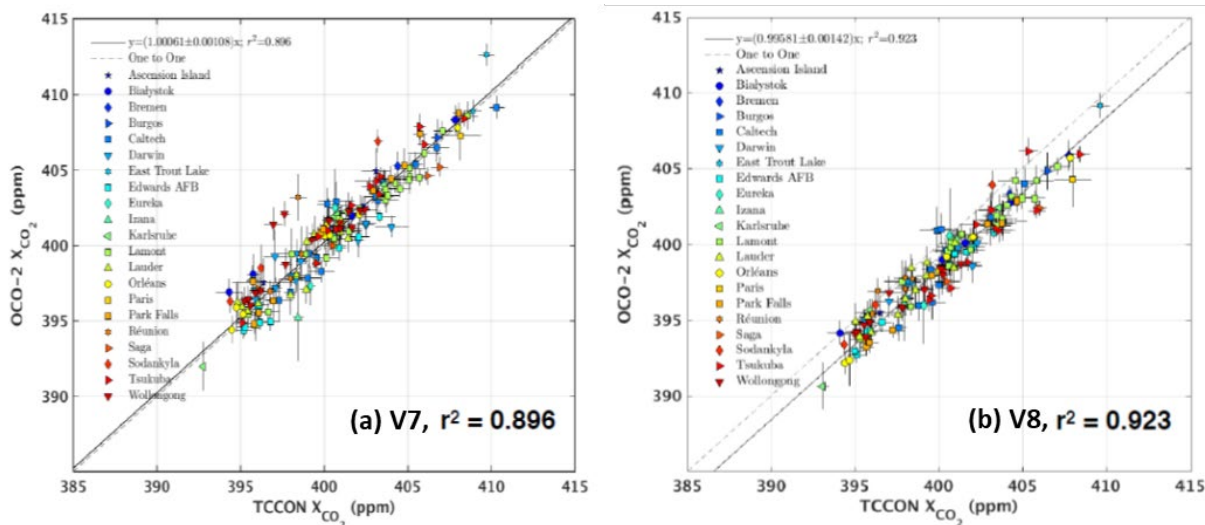


Figure A4-8: (a) Comparisons of the bias-corrected OCO-2 V7 XCO<sub>2</sub> estimates with XCO<sub>2</sub> estimates from 21 TCCON stations. (b) Same comparison for the OCO-2 V8 XCO<sub>2</sub> product, showing fewer outliers and improvements in the overall regression fit ( $r^2$ ).

While this TCCON-based validation architecture continues to be extremely useful for identifying and correcting biases in SCIAMACHY, GOSAT, and OCO-2 measurements on regional scales, improvements in both spatial resolution and accuracy will be needed to support future efforts to reduce uncertainties in national emission inventory reports and identify additional emission reduction opportunities. Networks of smaller, less costly, ground-based up-looking spectrometers, such as the EM27/SUN instruments (see Hedelius et al., 2017; Frey et al., 2018) provide the accuracy and deployment flexibility needed to validate space-based XCO<sub>2</sub> and XCH<sub>4</sub> estimates on the scale of a megacity, or even a single power plant.

Balloon-borne AirCore systems (Karion et al. 2010) are also becoming more widely used for validating space-based column measurements of CO<sub>2</sub> and CH<sub>4</sub>. These low-cost systems can acquire high-resolution *in situ* vertical profiles of these gases at altitudes between the surface and 25 km that can be compared directly to the WMO atmospheric standards. AirCore systems are currently being used to validate results from TCCON (Tukiainen et al. 2016; Wunch et al., 2015), facilitating its use as a transfer standard for the *in situ* standards maintained by WMO. These systems could be even more useful if methods could be developed to return the sample system to a designated landing location. Vertical profiles of CO<sub>2</sub> and CH<sub>4</sub> collected by instruments installed on commercial aircraft, like those being flown by the CONTRAIL experiment (Machida et al., 2008) and those being implemented by IAGOS (Verma et al., 2017), will also play an increasingly important role in validating both space-based XCO<sub>2</sub> and XCH<sub>4</sub> estimates and the CO<sub>2</sub> fluxes inferred from these measurements.

### A4.3 Resolution and coverage

Two factors limit the coverage and resolution provided by instruments like SCIAMACHY, GOSAT, OCO-2 and those that will be returning data in the near future. The first is the spatial sampling strategy adopted by these systems (Figure A4-9). SCIAMACHY provided contiguous spatial sampling over a 960-km wide swath, but the individual  $30 \text{ km} \times 60 \text{ km}$  footprints were so large that they were often contaminated by clouds and aerosols, compromising the accuracy of the retrieved  $\text{CO}_2$  and  $\text{CH}_4$  estimates.

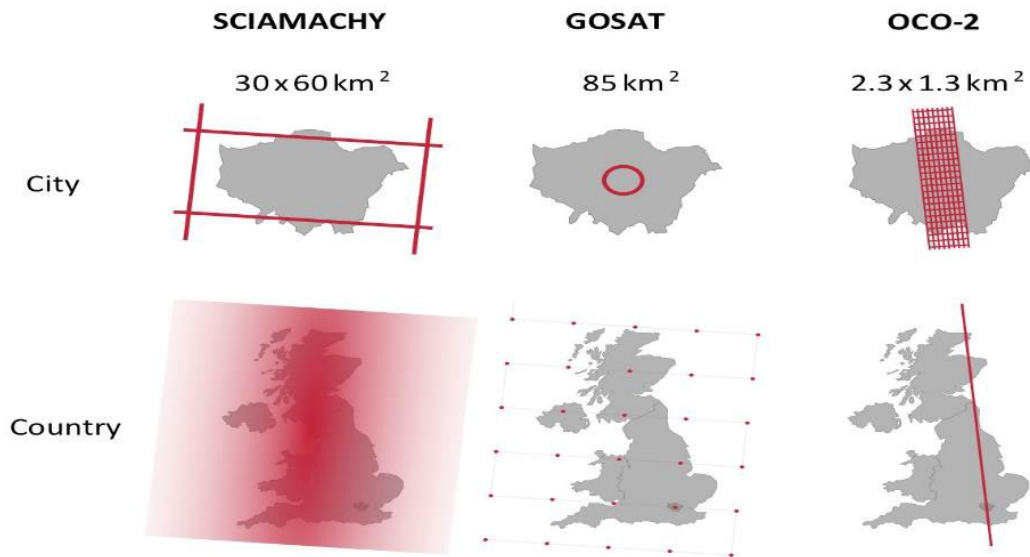


Figure A4-9: Spatial sampling of a city (Berlin) and a country (United Kingdom) by SCIAMACHY, GOSAT, and OCO-2 (credit: ESA 2015).

The instruments carried by GOSAT, Feng Yun-3D, GaoFen-5, and GOSAT-2 acquire soundings with relatively large surface footprints ( $> 10 \text{ km}$  diameter) and these footprints are typically separated by  $> 100 \text{ km}$ . Others, including OCO-2, TanSat and MicroCarb, collect data at higher spatial resolution along a narrow ( $10 - 25 \text{ km}$ ) swath, but the measurement tracks are separated by more than  $100 \text{ km}$  at most latitudes (Figure A4-9). Both approaches yield cloud free observations over  $< 1\%$  of the Earth's surface area on weekly to monthly time scales. These sampling limitations could be addressed by future instruments that are designed to acquire contiguous 2-D images of  $\text{XCO}_2$  and  $\text{XCH}_4$  across a wide ( $> 200 \text{ km}$ ) swath at high spatial resolution ( $2 \text{ km} \times 2 \text{ km}$ ) with high precision ( $\sim 0.1\%$ /sounding) and high accuracy ( $\ll 0.1\%$ ). Such instruments would fill the gap in  $\text{CO}_2$  and  $\text{CH}_4$  observations from regional to national to city scales.

The second factor that limits the spatial resolution and coverage of these first-generation NIR/SWIR sensors is optically thick clouds and aerosols (Figure A4-10). As noted above, even with its small ( $< 3 \text{ km}^2$ ) measurement footprint, only about 8% OCO-2 soundings are sufficiently free of cloud and aerosol contamination to yield reliable, full-column  $\text{XCO}_2$  estimates. GOSAT TANSO-FTS has a larger measurement footprint ( $85 \text{ km}^2$ ) and yields an even smaller fraction of cloud-free scenes (Yoshida et al. 2011; Crisp et al. 2012). For OCO-2, over 70% of the cloud free observations are collected while observing the glint spot over the ocean (Figure A4-10b).

Over land, roughly equal numbers of cloud-free observations are collected while observing the glint spot and the local nadir. This was somewhat of a surprise because glint observations have longer atmospheric path lengths and were expected to be more contaminated by clouds.

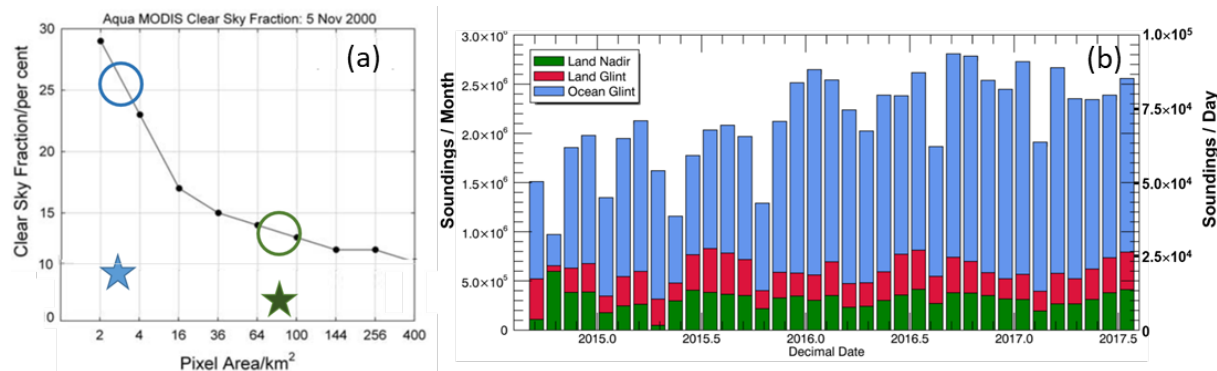


Figure A4-10: (a) Early in the evolution of the OCO and GOSAT missions, optically thick clouds were identified as a significant limitation on coverage. Based on MODIS cloud studies, the predicted clear sky yields were found to be strong function of footprint size. Much larger yields were predicted for OCO-2 (blue circle) than for GOSAT (green circle) due to the smaller footprint area of the OCO-2 footprint. The actual cloud-free yields for both OCO-2 (blue star) and GOSAT (green star) were much smaller than expected. (b) The actual monthly yields of cloud-free scenes for OCO-2 are shown as a function of observing mode. The majority of the cloud free-scenes are glint observations over the ocean (blue). Roughly equal numbers of cloud-free glint (red) and nadir (green) observations are collected over land (credit: NASA OCO-2 Project).

Recent experiments by Massie et al. (2017) show that realistic 3-dimensional (3-D) clouds can introduce optical path length uncertainties even in cloud-free footprints by scattering sunlight into these footprints or by casting shadows on them. This experience suggests that, even though a smaller measurement footprint improves the cloud-free yield, there is a point of diminishing returns below 5-10 km in many partially-cloudy regions. Active lidars, with lasers that transmit and receive near-vertical beams, are not affected by cloud scattering and shadowing and may therefore return more useful soundings in partially cloudy regions.

Even in areas without optically thick clouds and aerosols, scattering by optically thin clouds and aerosols can introduce uncertainties in the optical path length that can cause unacceptably large biases in XCO<sub>2</sub> and XCH<sub>4</sub> estimates. To mitigate these errors, the optical properties and vertical distribution of optically thin clouds and aerosols must be known to quantify the impact of their scattering on the optical path length. For most existing and near-term CO<sub>2</sub> and CH<sub>4</sub> missions, this information is provided by co-boresighted measurements acquired within the 0.765- $\mu\text{m}$  O<sub>2</sub> A-band and 2.06- $\mu\text{m}$  CO<sub>2</sub> (see Crisp et al., 2004). This approach, combined with cloud screening methods (Taylor et al., 2016), usually provides adequate accuracy when the combined cloud and aerosol optical depth is less than 0.3.

Some platforms augment these measurements with dedicated cloud and aerosol imagers (e.g. the GOSAT TANSO-CAI, TanSat Cloud and Aerosol Polarization Imager, CAPI). These sensors provide additional information about the horizontal distribution of clouds or aerosols within or around the CO<sub>2</sub> / CH<sub>4</sub> sounding footprint. However, these multi-channel imaging filter radiometer data provide little or no information about the aerosol optical depth and the vertical

distribution of optically thin aerosols or their impact on the optical path length modifications within CO<sub>2</sub> and CH<sub>4</sub> bands. This may explain why groups that have used TANSO-CAI data in TANSO-FTS retrievals (Yoshida et al. 2011) have not shown significant additional skill over those using TANSO-FTS A-Band and 2.06- $\mu\text{m}$  CO<sub>2</sub> data in their retrievals (Crisp et al. 2012).

Other efforts have exploited the tight formation flying between the OCO-2 and CALIPSO satellites and used the aerosol vertical profile data from the CALIPSO CALIOP lidar as the prior in XCO<sub>2</sub> retrievals (Merrelli et al. 2017). This approach substantially reduces the scatter in aerosol, surface albedo, and XCO<sub>2</sub> retrievals in some cases but not in others. An improved understanding of the scattering by optically thin aerosols would clearly improve the accuracy and coverage of space-based CO<sub>2</sub> and CH<sub>4</sub> measurements, but no space-based remote sensing methods currently available or planned are well suited for this application.

One approach that would substantially improve the coverage and resolution of full-column XCO<sub>2</sub> and XCH<sub>4</sub> soundings would be to integrate the existing satellites into an ad-hoc constellation and combine their measurements into a common, harmonized dataset. This approach exploits the different orbits and sampling strategies to provide enhanced spatial resolution and shorter revisit times. It should also provide better coverage of partially-cloudy regions because the various satellites sample at different times, and clouds move in response to the changing wind field.

#### A4.4 Benefits of cross-calibrating and cross-validating the GOSAT and OCO-2 products

To combine data from multiple satellites into a harmonized dataset, their measurements must be cross-calibrated and their retrieved products (XCO<sub>2</sub>, XCH<sub>4</sub>, SIF) must be cross-validated against common standards to quantify their relative precision and accurately identify any persistent biases. In addition, to retrieve CO<sub>2</sub> fluxes from this combined dataset, advanced assimilation methods are needed that can accommodate the spatial and temporal sampling and the differing uncertainties in the satellite measurements. This is a particularly challenging task for space-based CO<sub>2</sub> and CH<sub>4</sub> sensors because of the demanding requirements for accuracy and precision.

Early in the development of the OCO and GOSAT missions, the science teams of both missions recognized these challenges, but also realized the value of a combined, harmonized dataset. They therefore formed a close collaboration focused on addressing this need. The initial objectives of this collaboration were to cross-calibrate OCO and GOSAT instruments and develop methods to validate their XCO<sub>2</sub> estimates against common standards. During the development phases of these missions, the teams exchanged the radiometric standards used in the pre-launch calibration of the two instruments. These experiments uncovered subtle shortcomings in the calibration of both instruments that were addressed prior to launch (Sakuma et al., 2010), and reinforced the value of this collaboration.

After the loss of the OCO spacecraft, the GOSAT team invited the OCO team to join their efforts to analyze GOSAT data. NASA responded by reformulating the OCO science team as the

Atmospheric CO<sub>2</sub> Observations from Space (ACOS) team. The ACOS-GOSAT collaboration then focused on three primary areas:

- (1) Joint vicarious calibration campaigns in Railroad Valley, Nevada, USA, to track and correct changes in the radiometric calibration of TANSO-FTS;
- (2) Modification and use of the OCO retrieval algorithm to generate estimates of XCO<sub>2</sub> from GOSAT measurements; and
- (3) Validation of the ACOS and GOSAT XCO<sub>2</sub> retrievals against the ground-based FTS retrievals of XCO<sub>2</sub> from TCCON.

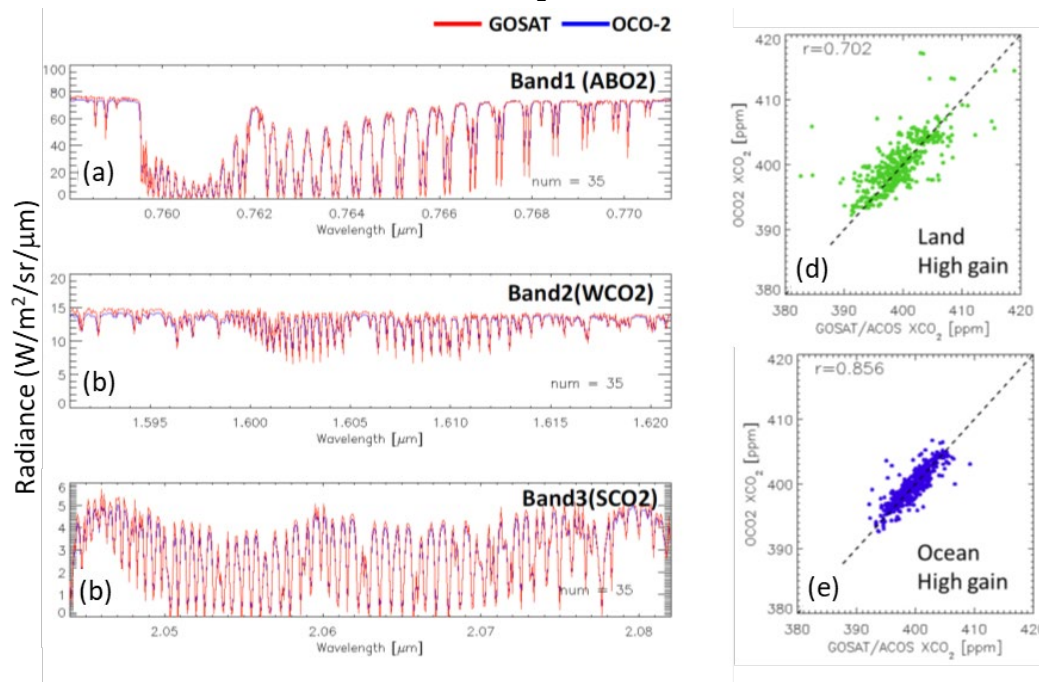


Figure A4-11: Coincident spectra of the (a) O<sub>2</sub> A-band, (b) 1.61 μm CO<sub>2</sub> band and (c) 2.06 μm CO<sub>2</sub> bands from GOSAT TANSO FTS (red) and OCO-2 (blue) collected over a cloud-free scene over the Pacific Ocean. (d) Comparison of coincident XCO<sub>2</sub> estimates from TANSO FTS high gain measurements and OCO-2 observations over land. (e) Same as (d) for measurements collected over ocean. (credit: Kataoka et al., 2017).

This collaboration has continued to yield benefits for both teams. The vicarious calibration experiments have helped to identify and correct drifts in the pre-launch GOSAT radiometric calibration (Kuze et al., 2011; 2014). These campaigns also helped to refine techniques for conducting ground-based vicarious calibration campaigns for OCO-2 and future satellite-based SWIR CO<sub>2</sub> and CH<sub>4</sub> sensors. The retrieval algorithm intercomparison effort accelerated the development of XCO<sub>2</sub> retrieval algorithms. Early comparisons of preliminary GOSAT and ACOS XCO<sub>2</sub> retrievals with TCCON results showed that the ACOS GOSAT retrievals were about 2% too low. About half of this bias has been attributed to a 1% high bias in the O<sub>2</sub> column abundance, which was first revealed as a 10 hPa overestimate in the retrieved surface pressure (Crisp et al. 2012) that was subsequently traced to uncertainties in the absorption cross sections for O<sub>2</sub> A-band. The remainder is associated with unresolved instrument calibration uncertainties,

errors in the CO<sub>2</sub> spectroscopy, and errors or oversimplifications in the retrieval algorithms (Kuze et al. 2012; Yoshida et al., 2016).

Once the OCO-2 satellite was launched, the focus of the collaboration was shifted back to the cross-calibration of the TANSO-FTS and OCO-2 measurements, and the cross-validation of their products. While the vicarious calibration campaigns in Railroad Valley have continued to play a primary role in the cross-calibration effort, co-incident measurements from a broad range of sites around the globe have been added to improve the range of scene brightness covered by this approach (Kataoka et al. 2017; Figure A4-11 a-c). These measurements are now yielding new insights into the radiometric and spectroscopic calibration of both instruments.

To facilitate the development of a harmonized OCO-2/GOSAT product, the OCO-2/ACOS team modified the OCO-2 Build 7 algorithm to process the TANSO-FTS L1B v200/201 product, generating the ACOS version 7.3 product. This product was validated against TCCON (Lindquist et al. 2015; Kulawik et al., 2016) and then cross-validated against OCO-2 using TCCON and EM27/SUN instruments (Hedelius et al., 2017; Frey et al., 2018) and by comparing co-incident measurements (Kataoka et al., 2017; Figure A4-11 d-e). The overlapping regions show very good agreement on regional scales at monthly intervals (Figure A4-12). This combined product has since been used for studies of the carbon cycle (see Chatterjee et al. 2017; Liu et al. 2017). An updated ACOS/GOSAT data product that uses the OCO-2 Build 8 algorithm was under development as this report was being written.

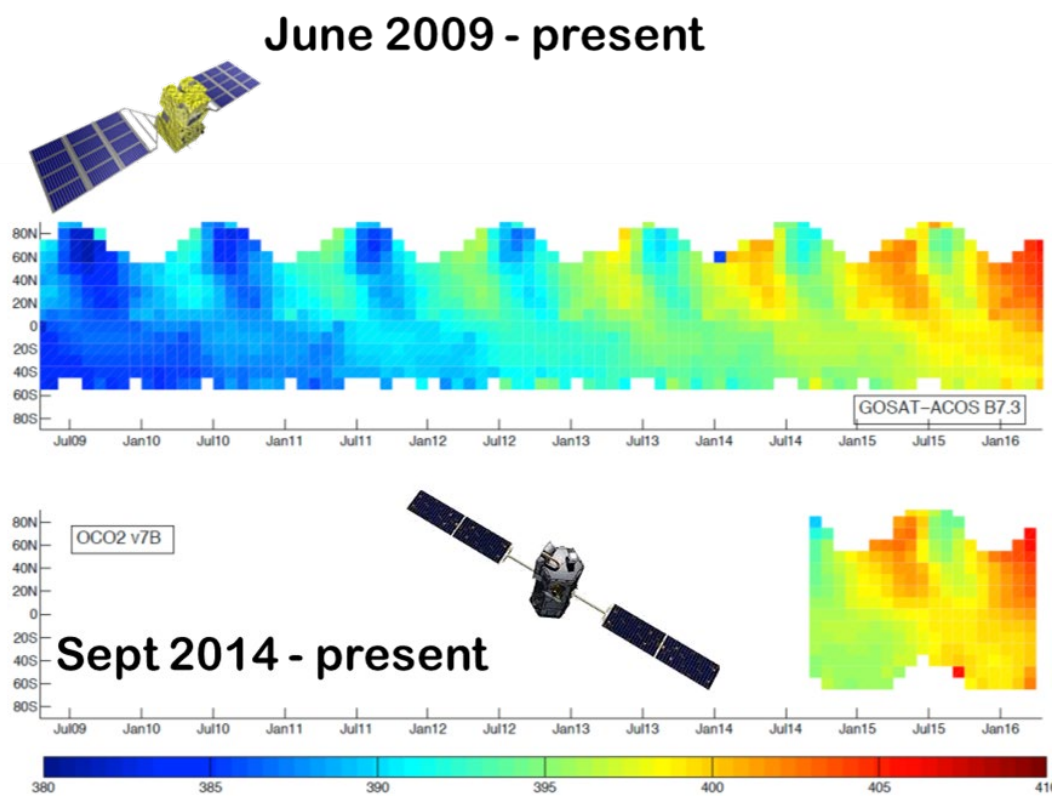


Figure A4-12: The GOSAT and OCO-2 measurements were cross-calibrated, and their data products were cross-validated to produce a continuous, harmonized data record that spanned the lifetimes of both missions.

Given the success of this collaboration, NASA and its GOSAT partners, MOE, NIES, and JAXA, have extended this effort to include the GOSAT-2 and OCO-3 missions. The SCIAMACHY team also adopted TCCON as a critical transfer standard for cross-calibrating their results against the WMO standard (Heymann et al. 2015; Buchwitz et al. 2015). Representatives from other missions including Sentinel 5 Precursor, MicroCarb, and TanSat, have also expressed interest in the Railroad Valley vicarious calibration and TCCON validation approach pioneered by the GOSAT and OCO-2 teams.

## APPENDIX 5: Greenhouse gas monitoring satellites from commercial organizations and non-governmental organizations

### A5.1 GHGSat-D

GHGSat-D or ‘Claire’ is a ~15 kg microsatellite equipped with an imaging Fabry-Perot Spectrometer (Figure A5-1). GHGSat-D was launched on June 21, 2016 into a 520 km sun-synchronous orbit with a 9:30 local equator crossing time. GHGSat is a commercial organization with the primary objective of providing CH<sub>4</sub> and CH<sub>4</sub> emission information to paying customers, such as companies in the oil and gas sector. The satellite operates in target mode only, rather than collecting global surveys. The Fabry-Perot spectrometer images CH<sub>4</sub> in the 1.6- $\mu$ m region at a spatial resolution of ~20-50 m over a 12 km  $\times$  12 km field of view.

Complications with GHGSat-D, including stray light, ghost images and detector degradation, have resulted in column CH<sub>4</sub> measurement uncertainties of order 10%. The GHGSat team has also attempted to retrieve CO<sub>2</sub> from the 1.6  $\mu$ m spectra, but these results had uncertainties of about 30%. With this performance, detecting strong sources may be possible when they are successfully targeted, but accurate quantification of source fluxes has not yet been demonstrated.

GHGSat-D was still in operation and returning data in late 2018. Building on lessons learned from this system, GHGSat is currently building two new microsatellites called GHGSat-C1 (scheduled for launch in 2019) and GHGSat-C2 (scheduled for launch in 2020).

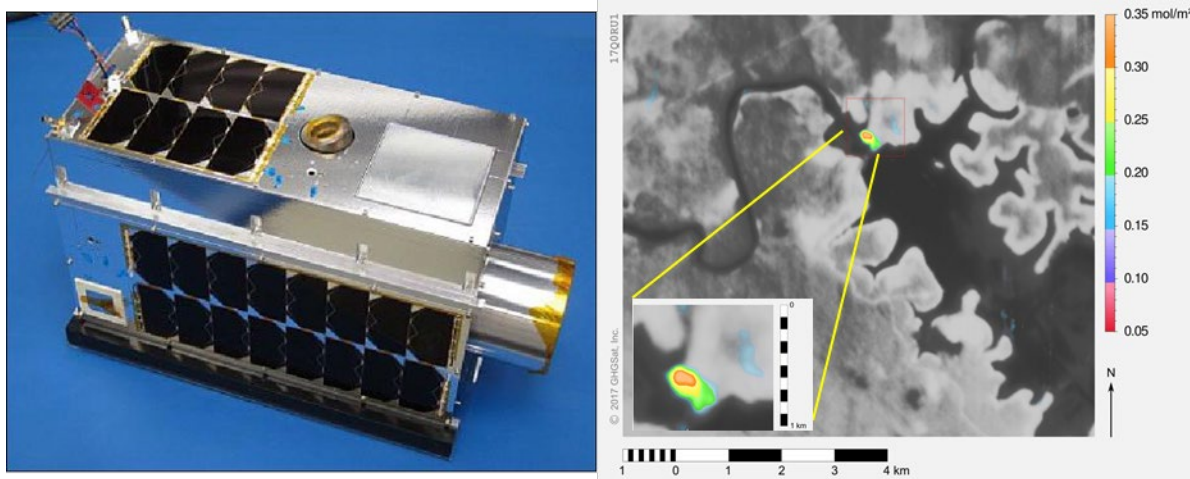


Figure A5-1: Left: Image of the GHGSat-D microsatellite (credit: University of Toronto, Institute for Aerospace Studies/ Space Flight Laboratory). Right: GHGSat-D measurement of excess CH<sub>4</sub> column from Lom Pangar Dam in Cameroon, April 20, 2017 (credit: GHGSat [http://www.ghgsat.com/?attachment\\_id=317](http://www.ghgsat.com/?attachment_id=317)).

### A5.2 Bluefield Technologies COOL

Bluefield Technologies plans to deploy a constellation of 20-kg CH<sub>4</sub> Observation Of Lower-troposphere (COOL) microsatellites in LEO at 550 km altitude. The orbit will be sun-

synchronous with a local nodal crossing time of noon  $\pm 90$  minutes. Each satellite will carry and point a sensor capable of detecting methane ground leaks at a spatial resolution of 20 m x 20 m (<http://bluefield.co>). Satellites will measure along the orbital track with a 25 km x 20 km field of view (FOV). An off-nadir pointing capacity of  $\pm 25^\circ$  cross-track angle with a 540 km east-west field of regard (FOR) allows additional coverage and increased ability to avoid clouds.

The CH<sub>4</sub> sensor is a gas filter correlation radiometer (GFCR), an approach used by the NASA Halogen Occultation Experiment (HALOE) on the Upper Atmosphere Research Satellite (UARS) and the CSA/NASA MOPITT instrument on the Terra spacecraft. The principle of operation of the GFCR instrument is illustrated in Figure A5-2. The CH<sub>4</sub> absorption band at 2.3  $\mu\text{m}$  was chosen because this band is factor 3 to 5 stronger than the one at 1.67  $\mu\text{m}$ , enabling the use of shorter gas correlation cells. This wavelength range has limited interference from water vapor and N<sub>2</sub>O contamination. The GFCR is accompanied by a small CMOS visible camera to register the GFCR FOV and to facilitate the detection of clouds and optically thick aerosols within the FOV. To minimize system complexity, the spacecraft Attitude Determination and Control Subsystem points the instrument and performs image motion compensation for about 5–10 s on each ground target as it passes within its FOV. The on-orbit calibration approach uses an on-board calibration system and observations of ground-based vicarious calibration sites, such as Railroad Valley, Nevada. Observations near TCCON stations will be used to validate the CH<sub>4</sub> products.

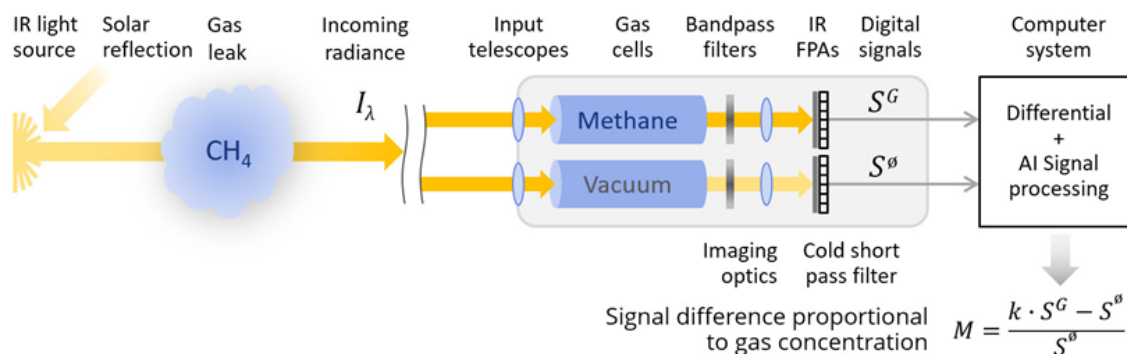


Figure A5-2: Gas Filter Correlation Radiometry (GFCR) general operation concept. Simultaneous high spatial resolution images of the same scene are collected in two channels that are identical, except that one channel includes an absorption cell filled with CH<sub>4</sub>, while the other includes an evacuated cell.

Data from the GFCR instruments will be downlinked and analyzed at ground processing stations to estimate the integrated concentration path-length readings (in ppm-m) using retrieval algorithms adapted from MOPITT (Deeter et al. 1999, Francis et al. 2017). The detection outputs will be delivered to clients as ground registered 2D maps.

Bluefield is launching its first two microsattellites in 2020, which will provide coverage of 727,000 km<sup>2</sup>/day over the course of their 5-year lifespan – sufficient for twice a week readings of every known land-based methane emitter on Earth above the detection threshold. In 2021, five (5) microsats phased within the same orbit will be able to give daily access to any area on Earth, by filling gaps between the other tracks. By 2023, Bluefield will operate a swarm of 10 or more

microsats, allowing targets closer together and more than one daily access to a larger number of ground targets, including some ocean targets observed in sun-glint reflection.

### A5.3 Environmental Defence Fund's MethaneSAT

A micro-satellite concept, called MethaneSAT, was recently announced by the Environmental Defense Fund (EDF; <https://www.nature.com/articles/d41586-018-04478-6>; Tolerson, 2018). This satellite will use an imaging grating spectrometer to return global measurements of CH<sub>4</sub> emissions at weekly intervals at an effective spatial resolution of ~1 km by 1 km across a 200-km wide swath. The objective is to quantify, rather than to simply identify, emissions sources, but there is a strong focus on precision to facilitate the detection of weak sources. The current expected XCH<sub>4</sub> precision goal is 0.1% (1.8 ppb) in each 1 km x 1 km sample. EDF has partnered with Harvard University and the Smithsonian Astrophysical Observatory to regularly monitor CH<sub>4</sub> emissions from the 50 largest oil and gas facilities, which account for ~80% of the global oil and gas production. The first launch is targeted for late 2020 or early 2021. Unlike the commercial efforts described above, a key feature of MethaneSAT is that, like the data from major space agencies, the data from MethaneSAT will be freely available to all users (<https://www.cfa.harvard.edu/news/fe201806>).

## APPENDIX 6: Advantages of LEO, GEO and HEO vantage points

### A6.1 Global observations from LEO constellations

Most existing and planned solar SWIR CO<sub>2</sub> and CH<sub>4</sub> sensors are deployed on platforms in low Earth orbit (LEO) because this vantage point offers a number of advantages in addition to the inherently lower cost of launch and operations. Sensors deployed in LEO can collect measurements over nearly the entire globe at high spatial resolution at weekly to monthly intervals. Because the entire Earth can be observed by the same sensor, no instrument-to-instrument cross calibration or cross validation is needed to harmonize regional-scale observations from instruments on different platforms, and each instrument can exploit ground-based calibration and validation facilities distributed across the globe. The observation strategy for LEO instruments can also be optimized to observe the glint spot to maximise the SNR over the ocean and provide useful constraints on the transport of CO<sub>2</sub> and CH<sub>4</sub> over the ocean basins.

Sun-synchronous LEO orbits, like those used by GOSAT, OCO-2, TanSat and Sentinel 5p, sample the Earth at a fixed time of day. This is ideal for tracking seasonal to inter-annual trends in CH<sub>4</sub> and CO<sub>2</sub>. However, these orbits preclude observations of the systematic changes in the emission sources of natural sinks of these gases over the diurnal cycle. They also preclude observations of diurnal variations in SIF that could provide insight into the uptake of CO<sub>2</sub> by the land biosphere. Instruments in low-inclination precessing orbits, such as OCO-3 on ISS, can collect measurements from dawn to dusk, but can observe only a limited range of latitudes ( $\pm 51^\circ$  for the ISS), and the orbit track never repeats exactly, complicating repeat observations of specific sites to track long-term trends at specific surface locations. These temporal sampling limitations can be mitigated to some extent by deploying some elements of the LEO constellation in morning orbits and others in afternoon orbits, as is done for meteorological sensors (Palmer et al., 2011). This approach is being considered for TanSat-2. However, the morning and evening elements of the constellation would have to be carefully coordinated to avoid aliasing diurnal changes in XCO<sub>2</sub>, XCH<sub>4</sub> and SIF with spatial or temporal changes associated with transport or other factors.

Another limitation of instruments on LEO platforms is their relatively-infrequent sampling of individual surface locations. Most of these satellites collect a “snapshot” of the CO<sub>2</sub> and CH<sub>4</sub> fields along their ground tracks at intervals of days (GOSAT) or weeks (OCO-2, TanSat). The revisit time of sensors on individual LEO platforms is dictated by the sensors’ sampling strategy and the orbit’s ground track repeat cycle. Most systems currently in operation, or planned in the near future, acquire observations of discrete points separated by large distances (GOSAT, Feng Yun-3D, GaoFen-5) or along a narrow swath (OCO-2, TanSat, OCO-3, MicroCarb) that sample only a small fraction of the Earth’s surface. This sampling strategy, combined with interference by optically thick clouds, limits the repeat frequency to a few samples per year.

The revisit time of LEO sensors can be minimized by deploying a well-coordinated constellation of satellites that each acquires contiguous observations at high spatial resolution over a wide

swath. For example, a constellation of 3 LEO satellites carrying instruments with 280-km wide swaths deployed at ~10-minute intervals along the same orbit would cover a contiguous, ~800 km wide swath over a 30-minute period. With an optimized orbit design, this constellation could provide contiguous sampling of that part of the globe not covered by clouds with a repeat cycle as short as half a week. Coordinated observations from wide-swath instruments on platforms in coordinated orbits are therefore a high priority of any future, purpose-built LEO CO<sub>2</sub>/CH<sub>4</sub> constellation. One example is the Copernicus CO<sub>2</sub> Sentinel described in Chapter 5.

Other instruments could be added to the LEO constellation to address specific needs. For example, the broad-swath XCO<sub>2</sub> and XCH<sub>4</sub> mapping measurements might be combined with targeted measurements by independent sensors that have lower precision and accuracy but much high spatial resolution to pinpoint intense point sources. Alternatively, one or more of the satellites in the constellation could be augmented by an active lidar to provide some sampling over the night side and at high latitudes. If the Lidar was co-manifested with a passive, wide-swath mapping instrument, data from this active-passive instrument suite could be used to assess errors in both products, since many of the sources of bias in the XCO<sub>2</sub> and XCH<sub>4</sub> products from active Lidars and passive solar instruments have different origins. It might be possible to apply the lessons learned from a single active-passive satellite across the entire passive LEO constellation, following the approach pioneered by the Global Precipitation Mission (GPM). If active CO<sub>2</sub> and CH<sub>4</sub> sensors are not available, nearly-coincident measurements collected by instruments on different members of the constellation can be compared to identify and mitigate the impact of anomalous observations collected by individual sensors.

While the first purpose-built LEO CO<sub>2</sub>/CH<sub>4</sub> constellation is being implemented, substantial reductions in revisit times could be realized by organizing all operating satellites into a virtual constellation, and combining their data into a common, harmonized data product. This approach can also provide additional observations in partially cloudy regions, such as the Tropics, because the clouds move between the satellite overpasses. The coverage provided by such a virtual constellation can be maximized by carefully coordinating the orbits of the satellites. CEOS could play a critical role in the implementation and coordination of this virtual constellation.

## A6.2 Time-resolved observations from GEO constellations

One way to address the diurnal sampling constraints and long revisit times of LEO observations is to acquire observations of XCO<sub>2</sub>, XCH<sub>4</sub>, and SIF from platforms deployed in a geosynchronous orbit (GEO). From this vantage point, 35800 km above a fixed longitude at the equator, a region up to 50 degrees of the sub-satellite point can be observed from sunup to sundown. Passive solar NIR/SWIR methods, like those used for imaging these gases from LEO, can work in this application, but require modifications to accommodate the ~50 times greater viewing distance.

Because of their position above the equator, GEO observations are ideal for monitoring changes in anthropogenic (fossil and biomass burning) CO<sub>2</sub> and CH<sub>4</sub> emissions in rapidly-developing tropical and subtropical regions. Time-dependent observations of CO<sub>2</sub>, CH<sub>4</sub>, and SIF over these

regions can record the response of the natural carbon cycle to land use change and climate change. These areas are a high priority for space-based CO<sub>2</sub> and CH<sub>4</sub> measurements, in part because of the difficulty in sustaining ground-based observations there, due to the lack of infrastructure and/or political turmoil.

In principal, time-resolved CO<sub>2</sub> and CH<sub>4</sub> observations from a GEO platform could facilitate the detection and quantification of diurnal variations in emissions from urban areas, individual large power plants, and other localized sources, by explicitly resolving the time-dependent effects of emission fluxes and transport. In addition, because CO<sub>2</sub> and CH<sub>4</sub> fluxes from the land biosphere and different anthropogenic emissions sectors have different diurnal emission profiles, continuous observations might facilitate efforts to discriminate emissions from these sources. The GEO observation strategy could also be optimized to provide some useful, cloud-free observations in even the cloudiest regions, by acquiring data as the clouds move. This capability could dramatically improve the resolution and coverage of CO<sub>2</sub> and CH<sub>4</sub> emissions and trends in tropical rain forests and other persistently-cloudy regions.

GEO observations also pose a number of challenges for CO<sub>2</sub> and CH<sub>4</sub> observations. For example, the equatorial vantage point provides no coverage of latitudes exceeding ~55° or longitudes more than ~55° east or west of the stationary longitude. Three or more satellites are therefore needed to cover the full range of longitudes spanned by the major land masses in Africa and Europe, North and South America, and South and East Asia. Observations of XCO<sub>2</sub> and XCH<sub>4</sub> over the ocean are limited because they can only be observed over a narrow range of latitudes and longitudes. In-orbit calibration and validation are also more challenging because platforms deployed at specific longitudes can only observe ground-based assets within their field of view, and these locations can only be viewed from a single, constant observing geometry. A coordinated, planet-encircling network of ground-based calibration and validation standards must therefore be maintained to cross-calibrate or cross-validate the measurements from different platforms in a GEO constellation.

Fortunately, there are straightforward ways to address these challenges. Telescopes with larger apertures and longer focal lengths will maintain spatial resolution and reduce the impact of the reduced signal levels. Exposure times can also be increased to help to compensate for the reduced signal levels without compromising spatial resolution, since, unlike a LEO platform, GEO satellites do not fly over the surface at ~7 km/second. Other challenges can be addressed by coordinating measurements from the GEO and LEO constellations. While GEO satellites provide little coverage of high latitudes, LEO satellites provide their most frequent observations at high latitudes where their swaths overlap due to the convergence of the meridians. Coincident measurements from under-flying LEO satellites can be used to cross-calibrate measurements and cross-validate the results from sensors on GEO satellites covering different longitude ranges.

GeoCarb is the first mission designed to exploit the GEO vantage point for measuring atmospheric CO<sub>2</sub> and CH<sub>4</sub>, CO, and SIF. If all goes as planned, GeoCarb will be stationed between 75° and 100° West longitude in the early 2020's. From there, it will produce contiguous spatial maps at least twice each day, which may extend as far north as the US/Canada border and as far south as Punta Arenas, Chile, with spatial resolution as high as ~7 km by 7 km at the sub-

spacecraft point (Polonsky et al., 2014; O'Brien et al. 2016). An even more ambitious GEO mission, called AbsoRption spectRometric patHfindEr for carboN regional flUx dynamicS (ARRHENIUS) was recently proposed to the ESA Earth Explorer 10 opportunity. With ARRHENIUS stationed over the equator at  $\sim 20^\circ$  E longitude, it could cover Africa, Europe, and the Middle East at a spatial resolution as high as 2 km by 2 km at the sub-spacecraft point. ARRHENIUS will complement the Sentinel constellations in LEO by sampling selected locations up to 5 times each day to capture diurnal variations in XCO<sub>2</sub>, XCH<sub>4</sub>, XCO and SIF over Africa's tropical rain forests, semi-arid, and arid regions, Europe's industrial and agricultural areas, and Middle Eastern fossil fuel extraction activities. Currently, there are no published plans to deploy a GEO CO<sub>2</sub>/CH<sub>4</sub> satellite over the heavily populated and rapidly-developing range of longitudes occupied by South or East Asia.

### A6.3 High latitude observations from HEO platforms

The carbon cycle in arctic and boreal regions is changing rapidly in response to increasing temperatures, changes in sea and land ice cover, and extended growing seasons. These regions are particularly challenging to monitor from the ground due to the difficulty and expense of deploying and maintaining instruments and stations at these latitudes. They also pose serious challenges for space-based CO<sub>2</sub> and CH<sub>4</sub> measurements due to low light conditions and persistent clouds during much of the year, and due to their lack of visibility from GEO orbits.

One way to improve the coverage of this region is to deploy CO<sub>2</sub> and CH<sub>4</sub> sensors on platforms in highly eccentric, elliptical orbits with their apogees over high northern latitudes. From a Highly Elliptical Orbit (HEO), these instruments could then collect time-resolved observations over the boreal and arctic regions similar to those provided by GEO platforms over low latitudes (Nassar et al., 2014). For example, a highly-eccentric elliptical orbit with a perigee near 8100 km and an apogee near 43,500 km would be able to view the Arctic and areas outside of GEO range for over half of each 16-hour orbit.

The Canadian Space Agency (CSA) has explored the benefits of these platforms for several years. One recent concept called AIM-North ([www.aim-north.ca](http://www.aim-north.ca)) would deploy a NIR/SWIR Imaging Fourier Transform Spectrometer (IFTS) to measure XCO<sub>2</sub>, XCH<sub>4</sub>, XCO and SIF, along with a dispersive ultraviolet-visible imaging spectrometer (UVS) to monitor NO<sub>2</sub>, SO<sub>2</sub> and other reactive trace gas species that affect air quality. This concept would employ a 12-hour Molniya orbit with a  $\sim 39000$  km apogee and a 800 km perigee to monitor both anthropogenic (fracking, mining, oil sands operations, other industry and urban areas) and natural carbon cycle activity (permafrost thaw and forest evolution and health) at latitudes between  $40^\circ$  N and  $80^\circ$  N. From this orbit, observations could be collected at 60 to 90 minute intervals throughout the day at a spatial resolution of 3 km by 3 km. By extending the CO<sub>2</sub>, CH<sub>4</sub> and air quality observations to high latitudes, HEO measurements will better quantify emissions for regulatory purposes, improve air quality forecasting, track climate-related changes in the boreal and Arctic ecosystems, and support national emission reduction goals and the transparency framework of the United Nations Paris Agreement.

## APPENDIX 7: CEOS Agencies implementing CO<sub>2</sub> and CH<sub>4</sub> missions

Canadian Space Agency (CSA)

- ACE FTS

Centre National d'Etudes Spatiales (CNES)

- IASI, IASI-NG, MicroCarb, MERLIN

Deutsches Zentrum für Luft-und Raumfahrt (DLR)

- MERLIN

European Commission (EC)

- Copernicus Sentinel 5 p TROPOMI, Copernicus Sentinel 5 UVNS, Copernicus CO<sub>2</sub>

European Space Agency (ESA)

- ENVISAT SCIAMACHY and MIPAS, Sentinel 5 p TROPOMI, Sentinel 5 UVNS, Sentinel CO<sub>2</sub>

European Organisation for the Exploitation of Meteorological Satellites (EUMETSAT)

- Metop-A IASI, Metop IASI-NG

Japan Aerospace Exploration Agency (JAXA)

- GOSAT TANSO-FTS, GOSAT-2 TANSO FTS-2

National Aeronautics & Space Administration (NASA)

- Aqua AIRS, Aura TES, OCO-2, OCO-3, GeoCarb

National Satellite Meteorological Center/China Meteorological Administration (NSMC/CMA)

- TanSat, FY-3D, GaoFen-5, FY-3G

National Oceanic and Atmospheric Administration (NOAA)

- NOAA-10 HIRS-2

## Appendix 8: Acronym List

2-D - Two-dimensional

A-Train - Afternoon Constellation

AC-VC - Atmospheric Composition Virtual Constellation

ACE - Atmospheric Chemistry Experiment

ACGS - Atmospheric CO<sub>2</sub> Grating Spectrometer (on TanSat)

ACOS - Atmospheric CO<sub>2</sub> Observations from Space

AGU - American Geophysical Union

AOD - Aerosol optical depth

CAI - Cloud and Aerosol Imager (GOSAT)

CALIOP – Cloud-Aerosol Lidar with Orthogonal Polarization (CALIPSO)

CALIPSO – Cloud-Aerosol Lidar and Infrared Pathfinder

CAPI - Cloud and Aerosol Polarization Imager (TanSat)

CAS - Chinese Academy of Sciences

CDIAC - Carbon Dioxide Information Analysis Center

CEOS - Committee on Earth Observation Satellites

CFC - Chlorofluorocarbons

CGMS - Coordination Group on Meteorological Satellites

CH<sub>4</sub> – Methane

CHEOS - China High-Resolution Earth Observation System

Cl – Chlorine

cm<sup>-1</sup> – Wavenumber

cm<sup>2</sup> – Square centimeter

CMA - China Meteorological Administration

CNES - Centre National d'Etudes Spatiales

CNSA - China National Space Administration

CO – Carbon monoxide

CO<sub>2</sub> – Carbon Dioxide

CONTRAIL – Comprehensive Observation Network for Trace gases by Airliner

COOL - CH<sub>4</sub> Observation Of Lower-troposphere (Bluefield)

COP21 - 21st session of the Conference of the Parties (of the UNFCCC)

COP29 = 29<sup>th</sup> session of the Conference of the Parties to be held in 2023

CTF - Carbon Task Force

DLR - Deutsches Zentrum für Luft- und Raumfahrt

EC - European Commission

ECMWF - European Centre for Medium-range Weather Forecasts

ECOSTRESS - Ecosystem Spaceborne Thermal Radiometer Experiment on Space Station

EDGAR - Emission Database for Global Atmospheric Research

EFU3 - Exposed Facility Unit 3 (JEM-EF, ISS)

ENVISAT - Environmental Satellite

ESA - European Space Agency

EUMETSAT - European Organisation for the Exploitation of Meteorological Satellites

FOV - Field of view

FSCRDS - Frequency-Stabilized Cavity Ring-Down Spectroscopy

FTS - Fourier Transform Spectrometer

FY-3D - Feng Yun 3D (China)

FY-3G - Feng Yun-3G (China)

G – Goal (ESA)

GAS - Greenhouse gases Absorption Spectrometer (FY-3D)

GAS-2 - Greenhouse gases Absorption Spectrometer-2 (FY-3G)

GAW - Global Atmospheric Watch

GCOS - Global Climate Observing System

GEDI - Global Ecosystem Dynamics Investigation (ISS)

GEIA -Global Emissions Initiative

GFCR - gas filter correlation radiometer (Bluefield)

GEO - Group on Earth Observations

GEO – Geostationary Earth orbit

GeoCarb - Geostationary Carbon Cycle Observatory

GHG – Greenhouse gas

GHG-CCI - Greenhouse Gas Climate Change Initiative

Gigaton – Billion tons

GMD - Global Atmospheric Monitoring Division (of NOAA)

GMI - Greenhouse-gases Monitoring instrument (GaoFen-5)

GOSAT - Greenhouse gases Observing SATellite

GtC – Billion tons of carbon

HALOE - Halogen Occultation Experiment (UARS)

HEO – High Earth orbit

HCFC - Hydrogenated chlorofluorocarbons

HISUI - Hyperspectral Imager Suite (ISS)

hPa – HectoPascals (a unit of pressure)

Hz – Hertz (cycles per second)

IAGOS - In-service Aircraft for a Global Observing System

ICOS - Integrated Carbon Observation System

IEA - International Energy Agency

IG<sup>3</sup>IS - Integrated Global Greenhouse Gas Information System

IGCO - Integrated Global Carbon Observing system

IPDA - Integrated Path Differential Absorption

IWGGMS - International Workshop on Greenhouse Gas Measurements from Space

IPCC- Intergovernmental Panel on Climate Change

ISS - International Space Station

JAXA 0 Japanese Aerospace Exploration Agency

JEM-EF - Japanese Equipment Module Exposed Facility

JRC – Joint Research Center (of the European Commission)

km<sup>2</sup> – Square kilometer

L1B – Level 1B (calibrated geolocated spectral radiances)

LEO – Low Earth orbit

Lidar - Light Detecting and Ranging

MAG - Mission Advisory Group (ESA)

MAP - multi-angle polarimeter (ESA)

MERIS - Medium Resolution Imaging Spectrometer (ENVISAT)

MERLIN -Methane Remote Sensing Lidar Mission (CNES/DLR)

MISR - Multi-angle Imaging SpectroRadiometer (Terra)

µm – Micron ( $10^{-6}$  meter)

MRD - Mission Requirements Document (ESA)

MODIS - Moderate Resolution Imaging Spectroradiometer (Terra, Aqua)

MOPITT - Measurement of Pollution in the Troposphere (Terra)

MOST - Ministry of Science and Technology (China)

MOE - Ministry of the Environment (Japan)

MRV - Measurement, Reporting and Verification

MVS - Monitoring and Verification Support

N<sub>2</sub>O – Nitrous oxide

NASA - National Aeronautics and Space Administration (USA)

Nd:YAG - Neodymium-doped yttrium aluminum garnet

NDC - Nationally-determined contributions (to a to a global GHG emissions reduction effort)

NIES - National Institute of Environmental Sciences

NIR - Near-infrared

NGO - Non-governmental organization

nm – Nanometer ( $10^{-9}$  meters)

NOAA - National Oceanic and Atmospheric Administration

NO<sub>x</sub> – Nitrogen oxides

NPP - National Polar-orbiting Partnership (USA)

NSO - Netherlands Space Office

O<sup>1</sup>D – Oxygen singlet D (an excited state of atomic oxygen)

O<sub>2</sub> – Molecular oxygen

O<sub>2</sub> <sup>1</sup>Δ<sub>g</sub> – Molecular oxygen singlet delta-g (and excited state)

OCO – Orbiting Carbon Observatory

OCO-2 - Orbiting Carbon Observaotry-2

OCO-3 - Orbiting Carbon Observaotry-3

ODIAC - Open-source Data Inventory for Anthropogenic CO<sub>2</sub>

OH – Hydroxyl

OMI - Ozone Monitoring Instrument (Aura)

OSCAR – Observing System Capability Analysis and Review (WMO)

ppb – Parts per billion by volume

PAS - Photo-Acoustic Spectroscopy

PFC - Perfluorocarbons

ppm – Parts per million by volume

ROLO - Robotic Lunar Observatory

S5P - Sentinel 5 Precursor

SARI - Shanghai Advanced Research Institute

SBSTA - Subsidiary Body for Scientific and Technological Advice (of the UNFCCC)

SCIAMACHY - SCanning Imaging Absorption spectroMeter for Atmospheric Cartography

SIF - Solar induced chlorophyll fluorescence

SNR - Signal-to-noise ratio

SWIR - Short wavelength infrared

SZA - Solar zenith angle

T – Threshold (ESA)

TANSO - Thermal and Near Infrared Sensor for Carbon Observation (GOSAT)

TCCON - Total Carbon Column Observing Network

TFI - Task Force on Greenhouse Gas Inventories

TIR - Thermal infrared

TROPOMI - TROPOspheric Monitoring Instrument (S5P)

UARS - Upper Atmosphere Research Satellite

UK – United Kingdom

UKSA - United Kingdom Space Agency

UNFCCC - United Nations Framework Convention on Climate Change

USA – United States of America

W/m<sup>2</sup> – Watts per square meter

WDCGG - World Data Centre for Greenhouse Gases

WGCapD – Working Group on Capacity Building and Data Democracy (CEOS)

WGCV - Working Group on Calibration and Validation (CEOS)

WMO - World Meteorological Organization

XCH<sub>4</sub> - Column-averaged CH<sub>4</sub> dry air mole fraction

XCO – Column-averaged CO dry air mole fraction

XCO<sub>2</sub> - Column-averaged CO<sub>2</sub> dry air mole fraction

## References Cited

- Aben, I., Hasekamp, O., and Hartmann, W.: Uncertainties in the space-based measurements of CO<sub>2</sub> columns due to scattering in the Earth's atmosphere, *J. Quant. Spect. Radiat. Trans.*, 104, 450-459, 2007.
- Alexe, M., Bergamaschi, P., Segers, A., Detmers, R., Butz, A., Hasekamp, O., Guerlet, S., Parker, R., Boesch, H., Frankenberg, C., Scheepmaker, R.-A., Dlugokencky, E., Sweeney, C., Wofsy, S.-C., and Kort, E. A.: Inverse modelling of CH<sub>4</sub> emissions for 2010-2011 using different satellite retrieval products from GOSAT and SCIAMACHY, *Atmos. Chem. Phys.*, 15, 113-133, 2015.
- Al-Saadi, J., Kim, J., Lambert, J.-C., Veihelmann, B., and Chance, K.: Geostationary Satellite Constellation for Observing Global Air Quality: Geophysical Validation Needs, CEOS Atmospheric Composition Constellation, in preparation, 2018.
- Alvarado, M. J., Payne, V. H., Cady-Pereira, K. E., Hegarty, J. D., Kulawik, S. S., Wecht, K. J., Worden, J. R., Pittman, J. V., and Wofsy, S. C.: Impacts of updated spectroscopy on thermal infrared retrievals of methane evaluated with HIPPO data, *Atmos. Meas. Tech.*, 8, 965-985, doi:10.5194/amt-8-965-2015, 2015.
- Anderson, J. M., Becker, K. J., Kieffer, H. H., and Dodd D. N.: Modeling the brightness of the Moon over 350 - 2500 nm for spacecraft calibration, *Pub. Astronomical Soc. Pacific* 111, 737-749, doi:10.1086/316375, 1999.
- Andres, R. J., Boden, T. A., Bréon, F.M., Ciais, P., Davis, S., Erickson, D., Gregg, J. S., Jacobson, A., Marland, G., Miller, J., Oda, T., Olivier, J. G. J., Raupach, M. R., Rayner, P., Treanton, K.: A synthesis of carbon dioxide emissions from fossil-fuel combustion, *Biogeosciences*, 9, 1845-1871, doi:10.5194/bg-9-1845-2012, 2012.
- Andrews, A. E., Kofler, J. D., Trudeau, M. E., Williams, J. C., Neff, D. H., Masarie, K. A., Chao, D. Y., Kitzis, D. R., Novelli, P. C., Zhao, C. L., Dlugokencky, E. J., Lang, P. M., Crotwell, M. J., Fischer, M. L., Parker, M. J., Lee, J. T., Baumann, D. D., Desai, A. R., Stanier, C. O., De Wekker, S. F. J., Wolfe, D. E., Munger, J. W., and Tans, P. P.: CO<sub>2</sub>, CO, and CH<sub>4</sub> measurements from tall towers in the NOAA Earth System Research Laboratory's Global Greenhouse Gas Reference Network: instrumentation, uncertainty analysis, and recommendations for future high-accuracy greenhouse gas monitoring efforts, *Atmos. Meas. Tech.*, 7, 647-687, <https://doi.org/10.5194/amt-7-647-2014>, 2014.
- Arnold, C. P. and Dey, C. H.: Observing-systems simulation experiments: Past, present, and future. *Bulletin of the American Meteorological Society*, 67(6):687-695, 1986.
- Baker, D. F., Doney, S. C., and Schimel, D. S.: Variational data assimilation for atmospheric CO<sub>2</sub>, *Tellus*, 58B, 359-365. doi:10.1111/j.1600-0889.2006a.00218.x, 2006a.
- Baker, D. F., Law, R. M., Gurney, K. R., Rayner, P., Peylin, P., Denning, A. S., Bousquet, P., Bruhwiler, L., Chen, Y. H., Ciais, P., Fung, I. Y., Heimann, M., John, J., Maki, T., Maksyutov, S., Masarie, K., Prather, M., Pak, B., Taguchi, S., and Zhu, Z.: TransCom 3

- inversion intercomparison: Impact of transport model errors on the interannual variability of regional CO<sub>2</sub> fluxes, 1988-2003. *Global Biogeochem. Cycles*, 20, 01 [GB1002], doi:10.1029/2004GB002439, 2006b.
- Baker, D. F., Boesch, H., Doney, S. C., O'Brien, D., and Schimel, D. S.: Carbon source/sink information provided by column CO<sub>2</sub> measurements from the Orbiting Carbon Observatory. *Atmos. Chem. Phys.*, 10, 4145–4165, doi:10.5194/acp-10-4145-2010, 2010.
- Basu, S., S. Guerlet, A. Butz, S. Houweling, O. Hasekamp, I. Aben, P. Krummel, P. Steele, R. Langenfelds, M. Torn, S. Biraud, B. Stephens, A. Andrews, and D. Worthy, Global CO<sub>2</sub> fluxes estimated from GOSAT retrievals of total column CO<sub>2</sub>, *Atmos. Chem. Phys.*, 13(17), 8695-8717, doi:10.5194/acp-13-8695-2013, 2013.
- Basu, S., Krol, M., Butz, A., Clerbaux, C., Sawa, Y., Machida, T., Matsueda, H., Frankenberg, C., Hasekamp, O. P., and Aben, I.: The seasonal variation of the CO<sub>2</sub> flux over Tropical Asia estimated from GOSAT, CONTRAIL, and IASI, *Geophys. Res. Lett.*, 41, 1809–1815, doi:10.1002/2013GL059105, 2014.
- Basu, S., Baker, D. F., Chevallier, F., Patra, P. K., Liu, J., Miller, J. B.: The impact of transport model differences on CO<sub>2</sub> surface flux estimates from OCO-2 retrievals of column average CO<sub>2</sub>, *Atmos. Chem. Phys.*, 18, 7189–7215, doi:10.5194/acp-18-7189-2018, 2018.
- Battersby, S., “News feature: The carbon detectives,” *Proceedings of the National Academy of Sciences*, 115, 6873–6877, 2018.
- Beer, C., Reichstein, M., Tomelleri, E., Ciais, P., Jung, M., Carvalhais, N., Rodenbeck, C., Arain, M. A., Baldocchi, D., Bonan, G. B., Bondeau, A., Cescatti, A., Lasslop, G., Lindroth, A., Lomas, M., Luyssaert, S., Margolis, H., Oleson, K. W., Rouspard, O., Veenendaal, E., Viovy, N., Williams, C., Woodward, F. I., and Papale, D.: Terrestrial gross carbon dioxide uptake: Global distribution and covariation with Climate. *Science*, 329,834-838, doi:10.1126/science.1184984, 2010.
- Benner, D. C., Rinsland, C. P., Devi, V. M., Smith, M. A. H and Atkins, D.: A multispectrum nonlinear least-squares fitting technique, *J. Quant. Spectrosc. Radiat. Transfer*, 53, 705-721, doi:10.1016/0022-4073(95)00015-D, 1995.
- Benner, D. C., V. M. Devi, K. Sung, L. R. Brown, C. E. Miller, V.H. Payne, B. J. Drouin, S. Yu, T. J. Crawford, A. W. Mantz, M. A. H. Smith and R. R. Gamache: Line parameters including temperature dependences of air- and self-broadened line shapes of (CO<sub>2</sub>)-C-12-O-16: 2.06- $\mu$ m region, *J. Mol. Spec.*, 326, 21-47, doi:10.1016/j.jms.2016.02.012, 2016.
- Bergamaschi, P., Frankenberg, C., Meirink, J. F., Krol, M., Villani, M. G., Houweling, S., Dentener, F., Dlugokencky, E. J., Miller, J. B., Gatti, L. V., Engel, A., and Levin, I.: Inverse modeling of global and regional CH<sub>4</sub> emissions using SCIAMACHY satellite retrievals, *J. Geophys. Res.*, 114, D22301, doi:10.1029/2009JD012287, 2009.
- Bergamaschi, P., Krol M., Meirink, J. F., Dentener, F., Segers A., van Aardenne, J., Monni, S., Vermeulen, A. T., Schmidt, M., Ramonet, M., Yver C., Meinhardt, F., Nisbet, E. G., Fisher, R. E., O'Doherty, S., and Dlugokencky, E. J.: Inverse modeling of European CH<sub>4</sub> emissions

2001–2006, *J. Geophys. Res.*, 115, D22309, doi:10.1029/2010JD014180, 2010.

- Bergamaschi, P., Houweling, S., Segers, A., Krol, M., Frankenberg, C., Scheepmaker, R. A., Dlugokencky, E., Wofsy, S. C., Kort, E. A., Sweeney, C., Schuck, T., Brenninkmeijer, C., Chen, H., Beck, V., and Gerbig, C.: Atmospheric CH<sub>4</sub> in the first decade of the 21st century: Inverse modeling analysis using SCIAMACHY satellite retrievals and NOAA surface measurements, *J. Geophys. Res. Atmos.*, 118, 7350–7369, doi:10.1002/jgrd.50480, 2013.
- Bergamaschi, P., A. Danila, R. F. Weiss, P. Ciais, R. L. Thompson, D. Brunner, I. Levin, Y. Meijer, F. Chevallier, G. Janssens-Maenhout, H. Bovensmann, D. Crisp, S. Basu, E. Dlugokencky, R. Engelen, C. Gerbig, D. Günther, S. Hammer, S. Henne, S. Houweling, U. Karstens, E. Kort, M. Maione, A. J. Manning, J. Miller, S. Montzka, S. Pandey, W. Peters, P. Peylin, B. Pinty, M. Ramonet, S. Reimann, T. Röckmann, M. Schmidt, M. Strogies, J. Sussams, O. Tarasova, J. van Aardenne, A. T. Vermeulen, F. Vogel: Atmospheric monitoring and inverse modelling for verification of greenhouse gas inventories, EUR 29276 EN, Publications Office of the European Union, Luxembourg, ISBN 978-92-79-88938-7, doi:10.2760/759928, JRC111789, 2018.
- Bernath, P. F., McElroy, C. T., Abrams, M. C., Boone, C. D., Butler, M., Camy-Peyret, C., Carleer, M., Clerbaux, C., Coheur, P. F., Colin, R., DeCola, P., Bernath, P. F., McElroy, C. T., Abrams, M. C., Boone, C. D., Butler, M., Camy-Peyret, C., Carleer, M., Clerbaux, C., Coheur, P. F., Colin, R., DeCola, P., DeMaziere, M., Drummond, J. R., Dufour, D., Evans, W. F. J., Fast, H., Fussen, D., Gilbert, K., Jennings, D. E., Llewellyn, E. J., Lowe, R. P., Mahieu, E., McConnell, J. C., McHugh, M., McLeod, S. D., Michaud, R., Midwinter, C., Nassar, R., Nichitiu, F., Nowlan, C., Rinsland, C. P., Rochon, Y. J., Rowlands, N., Semeniuk, K., Simon, P., Skelton, R., Sloan, J. J., Soucy, M. A., Strong, K., Tremblay, P., Turnbull, D., Walker, K. A., Walkty, I., Wardle, D. A., Wehrle, V., Zander, R., and Zou, J.: Atmospheric Chemistry Experiment (ACE): Mission overview, *Geophys. Res. Lett.*, 32, L15S01, doi:10.1029/2005GL022386, 2005.
- Bi, Y., Yang, Z., and Wang, Q.: TanSat ACGS prelaunch performance evaluation of radiometric calibration, International Workshop on Greenhouse Gas Measurements from Space (IWGGMS), Helsinki, Finland, <http://iwggms13.fmi.fi/presentations.html>, 2017.
- Birk, M., Wagner, G., Mondelain, D., Campargue, A., Hase, F., Orphal, J. and Tyuterev, V.: New spectroscopic data for TROPOMI/S5P in the 2.3 μm region for CH<sub>4</sub> and H<sub>2</sub>O and a new UV database for ozone, Proceedings of the 15<sup>th</sup> International HITRAN conference, Cambridge, MA, June 2018.
- Bloom, A. A., Palmer, P. I., Fraser, A. and Reay, D. S.: Seasonal variability of tropical wetland CH<sub>4</sub> emissions: the role of the methanogen-available carbon pool, *Biogeosciences*, 9, 2821–2830, doi:10.5194/bg-9-2821-2012, 2012.
- Bloom, A. A., Lauvaux, T., Worden, J., Yadav, V., Duren, R., Sander, S. P., and Schimel, D. S.: What are the greenhouse gas observing system requirements for reducing fundamental biogeochemical process uncertainty? Amazon wetland CH<sub>4</sub> emissions as a case study, *Atmos. Chem. Phys.*, 16, 15199–15218, doi:10.5194/acp-16-15199-2016, 2016.
- Boden, T. A., Marland, G., and Andres, R. J.: Global, Regional, and National Fossil-Fuel CO<sub>2</sub> Emissions, Carbon Dioxide Information Analysis Center, Oak Ridge National Laboratory,

U.S. Department of Energy, Oak Ridge, Tenn., USA, doi:10.3334/CDIAC/00001\_V2017, 2017.

Boesch H., G.C. Toon, B. Sen, R. A. Washenfelder, P.O. Wennberg, M. Buchwitz, R. de Beek, J. P. Burrows, D. Crisp, M. Christi, B. J. Connor, V. Natraj, and Y. L. Yung: Space-based near-infrared CO<sub>2</sub> measurements: Testing the Orbiting Carbon Observatory retrieval algorithm and validation concept using SCIAMACHY observations over Park Falls, Wisconsin, *J. Geophys. Res.* 111 (D23): Art. No. D23302, doi:10.1029/2006JD007080, 2006.

Boesch, H.; Baker, D., Connor, B., Crisp, D., and Miller, C.: Global Characterization of CO<sub>2</sub> Column Retrievals from Shortwave-Infrared Satellite Observations of the Orbiting Carbon Observatory-2 Mission. *Remote Sens.* 3, 270-304, doi:10.3390/rs3020270, 2011.

Borsdorff, T., Aan de Brugh, J., Hu, H., Aben, I., Hasekamp, O., & Landgraf, J.: Measuring carbon monoxide with TROPOMI: First results and a comparison with ECMWF-IFS analysis data. *Geophysical Research Letters*, 45, 2826–2832. doi:10.1002/2018GL077045, 2018.

Bousquet, P., Peylin, P., Ciais, P., Le Quéré, C., Friedlingstein, P., and Tans, P. P.: Regional changes in carbon dioxide fluxes of land and oceans since 1980, *Science*, 290, 1342-1346, 2000.

Bousquet, P., et al., Error budget of the MEthane Remote Lidar missioN (MERLIN) and its impact on the uncertainties of the global methane budget, accepted for publication in *JGR-A*, 2018.

Bousserez, N., Henze, D. K., Rooney, B., Perkins, A., Wecht, K. J., Turner, A. J., Natraj, V., and Worden, J. R.: Constraints on methane emissions in North America from future geostationary remote-sensing measurements, *Atmos. Chem. Phys.*, 16, 6175-6190, doi:10.5194/acp-16-6175-2016, 2016.

Bovensmann, H., Burrows, J. P., Buchwitz, M., Frerick, J., Noël, S., Rozanov, V. V., Chance, K. V., and Goede, A.: SCIAMACHY – Mission Objectives and Measurement Modes, *J. Atmos. Sci.*, 56, 127–150, 1999. doi:10.1175/1520-0469(1999).

Bovensmann, H., Buchwitz, M., Burrows, J. P., Reuter, M., Krings, T., Gerilowski, K., Erzinger, J. A remote sensing technique for global monitoring of power plant CO<sub>2</sub> emissions from space and related applications. *Atmospheric Measurement Techniques*, 3, 781–811, doi:10.5194/amt-3-781-2010, 2010.

Bowman, K. W., Liu, J., Bloom, A. A., Parazoo, N. C., Lee, M., Jiang, Z., Menemenlis, D., Gierach, M. M., Collatz, G. J., Gurney, K. R., and Wunch, D., “Global and Brazilian carbon response to El Niño Modoki 2011-2010,” *Earth and Space Science*, 4, 637-660, doi:10.1002/2016EA000204, 2017.

Bril, A., Maksyutov, S., Belikov, D., Oshchepkov, S., Yoshida, Y., Deutscher, N. M., Griffith,

- D., Hase, F., Kivi, R., Morino, I., Notholt, J., Pollard, D. F., Sussmann, R., Velazco, V. A., and Warneke, T.: EOF-based regression algorithm for the fast retrieval of atmospheric CO<sub>2</sub> total column amount from the GOSAT observations, *Journal of Quantitative Spectroscopy & Radiative Transfer*, 189, 258-266, 10.1016/j.jqsrt.2016.12.005, 2017.
- Brioude, J., Angevine, W. M., Ahmadov, R., Kim, S.-W., Evan, S., McKeen, S. A., Hsie, E.-Y., Frost, G. J., Neuman, J. A., Pollack, I. B., Peischl, J., Ryerson, T. B., Holloway, J., Brown, S. S., Nowak, J. B., Roberts, J. M., Wofsy, S. C., Santoni, G. W., Oda, T., and Trainer, M.: Top-down estimate of surface flux in the Los Angeles Basin using a mesoscale inverse modeling technique: assessing anthropogenic emissions of CO, NO<sub>x</sub> and CO<sub>2</sub> and their impacts, *Atmos. Chem. Phys.*, 13, 3661-3677, doi:10.5194/acp-13-3661-2013, 2013.
- Broquet, G., Bréon, F.-M., Renault, E., Buchwitz, M., Reuter, M., Bovensmann, H., Chevallier, F., Wu, L., and Ciais, P.: The potential of satellite spectro-imagery for monitoring CO<sub>2</sub> emissions from large cities, *Atmos. Meas. Tech.*, 11, 681-708, doi:10.5194/amt-11-681-2018, 2018.
- Brown, C. W., and Keeling, C. D.: The concentration of atmospheric carbon dioxide in Antarctica, *J. Geophys. Res.*, 70, 6077-6085, doi:10.1029/JZ070i024p06077, 1965.
- Buchwitz, M.; Rozanov, V.V.; Burrows, J.P.: A correlated-k distribution scheme for overlapping gases suitable for retrieval of atmospheric constituents from moderate resolution radiance measurements in the visible/near-infrared spectral region. *J. Geophys. Res.*, 105, 15247–15261, doi:10.1029/2000JD900171, 2000.
- Buchwitz, M., R. de Beek, S. Noël, J. P. Burrows, H. Bovensmann, H. Bremer, P. Bergamaschi, S. Körner, M. Heimann, Carbon monoxide, methane and carbon dioxide columns retrieved from SCIAMACHY by WFM-DOAS: year 2003 initial data set, *Atmos. Chem. Phys.*, 5, 3313-3329, 2005.
- Buchwitz, M., Schneising, O., Burrows, J. P., Bovensmann, H., Reuter, M., and Notholt, J.: First direct observation of the atmospheric CO<sub>2</sub> year-to-year increase from space, *Atmos. Chem. Phys.*, 7, 4249-4256, doi:10.5194/acp-7-4249-2007, 2007.
- Buchwitz, M., Reuter, M., Bovensmann, H., Pillai, D., Heymann, J., Schneising, O., Rozanov, V., Krings, T., Burrows, J. P., Boesch, H., Gerbig, C., Meijer, Y., and Löscher, A.: Carbon Monitoring Satellite (CarbonSat): assessment of atmospheric CO<sub>2</sub> and CH<sub>4</sub> retrieval errors by error parameterization, *Atmos. Meas. Tech.*, 6, 3477-3500, doi:10.5194/amt-6-3477-2013, 2013.
- Buchwitz, M., Reuter, M., Schneising, O., Boesch, H., Guerlet, S., Dils, B., Aben, I., Armante, R., Bergamaschi, P., Blumenstock, T., Bovensmann, H., Brunner, D., Buchmann, B., Burrows, J. P., Butz, A., Chédin, A., Chevallier, F., Crevoisier, C. D., Deutscher, N. M., Frankenberg, C., Hase, F., Hasekamp, O. P., Heymann, J., Kaminski, T., Laeng A., Lichtenberg, G., De Mazière, M., Noël, S., Notholt, J., Orphal, J., Popp, C., Parker R., Scholze, M., Sussmann, R., Stiller, G. P., Warneke, T., Zehner, C., Bril, A., Crisp D., Griffith, D. W. T., Kuze, A., O'Dell, C., Oshchepkov, S., Sherlock, V., Suto H., Wennberg, P., Wunch, D., Yokota, T., Yoshida, Y.: The Greenhouse Gas Climate Change Initiative (GHG-CCI): Comparison and quality assessment of near-surface-sensitive satellite derived CO<sub>2</sub> and CH<sub>4</sub> global data sets, *Remote Sensing of Environment*, 162, 344-362,

doi:10.1016/j.rse.2013.04.024, 2015.

Buchwitz, M., Reuter M., Schneising O., Hewson, W., Detmers, R.G., Boesch, H., Hasekamp, O.P., Aben I., Bovensmann, H., Burrows, J.P., Butz A., Chevallier, F., Dils, B., Frankenberg, C., Heymann, J., Lichtenberg, G., De Mazière, M., Notholt J., Parker R., Warneke, T., Zehner, C., Griffith D.W.T., Deutscher N.M., Kuze A., Suto, H., Wunch D.: Global satellite observations of column-averaged carbon dioxide and methane: The GHG-CCI XCO<sub>2</sub> and XCH<sub>4</sub> CRDP3 data set, *Remote Sensing of Environment*, 203, 276-205, doi:10.1016/j.rse.2016.12.027, 2017a.

Buchwitz, M., Schneising, O., Reuter, M., Heymann, J., Krautwurst, S., Bovensmann, H., Burrows, J. P., Boesch, H., Parker, R. J., Somkuti, P., Detmers, R. G., Hasekamp, O. P., Aben, I., Butz, A., Frankenberg, C., and Turner, A. J.: Satellite-derived methane hotspot emission estimates using a fast data-driven method, *Atmos. Chem. Phys.*, 17, 5751-5774, 10.5194/acp-17-5751-2017, 2017b.

Buchwitz, M., Reuter, M., Schneising, O., Noel, S., Gier, B., Bovensmann, H., Burrows, J. P., Boesch, H., Anand, J., Parker, R. J., Somkuti, P., Detmers, R. G., Hasekamp, O. P., Aben, I., Butz, A., Kuze, A., Suto, H., Yoshida, Y., Crisp, D., and O'Dell, C., Computation and analysis of atmospheric carbon dioxide annual mean growth rates from satellite observations during 2003-2016, *Atmos. Chem. Phys. Discuss.*, <https://doi.org/10.5194/acp-2018-158>. In review, 2018a.

Buchwitz, M., Reuter, M., Schneising, O., Bovensmann, H., Burrows, J. P., Boesch, H., Anand, J., Parker, R., Detmers, R. G., Aben, I., Hasekamp, O. P., Crevoisier, C., Armante, R., Zehner, C., Schepers, D., Copernicus Climate Change Service (C3S) Global Satellite Observations of Atmospheric Carbon Dioxide and Methane, *Adv. Astronaut. Sci. Technol.*, <https://doi.org/10.1007/s42423-018-0004-6>, 2018b.

Burrows J. P., Hölzle, E., Goede, A. P. H., Visser, H. and Fricke, W.: SCIAMACHY - Scanning Imaging Absorption Spectrometer for Atmospheric Cartography. *ACTA ASTRONAUTICA* Volume: 35 Issue: 7 Pages: 445-451 Published: APR 1995, Source: ACTA ASTRONAUTICA Volume: 35 Issue: 7 Pages: 445-451 DOI: 10.1016/0094-5765(94)00278-T, 1995.

Burrows, J.P. and Bovensmann, H. and Bergametti, G. and Flaud, J.M. and Orphal, J. and Noël, S. and Monks, P.S. and Corlett, G.K. and Goede, A.P. and VonClarmann, T. and Steck, T. and Fischer, H. and Friedl-Vallon, F.: The geostationary tropospheric pollution explorer (GeoTROPE) missions: objects requirements and mission concept. *Advances in Space Research*, 34, 682-687, 2004.

Butz, A., O. P. Hasekamp, C. Frankenberg, I. Aben, Retrievals of atmospheric CO<sub>2</sub> from simulated space-borne measurements of backscattered near-infrared sunlight: accounting for aerosol effects, *Appl. Opt.*, 48, 18, 3322 – 3336, doi:10.1364/AO.48.003322, 2009.

Butz, A., Guerlet, S., Hasekamp, O., Schepers, D., Galli, A., Aben I., Frankenberg, C., Hartmann, J.-M., Tran, H., Kuze, A., Keppel-Aleks, G., Toon, G., Wunch, D., Wennberg, P., Deutscher, N., Griffith, D., Macatangay, R., Messerschmidt, J., Notholt, J., and Warneke, T.: Toward accurate CO<sub>2</sub> and CH<sub>4</sub> observations from GOSAT, *Geophys. Res. Lett.*, 38, L14812, doi:10.1029/2011GL047888, 2011.

- Byrne, B., Jones, D. B. A., Strong, K., Zeng, Z.-C., Deng, F., and Liu, J.: Sensitivity of CO<sub>2</sub> surface flux constraints to observational coverage, *J. Geophys. Res. Atmos.*, 122, 6672–6694, doi:10.1002/2016JD026164, 2017.
- Cambaliza, M. O. L., Shepson, P. B., Caulton, D. R., Stirn, B., Samarov, D., Gurney, K. R., Turnbull, J., Davis, K. J., Possolo, A., Karion, A., Sweeney, C., Moser, B., Hendricks, A., Lauvaux, T., Mays, K., Whetstone, J., Huang, J., Razlivanov, I., Miles, N. L., and Richardson, S. J.: Assessment of uncertainties of an aircraft-based mass balance approach for quantifying urban greenhouse gas emissions, *Atmos. Chem. Phys.*, 14, 9029–9050, doi:10.5194/acp-14-9029-2014, 2014.
- Carouge, C., Bousquet, P., Peylin, P., Rayner, P. J., and Ciais, P.: What can we learn from European continuous atmospheric CO<sub>2</sub> measurements to quantify regional fluxes – Part 1: Potential of the 2001 network, *Atmos. Chem. Phys.*, 10, 3107–3117, doi:10.5194/acp-10-3107-2010, 2010.
- CEOS Strategy for Carbon Observations from Space. The Committee on Earth Observation Satellites (CEOS) Response to the Group on Earth Observations (GEO) Carbon Strategy. Issued date: September 30 2014.
- Chahine, M. T., Barnet, C. D., Olsen, E. T., Chen, L. and Maddy, E.: On the determination of atmospheric minor gases by the method of vanishing partial derivatives with application to CO<sub>2</sub>, *Geophys. Res. Lett.*, 32, L22803, doi:10.1029/2005GL024165, 2005.
- Chatterjee, A., M. Gierach, A. Sutton, D. Crisp, A. Eldering, R. A. Feely, M. Gunson, C. W. O'Dell, B. B. Stephens, D. Schimel: Influence of El Niño on atmospheric CO<sub>2</sub> over the tropical Pacific Ocean: Findings from NASA's OCO-2 mission. *Science* 358, eaam5776, doi:10.1126/science.aam5776, 2017.
- Chédin, A., Serrar, S., Scott, N. A., Pierangelo, C., and Ciais, P.: Impact of tropical biomass burning emissions on the diurnal cycle of upper tropospheric CO<sub>2</sub> retrieved from NOAA 10 satellite observations, *Journal Geophys. Res.*, 110, D11309, doi:10.1029/2004JD005540, 2005.
- Chen, L., Mission Overview GaoFen-5, CEOS-ACC-12 Meeting, Seoul, Korea, <http://ceos.org/meetings/ac-vc-12/>, 13-15 October 2016.
- Chevallier, F., Engelen R. J., and Peylin, P.: The contribution of AIRS data to the estimation of CO<sub>2</sub> sources and sinks. *Geophys. Res. Lett.*, 32, L23801, doi:10.1029/2005GL024229, 2005a.
- Chevallier, F., Fisher, M., Peylin, P., Serrar, S., Bousquet, P., Bréon, F.-M., and Chédin, A.: Inferring CO<sub>2</sub> sources and sinks from satellite observations: Method and application to TOVS data, *J. Geophys. Res.*, 110, D24309, doi:10.1029/2005JD006390, 2005b.
- Chevallier, F., Viovy, N., Reichstein, M., and Ciais, P.: On the assignment of prior errors in Bayesian inversions of CO<sub>2</sub> surface fluxes, *Geophys. Res. Lett.*, 33, L13802,

doi:10.1029/2006GL026496, 2006.

- Chevallier, F., Bréon, F.-M., and Rayner, P. J.: The contribution of the Orbiting Carbon Observatory to the estimation of CO<sub>2</sub> sources and sinks: Theoretical study in a variational data assimilation framework, *J. Geophys. Res.*, 112, D09307, doi:10.1029/2006JD007375, 2007.
- Chevallier, F., Ciais, P., Conway, T. J., Aalto, T., Anderson, B. E., Bousquet, P., Brunke, E. G., Ciattaglia, L., Esaki, Y., Frohlich, M., Gomez, A. J., Gomez-Pelaez, A. J., Haszpra, L., Krummel, P., Langenfelds, R., Leuenberger, M., Machida, T., Maignan, F., Matsueda, H., Morgui, J. A., Mukai, H., Nakazawa, T., Peylin, P., Ramonet, M., Rivier, L., Sawa, Y., Schmidt, M., Steele, P., Vay, S. A., Vermeulen, A. T., Wofsy, S., and Worthy, D.: CO<sub>2</sub> surface fluxes at grid point scale estimated from a global 21-year reanalysis of atmospheric measurements, *J. Geophys. Res.*, 115, D21307, doi:10.1029/2010JD013887, 2010a.
- Chevallier, F., L. Feng, H. Bösch, P. I. Palmer, and P. J. Rayner: On the impact of transport model errors for the estimation of CO<sub>2</sub> surface fluxes from GOSAT observations, *Geophys. Res. Lett.*, 37, L21803, doi:10.1029/2010GL04465, 2010b.
- Chevallier, F., Palmer, P. I., Feng, L., Boesch, H., O'Dell, C. W., and Bousquet, P.: Toward robust and consistent regional CO<sub>2</sub> flux estimates from *in situ* and spaceborne measurements of atmospheric CO<sub>2</sub>, *Geophys. Res. Lett.*, 41, 1065–1070, doi:10.1002/2013GL058772, 2014.
- Chevallier, F.: On the statistical optimality of CO<sub>2</sub> atmospheric inversions assimilating CO<sub>2</sub> column retrievals, *Atmos. Chem. Phys.*, 15, 11133–11145, doi:10.5194/acp-15-11133-2015, 2015.
- Chevallier, F., P. Bergamaschi, D. Brunner, L. Feng, S. Houweling, T. Kaminski, W. Knorr, J. Marshall, P. I. Palmer, S. Pandey, M. Reuter, M. Scholze, and M. Voßbeck, *Climate Assessment Report for the GHG-CCI project of ESA's Climate Change Initiative*, pp. 96, version 4, 28 March 2017.
- Ciais, P., Rayner, P., Chevallier, F., Bousquet, P., Logan, M., Peylin, P., and Ramonet, M.: Atmospheric inversions for estimating CO<sub>2</sub> fluxes: methods and perspectives, *Climatic Change*, 103(1), 69–92, 2010.
- Ciais, P., Sabine, C., Bala, G., Bopp, L., Brovkin, V., Canadell, J., Chhabra, A., DeFries R., Galloway, J., Heimann, M., Jones, C., Le Quéré, C., Myneni, R.B., Piao, S. and Thornton, P.: Carbon and Other Biogeochemical Cycles. In: *Climate Change 2013: The Physical Science Basis. Contribution of Working Group I to the Fifth Assessment Report of the Intergovernmental Panel on Climate Change* [Stocker, T.F., D. Qin, G.-K. Plattner, M. Tignor, S.K. Allen, J. Boschung, A. Nauels, Y. Xia, V. Bex and P.M. Midgley (eds.)]. Cambridge University Press, Cambridge, United Kingdom and New York, NY, USA, 2013.
- Ciais, P., Dolman, A. J., Bombelli, A., Duren, R., Pregon, A., Rayner, P. J., Miller, C., Gobron, N., Kinderman, G., Marland, G., Gruber, N., Chevallier, F., Andres, R. J., Balsamo, G., Bopp, L., Bréon, F.-M., Broquet, G., Dargaville, R., Battin, T. J., Borges, A., Bovensmann, H., Buchwitz, M., Butler, J., Canadell, J. G., Cook, R. B., DeFries, R., Engelen, R., Gurney,

- K. R., Heinze, C., Heimann, M., Held, A., Henry, M., Law, B., Luyssaert, S., Miller, J., Moriyama, T., Moulin, C., Myneni, R. B., Nussli, C., Obersteiner, M., Ojima, D., Pan, Y., Paris, J.-D., Piao, S. L., Poulter, B., Plummer, S., Quegan, S., Raymond, P., Reichstein, M., Rivier, L., Sabine, C., Schimel, D., Tarasova, O., Valentini, R., Wang, R., van der Werf, G., Wickland, D., Williams, M., and Zehner, C.: Current systematic carbon-cycle observations and the need for implementing a policy-relevant carbon observing system, *Biogeosciences*, 11, 3547-3602, doi:10.5194/bg-11-3547-2014, 2014.
- Ciais, P., Crisp, D., Denier Van Der Gon, H., Engelen, R., Heimann, M., Janssens-Maenhout, G., Rayner, P. and Scholze, M.: Towards a European Operational Observing System to Monitor Fossil CO<sub>2</sub> emissions, European Commission – ISBN 978-92-79-53482-9, doi:10.2788/350433, 2015.
- Cich, M., Lunny, E. M., Bui, T. Q., Stroschio, G. D., Bray, C., Hogan, D., Rupsingha, P., Crawford, T. J., Long, D. A., Hodges, J. T., Drouin, B. J., Miller, C. E. and Okumura, M.: Photoacoustic spectroscopy to improve accuracy of ABSCO's oxygen A-band model. Presentation at OCO-2 Science Team Meeting, Boulder, CO, October 2017.
- Cogan, A. J., Boesch, H., Parker, R. J., Feng, L., Palmer, P. I., Blavier, J.-F. L., Deutscher, N. M., Macatangay, R., Notholt, J., Roehl, C., Warneke, T., Wunch, D., A. J. Cogan, H. Boesch, R. J. Parker, L. Feng, P. I. Palmer, J.-F. L. Blavier, N. M. Deutscher, R. Macatangay, J. Notholt, C. Roehl, T. Warneke, D. Wunch. Atmospheric carbon dioxide retrieved from the Greenhouse gases Observing SATellite (GOSAT): Comparison with ground-based TCCON observations and GEOS-Chem model calculations, *J. Geophys. Res.*, 117, doi:10.1029/2012JD018087, 2012.
- COM (2011) European Commission, Communication from the Commission to the European Parliament, the Council, the European Economic and Social Committee and the Committee of the Regions - A Roadmap for moving to a competitive low carbon economy in 2050, 112 final, <http://eur-lex.europa.eu/legal-content/EN/TXT/?uri=CELEX:52011DC0112>, 2011.
- Conley, S., Franco, G., Faloona, I., Blake, D.R., Peischl, J., and Ryerson, T.B.: Methane emissions from the 2015 Aliso Canyon blowout in Los Angeles, CA. *Science*, 351(6279), doi:10.1126/science.aaf2348, 2016.
- Connor, B. J., Bösch, H., Toon, G., Sen, B., Miller, C. E., and Crisp, D.: Orbiting carbon observatory: Inverse method and prospective error analysis, *J. Geophys. Res.*, 113, doi:10.1029/2006JD008336, 2008.
- Connor, B., Bösch, H., McDuffie, J., Taylor, T., Fu, D., Frankenberg, C., O'Dell, C. O., Payne, V. H., Gunson, G., Pollock, R., Hobbs, J., Oyafuso, F., and Jiang, Y.: Quantification of Uncertainties in OCO-2 Measurements of XCO<sub>2</sub>: Simulations and Linear Error Analysis, *Atmos. Meas. Tech.*, 9, 5227–5238, doi:10.5194/amt-9-5227-201, 2016.
- Corbin, K. D., A. S. Denning, and N. C. Parazoo: Assessing temporal clear-sky errors in assimilation of satellite CO<sub>2</sub> retrievals using a global transport model. *Atmos. Chem. Phys.*, 9, 3043–3048, doi:10.5194/acp-9-3043-2009, 2009.
- Cressot, C., Chevallier, F., Bousquet, P., Crevoisier, C., Dlugokencky, E. J., Fortems-Cheiney,

- A., Frankenberg, C., Parker, R., Pison, I., Scheepmaker, R. A., Montzka, S. A., Krummel, P. B., Steele, L. P., and Langenfelds, R. L.: On the consistency between global and regional methane emissions inferred from SCIAMACHY, TANSO-FTS, IASI and surface measurements, *Atmos. Chem. Phys.*, 14, 577-592, 2014, doi:10.5194/acp-14-577-2014.
- Crevoisier, C., Heilliette, S., Chédin, A., Serrar, S., Armante, R., and Scott, N. A.: Midtropospheric CO<sub>2</sub> concentration retrieval from AIRS observations in the tropics, *Geophys. Res. Lett.*, 31, L17106, doi:10.1029/2004GL020141, 2004.
- Crevoisier, C., Nobileau, D., Fiore, A. M., Armante, R., Chédin, A., and Scott, N. A.: Tropospheric methane in the tropics – first year from IASI hyperspectral infrared observations, *Atmos. Chem. Phys.*, 9, 6337–6350, doi:10.5194/acp-9-6337-2009, 2009a.
- Crevoisier C., Nobileau D., Fiore A., Armante R., Chédin A., and Scott N. A., Tropospheric methane in the tropics - first year from IASI hyperspectral infrared observations, *Atmos. Chem. Phys.*, 9, 6337-6350, 2009b.
- Crevoisier C., Clerbaux, C., Guidard, V., Phulpin, T., Armante, R., Barret, B., Camy-Peyret, C., Chaboureaud, J.-P., Coheur, P.-F., Crépeau, L., Dufour, G., Labonnote, L., Lavanant, L., Hadji-Lazaro, J., Herbin, H., Jacquinet-Husson, N., Payan, S., Péquignot, E., Pierangelo, C., Sellitto, P., and Stubenrauch, C.: Towards IASI-New Generation (IASI-NG): impact of improved spectral resolution and radiometric noise on the retrieval of thermodynamic, chemistry and climate variables, *Atmos. Meas. Tech.*, 7, 4367-4385, 2014.
- Crevoisier C.: Use of Hyperspectral Infrared Radiances to Infer Atmospheric Trace Gases. In S. Liang (Ed.), *Comprehensive Remote Sensing*, 7, 345–387. Oxford: Elsevier, 2018.
- Crisp, D., Atlas, R.M., Bréon, F.-B., Brown, L.R., Burrows, J.P., Ciais, P., Connor, B.J., Doney, S.C., Fung, I.Y., Jacob, D.J., Miller, C.E., O'Brien, D., Pawson, S., Randerson, J.T., Rayner, P., Salawitch, R.J., Sander, S.P., Sen, B., Stephens, G.L., Tans, P.P., Toon, G.C., Wennberg, P.O., Wofsy, S.C., Yung, Y.L., Kuang, Z., Chudasama, B., Sprague, G., Weiss, B., Pollock, R., Kenyon, D., Schroll, S.: The Orbiting Carbon Observatory (OCO) mission, *Advances in Space Research*, 34, 700–709, doi: 10.1016/j.asr.2003.08.062, 2004.
- Crisp, D., Miller, C.E., and DeCola, P.L.: NASA Orbiting Carbon Observatory: measuring the column averaged carbon dioxide mole fraction from space, *J. Appl. Remote Sens.*, 2, 023508; doi:10.1117/1.2898457, 2008.
- Crisp, D., Fisher, B. M., O'Dell, C., Frankenberg, C., Basilio, R., Bösch, H., Brown, L. R., Castano, R., Connor, B., Deutscher, N. M., Eldering, A., Griffith, D., Gunson, M., Kuze, A., Mandrake, L., McDuffie, J., Messerschmidt, J., Miller, C. E., Morino, I., Natraj, V., Notholt, J., O'Brien, D. M., Oyafuso, F., Polonsky, I., Robinson, J., Salawitch, R., Sherlock, V., Smyth, M., Suto, H., Taylor, T. E., Thompson, D. R., Wennberg, P. O., Wunch, D., and Yung, Y. L.: The ACOS CO<sub>2</sub> retrieval algorithm – Part II: Global XCO<sub>2</sub> data characterization, *Atmos. Meas. Tech.*, 5, 687–707, doi:10.5194/amt-5-687-2012, 2012.
- Crisp, D. for the OCO-2 Team: Measuring Atmospheric Carbon Dioxide from Space with the Orbiting Carbon Observatory-2 (OCO-2), *Proc. SPIE 9607, Earth Observing Systems XX*, 960702, doi: 10.1117/12.2187291, 2015.

- Crisp, D., Pollock, H. R., Rosenberg, R., Chapsky, L., Lee, R. A. M., Oyafuso, F. A., Frankenberg, C., O'Dell, C. W., Bruegge, C. J., Doran, G. B., Eldering, A., Fisher, B. M., Fu, D., Gunson, M. R., Mandrake, L., Osterman, G. B., Schwandner, F. M., Sun, K., Taylor, T. E., Wennberg, P. O., and Wunch, D.: The On-Orbit Performance of the Orbiting Carbon Observatory-2 (OCO-2) Instrument and its Radiometrically Calibrated Products, *Atmos. Meas. Tech.* 10, 59-81, doi:10.5194/amt-10-59-2017, 2017.
- DeCola, P. and Tarasova, O.: An Integrated Global Greenhouse Gas Information System (IG<sup>3</sup>IS). WMO Bulletin, 66, 38-45, 2017.
- Deeter M.N., J. Wang; J. C. Gille, P. L. Bailey: "Retrieval of tropospheric methane from MOPITT measurements: algorithm description and simulations", SPIE Proceedings, 3756, Optical Spectroscopic Techniques and Instrumentation for Atmospheric and Space Research III; <https://doi.org/10.1117/12.366401>, 1999.
- Delahaye, T., Maxwell, S. E., Reed, Z. D., Lin, H., Hodges, J. T., Sung, K., Devi, V. M., Warneke, T., Spietz, P. and Tran, H.: Precise methane absorption measurements in the 1.64 mm spectral region for the MERLIN mission. *J. Geophys. Res. Atmos.*, 121, 7360-7370, doi: 10.1002/2016JD025024, 2016.
- De Mazière, M., Vigouroux, C., Bernath, P. F., Baron, P., Blumenstock, T., Boone, C., Brogniez, C., Catoire, V., Coffey, M., Duchatelet, P., Griffith, D., Hannigan, J., Kasai, Y., Kramer, I., Jones, N., Mahieu, E., Manney, G. L., Piccolo, C., Randall, C., Robert, C., Senten, C., Strong, K., Taylor, J., Tétard, C., Walker, K. A., and Wood, S.: Validation of ACE-FTS v2.2 methane profiles from the upper troposphere to the lower mesosphere, *Atmos. Chem. Phys.*, 8, 2421-2435, doi:10.5194/acp-8-2421-2008, 2008.
- Deng, F., Jones, D. B. A., Walker, T. W., Keller, M., Bowman, K. W., Henze, D. K., Nassar, R., Kort, E. A., Wofsy, S. C., Walker, K. A., Bourassa, A. E., and Degenstein, D. A.: Sensitivity analysis of the potential impact of discrepancies in stratosphere-troposphere exchange on inferred sources and sinks of CO<sub>2</sub>, *Atmos. Chem. Phys.*, 15, 11773-11788, doi:10.5194/acp-15-11773-2015, 2015.
- Deng, F., Jones, D. B. A., O'Dell, C. W., Nassar, R., and Parazoo, N. C.: Combining GOSAT XCO<sub>2</sub> observations over land and ocean to improve regional CO<sub>2</sub> flux estimates. *J. Geophys. Res. Atmos.*, 121, 1896–1913, doi:10.1002/2015JD024157, 2016.
- Denning, A. S., Collatz, G. J., Zhang, C., Randall, D. A., Berry, J. A., Sellers, P. J., Colello, G. D., and Dazlich, D. A.: Simulations of terrestrial carbon metabolism and atmospheric CO<sub>2</sub> in a general circulation model. Part 2: simulated CO<sub>2</sub> concentrations, *Tellus*, 48B, 543-567, 1996.
- Detmers, R. G., O. Hasekamp, I. Aben, S. Houweling, T. T. van Leeuwen, A. Butz, J. Landgraf, P. Köhler, L. Guanter, and B. Poulter: Anomalous carbon uptake in Australia as seen by GOSAT, *Geophys. Res. Lett.*, 42, 8177–8184, doi:10.1002/2015GL065161, 2015.

- Devi, M., Benner, C., Sung, K., Brown, L., Miller, C. E., Payne, V., Drouin, B., Yu, S., Crawford, T. J., Mantz, A.W., Smith, M. A. H., Gamache, R. R.: Line parameters including temperature dependences of self- and air-broadened line shapes of (CO<sub>2</sub>)-C-12-O-16: 1.6- $\mu$ m region. *J. Quant. Spectrosc. Radiat. Transf.*, 17, 117-144, doi:10.1016/j.jqsrt.2015.12.020, 2016.
- Drouin, B., Benner, D.C., Brown, L., Cich, M. J., Crawford, T. J., Devi, M., Guillaume, A., Hodges, J., Mlawer, E. J., Robichaud, D. J., Oyafuso, F., Payne, V., Sung, K., Wishnow, E. H., Yu, S.: Multispectrum analysis of the Oxygen A-band, *J. Quant. Spectrosc. Radiat. Transf.*, 186, 118-136, doi:10.1016/j.jqsrt.2016.03.037, 2016.
- Drouin, B. J., Cich, M. J., Sung, K., Adkins, E., Hodges, J. T., Lunny, E. and Okumura, M.: Multispectrum analysis of the oxygen A-band. Proceedings of the 15<sup>th</sup> International HITRAN Conference, Cambridge, MA, June 2018.
- Drummond, J. R.: Measurements of Pollution in the Troposphere (MOPITT). The use of EOS for studies of atmospheric physics, edited by J. C. Gille and G. Visconti, 77–101, 1992.
- Edwards, D. P., Arellano, J., Avelino F., and Deeter, M. N.: A satellite observation system simulation experiment for carbon monoxide in the lowermost troposphere. *J. Geophys. Res.*, 114, D14304, doi:10.1029/2008JD011375, 2009.
- Ehret, G.; Bousquet, P.; Pierangelo, C.; Alpers, M.; Millet, B.; Abshire, J.B.; Bovensmann, H.; Burrows, J.P.; Chevallier, F.; Ciais, P.; Crevoisier, C.; Fix, A.; Flamant, P.; Frankenberg, C.; Gibert, F.; Heim, B.; Heimann, M.; Houweling, S.; Hubberten, H.W.; Jöckel, P.; Law, K.; Löw, A.; Marshall, J.; Agustí-Panareda, A.; Payan, S.; Prigent, C.; Rairoux, P.; Sachs, T.; Scholze, M.: MERLIN: A French-German Space Lidar Mission Dedicated to Atmospheric Methane, *Remote Sensing*, 9, 1052, doi:10.3390/rs9101052, 2017.
- Eldering, A., O'Dell, C. W., Wennberg, P. O., Crisp, D., Gunson, M. R., Viatte, C., Avis, C., Braverman, A., Castano, R., Chang, A., Chapsky, L., Cheng, C., Connor, B., Dang, L., Doran, G., Fisher, B., Frankenberg, C., Fu, D., Granat, R., Hobbs, J., Lee, R. A. M., Mandrake, L., McDuffie, J., Miller, C. E., Myers, V., Natraj, V., O'Brien, D., Osterman, G. B., Oyafuso, F., Payne, V. H., Pollock, H. R., Polonsky, I., Roehl, C. M., Rosenberg, R., Schwandner, F., Smyth, M., Tang, V., Taylor, T. E., To, C., Wunch, D., and Yoshimizu, J.: The Orbiting Carbon Observatory-2: first 18 months of science data products, *Atmos. Meas. Tech.*, 10, 549– 563, doi:10.5194/amt-10-549-2017, 2017.
- Emmert, J. T., Stevens, M. H., Bernath, P. F., Drob, D. P., and Boone, C. D.: Observations of increasing carbon dioxide concentration in Earth's thermosphere, *Nat. Geosci.*, 5, 868–871, doi:10.1038/ngeo1626, 2012.
- Enting, I. G.: *Inverse Problems in Atmospheric Constituent Transport*, Cambridge University Press, Cambridge, doi: 10.1017/CBO9780511535741, 2002.
- Errico, R. M., Privé, N. C., Carvalho, D., Sienkiewicz, M., Akkraoui, A. E., Guo, J., Todling, R., McCarty, W., Putman, W. M., da Silva, A., Gelaro, R., Moradi, I.: Description of the GMAO OSSE for Weather Analysis Software Package: Version 3. NASA/TM-2017-104606, 48, 156 pp. 2017. <https://gmao.gsfc.nasa.gov/pubs/docs/Errico987.pdf>

- ESA 2015, Report for Mission Selection: CarbonSat, ESA SP-1330/1 (2 volume series), European Space Agency, Noordwijk, The Netherlands, 2015, [https://esamultimedia.esa.int/docs/EarthObservation/SP1330-1\\_CarbonSat.pdf](https://esamultimedia.esa.int/docs/EarthObservation/SP1330-1_CarbonSat.pdf)
- Falge, E., M. Aubinet, P.S. Bakwin, D. Baldocchi, P. Berbigier, C. Bernhofer, T.A. Black, R. Ceulemans, K.J. Davis, A.J. Dolman, A. Goldstein, M.L. Goulden, A. Granier, D.Y. Hollinger, P.G. Jarvis, N. Jensen, K. Pilegaard, G. Katul, P. Kyaw Tha Paw, B.E. Law, A. Lindroth, D. Loustau, Y. Mahli, R. Monson, P. Moncrieff, E. Moors, J.W. Munger, T. Meyers, W. Oechel, E.-D. Schulze, H. Thorgeirsson, J. Tenhunen, R. Valentini, S.B. Verma, T. Vesala, and S.C. Wofsy: FLUXNET Research Network Site Characteristics, Investigators, and Bibliography, 2016. ORNL DAAC, Oak Ridge, Tennessee, USA, doi:10.3334/ORNLDAAC/1530, 2017
- Feng, L., Palmer, P. I., Bösch, H., and Dance, S.: Estimating surface CO<sub>2</sub> fluxes from space-borne CO<sub>2</sub> dry air mole fraction observations using an ensemble Kalman Filter, *Atmos. Chem. Phys.*, 9, 2619-2633, doi:10.5194/acp-9-2619-2009, 2009.
- Feng, L., Palmer, P. I., Parker, R. J., Deutscher, N. M., Feist, D. G., Kivi, R., Morino, I., and Sussmann, R.: Estimates of European uptake of CO<sub>2</sub> inferred from GOSAT X-CO<sub>2</sub> retrievals: sensitivity to measurement bias inside and outside Europe, *Atmospheric Chemistry And Physics*, 16, 1289-1302, doi:10.5194/acp-16-1289-2016, 2016.
- Filges, A., Gerbig, C., Chen, H., Franke, H., Klaus, C. and Jordan, A. The IAGOS-core greenhouse gas package: a measurement system for continuous airborne observations of CO<sub>2</sub>, CH<sub>4</sub>, H<sub>2</sub>O and CO, *Tellus B: Chemical and Physical Meteorology*, 67:1, 27989, doi:10.3402/tellusb.v67.27989, 2015.
- Foucher P.-Y., Chédin, A., Armante, R., Boone, C. D., Crevoisier, C., and Bernath, P., Carbon dioxide atmospheric vertical profiles retrieved from space observation using ACE-FTS solar occultation instrument. *Atmos. Chem. Phys.*, 11, 2455–2470, doi:10.5194/acp-11-2455-2011, 2011.
- Francis G. L., M. N. Deeter, S. Martinez-Alonso, J. C. Gille, D. P. Edwards, D. Mao, H. M. Worden, and D. Ziskin: MOPITT Algorithm Theoretical Basis Document (ATBD). Atmospheric Chemistry Observations and Modeling Laboratory, National Center for Atmospheric Research (NCAR), Boulder, June 2017.
- Frankenberg, C., Meirink, J. F., van Weele, M., Platt, U., and Wagner, T.: Assessing Methane Emissions from Global Space-Borne Observations, *Science*, 308, 1010–1014, doi:10.1126/science.1106644, 2005.
- Frankenberg, C., T. Warneke, A. Butz, L. R. Brown, F. Hase, P. Spietz, and I. Aben: Methane spectroscopy in the near infrared and its implication on atmospheric retrievals, *Atmos. Chem. Phys. Disc.*, 8, 10,021–10,055, 2008a.
- Frankenberg, C., P. Bergamaschi, A. Butz, S. Houweling, J. F. Meirink, J. Notholt, A. K. Petersen, H. Schrijver, T. Warneke, and I. Aben (2008), Tropical methane emissions: A revised view from SCIAMACHY onboard ENVISAT, *Geophys. Res. Lett.*, 35, L15811,

doi:10.1029/2008GL034300, 2008b.

Frankenberg, C., Butz, A., Toon, G.C., Disentangling chlorophyll fluorescence from atmospheric scattering effects in O<sub>2</sub> A-band spectra of reflected sun-light. *Geophys. Res. Lett.*, 38, L03801, doi:10.1029/2010GL045896, 2011a.

Frankenberg, C., Fisher, J.B., Worden, J., Badgley, G., Saatchi, S.S., Lee, J.-E., Toon, G.C., Butz, A., Jung, M., Kuze, A., Yokota, T., 2011b. New global observations of the terrestrial carbon cycle from GOSAT: patterns of plant fluorescence with gross primary productivity. *Geophys. Res. Lett.* 38, doi:10.1029/2011GL048738, 2011b.

Frankenberg, C., Pollock, R., Lee, R. A. M., Rosenberg, R., Blavier, J.-F., Crisp, D., O'Dell, C.W., Osterman, G. B., Roehl, C., Wennberg, P. O., and Wunch, D.: The Orbiting Carbon Observatory (OCO-2): spectrometer performance evaluation using pre-launch direct sun measurements, *Atmos. Meas. Tech.*, 7, 1–10. [www.atmos-meas-tech.net/7/1/2014/doi:10.5194/amt-7-1-2014](http://www.atmos-meas-tech.net/7/1/2014/doi:10.5194/amt-7-1-2014), 2014.

Frankenberg, C., Aben, I., Bergamaschi, P., Dlugokencky, E. J., van Hees, R., Houweling, S., van der Meer, P., Snel, R., and Tol, P., Global column-averaged methane mixing ratios from 2003 to 2009 as derived from SCIAMACHY: Trends and variability. *J. Geophys. Res.*, 116, D04302, doi:10.1029/2010JD014849, 2016a.

Frankenberg, C., S. S. Kulawik, S. Wofsy, F. Chevallier, B. Daube, E. A. Kort, C. O'Dell, E. T. Olsen, and G. Osterman, Using airborne HIAPER Pole-to-Pole Observations (HIPPO) to evaluate model and remote sensing estimates of atmospheric carbon dioxide. *Atmos. Chem. Phys.*, 16, 7867–7878, doi:10.5194/acp-16-7867-2016, 2016.

Frankenberg, C., Thorpe, A.K., Thompson, D.R., Hulley, G., Kort, E.A., Vance, N., Borchardt, J., Krings, T., Gerilowski, K., Sweeney, C., and Conley, S.: Airborne methane remote measurements reveal heavy-tail flux distribution in Four Corners region. *Proceedings of the National Academy of Sciences*, 113(35), 9734-9739, doi:10.1073/pnas.1605617113, 2016.

Fraser, A., Palmer, P. I., Feng, L., Boesch, H., Cogan, A., Parker, R., Dlugokencky, E. J., Fraser, P. J., Krummel, P. B., Langenfelds, R. L., O'Doherty, S., Prinn, R. G., Steele, L. P., van der Schoot, M., and Weiss, R. F.: Estimating regional methane surface fluxes: the relative importance of surface and GOSAT mole fraction measurements, *Atmos. Chem. Phys.*, 13, 5697–5713, doi:10.5194/acp-13-5697-2013, 2013.

Frey, M., Kumar, M., Hase, F., Kiel, M., Blumenstock, T., Harig, R., Surawicz, G., Deutscher, M., Shiomi, K., Franklin, J., Bösch, H., Chen, J., Grutter, M., Ohyama, H., Sun, Y., Butz, A., Mengistu, G., Ene, D., Wunch, D., Cao, Z., Garcia, O., Ramonet, M., Vogel, F., and Orphal, J.: Building the COllaborative Carbon Column Observing Network (COCCON): Long term stability and ensemble performance of the EM27/SUN Fourier transform spectrometer., *Atmos. Meas. Tech. Discuss.*, doi:10.5194/amt-2018-146, 2018.

Ganesan, A.L., Rigby, M., Lunt, M.F., Parker, R.J., Boesch, H., Goulding, N., Umezawa, T., Zahn, A., Chatterjee, A., Prinn, R.G., Tiwari, Y.K., van der Schoot, M., and Krummel, P.B. Atmospheric observations show accurate reporting and little growth in India's methane emissions, *Nature Communications*, 8, doi:10.1038/s41467-017-00994-7, 2017.

- Gatti, L. V., J. B. Miller, M. T. S. D'Amelio, A. Martinewski, L. S. Basso, M. E. Gloor, S. Wofsy, and P. Tans: Vertical profiles of CO<sub>2</sub> above eastern Amazonia suggest a net carbon flux to the atmosphere and balanced biosphere between 2000 and 2009, *Tellus, Ser. B*, 62(5), 581-594, 2010.
- Geddes, A., and Bösch, H.: Tropospheric aerosol profile information from high-resolution oxygen A-band measurements from space, *Atmos. Meas. Tech.*, 8, 859-874, doi:10.5194/amt-8-859-2015, 2015.
- GCOS, 2011: Systematic Observation Requirements for Satellite-based Products for Climate: Supplemental details to the satellite-based component of the Implementation Plan for the Global Observing System for Climate in Support of the UNFCCC (2010 Update)". GCOS-154, WMO, Geneva, December 2011.
- GCOS, 2016: The Global Observing System for Climate: Implementation Needs". GCOS-200, GOOS-214, WMO, Geneva, December 2016.
- Gloor, M., Fan, S.-M., Pacala, S., and Sarmiento J.: Optimal sampling of the atmosphere for purpose of inverse modeling: A model study. *Global Biogeochem. Cycles*, 14(1):407–428, doi: 10.1029/1999GB900052, 2000.
- Gloudemans, A. M. S., Schrijver, H., Kleipool, Q., van den Broek, M. M. P., Straume, A. G., Lichtenberg, G., van Hees, R. M., Aben, I., and Meirink, J. F.: The impact of SCIAMACHY near-infrared instrument calibration on CH<sub>4</sub> and CO total columns, *Atmos. Chem. Phys.*, 5, 2369-2383, doi:10.5194/acp-5-2369-2005, 2005.
- Gordon, I. E., Rothman, L. S., Hill, C., Kochanov, R. V., Tan, Y. et al.: The HITRAN2016 molecular spectroscopic database. *J. Quant. Spectrosc. Radiat. Transfer*, 203, 3-69, doi: 10.1016/j.jqsrt.2017.06.038, 2017.
- Gottwald, M., Bovensmann, H., Döhler, W., Herbst, E., Krieg, E., Kröger, H., Lichtenberg, G., Lützw-Wentzky, P., Mager, R., Nießen, T., Noël, S., and Wuttke, M. W.: SCIAMACHY operations support overview, in *Proc. ENVISAT Calibration Review*, ESTEC/Noordwijk, SP-520, 2002 (published on CD, ISBN 92-9092-830-1).
- Gottwald, M., Bovensmann, H. (eds.), SCIAMACHY - Exploring the Changing Earth's Atmosphere. Springer Heidelberg Dordrecht London New York, ISBN 978-90-481-9895-5, doi:10.1007/978-90-481-9896-2, 2011.
- Guanter, L., Frankenberg, C., Dudhia, A., Lewis, P.E., Gómez-Dans, J., Kuze, A., Suto, H., and Grainger, R. G.: Retrieval and global assessment of terrestrial chlorophyll fluorescence from GOSAT space measurements. *Remote Sens. Environ.* 121, 236–251. doi:10.1016/j.rse.2012.02.006, 2012.
- Guerlet, S., A. Butz, D. Schepers, S. Basu, O. P. Hasekamp, A. Kuze, T. Yokota, J.-F. Blavier, N. M. Deutscher, D. W. T. Griffith, F. Hase, E. Kyro, I. Morino, V. Sherlock, R. Sussmann, A. Galli, and I. Aben, Impact of aerosol and thin cirrus on retrieving and validating XCO<sub>2</sub>

from GOSAT shortwave infrared measurements. *J. Geophys. Res.*, 118, 10, 4887-4905, doi:10.1002/jgrd.50332, 2013.

Gurney, K. R., Law, R. M., Denning, A. S., Rayner, P. J., Baker, D., Bousquet, P., Bruhwiler, L., Chen, Y.-H., Ciais, P., Fan, S., Fung, I. Y., Gloor, M., Heimann, M., Higuchi, K., John, J., Maki, T., Maksyutov, S., Masarie, K., Peylin, P., Prather, M., Pak, B. C., Randerson, J., Sarmiento, J., Taguchi, S., Takahashi, T., and Yuen, C.-W.: Towards robust regional estimates of CO<sub>2</sub> sources and sinks using atmospheric transport models, *Nature*, 415, 626-630, 2002.

Hakkarainen, J., Ialongo, I., and Tamminen, J.: Direct space-based observations of anthropogenic CO<sub>2</sub> emission areas from OCO-2, *Geophysical Research Letters*, 43(21), 11400-11406, 2016.

Hakkarainen, J., Ialongo, I., Maksyutov, S., and Crisp, D.: Global XCO<sub>2</sub> anomalies as seen by Orbiting Carbon Observatory-2, *Atmos. Chem. Phys. Discuss.*, <https://doi.org/10.5194/acp-2018-649>, in review, 2018.

Harlander, J., Reynolds, R. J., and Roesler, F. L.: "Spatial heterodyne spectroscopy for the exploration of diffuse interstellar emission lines at far ultraviolet wavelengths," *Astrophys. J.* **396**, 730-740, 1992.

Harlander, J., Roesler, F.L., Cardon, J.G., Englert, C.R., and Conway, R.R.: Shimmer: a spatial heterodyne spectrometer for remote sensing of Earth' middle atmosphere, *Applied Optics*, 41, 1343-1352, 2002.

Hasekamp, O. P., and J. Landgraf, A linearized vector radiative transfer model for atmospheric trace gas retrieval, *J. Quant. Spectrosc. Radiat. Transfer*, 75, 221-238, doi:10.1016/S0022-4073(01)00247-3, 2002.

Hasekamp, O., Hu, H., Galli, A., Tol, P., Landgraf, J., and Butz, A.: Algorithm Theoretical Baseline Document for Sentinel-5 Precursor methane retrieval, Report, SRON Netherlands Institute for Space Research, available at: [http://www.tropomi.eu/sites/default/files/files/SRON-S5P-LEV2-RP-001\\_TROPOMI\\_ATBD\\_CH4\\_v1p0p0\\_20160205.pdf](http://www.tropomi.eu/sites/default/files/files/SRON-S5P-LEV2-RP-001_TROPOMI_ATBD_CH4_v1p0p0_20160205.pdf), 2016.

Hedelius, J. K., Feng, S., Roehl, C. M., Wunch, D., Hillyard, P. W., Podolski, J. R., Iraci, L. T., Patarasuk, R., Rao, P., O'Keefe, D., Gurney, K. R., Lauvaux, T., Wennberg, P. O.: Emissions and topographic effects on column CO<sub>2</sub> (XCO<sub>2</sub>) variations, with a focus on the Southern California Megacity, *J. Geophys. Res. Atmos.*, 122, 7200-7215, doi:10.1002/2017JD026455, 2017.

Heymann, J., Reuter, M., Hilker, M., Buchwitz, M., Schneising, O., Bovensmann, H., Burrows, J.P., Kuze, A., Suto, H., Deutscher, N.M., Dubey, M.K., Griffith, D.W.T., Hase, F., Kawakami, S., Kivi, R., Morino, I., Petri, C., Roehl, C., Schneider, M., Sherlock, V., Sussmann, R., Velasco, V.A., Warneke, T., and Wunch, D.: Consistent satellite XCO<sub>2</sub> retrievals from SCIAMACHY and GOSAT using the BESD algorithm, *Atmos. Meas. Tech.*, 8, 2961-2980, 2015.

- Heymann, J., Reuter, M., Buchwitz, M., Schneising, O., Bovensmann, H., Burrows J. P., Massart, S., Kaiser, J. W., Crisp, D., and O'Dell, C. W.: CO<sub>2</sub> emission of Indonesian fires in 2015 estimated from satellite-derived atmospheric CO<sub>2</sub> concentrations. *Geophys. Res. Lett.* 44, 1537–1544. doi: 10.1002/2016GL072042, 2017.
- Hilton, F., Atkinson, N. C., English S. J., and Eyre J. R.: Assimilation of IASI at the Met Office and assessment of its impact through observing system experiments. *Quarterly Journal of the Royal Meteorological Society*, 135(639):495–505, 2009.
- Houweling, S., Bréon, F.-M., Aben, I., Rodenbeck, C., Gloor, M., Heimann, M., and Ciais, P.: Inverse modeling of CO<sub>2</sub> sources and sinks using satellite data: a synthetic inter-comparison of measurement techniques and their performance as a function of space and time, *Atmos. Chem. Phys.*, 4, 523 – 538, 2004.
- Houweling, S., Baker, D., Basu, S., Boesch, H., Butz, A., Chevallier, F., Deng, F., Dlugokencky, E.J., Feng, L., Ganshin, A., Hasekamp, O., Jones, D., Maksyutov, S., Marshall, J., Oda, T., O'Dell, C.W., Oshchepkov, S., Palmer, P.I., Peylin, P., Pousl, Z., Reum, F., Takagi, H., Yoshida, Y., and Zhuravlev, R.: An intercomparison of inverse models for estimating sources and sinks of CO<sub>2</sub> using GOSAT measurements. *J. Geophys. Res. Atmos.*, 120, 5253–5266, doi:10.1002/2014JD022962, 2015.
- Houweling, S., Bergamaschi, P., Chevallier, F., Heimann, M., Kaminski, T., Krol, M., Michalak, A. M., and Patra, P.: Global inverse modeling of CH<sub>4</sub> sources and sinks: an overview of methods, *Atmos. Chem. Phys.*, 17, 235-256, <https://doi.org/10.5194/acp-17-235-2017>, 2017.
- Hu, H., Hasekamp, O., Butz, A., Galli, A., Landgraf, J., Aan de Brugh, J., Borsdorff, T., Scheepmaker, R., and Aben, I.: The operational methane retrieval algorithm for TROPOMI, *Atmos. Meas. Tech.*, 9, 5423-5440, doi:10.5194/amt-9-5423-2016, 2016.
- Hu, H., Landgraf, J., Detmers, R., Borsdorff, T., Aan de Brugh, J., Aben, I., Butz, and A., Hasekamp, O.: Toward global mapping of methane with TROPOMI: First results and intersatellite comparison to GOSAT. *Geophysical Research Letters*, 45, 3682–3689, doi:10.1002/2018GL077259, 2018.
- Huijnen, V., Wooster, M. J., Kaiser, J. W., Gaveau, D. L. A., Flemming, J., Parrington, M., Inness, A., Murdiyarso, D., Main, B., and van Weele, M.: Fire carbon emissions over maritime Southeast Asia in 2015 largest since 1997, *Nature Sci. Rep.*, 6, 26, 886, doi:10.1038/srep26886, 2016.
- Hungershofer, K., Bréon, F. M., Peylin, P., Chevallier, F., Rayner, P., Klonecki, A., Houweling, S., and Marshall, J.: Evaluation of various observing systems for the global monitoring of CO<sub>2</sub> surface fluxes. *Atmos. Chem. Phys.*, 10, 10503–10520, 11 2010.
- IEA: (International Energy Agency): CO<sub>2</sub> Emissions from fuel combustion 2017 Edition. ISBN PRINT 978-92-64-27818-9 / PDF 978-92-64-27819-6. See also [http://www.iea.org/bookshop/757-CO<sub>2</sub> Emissions from Fuel Combustion 2017](http://www.iea.org/bookshop/757-CO2_Emissions_from_Fuel_Combustion_2017)
- IPCC, 2013: Climate Change 2013: The Physical Science Basis. Contribution of Working Group

I to the Fifth Assessment Report of the Intergovernmental Panel on Climate Change [Stocker, T.F., D. Qin, G.-K. Plattner, M. Tignor, S.K. Allen, J. Boschung, A. Nauels, Y. Xia, V. Bex and P.M. Midgley (eds.)]. Cambridge University Press, Cambridge, United Kingdom and New York, NY, USA, 1535 pp.

Jacob, D.J., Turner, A.J., Maasakkers, J.D., Sheng, J., Sun, K., Liu, X., Chance, K., Aben, I., McKeever, J., and 30 Frankenberg, C.: Satellite observations of atmospheric methane and their value for quantifying methane emissions. *Atmos. Chem. Phys.*, 16, 14371-14396, doi:10.5194/acp-16-14371-2016, 2016.

Janardanan, R., Maksyutov, S., Oda, T., Saito, M., Kaiser, J. W., Ganshin, A., Stohl, A., Matsunaga, T., Yoshida, Y. and Yokota, T.: Comparing GOSAT observations of localized CO<sub>2</sub> enhancements by large emitters with inventory-based estimates, *Geophys. Res. Lett.*, 43(7), 3486–3493, doi:10.1002/2016GL067843, 2016.

Janardanan, R., Maksyutov, S., Ito, A., Yoshita, Y., and Matsunaga, T.: Assessment of Anthropogenic Methane Emissions over Large Regions Based on GOSAT Observations and High Resolution Transport Modeling, *Remote Sensing*, 9(9), 941, doi:10.3390/rs9090941, 2017.

Janssens-Maenhout, G., M. Crippa, D. Guizzardi, M. Muntean, E. Schaaf, F. Dentener, P. Bergamaschi, V. Pagliari, J. G. J. Olivier, J. A. H. W. Peters, J. A. van Aardenne, S. Monni, U. Doering, and A. M. R. Petrescu, EDGAR v4.3.2 Global Atlas of the three major Greenhouse Gas Emissions for the period 1970–2012, *Earth Syst. Sci. Data Discuss.*, doi:10.5194/essd-2017-79, 2017.

Joiner, J., Yoshida, Y., Vasilkov, A. P., Yoshida, Y., Corp, L. A., and Middleton, E. M.: First observations of global and seasonal terrestrial chlorophyll fluorescence from space, *Biogeosciences*, 8, 637-651, doi:10.5194/bg-8-637-2011, 2011.

Joiner, J., Yoshida, Y., Vasilkov, A.P., Middleton, E.M., Campbell, P.K.E., Kuze, A., Corp, L.A.: Filling-in of near-infrared solar lines by terrestrial fluorescence and other geophysical effects: Simulations and space-based observations from SCIAMACHY and GOSAT. *Atmos. Meas. Tech.* 5, 809–829, doi:10.5194/amt-5-809-2012, 2012.

Jones, D. B. A., Bowman, K. W., Palmer, P. I., Worden, J. R., Jacob, D. J., Hoffman, R. N., Bey I., and Yantosca R. M.: Potential of observations from the Tropospheric Emission Spectrometer to constrain continental sources of carbon monoxide. *J. Geophys. Res. Atmos.*, 108(D24):4789, doi:10.1029/2003JD003702, 2003.

Jung, Y., Kim, J., Kim, W., Boesch, H., Lee, H., Cho, C., Goo, T.-Y.: Impact of Aerosol Property on the Accuracy of a CO<sub>2</sub> Retrieval Algorithm from Satellite Remote Sensing. *Remote Sens.*, 8, 322, doi:10.3390/rs8040322, 2016.

Kalnay, E.: *Atmospheric Modeling, Data Assimilation, and Predictability*. Cambridge University Press, 2003.

Karion, A., Sweeney, C., Tans, P. P., and Newberger, T.: AirCore: An Innovative Atmospheric Sampling System, *Journal of Atmospheric and Oceanic Technology*, 27, 1839–1853,

doi:10.1175/2010JTECHA1448.1, 2010.

- Karion, A., Sweeney, C., Petron, G., Frost, G., Hardesty, R. M., Kofler, J., Miller, B. R., Newberger, T., Wolter, S., Banta, R., Brewer, A., Dlugokencky, E., Lang, P., Montzka, S.A., Schnell, R., Tans, P., Trainer, M., Zamora, R., and Conley, S. Methane emissions estimate from airborne measurements over a western United States natural gas field, *Geophysical Research Letters*, 40, 4393–4397, doi:10.1002/grl.50811, 2013.
- Kataoka, F., Crisp, D., Taylor, T.E., O'Dell, C.W., Kuze, A., Shiomi, K., Suto, H., Bruegge, C., Schwandner, F., Rosenberg, R., Chapsky, L., and Lee, R.A.M.: The Cross-Calibration of Spectral Radiances and Cross-Validation of CO<sub>2</sub> Estimates from GOSAT and OCO-2. *Remote Sens.* 9, 1158, doi:10.3390/rs9111158, 2017.
- Keppel-Aleks, G., Wennberg, P. O., Washenfelder, R. A., Wunch, D., Schneider, T., Toon, G. C., Andres, R. J., Blavier, J. F., Connor, B., Davis, K. J., Desai, A. R., Messerschmidt, J., Notholt, J., Roehl, C. M., Sherlock, V., Stephens, B. B., Vay, S. A. and Wofsy, S. C.: The imprint of surface fluxes and transport on variations in total column carbon dioxide, *Biogeosciences*, 9(3), 875–891, doi:10.5194/bg-9-875-2012, 2012.
- Keppel-Aleks, G., Wennberg, P. O. and Schneider, T.: Sources of variations in total column carbon dioxide, *Atmospheric Chemistry and Physics*, 11(8), 3581–3593, doi:10.5194/acp-11-3581-2011, 2011.
- Keppel-Aleks, G., Wennberg, P. O., Washenfelder, R. A., Wunch, D., Schneider, T., Toon, G. C., Andres, R. J., Blavier, J. F., Connor, B., Davis, K. J., Desai, A. R., Messerschmidt, J., Notholt, J., Roehl, C. M., Sherlock, V., Stephens, B. B., Vay, S. A. and Wofsy, S. C.: The imprint of surface fluxes and transport on variations in total column carbon dioxide, *Biogeosciences*, 9(3), 875–891, doi:10.5194/bg-9-875-2012, 2012.
- Kim, W., J. Kim, Y. Jung, H. Boesch, H. Lee, S. Lee, T.-Y. Goo, U. Jeong, M. Kim, C.-H. Cho and M.-L. Ou, Retrieving XCO<sub>2</sub> from GOSAT FTS over East Asia Using Simultaneous Aerosol Information from CAI, *Remote Sens.*, 8, 994, doi:10.3390/rs8120994, 2016.
- Kondo, M., Ichii, K., Takagi, H., and Sasakawa, M., Comparison of the data-driven top-down and bottom-up global terrestrial CO<sub>2</sub> exchanges: GOSAT CO<sub>2</sub> inversion and empirical eddy flux upscaling, *J. Geophys. Res. Biogeo.* 120, 1226-1245, 2015.
- Kort, E. A., Frankenberg, C., Costigan, K. R., Lindenmaier, R., Dubey, M. K., and Wunch, D.: Four corners: The largest US methane anomaly viewed from space, *Geophys. Res. Lett.*, 41, doi:10.1002/2014GL061503, 2014.
- Krings, T., Gerilowski, K., Buchwitz, M., Reuter, M., Tretner, A., Erzinger, J., Heinze, D., Pflüger, U., Burrows, J.P., and Bovensmann, H.: MAMAP-a new spectrometer system for column-averaged methane and carbon dioxide observations from aircraft: retrieval algorithm and first inversions for point source emission rates. *Atmospheric Measurement Techniques*, 4(9), 1735-1758, doi:10.5194/amt-4-1735-2011, 2011.
- Krings, T., Gerilowski, K., Buchwitz, M., Hartmann, J., Sachs, T., Erzinger, J., Burrows, J.P., and Bovensmann, H.: Quantification of methane emission rates from coal mine ventilation

shafts using airborne remote sensing data. *Atmospheric Measurement Techniques*, 6(1), 151-166, doi:10.5194/amt-6-151-2013, 2013.

Kuai, L., Worden, J., Kulawik, S., Bowman, K., Lee, M., Biraud, S. C., Abshire, J. B., Wofsy, S. C., Natraj, V., Frankenberg, C., Wunch, D., Connor, B., Miller, C., Roehl, C., Shia, R. L., and Yung, Y., “Profiling tropospheric CO<sub>2</sub> using Aura TES and TCCON instruments,” *Atmos. Meas. Tech.*, 6, 63–79, 01 2013.

Kuhlmann, G., J. Marshall, V. Clément, and D. Brunner, Study on use of satellite measurements of auxiliary reactive trace gases for fossil fuel carbon dioxide emission estimation deliverable 3: Description of model setup and simulated satellite observations, Version 1.0., ESA Project SMARTCARB, 2018. <https://www.empa.ch/web/s503/smartcarb>

Kulawik, S. S., Jones, D. B. A., Nassar, R., Irion, F. W., Worden, J. R., Bowman, K. W., Machida, T., Matsueda, H., Sawa, Y., Biraud, S. C., Fischer, M. L., and Jacobson, A. R.: Characterization of Tropospheric Emission Spectrometer (TES) CO<sub>2</sub> for carbon cycle science. *Atmos. Chem. Phys.*, 10, 5601–5623, 2010.

Kulawik, S. S., O'Dell, C., Payne, V. H., Kuai, L., Worden, H. M., Biraud, S. C., Sweeney, C., Stephens, B., Iraci, L. T., Yates, E. L., and Tanaka, T.: Lower-tropospheric CO<sub>2</sub> from near-infrared ACOS-GOSAT observations, *Atmos. Chem. Phys.*, 17, 5407-5438, <https://doi.org/10.5194/acp-17-5407-2017>, 2017. Lauvaux, T. and Davis, K. J.: Planetary boundary layer errors in mesoscale inversions of column-integrated CO<sub>2</sub> measurements, *J. Geophys. Res.-Atmos.*, 119, 490-508, doi:10.1002/2013jd020175, 2014.

Kulawik, S., Wunch, D., O'Dell, C., Frankenberg, C., Reuter, M., Oda, T., Chevallier, F., Sherlock, V., Buchwitz, M., Osterman, G., Miller, C. E., Wennberg, P. O., Griffith, D., Morino, I., Dubey, M. K., Deutscher, N. M., Notholt, J., Hase, F., Warneke, T., Sussmann, R., Robinson, J., Strong, K., Schneider, M., De Mazière, M., Shiomi, K., Feist, D. G., Iraci, L. T., and Wolf, J.: Consistent evaluation of ACOS-GOSAT, BESD-SCIAMACHY, CarbonTracker, and MACC through comparisons to TCCON, *Atmos. Meas. Tech.*, 9, 683-709, doi:10.5194/amt-9-683-2016, 2016.

Kulawik, S. S., O'Dell, C., Payne, V. H., Kuai, L., Worden, H. M., Biraud, S. C., Sweeney, C., Stephens, B., Iraci, L. T., Yates, E. L., and Tanaka, T.: Lower-tropospheric CO<sub>2</sub> from near-infrared ACOS-GOSAT observations, *Atmos. Chem. Phys.*, 17, 5407-5438, <https://doi.org/10.5194/acp-17-5407-2017>, 2017.

Kuze, A., Suto, H., Shiomi, K., Nakajima, M., and Hamazaki, T.: On-orbit performance and level 1 data processing of TANSO-FTS and CAI on GOSAT, *Sensors, Systems, and Next-Generation Satellites XIII*, edited by Roland Meynart, Steven P. Neeck, Haruhisa Shimoda, Proc. of SPIE, 7474, 74740I, doi:10.1117/12.830152, 2009b.

Kuze, A., O'Brien, D. M., Taylor, T. E., Day, J. O., O'Dell, C. W., Kataoka, F., Yoshida, M., Mitomi, Y., Bruegge, C. J., Pollock, H., Basilio, R., Helmlinger, M., Matsunaga, T., Kawakami, S., Shiomi, K., Urabe, T., and Suto, H.: Vicarious calibration of the GOSAT sensors using the Railroad Valley desert playa, *IEEE Trans. Geosci. Remote Sens.* 49, 1781-1795, doi:10.1109/TGRS.2010.2089527, 2011.

- Kuze, A., Suto, H., Shiomi, K., Urabe, T., Nakajima, M., Yoshida, J., Kawashima, T., Yamamoto, Y., Kataoka, F., and Buijs, H.: Level 1 algorithms for TANSO on GOSAT: processing and on-orbit calibrations, *Atmos. Meas. Tech.*, 5, 2447–2467, doi:10.5194/amt-5-2447-2012, 2012.
- Kuze, A., T. E. Taylor, F. Kataoka, C. J. Bruegge, D. Crisp, M. Harada, M. Helmlinger, M. Inoue, S. Kawakami, N. Kikuchi, Y. Mitomi, J. Murooka, M. Naitoh, D. M. O'Brien, C. W. O'Dell, H. Ohyama, H. Pollock, F. M. Schwandner, K. Shiomi, H. Suto, T. Takeda, T. Tanaka, T. Urabe, T. Yokota, and Y. Yoshida, Long-Term Vicarious Calibration of GOSAT Short-Wave Sensors: Techniques for Error Reduction and New Estimates of Radiometric Degradation Factors, *IEEE Transactions On Geoscience and Remote Sensing*, 52, 3991–4004, doi:10.1109/TGRS.2013.2278696, 2014.
- Laeng, A., Plieninger, J., von Clarmann, T., Grabowski, U., Stiller, G., Eckert, E., Glatthor, G., Haenel, F., Kellmann, S., Kiefer, M., Linden, A., Lossow, S., Deaver, L., Engel, A., Hervig, M., Levin, I., McHugh, M., Noël, S., Toon, G., Walker, K.: Validation of MIPAS IMK/IAA methane profiles, *Atmos. Meas. Tech.*, 8, 5251–5261, 2015.
- Lamouroux, J., Regalia, L., Thomas, X., Vander Auwera, J., Gamache, R. R. and Hartmann, J-M.: CO<sub>2</sub> line-mixing database and software update and its tests in the 2.1 and 4.3  $\mu\text{m}$  regions. *J. Quant. Spectrosc. Radiat. Transfer*, 151, p88–96, doi:10.1016/j.jqsrt.2014.09.017, 2015.
- Landgraf, J., aan de Brugh, J., Scheepmaker, R., Borsdorff, T., Hu, H., Houweling, S., Butz, A., Aben, I., and Hasekamp, O.: Carbon monoxide total column retrievals from TROPOMI shortwave infrared measurements, *Atmos. Meas. Tech.*, 9, 4955–4975, doi:10.5194/amt-9-4955-2016, 2016.
- Lauvaux, T., O. Pannekoucke, C. Sarrat, F. Chevallier, P. Ciais, J. Noilhan, and P. J. Rayner. Structure of the transport uncertainty in meso-scale inversions of CO<sub>2</sub> sources and sinks using ensemble model simulations, *Biogeosciences*, 5, 4813–4846, 2009.
- Law, R. M., Rayner, P. J., Steele, L. P., and Enting, I. G.: Data and modelling requirements for CO<sub>2</sub> inversions using high-frequency data. *Tellus B*, 55(2):512–521, 2003.
- L'Ecuyer, T. S. and Jiang, J. H.: Touring the atmosphere aboard the A-Train, *Physics Today*, 63(7), doi:10.1063/1.3463626, 2010.
- Le Quéré, C., Andrew, R. M., Friedlingstein, P., Sitch, S., Pongratz, J., Manning, A. C., Korsbakken, J. I., Peters, G. P., Canadell, J. G., Jackson, R. B., Boden, T. A., Tans, P. P., Andrews, O. D., Arora, V. K., Bakker, D. C. E., Barbero, L., Becker, M., Betts, R. A., Bopp, L., Chevallier, F., Chini, L. P., Ciais, P., Cosca, C. E., Cross, J., Currie, K., Gasser, T., Harris, I., Hauck, J., Haverd, V., Houghton, R. A., Hunt, C. W., Hurtt, G., Ilyina, T., Jain, A. K., Kato, E., Kautz, M., Keeling, R. F., Klein Goldewijk, K., Körtzinger, A., Landschützer, P., Lefèvre, N., Lenton, A., Lienert, S., Lima, I., Lombardozi, D., Metzl, N., Millero, F., Monteiro, P. M. S., Munro, D. R., Nabel, J. E. M. S., Nakaoka, S.-I., Nojiri, Y., Padin, X. A., Peregón, A., Pfeil, B., Pierrot, D., Poulter, B., Rehder, G., Reimer, J., Rödenbeck, C., Schwinger, J., Séférian, R., Skjelvan, I., Stocker, B. D., Tian, H., Tilbrook, B., Tubiello, F.

- N., van der Laan-Luijkx, I. T., van der Werf, G. R., van Heuven, S., Viovy, N., Vuichard, N., Walker, A. P., Watson, A. J., Wiltshire, A. J., Zaehle, S., and Zhu, D.: Global Carbon Budget 2017, *Earth Syst. Sci. Data*, 10, 405-448, doi:10.5194/essd-10-405-2018, 2018.
- Li, Z., Lin, C., Li, C., Wang, L., Ji, Z., Xue, H., Wei, Y., Gong, C., Gao, M., Liu, L., Gao, Z., Zheng, Y., Prelaunch spectral calibration of a carbon dioxide spectrometer, *Meas. Sci. Technol.* 28065801, doi.org/10.1088/1361-6501/aa6507, 2017.
- Lichtenberg, G., Kleipool, Q., Krijger, J. M., van Soest, G., van Hees, R., Tilstra, L. G., Acarreta, J. R., Aben, I., Ahlers, B., Bovensmann, H., Chance, K., Gloudemans, A. M. S., Hoogeveen, R. W. M., Jongma, R. T. N., Noël, S., Pipers, A., Schrijver, H., Schrijvers, C., Sioris, C. E., Skupin, J., Slijkhuis, S., Stammes, P., and Wuttke, M.: SCIAMACHY Level 1 data: Calibration concept and in-flight calibration, *Atmos. Chem. Phys.*, 6, 5347-5367, 2006.
- Lindqvist, H., O'Dell, C.W., Basu, S., Boesch, H., Chevallier, F., Deutscher, N., Feng, L., Fisher, B., Hase, F., Inoue, M., Kivi, R., Morino, I., Palmer, P.I., Parker, R., Schneider, M., Sussmann, R., Yoshida, Y.: Does GOSAT capture the true seasonal cycle of CO<sub>2</sub>?, *Atmos. Chem. Phys.*, 15, 13023-13040, doi:10.5194/acp-15-13023-2015, 2015.
- Liu, J., I. Fung, E. Kalnay, and J.-S. Kang: CO<sub>2</sub> transport uncertainties from the uncertainties in meteorological fields, *Geophys. Res. Lett.*, 38, L12808, doi:10.1029/2011GL047213, 2011.
- Liu, J., Bowman, K. W., Lee, M., Henze, D. K., Bousseres, N., Brix, H., Collatz, G. J., Menemenlis, D., Ott, L., Pawson, S., Jones, D. and Nassar, R.: Carbon monitoring system flux estimation and attribution: impact of ACOS-GOSAT XCO<sub>2</sub> sampling on the inference of terrestrial biospheric sources and sinks. *Tellus B*, 66, 1600-0889, doi:10.3402/tellusb.v66.22486, 2014.
- Liu, J., Bowman, K.W., and Henze, D.K.: Source-receptor relationships of column-average CO<sub>2</sub> and implications for the impact of observations on flux inversions, *J. Geophys. Res. Atmos.*, 120, 5214-5236, 2015.
- Liu, J., and Bowman, K.: A method for independent validation of surface fluxes from atmospheric inversion: Application to CO<sub>2</sub>, *Geophys. Res. Lett.*, 43, 3502-3508, doi: 10.1002/2016GL067828, 2016.
- Liu, J., K. Bowman, D. Schimel, N. Parazoo, Z. Jiang, M. Lee, A. Bloom, D. Wunch, K. Gurney, D. Menemenlis, M. Gierach, D. Crisp, and A. Eldering: Contrasting carbon cycle responses of the tropical continents to the 2015-2016 El Niño. *Science* 358, eaam5690, doi:10.1126/science.aam5690, 2017.
- Locatelli, R., Bousquet, P., Saunois, M., Chevallier, F., and Cressot, C.: Sensitivity of the recent methane budget to LMDz subgrid-scale physical parameterizations, *Atmos. Chem. Phys.*, 15, 9765-9780, doi:10.5194/acp-15-9765-2015, 2015.
- Long, D. A., Bielska, K., Lisak, D., Havey, D. K., Okumura, M., Miller, C. E., and Hodges, J. T.: The air-broadened, near-infrared CO<sub>2</sub> line shape in the spectrally isolated regime: Evidence of simultaneous Dicke narrowing and speed dependence, *J. Chem. Phys.*, 135, 064308, doi:10.1063/1.3624527, 2011.

- Long, D. A., Robichaud, D.J., and Hodges, J.T., Frequency-stabilized cavity ring-down spectroscopy measurements of line mixing and collision-induced absorption in the O<sub>2</sub> A-band, *J. Chem. Phys.*, 137, 014307, doi:10.1063/1.4731290, 2012.
- Long, D. A., and Hodges, J.T. On spectroscopic models of the O<sub>2</sub> A-band and their impact upon atmospheric retrievals, *J. Geophys. Res.*, 117, D12309, doi:10.1029/2012JD017807, 2012.
- Lu, F., Recent Development and plans in CMA, Expert Team on Satellite Systems (ET-SAT) 11th SESSION, 4-6 April 2017, WMO Headquarters, Geneva, Switzerland, 2017.  
<http://www.wmo.int/pages/prog/sat/meetings/ET-SAT-11/ET-SAT-11.html> (last accessed 7 Jan 2018).
- Lunt, M., Rigby, M., Ganesan, A., and Manning, A.: Estimation of trace gas fluxes with objectively determined basis functions using reversible-jump Markov chain Monte Carlo, *Geoscientific Model Development*, 9, 10.5194/gmd-9-3213-2016, 2016.
- Machida, T., Matsueda, H., Sawa, Y., Nakagawa, Y., Hirokuni, K., Kondo, N., Goto, K., Nakazawa, T., Ishikawa, K., and Ogawa, T.: Worldwide measurements of atmospheric CO<sub>2</sub> and other trace gas species using commercial airlines, *J. Atmos. Ocean. Tech.*, 25, 1744–1754, 2008.
- Maksyutov, S., Takagi, H., Valsala, V. K., Saito, M., Oda, T., Saeki, T., Belikov, D. A., Saito, R., Ito, A., Yoshida, Y., Morino, I., Uchino, O., Andres, R. J., and Yokota, T.: Regional CO<sub>2</sub> flux estimates for 2009-2010 based on GOSAT and ground-based CO<sub>2</sub> observations, *Atmospheric Chemistry and Physics*, 13, 9351-9373, 10.5194/acp-13-9351-2013, 2013.
- Mandrake, L., Frankenberg, C., O'Dell, C. W., Osterman, G., Wennberg, P., and Wunch, D.: Semi -autonomous sounding selection for OCO-2, *Atmos. Meas. Tech.*, 6, 2851-2864, doi:10.5194/amt-6-2851-2013, 2013.
- Masarie, K. A., Peters, W., Jacobson, A. R., and Tans, P. P.: ObsPack: a framework for the preparation, delivery, and attribution of atmospheric greenhouse gas measurements, *Earth Syst. Sci. Data*, 6, 375-384, doi:10.5194/essd-6-375-2014, 2014.
- Massart, S. Agusti-Panareda A., Aben I., Butz A., Chevallier F., Crevoisier C., Engelen R., Frankenberg C., and Hasekamp O., Assimilation of atmospheric methane products in the MACC-II system: from SCIAMACHY to TANSO and IASI, *Atmos. Chem. Phys.*, 14, 6139-6158 doi:10.5194/acp-14-6139-2014, 2014.
- Massie, S., Schmidt, K. S., Eldering, A., and Crisp, D.: Observational Evidence of 3D Cloud Effects in OCO-2 CO<sub>2</sub> Retrievals. *J. Geophys. Res. Atmos.*, 122, 7064–7085, doi:10.1002/2016JD026111, 2017.
- Masutani, M., Woollen, J. S., Lord, S. J., Emmitt, G. D., Kleespies, T. J., S. Wood, A., Greco, S., Sun, Terry, H., J., Kapoor, V., Treadon, R., and Campana, K. A.: Observing system simulation experiments at the National Centers for Environmental Prediction. *J. Geophys. Res.*, 115: D07101, doi:10.1029/2009JD012528, 2010.

- Matsueda, H., T. Machida, Y. Sawa, Y. Niwa: Long-term change of CO<sub>2</sub> latitudinal distribution in the upper troposphere, *Geophys. Res. Lett.*, 42, doi:10.1002/2014GL062768, 2015.
- Meirink, J. F., Bergamaschi, P., and Krol, M. C.: Four-dimensional variational data assimilation for inverse modelling of atmospheric methane emissions: method and comparison with synthesis inversion, *Atmos. Chem. Phys.*, 8, 6341-6353, doi:10.5194/acp-8-6341-2008, 2008.
- Merrelli, A. J., Bennartz, R., and O'Dell, C.; Evaluating XCO<sub>2</sub> Retrievals from OCO-2 with CALIOP-Derived Aerosol Priors. American Geophysical Union Fall Meeting, 2017.
- Michalak, A. M., Bruhwiler, L., and Tans, P. P.: A geostatistical approach to surface flux estimation of atmospheric trace gases, *J. Geophys. Res. Atmos.*, 109, 10.1029/2003JD004422, 2004.
- Michalak, A. M., A. Hirsch, L. Bruhwiler, K. R. Gurney, W. Peters, and P. P. Tans, Maximum likelihood estimation of covariance parameters for Bayesian atmospheric trace gas surface flux inversions, *J. Geophys. Res.*, 110, D24107, doi: 10.1029/2005JD005970, 2005.
- Miles, N.L., S.J. Richardson, K.J. Davis, A.E. Andrews, T.J. Griffis, V. Bandaru, and K.P. Hosman: NACP MCI: Tower Atmospheric CO<sub>2</sub> Concentrations, Upper Midwest Region, USA, 2007-2009. ORNL DAAC, Oak Ridge, Tennessee, USA. doi:10.3334/ORNLDAAC/1202. 2013.
- Miller, C. E., Crisp, D., DeCola, P. L., Olsen, S.C., Randerson, J. T., Michalak, A. M., Alkhaled, A., Rayner, P., Jacob, D. J., Suntharalingam, P., Jones, D. B. A., Denning, A. S., Nicholls, M. E., Doney, S. C., Pawson, S., Boesch, H., Connor, B. J., Fung, I. Y., O'Brien, D., Salawitch, R. J., Sander, S. P., Sen, B., Tans, P. P., Toon, G. C., Wennberg, P. O., Wofsy, S. C., Yung, Y. L., Law, R. M.: Precision requirements for space-based XCO<sub>2</sub> data. *J. Geophys. Res.*, 112, D10314, doi:10.1029/2006JD007659, 2007.
- Myhre, G., D. Shindell, F.-M. Bréon, W. Collins, J. Fuglestedt, J. Huang, D. Koch, J.-F. Lamarque, D. Lee, B. Mendoza, T. Nakajima, A. Robock, G. Stephens, T. Takemura and H. Zhang: Anthropogenic and Natural Radiative Forcing. In: *Climate Change 2013: The Physical Science Basis. Contribution of Working Group I to the Fifth Assessment Report of the Intergovernmental Panel on Climate Change* [Stocker, T.F., D. Qin, G.-K. Plattner, M. Tignor, S.K. Allen, J. Boschung, A. Nauels, Y. Xia, V. Bex and P.M. Midgley (eds.)]. Cambridge University Press, Cambridge, United Kingdom and New York, NY, USA, 2013.
- Nassar, R., Jones, D. B. A., Kulawik, S. S., Worden, J. R., Bowman, K. W., Andres, R. J., Suntharalingam, P., Chen, J. M., Brenninkmeijer, C. A. M., Schuck, T. J., Conway, T. J., and Worthy, D. E.: Inverse modeling of CO<sub>2</sub> sources and sinks using satellite observations of CO<sub>2</sub> from TES and surface flask measurements, *Atmospheric Chemistry and Physics*, 11, 6029-6047, 2011.
- Nassar, R., Napier-Linton, L., Gurney, K. R., Andres, R. J., Oda, T., Vogel, F. R., and Deng, F.: Improving the temporal and spatial distribution of CO<sub>2</sub> emissions from global fossil fuel emission data sets, *J. Geophys. Res. Atmos.*, 118, 917-933, doi:10.1029/2012JD018196, 2013.

- Nassar, R., C.E. Sioris, D.B.A. Jones, J.C. McConnell. Satellite observations of CO<sub>2</sub> from a Highly Elliptical Orbit (HEO) for studies of the Arctic and boreal carbon cycle, *J. Geophys. Res. Atmos.*, 119, 2654-2673, doi:10.1002/2013JD020337, 2014.
- Nassar, R., T. G. Hill, C. A. McLinden, D. Wunch, D. B.A. Jones, and D. Crisp: Quantifying CO<sub>2</sub> emissions from individual power plants from space. *Geophys. Res. Lett.*, 44, doi:10.1002/2017GL074702, 2017.
- Natraj, V., & Spurr, R. J. D.: A fast linearized pseudo-spherical two orders of scattering model to account for polarization in vertically inhomogeneous scattering-absorbing media. *Journal of Quantitative Spectroscopy and Radiative Transfer*, 107(2), 263–293, doi:10.1016/j.jqsrt.2007.02.011, 2007.
- Nikitin, A.-V., Lyulin, O.-M., Mikhailenko, S.-N., Perevalov, V.-I., Filippov, N.-N., Grigoriev, I.-M., Morino, I., Yoshida, Y., and Matsunaga, T.: GOSAT-2014 methane spectral line list, *J. Quant. Spectrosc. Radiat. Transfer*, 154, 63-71, 2015.
- Noël, S., Bovensmann, H., Skupin, J., Wuttke, M.W, Burrows, J.P., Gottwald, M., and Krieg, E.: The SCIAMACHY calibration/monitoring concept and first results. *Adv. Space Res.*, 32, 2123-2128, 2003.
- Noël, S., Bramstedt, K., Hilker, M., Liebing, P., Plieninger, J., Reuter, M., Rozanov, A., Sioris, C. E., Bovensmann, H., Burrows, J.: Stratospheric CH<sub>4</sub> and CO<sub>2</sub> profiles derived from SCIAMACHY solar occultation measurements, *Atmos. Meas. Tech.*, 9, 1485–1503, doi:10.5194/amt-9-1485-2016, 2016.
- O'Brien, D. M, I. N. Polonsky, S. R. Utembe and P. J. Rayner. Potential of a geostationary geoCARB mission to estimate surface emissions of CO<sub>2</sub>, CH<sub>4</sub> and CO in a polluted urban environment: case study Shanghai, *Atmospheric Measurements Techniques*, 9, 4633–4654, 2016.
- Oda, T., and S. Maksyutov, A very high-resolution (1 km×1 km) global fossil fuel CO<sub>2</sub> emission inventory derived using a point source database and satellite observations of nighttime lights, *Atmos. Chem. Phys.*, 11(2), 543-556, doi: 10.5194/acp-11-543-2011, 2011.
- Oda, T., Maksyutov, S., and Andres, R. J.: The Open-source Data Inventory for Anthropogenic CO<sub>2</sub>, version 2016 (ODIAC2016): a global monthly fossil fuel CO<sub>2</sub> gridded emissions data product for tracer transport simulations and surface flux inversions, *Earth Syst. Sci. Data*, 10, 87-107, doi:10.5194/essd-10-87-2018, 2018.
- O'Dell, C. W.: Acceleration of multiple-scattering, hyperspectral radiative transfer calculations via low-streams interpolation. *J. Geophys. Res.*, 115, 1–15, doi:10.1029/2009JD012803, 2010.
- O'Dell, C. W., Connor, B. J., Bösch, H., O'Brien, D. M., Frankenberg, C., Castano, R., Christi, M., Eldering, A., Fisher, B., Gunson, M., McDuffie, J., Miller, C. E., Natraj, V., Oyafuso, F. A., Polonsky, I., Smyth, M., Taylor, T. E., Toon, G. C., Wennberg, P. O., and Wunch, D.: The ACOS CO<sub>2</sub> retrieval algorithm – Part 1: Description and validation against synthetic observations, *Atmospheric Measurement Techniques*, 5, 99–121, doi:10.5194/amt-5-99-

2012, 2012.

- O'Dell, C., Eldering, A., Wennberg, P., Crisp, D., Gunson, M., Fisher, B., Frankenberg, C., Kiel, M., Lindqvist, H., Mandrake, L., Merrelli, A., Natraj, V., Nelson, R., Osterman, G., Payne, V., Taylor, T., Wunch, D., Drouin, B., Oyafuso, F., Chang, A., McDuffie, J., Smyth, M., Baker, D., Basu, S., Chevallier, F., Crowell, S., Feng, L., Palmer, P., Dubey, M., Garcia, O., Griffith, D., Hase, F., Iraci, L., Kivi, R., Morino, I., Notholt, J., Ohyama, H., Petri, C., Roehl, C., Sha, M., Strong, K., Te, Y., Uchino, O., and Velazco, V.: Retrievals of Carbon Dioxide from the Orbiting Carbon Observatory-2 with the ACOS algorithm, *Atmospheric Measurement Techniques Discussion*, Submitted July 2018.
- Oshchepkov, S., A. Bril, T. Yokota, P. O. Wennberg, N. M. Deutscher, D. Wunch, G. C. Toon, Y. Yoshida, C. W. O'Dell, D. Crisp, C. E. Miller, C. Frankenberg, A. Butz, I. Aben, S. Guerlet, O. Hasekamp, H. Boesch, A. Cogan, R. Parker, D. Griffith, R. Macatangay, J. Notholt, R. Sussmann, M. Rettinger, V. Sherlock, J. Robinson, E. Kyrö, P. Heikkinen, D. G. Feist, I. Morino, N. Kadyrov, D. Belikov, S. Maksyutov, T. Matsunaga, O. Uchino, and H. Watanabe, Effects of atmospheric light scattering on spectroscopic observations of greenhouse gases from space. Part 2: Algorithm intercomparison in the GOSAT data processing for CO<sub>2</sub> retrievals over TCCON sites, *J. Geophys. Res. Atmos.*, 118, 1493–1512, doi:10.1002/jgrd.50146, 2012.
- Osterman, G., Eldering, A., Mandrake, L., O'Dell, C., Wunch, D., Wennberg, P.O., Fisher, B., and Marchetti, Y., Orbiting Carbon Observatory-2 (OCO-2) Warn Level, Bias Correction, and Lite File Product Description, Version 2.0, 2017;  
[https://docs.server.gesdisc.eosdis.nasa.gov/public/project/OCO/OCO2\\_XCO2\\_Lite\\_Files\\_and\\_Bias\\_Correction.pdf](https://docs.server.gesdisc.eosdis.nasa.gov/public/project/OCO/OCO2_XCO2_Lite_Files_and_Bias_Correction.pdf) (last referenced 11 February 2018).
- Oyafuso, F., V. H. Payne, B. J. Drouin, V. M. Devi, D. C. Benner, K. Sung, S. Yu, I. E. Gordon, R. Kochanov, Y. Tan, D. Crisp, E. J. Mlawer, A. Guillaume: High accuracy absorption coefficients for the Orbiting Carbon Observatory-2 (OCO-2) mission: Validation of updated carbon dioxide cross-sections using atmospheric spectra, *Journal of Quantitative Spectroscopy & Radiative Transfer*, 203, 213-22, doi.org/10.1016/j.jqsrt.2017.06.012, 2017.
- Pacala, S. W., Breidenich, C., Brewer, P.G. Fung, I., Gunson, M. R., Heddle, G., Law, B., Marland, G., Paustian, K., Prather, M., Randerson, J., T., Tans, P., and Wofsy, S. C.: *Verifying Greenhouse Gas Emissions: Methods to Support International Climate Agreements*. National Academies Press, 2010.
- Pales, J. C., and Keeling, C. D.: The concentration of atmospheric carbon dioxide in Hawaii, *J. Geophys. Res.*, 70, 6053-6076, doi:10.1029/JZ070i024p06053, 1965.
- Palmer, P. I., Feng, L., and Boesch, H., Spatial resolution of tropical terrestrial CO<sub>2</sub> fluxes inferred using space-borne column CO<sub>2</sub> sampled in different earth orbits: the role of spatial error correlations, *Atmos. Meas. Tech.*, 4, 1995-2006, doi:10.5194/amt-4-1995-2011, 2011.
- Parazoo, N. C., Denning, A. S., Kawa, S. R., Pawson, S., and Lokupitiya, R.: CO<sub>2</sub> flux estimation errors associated with moist atmospheric processes, *Atmos. Chem. Phys.*, 12, 6405-6416, doi:10.5194/acp-12-6405-2012, 2012.

- Parker, R., H. Boesch, A. Cogan, A. Fraser, L. Feng, P. I. Palmer, J. Messerschmidt, N. Deutscher, D. W. T. Griffiths, J. Notholt, P. O. Wennberg, and D. Wunch, Methane observations from the Greenhouse gases Observing SATellite: validation and model comparison, *Geophys. Res. Lett.*, 38, L15807, doi:10.1029/2011GL047871, 2011.
- Parker, R. J., Boesch, H., Byckling, K., Webb, A. J., Palmer, P. I., Feng, L., Bergamaschi, P., Chevallier, F., Notholt, J., Deutscher, N., Warneke, T., Hase, F., Sussmann, R., Kawakami, S., Kivi, R., Griffith, D. W. T., and Velazco, V.: Assessing 5 years of GOSAT Proxy XCH<sub>4</sub> data and associated uncertainties, *Atmos. Meas. Tech.*, 8, 4785-4801. doi:10.5194/amt-8-4785-2015, 2015.
- Patra, P. K., Maksyutov, S.: TRANSCOM-3 Modelers. Sensitivity of optimal extension of CO<sub>2</sub> observation networks to model transport. *Tellus B*, 55(2):498–511, 2003.
- Patra, P. K., Houweling, S., Krol, M., Bousquet, P., Belikov, D., Bergmann, D., Bian, H., Cameron-Smith, P., Chipperfield, M. P., Corbin, K., Fortems-Cheiney, A., Fraser, A., Gloor, E., Hess, P., Ito, A., Kawa, S. R., Law, R. M., Loh, Z., Maksyutov, S., Meng, L., Palmer, P. I., Prinn, R. G., Rigby, M., Saito, R., and Wilson, C.: TransCom model simulations of CH<sub>4</sub> and related species: linking transport, surface flux and chemical loss with CH<sub>4</sub> variability in the troposphere and lower stratosphere, *Atmos. Chem. Phys.*, 11, 12813–12837, doi:10.5194/acp-11-12813-2011, 2011.
- Patra, P., Crisp, D., Kaiser, J., Wunch, D., Saeki, T., Ichii, K., Sekiya, T., Wennberg, P., Feist, D., Pollard, D., Griffith, D., Velazco, V., De Maziere, M., Sha, M. K., Roehl, C., and Chatterjee, A.: Orbiting Carbon Observatory-2 (OCO-2) tracks 2-3 peta-grams increase of carbon release to the atmosphere during the 2014-2016 El Niño. *Nature Scientific Reports*, 7: 13567, doi:10.1038/s41598-017-13459-0, 2017.
- Peters, W., Miller, J. B., Whitaker, J., Denning, A. S., Hirsch, A., Krol, M. C., Zupanski, D., Bruhwiler, L., and Tan, P. P. s: An ensemble data assimilation system to estimate CO<sub>2</sub> surface fluxes from atmospheric trace gas observations, *J. Geophys. Res.*, 110, D24304, doi:10.1029/2005JD006157, 2005.
- Peters, Wouter, Jacobson, Andrew R., Sweeney, Colm, Andrews, Arlyn E., Conway, Thomas J., Masarie, Kenneth, Miller, John B., Bruhwiler, Lori M. P., Petron, Gabrielle, Hirsch, Adam I., Worthy, Douglas E. J., van der Werf, Guido R., Randerson, James T., Wennberg, Paul O., Krol, Maarten C., and Tans, Pieter P.: An atmospheric perspective on North American carbon dioxide exchange: CarbonTracker, *Proceedings Of The National Academy Of Sciences Of The United States Of*, 104, 18925-18930, doi:10.1073/pnas.0708986104, 2007.
- Peylin, P., Baker, D., Sarmiento, J., Ciais, P., and Bousquet, P.: Influence of transport uncertainty on annual mean and seasonal inversions of atmospheric CO<sub>2</sub> data. *J. Geophys. Res.*, 107, 10, 2002.
- Pillai, D., M. Buchwitz, C. Gerbig, T. Koch, M. Reuter, H. Bovensmann, J. Marshall and J. P. Burrows (2016) Tracking city CO<sub>2</sub> emissions from space using a high-resolution inverse modelling approach: a case study for Berlin, Germany , *Atmospheric Chemistry and Physics*, 16, 9591–9610, doi:10.5194/acp-16-9591-2016, 2016.

- Pinty B., G. Janssens-Maenhout, M. Dowell, H. Zunker, T. Brunhes, P. Ciais, D. Dee, H. Denier van der Gon, H. Dolman, M. Drinkwater, R. Engelen, M. Heimann, K. Holmlund, R. Husband, A. Kentarchos, Y. Meijer, P. Palmer and M. Scholze: An Operational Anthropogenic CO<sub>2</sub> Emissions Monitoring & Verification Support capacity - Baseline Requirements, Model Components and Functional Architecture, doi:10.2760/39384, 2017. European Commission Joint Research Centre, EUR 28736 EN.
- Plieninger, J., von Clarmann, T., Stiller, G. P., Grabowski, U., Glatthor, N., Kellmann, S., Linden, A. Haenel, F., Kiefer, M., Höpfner, M., Laeng, A., and Lossow, S.: Methane and nitrous oxide retrievals from MIPAS-ENVISAT. *Atmos. Meas. Tech.*, 8, 4657-4670, 2015.
- Plieninger, J., Laeng, A., Lossow, S., von Clarmann, T., Stiller, G. P., Kellmann, S., Linden, A., Kiefer, M., Walker, K. A., Noël, S., Hervig, M., McHugh, M., Lambert, A., Urban, J., Elkins, J. W., Murtagh, D.: Validation of revised methane and nitrous oxide profiles from MIPAS-ENVISAT, *Atmos. Meas. Tech.*, 9, 765-779, 2016.
- Polavarapu, S. M., Neish, M., Tanguay, M., Girard, C., de Grandpré, J., Semeniuk, K., Gravel, S., Ren, S., Roche, S., Chan, D., and Strong, K., Greenhouse gas simulations with a coupled meteorological and transport model: the predictability of CO<sub>2</sub>, *Atmos. Chem. Phys.*, 16, 12005–12038, doi:10.5194/acp-16-12005-2016, 2016.
- Polavarapu, S. M., Deng, F., Byrne, B., Jones, D. B. A., Neish, M.: A comparison of atmospheric CO<sub>2</sub> flux signals obtained from GEOSChem flux inversions constrained by *in situ* or GOSAT observations, *Atmos. Chem. Phys. Discuss.*, doi:10.5194/acp-2017-1235, 2018.
- Polonsky, I. N., O' Brien, D. M., Kumer, J. B., O' Dell, C. W. and the geoCARB team: Performance of a geostationary mission, geoCARB, to measure CO<sub>2</sub>, CH<sub>4</sub> and CO column-averaged concentrations, *Atmospheric Measurement Techniques*, 7, 959-981, doi:10.5194/amt-7-959-2014, 2014.
- Prather, M. J.; Zhua, X; Strahan, SE; Steenrod, SD; Rodriguez, JM, Quantifying errors in trace species transport modeling. *Proceedings of the National Academy of Sciences of the United States of America* 105(50), 19617-19621. DOI: 10.1073/pnas.0806541106, Dec 16, 2008.
- Putman, W., da Silva, A.M., Ott, L.E. and Darmenov, A.: Model Configuration for the 7-km GEOS-5 Nature Run, Ganymed Release (Non-hydrostatic 7 km Global Mesoscale Simulation). GMAO Office Note No. 5 (Version 1.0), 18 pp, 2014. (Available from [http://gmao.gsfc.nasa.gov/pubs/office\\_notes](http://gmao.gsfc.nasa.gov/pubs/office_notes) )
- Rayner, P. J., Enting, I. G., and Trudinger, C. M., “Optimizing the CO<sub>2</sub> observing network for constraining sources and sinks,” *Tellus B*, 48, 433–444, 1996.
- Rayner, P. J. and O'Brien, D. M.: The utility of remotely sensed CO<sub>2</sub> concentration data in surface source inversions, *Geophys. Res. Lett.*, 28, 175-178, doi:10.1029/2001GL013115, 2001.
- Rayner, P., Scholze, M., Knorr, W., Kaminski, T., Giering, R., and Widmann, H.: Two decades of terrestrial carbon fluxes from a carbon cycle data assimilation system (CCDAS), *Global Biogeochem. Cy.*, doi:10.1029/2004gb002254, 2005.

- Rayner, P. J., Raupach, M. R., Paget, M., Peylin, P., and Koffi, E.: A new global gridded data set of CO<sub>2</sub> emissions from fossil fuel combustion: Methodology and evaluation, *J. Geophys. Res. Atmos.*, 115, D19306, doi:10.1029/2009jd013439, 2010.
- Rayner, P., Koffi, E., Scholze, M., Kaminski, T., and Dufresne, J.-L.: Constraining predictions of the carbon cycle using data, *Phil. Trans. R. Soc. A*, 369, 1955–1966, doi:10.1098/rsta.2010.0378, 2011.
- Rayner, P. J. and Utembe, S. R. and Crowell, S.: Constraining regional greenhouse gas emissions using geostationary concentration measurements: a theoretical study. *Atmos. Meas. Tech.*, 7, 3285-3293, 2014. doi: 10.5194/amt-7-3285-2014.
- Reuter, M., Buchwitz, M., Schneising, O., Heymann, J., Bovensmann, H., and Burrows, J. P., A method for improved SCIAMACHY CO<sub>2</sub> retrieval in the presence of optically thin clouds, *Atmos. Meas. Tech.*, 3, 209-232, 2010.
- Reuter, M., Bovensmann, H., Buchwitz, M., et al., Retrieval of atmospheric CO<sub>2</sub> with enhanced accuracy and precision from SCIAMACHY: Validation with FTS measurements and comparison with model results, *J. Geophys. Res.*, 116, D04301, doi:10.1029/2010JD015047, 2011.
- Reuter, M., Buchwitz, M., Hilker, M., Heymann, J., Schneising, O., Pillai, D., Bovensmann, H., Burrows, J. P., Bösch, H., Parker, R., Butz, A., Hasekamp, O., O'Dell, C. W., Yoshida, Y., Gerbig, C., Nehrkorn, T., Deutscher, N. M., Warneke, T., Notholt, J., Hase, F., Kivi, R., Sussmann, R., Machida, T., Matsueda, H., and Sawa, Y.: Satellite-inferred European carbon sink larger than expected, *Atmos. Chem. Phys.*, 14, 13739-13753, doi:10.5194/acp-14-13739-2014, 2014.
- Reuter, M., Buchwitz, M., Schneising, O., Noël, S., Bovensmann, H., and Burrows, J.P.: A Fast Atmospheric Trace Gas Retrieval for Hyperspectral Instruments Approximating Multiple Scattering—Part 2: Application to XCO<sub>2</sub> Retrievals from OCO-2, *Remote Sens.*, 9, 1159, doi:10.3390/rs9111159, 2017a.
- Reuter, M., Buchwitz, Hiker, M., Heymann, J., Bovensmann, H., Burrows, J.P., Houweling, S., Liu, Y.Y., Nassar, R., Chevallier, F., Ciais, P., Marshall, J., and Reichstein, M.: How Much CO<sub>2</sub> Is Taken Up by the European Terrestrial Biosphere? *Bull., Amer. Meteor. Soc.*, 665-671, doi: 10.1175/BAMS-D-15-00310.1, 2017b.
- Rigby, M., Montzka, S. A., Prinn, R. G., White, J. W. C., Young, D., O'Doherty, S., Lunt, M. F., Ganesan, A. L., Manning, A. J. , Simmonds, P. G., Salameh, P. K., Harth, C. M., Mühle, J., Weiss, R. F., Fraser P. J., Steele L. P., Krummel, P. B., McCulloch, A., and Park S.: Role of atmospheric oxidation in recent methane growth, *Proceedings of the National Academy of Sciences*, 114(21), 5373-5377, doi:10.1073/pnas.1616426114, 2017.
- Rödenbeck, C., Houweling, S., Gloor, M., and Heimann, M.: CO<sub>2</sub> flux history 1982–2001 inferred from atmospheric data using a global inversion of atmospheric transport, *Atmos. Chem. Phys.*, 3, 1919-1964, <https://doi.org/10.5194/acp-3-1919-2003>, 2003.

- Rosenberg, R., Maxwell, S., Johnson, B. C., Chapsky, L., Lee, R. A. M., and R. Pollock: Preflight radiometric calibration of Orbiting Carbon Observatory 2. *IEEE Trans. Geoscience Remote Sensing*, 55, doi 10.1109/TGRS.2016.2634023, 2017.
- Sakuma, F., Bruegge, C.J., Rider, D., Brown, D., Geier, S., Kawakami, S., and Kuze, A.: OCO/GOSAT Preflight Cross-Calibration Experiment, *IEEE Transactions on Geoscience And Remote Sensing*, 48, 2010.
- Saunio, M., Bousquet, P., Poulter, B., Peregón, A., Ciais, P., Canadell, J. G., Dlugokencky, E. J., Etiope, G., Bastviken, D., Houweling, S., Janssens-Maenhout, G., Tubiello, F. N., Castaldi, S., Jackson, R. B., Alexe, M., Arora, V. K., Beerling, D. J., Bergamaschi, P., Blake, D. R., Brailsford, G., Brovkin, V., Bruhwiler L., Crevoisier, C., Crill, P., Covey, K., Curry, C., Frankenberg, C., Gedney, N., Höglund-Isaksson, L., Ishizawa, M., Ito, A., Joos, F., Kim, H.-S., Kleinen, T., Krummel, P., Lamarque, J.-F., Langenfelds, R., Locatelli, R., Machida, S., Maksyutov, K. C. McDonald, J. Marshall, J. R. Melton, I. Morino, V. Naik, S. O'Doherty, T., Parmentier, F.-J. W., Patra, P. K., Peng, C., Peng, S., Peters, G. P., Pison, I., Prigent, C., Prinn, R., Ramonet, M., Riley, W. J., Saito, M., Santini, M., Schroeder, R., Simpson, I. J., Spahni, P., Steele, A. Takizawa, B. F. Thornton, H. Tian, Y. Tohjima, N. Viovy, A. Voulgarakis, R., van Weele, M., van der Werf, G. R., Weiss, R., Wiedinmyer, C., Wilton, D. J., Wiltshire, A., Worthy, D., Wunch, D., Xu, X., Yoshida, Y., Zhang, B., Zhang, Z., and Zhu, Q.: The global methane budget 2000–2012, *Earth Syst. Sci. Data*, 8(2), 697–751, doi:10.5194/essd-8-697-2016, 2016.
- Schepers, D., et al., Methane retrievals from Greenhouse Gases Observing Satellite (GOSAT) shortwave infrared measurements: Performance comparison of proxy and physics retrieval algorithms, *J. Geophys. Res.*, 117, doi: 10.1029/2012jd017549, 2012.
- Schneising, O., Buchwitz M., Burrows J. P., Bovensmann H., Reuter M., Notholt J., Macatangay R., and Warneke T., Three years of greenhouse gas column-averaged dry air mole fractions retrieved from satellite – Part 1: Carbon dioxide, *Atmos. Chem. Phys.*, 8, 3827–3853, 2008.
- Schneising, O., et al. Anthropogenic carbon dioxide source areas observed from space: assessment of regional enhancements and trends. *Atmos. Chem. Phys.*, 13, 2445–2454, doi:10.5194/acp-13- 2445-2013, 2013.
- Schneising, O., J. P. Burrows, R. R. Dickerson, M. Buchwitz, M. Reuter, and H. Bovensmann, Remote sensing of fugitive methane emissions from oil and gas production in North American tight geologic formations, *Earth's Future*, 2, 548–558, doi:10.1002/2014EF000265, 2014.
- Scholze, M., Kaminski, T., Rayner, P., Knorr, W., and Giering, R.: Propagating uncertainty through prognostic carbon cycle data assimilation system simulations, *J. Geophys. Res.*, 112, doi:doi:10.1029/2007JD008642, 2007.
- Schwandner, F. M., Verhulst, K., Eldering, A., Miller, C., Nguyen, H., Kahn, B., Oda, T., Rao, P., O'Dell, C., Crisp, D., Frankenberg, C., Gunson M., and Pollock, H.: Spaceborne detection of localized carbon dioxide sources. *Science* 358, eaam5782, doi:10.1126/science.aam5782, 2017.

- Shiomi, K., Kawakami, S., Kina, T., Mitomi, Y., Yoshida, M., Sekio, N., Kataoka, F., and Higuchi, R.: Calibration plan of GOSAT sensors. *Sensors, Systems, and Next-Generation Satellites XI, Proc. of SPIE*, 6744, 67440G, doi:10.1117/12.738206, 2007.
- Shiomi, K., Kawakami, S., Kuze, A., Suto, H., Hashiguchi, T., Kataoka, F., Higuchi, R., Bruegge, C., and Schwandner, F.: On orbit lunar calibration compared with vicarious calibration for GOSAT, AGU Fall Meeting, San Francisco, USA, 9–13 December 2013, A21G-0159, 2013.
- Singh, K., Sandu, A., Jardak, M., Bowman, K., and Lee, M., “A practical method to estimate information content in the context of 4d-var data assimilation,” *SIAM/ASA Journal on Uncertainty Quantification*, 1, 106–138, Sept. 2013.
- Sioris, C. E., Boone, C. D., Nassar, R., Sutton, K. J., Gordon, I. E., Walker, K. A., and Bernath, P.F., Retrieval of carbon dioxide vertical profiles from solar occultation observations and associated error budgets for ACE-FTS and CASS-FTS, *Atmos. Meas. Tech.*, 7, 2243–2262, doi:10.5194/amt-7-2243-2014, 2014.
- Somkuti, P., Boesch, H., Vijay, N., and Kopparla, P.: Application of a PCA-based fast radiative transfer model to XCO<sub>2</sub> retrievals in the shortwave infrared. *J. Geophys. Res. Atmos.*, 122, doi:10.1002/2017JD027013, 2017.
- Spurr, R. J. D., Kurosu, T. P., and Chance, K. V.: A linearized discrete ordinate radiative transfer model for atmospheric remote-sensing retrieval, *J. Quant. Spectrosc. Radiat. Trans.*, 68, 689–735, doi:10.1016/S0022-4073(00)00055-8, 2001.
- Staufer, J., Broquet, G., Bréon, F.-M., Puygrenier, V., Chevallier, F., Xueref-Rémy, I., Dieudonné, E., Lopez, M., Schmidt, M., Ramonet, M., Perrussel, O., Lac, C., Wu, L., and Ciais, P.: The first 1-year-long estimate of the Paris region fossil fuel CO<sub>2</sub> emissions based on atmospheric inversion, *Atmos. Chem. Phys.*, 16, 14703–14726, doi:10.5194/acp-16-14703-2016, 2016.
- Stavros, E. N., Schimel, D., Pavlick, R., Serbin, S., Swann, A., Duncanson, L., Fisher, J. B., Fassnacht, F., Ustin, S., Dubayah, R., Schweiger, A., and P. Wennberg, ISS observations offer insights into plan function. *Nature Ecology and Evolution*, 1, 0194, doi:10.1038/s41559-017-0194, 2017.
- Stephens, B. B., Gurney, K. R., Tans, P. P., Sweeney, C., Peters, W., Bruhwiler, L., Ciais, P., Ramonet, M., Bousquet, P., Nakazawa, T., Aoki, S., Machida, T., Inoue, G., Vinnichenko, N., Lloyd, J., Jordan, A., Heimann, M., Shibistova, O., Langenfelds, R. L., Steele, L. P., Francey, R. J. and Denning, A. S.: Weak northern and strong tropical land carbon uptake from vertical profiles of atmospheric CO<sub>2</sub>, *Science*, 316(5832), 1732–1735, doi:10.1126/science.1137004, 2007.
- Stohl, A., Seibert, P., Arduini, J., Eckhardt, S., Fraser, P., Grealley, B., Lunder, C., Maione, M., Muhle, J., O'Doherty, S., Prinn, R., Reimann, S., Saito, T., Schmidbauer, N., Simmonds, P., Vollmer, M., Weiss, R., and Yokouchi, Y.: An analytical inversion method for determining regional and global emissions of greenhouse gases: Sensitivity studies and application to halocarbons, *Atmospheric Chemistry and Physics*, 9, 1597-1620, 2009.

- Sun, K., Xiong Liu, C. R. Nowlan, Z. Cai, K. Chance, C. Frankenberg, R. A. M. Lee, R. Rosenberg, and D. Crisp: Characterization of the OCO-2 instrument line shape functions using on-orbit solar measurements., *Atmos. Meas. Tech.*, 10, 939–953, doi:10.5194/amt-10-939-2017, 2017.
- Sun, Y., Frankenberg, C., Wood, J. D., Schimel, D. S., Jung, M., Guanter, L., Drewry, D. T., Verma, M., Porcar-Castell, A., Griffis, T. J., Gu, L., Magney, T. S., Köhler, P., Evans, B., and Yuen, K. OCO-2 advances photosynthesis observation from space via solar induced chlorophyll fluorescence. *Science* 358, eaam5747, doi:10.1126/science.aam5747, 2017.
- Sun, Y., Frankenberg, C., Jung, M., Joiner, J., Guanter, L., Köhler, P., & Magney, T.: Overview of solar-induced fluorescence (SIF) from the Orbiting Carbon Observatory-2: Retrieval, cross-mission comparison, and global monitoring for GPP. *Remote Sensing of Environment*, 209, 808–823, doi:10.1016/j.rse.2018.02.016, 2018.
- Suntharalingam, P., Spivakovsky, C. M., Logan, J. A., and McElroy, M. B.: Estimating the distribution of terrestrial CO<sub>2</sub> sources and sinks from atmospheric measurements: Sensitivity to configuration of the observation network. *J. Geophys. Res.*, 108, 4452, doi:10.1029/2002JD002207, 2003.
- Suto, H., Kawashima, T., Yoshida, J., Ishida, J., Kuze, A., Nakajima, M., and Hamazaki, T.: The prelaunch performance test and calibration results of thermal and near-infrared sensor for carbon observation (TANSO) on GOSAT,” *Proc. SPIE* 7106, 710620, 2008.
- Suto, H., Kuze, A., Shiomi, K., and Nakajima, M.: Updated level-1 processing after two-years operation of TANSO-FTS. *Proc. SPIE* 8154, *Infrared Remote Sensing and Instrumentation XIX*, 81541A, doi:10.1117/12.893405, 2011.
- Takagi, H., Houweling, S., Andres, R. J., Belikov, D., Bril, A., Boesch, H., Butz, A., Guerlet, S., Hasekamp O., Maksyutov S., Morino I., Oda T., O’Dell, C. W., Oshchepkov, S., Parker, R., Saito, M., Uchino, O., Yokota, T., Yoshida, Y., and Valsala, V., Influence of differences in current GOSAT XCO<sub>2</sub> retrievals on surface flux estimation, *Geophysical Research Letters*, 41, 2013GL059174, 2014.
- Taylor, T.E., C.W. O’Dell, D.M. O’Brien, N. Kikuchi, T. Yokota, T.Y. Nakajima, H. Ishida, D. Crisp, and T. Nakajima, Comparison of Cloud-Screening Methods Applied to GOSAT Near-Infrared Spectra, *IEEE Trans. Geosci. Remote Sens.*, 50, 295-309, doi:10.1109/TGRS.2011.2160270, 2012.
- Taylor, T. E., O’Dell, C. W., Frankenberg, C., Partain, P., Cronk, H. Q., Savtchenko, A., Nelson, R. R., Rosenthal, E. J., Chang, A. Y., Fisher, B., Osterman, G., Pollock, R. H., Crisp, D., Eldering, A., and Gunson, M. R: Orbiting Carbon Observatory-2 (OCO-2) cloud screening algorithms; validation against collocated MODIS and CALIOP data, *Atmos. Meas. Tech.*, 9, 973-989, <http://www.atmos-meas-tech.net/9/973/2016/>doi:10.5194/amt-9-973-2016, 2016.
- Thompson, D.R., Benner, D. C., Brown, L. R., Crisp, D., Devi, V. M., Jiang, Y., Natraj, V., Oyafuso, F., Sung, K., Wunch, D., Castano, R., Miller, C. E.: Atmospheric Validation of High Accuracy CO<sub>2</sub> Absorption Coefficients for the OCO-2 Mission, *J. Quant. Spectro.*

Radiat. Trans., 113, 2265-2276, ISSN 0022-4073, 10.1016/j.jqsrt.2012.05.021, 2012.

Thompson, D.R., Thorpe, A.K., Frankenberg, C., Green, R.O., Duren, R., Guanter, L., Hollstein, A., Middleton, E., Ong, L. and Ungar, S.: Space-based remote imaging spectroscopy of the Aliso Canyon CH<sub>4</sub> superemitter. *Geophys. Res. Lett.*, 43, 6571-6578, doi:10.1002/2016GL069079, 2016.

Tian, X., Xie, Z., Liu, Y., Cai, Z., Fu, Y., Zhang, H., and Feng, L.: A joint data assimilation system (Tan-Tracker) to simultaneously estimate surface CO<sub>2</sub> fluxes and 3-D atmospheric CO<sub>2</sub> concentrations from observations, *Atmos. Chem. Phys.*, 14, 13281-13293, 10.5194/acp-14-13281-2014, 2014.

Tol, P. J. J., van Kempen, T. A., van Hees, R. M., Krijger, M., Cadot, S., Snel, R., Persijn, S. T., Aben, I., and Hoogeveen, R. W. M.: Characterization and correction of stray light in TROPOMI-SWIR, *Atmos. Meas. Tech.*, 11, 4493-4507, doi:10.5194/amt-11-4493-2018, 2018.

Tolerson, J.: US environmental group wins millions to develop methane-monitoring satellite, *Nature* 556, 283, doi:10.1038/d41586-018-04478-6, 2018.

Tran H and Hartmann J. M.: An improved O-2 A-Band Absorption Model and its Consequences for Retrievals of Photon Paths and Surface Pressures. *J. Geophys. Res. Atmos.* 113, doi:10.1029/2008JD010011, 2008.

Tukiainen, S., Railo, J., Laine, M., Hakkarainen, J., Kivi, R., Heikkinen, P., Chen, H. and Tamminen, J., Retrieval of atmospheric CH<sub>4</sub> profiles from Fourier transform infrared data using dimension reduction and MCMC, *J. Geophys. Res.*, 121, doi:10.1002/2015JD024657, 2016.

Turner, A.J., Jacob, D. J., Wecht, K. J., Maasackers, J. D., Lundgren, E., Andrews, A. E., Biraud, S.C., Boesch, H., Bowman, K.W., Deutscher, N. M., Dubey, M. K., Griffith, D. W. T., Hase, F., Kuze, A., Notholt, J., Ohyama, H., Parker, R., Payne, V. H., Sussmann, R., Sweeney, C., Velasco, V.A., Warneke, T., Wennberg, P. O., and Wunch, D.: Estimating global and North American methane emissions with high spatial resolution using GOSAT satellite data. *Atmos. Chem. Phys.*, 15, 7049–7069, 2015a.

Turner, A. J., and Jacob, D. J.: Balancing aggregation and smoothing errors in inverse models, *Atmos. Chem. Phys.*, 15, 7039-7048, 10.5194/acp-15-7039-2015, 2015bW

Turner, A. J., D. J. Jacob, J. Benmergui, S. C. Wofsy, J. D. Maasackers, A. Butz, O. Hasekamp, and S. C. Biraud: A large increase in U.S. methane emissions over the past decade inferred from satellite data and surface observations, *Geophys. Res. Lett.*, 43, 2218–2224, doi:10.1002/2016GL067987, 2016.

UNFCCC, 2015: Paris Agreement. United Nations Framework Convention on Climate Change, [Bonn, Germany]. 25 pp.  
[http://unfccc.int/files/essential\\_background/convention/application/pdf/english\\_paris\\_agreement.pdf](http://unfccc.int/files/essential_background/convention/application/pdf/english_paris_agreement.pdf)

- van Hees, R. M., Tol, P. J. J., Cadot, S., Krijger, M., Persijn, S. T., van Kempen, T. A., Snel, R., Aben, I., and Hoogeveen, R. W. M.: New method to determine the instrument spectral response function, applied to TROPOMI-SWIR, *Atmos. Meas. Tech.*, 11, 4493–4507, doi:10.5194/amt-11-4493-2018, 2018.
- Varon, D. J., Jacob, D. J., McKeever, J., Jervis, D., Durak, B. O. A., Xia, Y., and Huang, Y.: Quantifying methane point sources from fine-scale (GHGSat) satellite observations of atmospheric methane plumes, *Atmos. Meas. Tech. Discuss.*, doi:10.5194/amt-2018-171, in review, 2018.
- Veefkind, J. P., Aben, I., McMullan, K., Förster, H., De Vries, J., Otter, G., Claas, J., Eskes, H. J., De Haan, J. F., Kleipool, Q., Van Weele, M., Hasekamp, O., Hoogeveen, R., Landgraf, J., Snel, R., Tol, P., Ingmann, P., Voors, R., Kruizinga, B., Vink, R., Visser, H., and Levelt, P. F.: TROPOMI on the ESA Sentinel-5 Precursor: A GMES mission for global observations of the atmospheric composition for climate, air quality and ozone layer applications, *Remote Sensing of Environment*, 120, 70–83, doi:10.1016/j.rse.2011.09.027, 2012.
- Veefkind et al., Early Results from TROPOMI on the Copernicus Sentinel 5 Precursor, 2017 AGU Fall Meeting, New Orleans, LA, USA, December, 2017.  
<https://agu.confex.com/agu/fm17/meetingapp.cgi/Paper/215366> (last visited 7 Jan 2018).
- Velazco, V. A., Buchwitz, M., Bovensmann, H., Reuter, M., Schneising, O., Heymann, J., Krings, T., Gerilowski, K., and Burrows, J. P.: Towards space based verification of CO<sub>2</sub> emissions from strong localized sources: fossil fuel power plant emissions as seen by a CarbonSat constellation, *Atmos. Meas. Tech.*, 4, 2809–2822, doi:10.5194/amt-4-2809-2011, 2011.
- Verma, S.; Marshall, J.; Gerbig, C.; Rödenbeck, C.; Totsche, K. U.: The constraint of CO<sub>2</sub> measurements made onboard passenger aircraft on surface-atmosphere fluxes: the impact of transport model errors in vertical mixing. *Atmospheric Chemistry and Physics*, 17, 5665–5675, 2017.
- Wang, Y., G. Broquet, P. Ciais, F. Chevallier, F. Vogel, N. Kadyrov, L. Wu, Y. Yin, R. Wang, and S. Tao, Estimation of observation errors for large-scale atmospheric inversion of CO<sub>2</sub> emissions from fossil fuel combustion, *Tellus B: Chemical and Physical Meteorology*, 69(1), 1325723, doi:10.1080/16000889.2017.1325723, 2017.
- Washenfelder, R. A., Toon, G. C., Blavier, J. F., Yang, Z., Allen, N. T., Wennberg, P. O., Vay, S. A., Matross, D. M. & Daube, B. C.: Carbon dioxide column abundances at the Wisconsin Tall Tower site. *J. Geophys. Res.* 111, D22305. doi:10.1029/2006JD007154, 2006.
- Wecht, K. J., Jacob, D. J., Sulprizio, M. P., Santoni, G. W., Wofsy, S. C., Parker, R., Boesch, H., and Worden J.: Spatially resolving methane emissions in California: constraints from the CalNex aircraft campaign and from present (GOSAT, TES) and future (TROPOMI, geostationary) satellite observations, *Atmos. Chem. Phys.*, 14, 8173–8184, 08 2014.
- White, W.H., Anderson, J.A., Blumenthal, D.L., Husar, R.B., Gillani, N.V., Husar, J.D., and Wilson, W.E.: Formation and transport of secondary air pollutants: ozone and aerosols in the

St. Louis urban plume. *Science*, 194(4261), 187-189, web:  
<http://www.jstor.org/stable/1742680>, 1976.

WMO, 2009: Technical Report of Global Analysis Method for Major Greenhouse Gases by the World Data Centre for Greenhouse Gases (Y. Tsutsumi, K. Mori, T. Hirahara, M. Ikegami and T.J. Conway). GAW Report No. 184 (WMO/TD-No. 1473), Geneva, 29 pp.

WMO 2011: Report of the 15th WMO/IAEA Meeting of Experts on Carbon Dioxide, Other Greenhouse Gases, and Related Tracers Measurement Techniques, Jena, Germany, 7–10 September 2009, GAW 194, available at: <http://www.wmo.int/pages/prog/arep/gaw/gaw-reports.html> (last access: 28 January 2014), World, Meteorological Organization, Geneva, Switzerland, 2011.

WMO, 2017: The State of Greenhouse Gases in the Atmosphere Based on Global Observations through 2016, WMO Greenhouse Gas Bulletin, No. 13, 30 October 2017

WMO OSCAR Web Site <https://www.wmo-sat.info/oscar/satellites/view/116> Last accessed 7 Jan 2018.

Wofsy, S. C., B. Daube, R. Jimenez, E. Kort, J. V. Pittman, S. Park, R. Commane, B. Xiang, G. Santoni, D. Jacob, J. Fisher, C. Pickett-Heaps, H. Wang, K. J. Wecht, Q.-Q. Wang, B. B. Stephens, S. Shertz, P. Romashkin, T. Campos, J. Haggerty, W. A. Cooper, D. Rogers, S. Beaton, R. Hendershot, J. W. Elkins, D. Fahey, R. Gao, F. Moore, S. A. Montzka, J. Schwarz, D. Hurst, B. Miller, C. Sweeney, S. Oltmans, D. Nance, E. Hints, G. Dutton, L. Watts, R. Spackman, K. Rosenlof, E. Ray, M. A. Zondlo, M. Diao, R. Keeling, J. Bent, E. Atlas, R. Lueb, M. J. Mahoney, M. Chahine, E. Olson, P. Patra, K. Ishijima, R. Engelen, J. Flemming, R. Nassar, D. B. A. Jones, and S. E. M. Fletcher: HIAPER Pole-to-Pole Observations (HIPPO): Fine-grained, global scale measurements of climatically important atmospheric gases and aerosols, *Philosophical Transactions of the Royal Society of London A*, 369, 2073-2086, doi:10.1098/rsta.2010.0313, 2011.

Worden, J., Kulawik, S., Frankenberg, C., Payne, V., Bowman, K., Cady-Peirara, K., Wecht, K., Lee, J.-E., and Noone, D.: Profiles of CH<sub>4</sub>, HDO, H<sub>2</sub>O, and N<sub>2</sub>O with improved lower tropospheric vertical resolution from Aura TES radiances, *Atmos. Meas. Tech.*, 5, 397-411, doi:10.5194/amt-5-397-2012, 2012.

Worden, J., Jiang, Z., Jones, D. B. A., Alvarado, M., Bowman, K., Frankenberg, C., Kort, E. A., Kulawik, S. S., Lee, M., Liu, J., Payne, V., Wecht, K. and Worden, H.: El Niño, the 2006 Indonesian Peat Fires, and the distribution of atmospheric methane, *Geophys. Res. Lett.*, n/a–n/a, doi:10.1002/grl.50937, 2013.

Worden, J. R., Turner, A. J., Bloom, A., Kulawik, S. S., Liu, J., Lee, M., Weidner, R., Bowman, K., Frankenberg, C., Parker, R., and Payne, V. H.: Quantifying lower tropospheric methane concentrations using GOSAT near-IR and TES thermal IR measurements, *Atmos. Meas. Tech.*, 8, 3433-3445, doi:10.5194/amt-8-3433-2015, 2015.

Worden, J., Doran, G., Kulawik, S., Eldering, A., Crisp, D., Frankenberg, C., O'Dell, C., and Bowman, K.: Evaluation and Attribution of OCO-2 XCO<sub>2</sub> Uncertainties, *Atmos. Meas. Tech.*, 10, 2759–2771, 2017 <https://doi.org/10.5194/amt-10-2759-2017>.

- Worden, J. R., Bloom, A. A., Pandey, S., Jiang, Z., Worden, H. M., Walker, T. W., Houweling, S., and Röckmann, T.: Reduced biomass burning emissions reconcile conflicting estimates of the post-2006 atmospheric methane budget, *Nat. Commun.*, 8, 2227, doi:10.1038/s41467-017-02246-0, 2017.
- Wu, L., Hasekamp, O., Hu, H., Landgraf, J., Butz, A., de Brugh, J. a., Aben, I., Pollard, D. F., Griffith, D. W. T., Feist, D. G., Koshelev, D., Hase, F., Toon, G. C., Ohyama, H., Morino, I., Notholt, J., Shiomi, K., Iraci, L., Schneider, M., de Mazière, M., Sussman, R., Kivi, R., Warneke, T., Goo, T.-Y., Té, Y.: Carbon dioxide retrieval from OCO-2 satellite observations using the RemoTeC algorithm and validation with TCCON measurements. *Atmospheric Measurement Techniques Discussions*, doi:10.5194/amt-2017-415, 2018.
- Wunch, D., Toon, G. C., Wennberg, P. O., Wofsy, S. C., Stephens, B. B., Fischer, M. L., Uchino, O., Abshire, J. B., Bernath, P., Biraud, S. C., Blavier, J.-F. L., Boone, C., Bowman, K. P., Browell, E. V., Campos, T., Connor, B. J., Daube, B. C., Deutscher, N. M., Diao, M., Elkins, J. W., Gerbig, C., Gottlieb, E., Griffith, D. W. T., Hurst, D. F., Jiménez, R., Keppel-Aleks, G., Kort, E. A., Macatangay, R., Machida, T., Matsueda, H., Moore, F., Morino, I., Park, S., Robinson, J., Roehl, C. M., Sawa, Y., Sherlock, V., Sweeney, C., Tanaka, T., and Zondlo, M. A.: Calibration of the Total Carbon Column Observing Network using aircraft profile data, *Atmos. Meas. Tech.*, 3, 1351–1362, doi:10.5194/amt-3-1351-2010, 2010.
- Wunch, D., Toon, G. C., Blavier, J.-F. L., Washenfelder, R. A., Notholt, J., Connor, B. J., Griffith, D. W., Sherlock, V., and Wennberg, P. O.: The total carbon column observing network, *Philos. T. R. Soc. A*, 369, 2087–2112, doi:10.1098/rsta.2010.0240, 2011a.
- Wunch, D., Wennberg, P. O., Toon, G. C., Connor, B. J., Fisher, B., Osterman, G. B., Frankenberg, C., Mandrake, L., O'Dell, C., Ahonen, P., Biraud, S. C., Castano, R., Cressie, N., Crisp, D., Deutscher, N. M., Eldering, A., Fisher, M. L., Griffith, D. W. T., Gunson, M., Heikkinen, P., Keppel-Aleks, G., Kyrö, E., Lindenmaier, R., Macatangay, R., Mendonca, J., Messerschmidt, J., Miller, C. E., Morino, I., Notholt, J., Oyafuso, F. A., Rettinger, M., Robinson, J., Roehl, C. M., Salawitch, R. J., Sherlock, V., Strong, K., Sussmann, R., Tanaka, T., Thompson, D. R., Uchino, O., Warneke, T., and Wofsy, S. C: A method for evaluating bias in global measurements of CO<sub>2</sub> total columns from space, *Atmos. Chem. Phys.*, 11, 20899–20946, doi:10.5194/acpd-11-20899-2011, 2011b.
- Wunch, D., Toon, G. C., Sherlock, V., Deutscher, N. M., Liu, C., Feist, D. G., and Wennberg, P. O.: The Total Carbon Column Observing Network's GGG2014 Data Version, Tech. rep., California Institute of Technology, Carbon Dioxide Information Analysis Center, Oak Ridge National Laboratory, Oak Ridge, Tennessee, USA, <https://doi.org/10.14291/tcon.ggg2014.documentation.R0/1221662>, 2015.
- Wunch, D., Wennberg, P. O., Osterman, G., Fisher, B., Naylor, B., Roehl, C. M., O'Dell, C., Mandrake, L., Viatte, C., Griffith, D. W., Deutscher, N. M., Velazco, V. A., Notholt, J., Warneke, T., Petri, C., de Mazière, M., Sha, M. K., Sussmann, R., Rettinger, M., Pollard, D., Robinson, J., Morino, I., Uchino, O., Hase, F., Blumenstock, T., Kiel, M., Feist, D. G., Arnold, S. G., Strong, K., Mendonca, J., Kivi, R., Heikkinen, P., Iraci, L., Podolske, J., Hillyard, P. W., Kawakami, S., Dubey, M. K., Parker, H. A., Sepulveda, E., Rodriguez, O. E. G., Te, Y., Jeseck, P., Gunson, M. R., Crisp, D., and Eldering, A.: Comparisons of the Orbiting Carbon Observatory-2 (OCO-2) XCO<sub>2</sub> measurements with TCCON, *Atmos. Meas.*

Tech., 10, 2209–2238, doi:10.5194/amt-10-2209-2017, 2017.

Xiong, X., C. Barnet, E. Maddy, C. Sweeney, X. Liu, L. Zhou, and M. Goldberg (2008), Characterization and validation of methane products from the Atmospheric Infrared Sounder (AIRS), *J. Geophys. Res.*, 113, G00A01, doi:10.1029/2007JG000500, 2008.

Yang, Z., Bi, Y., Wang, Q.: Preliminary Assessment of TanSat Atmospheric Carbon Dioxide Grating Spectroradiometer on-orbit Performance, International Workshop on Greenhouse Gas Measurements from Space (IWGGMS), Helsinki, Finland, June 2017.  
<http://iwggms13.fmi.fi/presentations.html>

Yang, D. X., Y. Liu, Z. N. Cai, X. Chen, L. Yao, and D. R. Lu: First global carbon dioxide maps produced from TanSat measurements. *Adv. Atmos. Sci.*, 35(6), 621–623, doi:10.1007/s00376-018-7312-6, 2018.

Yates, E.L., Schiro, K., Lowenstein, M., Sheffner, E.J., Iraci, L.T., Tadic, J.M., and Kuze, A., Carbon Dioxide and Methane at a Desert Site—A Case Study at Railroad Valley Playa, Nevada, USA, *Atmosphere*, 2, 702-714, doi:10.3390/atmos2040702, 2011.

Ye, X., Lauvaux, T, Eric Kort, E. A., Oda, T., Feng, S., Lin, J. C., Yang E., Wu, D.: Constraining fossil fuel CO<sub>2</sub> emissions from urban area using OCO-2 observations of total column CO<sub>2</sub>, *Atmos. Chem. Phys. Discuss.*, doi:10.5194/acp-2017-1022, 2017.

Yoshida, Y., Ota, Y., Eguchi, N., Kikuchi, N., Nobuta, K., Tran, H., Morino, I., and Yokota, T.: Retrieval algorithm for CO<sub>2</sub> and CH<sub>4</sub> column abundances from short-wavelength infrared spectral observations by the Greenhouse Gases Observing Satellite, *Atmos. Meas. Tech.*, 4, 717–734, doi:10.5194/amt-4-717-2011, 2011.

Yoshida, Y., et al.: Improvement of the retrieval algorithm for GOSAT SWIR XCO<sub>2</sub> and XCH<sub>4</sub> and their validation using TCCON data, *Atmos. Meas. Tech.*, 6, 1533–1547, doi:10.5194/amt-6-1533-2013, 2013.

Yu, K., Keller, C. A., Jacob, D. J., Molod, A. M., Eastham, S. D., and Long, M. S.: Errors and improvements in the use of archived meteorological data for chemical transport modeling: an analysis using GEOS-Chem v11-01 driven by GEOS-5 meteorology, *Geosci. Model Dev.*, 11, 305-319, <https://doi.org/10.5194/gmd-11-305-2018>, 2018.

Zhang, B., Cressie, N., and Wunch, D.: Statistical properties of atmospheric greenhouse gas measurements: Looking down from space and looking up from the ground, *Chemom. Intell. Lab. Syst.*, 162, 214–222, doi:10.1016/j.chemolab.2016.11.014, 2017.

Zhang, B., Cressie, N., and Wunch, D.: Inference for Errors-in-Variables Models in the Presence of Systematic Errors with an Application to a Satellite Remote Sensing Campaign, *Technometrics*, 1706, 1–43, doi:10.1080/00401706.2018.1476268, 2018.

Zhang, H., Lin, C., Zheng, Y, Wang, W., Tian, L., Liu, D., and Li, S.: Development and characterization of Carbon Observing Satellite, *J. Appl. Remote Sens.*, 10, 024003, doi:10.1117/1.JRS.10.024003, 2016.

Zhuravlev, R., Khattatov, B., Kiryushov, B., and Maksyutov, S.: Technical Note: A novel approach to estimation of time-variable surface sources and sinks of carbon dioxide using empirical orthogonal functions and the Kalman filter, *Atmos. Chem. Phys.*, 11, 10305-10315, 10.5194/acp-11-10305-2011, 2011.